

Emergence and dynamics of pointer states

Dissertation der Fakultät für Physik
der Ludwig-Maximilians-Universität München



vorgelegt von Marc Busse
aus Starnberg

München, den 09. April 2010

1. Gutachter: PD Dr. Klaus Hornberger
 2. Gutachter: Prof. Dr. Stefan Kehrein
- Tag der mündlichen Prüfung: 28. Mai 2010

Zusammenfassung

In dieser Arbeit wird der Übergang von der quanten- zur klassischen Mechanik für ein Testteilchen untersucht, das mit einem idealen Gas wechselwirkt. Ein derartiges System wird durch die lineare Quanten-Boltzmann-Gleichung beschrieben, die sich auf reine Stoßdekohärenz vereinfachen lässt, wenn es sich um eine Wechselwirkung zwischen viel schwereren Testteilchen und leichten Gasteilchen handelt. Im ersten Teil der Arbeit untersuchen wir die Entstehung und Dynamik von Zeigerzuständen, die durch Stoßdekohärenz induziert werden. Diese, durch die Umgebung ausgezeichneten Zustände sind exponentiell lokalisierte solitonische Wellenfunktionen, die sich nach den klassischen Hamiltonschen Gleichungen bewegen. Basierend auf dem "orthogonalen Unraveling" der quanten Mastergleichung kann ihre Entstehung und Dynamik charakterisiert werden und es lässt sich zeigen, dass die statistischen Gewichte, die von einem anfänglichen Superpositionszustand ausgehen, durch die erwarteten Projektionen gegeben sind. Darüber hinaus gehende Aussagen der linearen Quanten-Boltzmann-Gleichung werden im zweiten Teil unserer Arbeit beschrieben. Ein effizienter stochastischer Algorithmus, der auf der Monte Carlo Wellenfunktions-Methode basiert, wird genutzt um eine Reihe von physikalischen Prozessen zu simulieren: Den Verlust von räumlicher Kohärenz, die Entstehung von Interferenzmustern, Relaxation und Thermalisierung und den Übergang von quanten Dispersion zu klassischer Diffusion. Die Eignung des Algorithmus wird durch die Analyse der verschiedenen Grenzfälle der linearen Quanten-Boltzmann-Gleichung verifiziert.

Abstract

We study the quantum-to-classical transition in the motion of a quantum test particle interacting with an ideal gas environment. Such a system is described by the quantum linear Boltzmann equation, which simplifies to the master equation of pure collisional decoherence if the test particle is much heavier than the gas particles. In the first part of the thesis, we study the emergence and dynamics of pointer states induced by collisional decoherence. These environmentally distinguished states are shown to be exponentially localized solitonic wave functions which evolve according to the classical equations of motion. Based on the orthogonal unraveling of the quantum master equation, we characterize their formation and dynamics, and we demonstrate that the statistical weights arising from an initial superposition state are given by the required projection. The second part of the thesis is devoted to the general case described by the quantum linear Boltzmann equation. We provide an efficient stochastic algorithm in terms of the Monte Carlo wave function method. This algorithm is used to study a variety of physical processes: the loss of spatial coherences, the formation of interference patterns, relaxation and thermalization, and the transition from quantum dispersion to classical diffusion. The accuracy of the results is verified by exploiting the various limiting forms of the quantum linear Boltzmann equation.

To my parents

Acknowledgments

It is a pleasure to thank my supervisor Klaus Hornberger for the choice of this fundamental subject, which offered a lot of potential for fascinating research. Moreover, I am thankful to Klaus for his intensive support, and for allowing me to “bother” him with questions at any time – even on Saturday evening. Over the three years working and discussing with Klaus I had the opportunity both to improve my mathematical as well as my verbal skills, and to learn working with the required accuracy.

I also enjoyed working together with Piotr Pietrulewicz on the simulations of the quantum linear Boltzmann equation. Thank you Piotr for this fruitful teamwork, which made the second part of this thesis possible! At this point, I would also like to thank Heinz-Peter Breuer, with whom we had a very constructive collaboration on this topic.

For being nice colleagues and for having a pleasant time at the institute I would like to thank Johannes, Clemens and Stefan.

Finally, I am grateful to the members of the QCCC PhD programme, in particular to Thomas Schulte-Herbrüggen for inviting me to the seminars. I benefited a lot from the various opportunities offered by the network.

Contents

1	Introduction	1
1.1	Overview of the results	2
1.2	Structure of the thesis	3
2	Concepts of open quantum systems	5
2.1	Density operators	5
2.1.1	Pure versus mixed states	6
2.1.2	Ensemble interpretation	7
2.1.3	The reduced density operator	7
2.1.4	Matrix elements of the density operator	8
2.2	Dynamics of open quantum systems	9
2.2.1	Dynamical maps	9
2.2.2	Master equations in Lindblad form	12
3	Exemplary master equations and their microscopic derivations	17
3.1	The weak coupling formulation	17
3.2	The damped harmonic oscillator	19
3.3	The Caldeira-Leggett equation	20
3.3.1	Sketch of the derivation	20
3.3.2	Extension to Lindblad form	21
3.3.3	Relaxation	22
3.3.4	Decoherence	23
3.4	The monitoring approach	24
3.5	Collisional decoherence	25
3.5.1	Relation to microscopic quantities	26
3.5.2	Dynamic reduction models	27
4	The pointer basis	31
4.1	The damped harmonic oscillator	32
4.2	Definition of pointer states	33
4.3	The predictability sieve	34
4.4	Nonlinear equation for pointer states	35
4.4.1	Pointer states of pure dephasing	35
4.4.2	General Markovian master equations	37
4.4.3	Pointer states of the damped harmonic oscillator	39
4.4.4	Pointer states of the linear coupling model	40

5	Pointer states of collisional decoherence	43
5.1	Determining the pointer states of collisional decoherence	43
5.2	Properties of the solitons	46
5.2.1	Consequences of the continuity equation	47
5.2.2	Asymptotic form of the solitons	48
5.2.3	Size of the solitons	49
5.2.4	Completeness of the soliton basis	52
5.3	Dynamics in an external potential	54
5.4	Extensions to 3D	56
5.4.1	Estimation of the localization length scale	56
5.4.2	Estimation of the pointer size	58
5.4.3	Determining the coherence length	59
6	Classical stochastic processes	61
6.1	Classical Markov processes	61
6.2	Diffusion processes	63
6.2.1	Wiener process	64
6.2.2	Stochastic integration	65
6.2.3	Stochastic differential equations (SDEs)	68
6.3	Piecewise deterministic processes (PDPs)	73
6.3.1	Poisson process	73
6.3.2	Stochastic calculus for PDPs	75
7	Quantum trajectories	79
7.1	The quantum Markov process	79
7.2	Diffusive unravelings	81
7.2.1	Derivation of the drift and diffusion terms	83
7.2.2	Quantum Stratonovich SDEs	85
7.3	Piecewise deterministic unravelings	86
7.3.1	Derivation of the Monte Carlo unraveling	87
7.3.2	Derivation of the orthogonal unraveling	88
8	Unraveling collisional decoherence	91
8.1	Pointer states and quantum trajectories	91
8.2	Application to collisional decoherence	93
8.2.1	Deterministic evolution	93
8.2.2	Stochastic part	99
8.3	The statistical weights of the pointer states	101
8.3.1	Superposition of two localized states	101
8.3.2	Superposition of $N > 2$ localized states	103
9	Unraveling the quantum linear Boltzmann equation	105
9.1	The quantum linear Boltzmann equation (QLBE)	106
9.2	Limiting forms	107
9.2.1	Classical linear Boltzmann equation (CLBE)	107
9.2.2	Pure collisional decoherence	108
9.2.3	Born approximation	108
9.2.4	Quantum Brownian limit	109
9.3	Monte Carlo unraveling	109
9.3.1	The general algorithm	110

9.3.2	Unraveling the QLBE	111
9.3.3	Unraveling the QLBE in the momentum basis	112
10	Numerical results	119
10.1	Scattering amplitudes	120
10.1.1	s-wave hard-sphere scattering	120
10.1.2	Gaussian potential	120
10.2	Decoherence in momentum	124
10.3	Decoherence in position	126
10.3.1	Measuring spatial coherences	126
10.3.2	Measuring the localization rate	128
10.4	Interference and decoherence	129
10.5	Relaxation and thermalization	131
10.6	Diffusion	134
10.7	Summary	136
11	Conclusions	137
11.1	Pointer states and the orthogonal unraveling	137
11.2	Stochastic simulation of the quantum linear Boltzmann equation	138

Chapter 1

Introduction

Quantum mechanics provides the most accurate description of atomic and subatomic physics currently known. Since any object is composed of atoms and molecules, it seems suggestive that this theory holds as well on the macroscopic scale. The observations made in our everyday world are, however, in sharp contrast to the laws of quantum mechanics. For instance, the electron in a hydrogen atom is completely delocalized across the atom; its dynamics along this probability cloud is governed by the Schrödinger equation. The center of mass of a macroscopic soccer ball, on the other hand, moves on a spatially localized trajectory, which is determined by Newton's equation of motion. Due to this discrepancy, the nontrivial question arises how the laws of classical physics can be explained within the framework of quantum mechanics.

Only at the beginning of the eighties, it was recognized that the influence of environmental degrees of freedom is responsible for this *quantum-to-classical transition* [1–3]. A soccer ball flying through the air, for instance, collides with a tremendous number of photons, gas molecules and dust particles. Due to this openness, the reduced dynamics of the soccer ball is now longer described by Schrödinger's equation. Instead it is replaced by a quantum master equation, which is obtained by disregarding the environmental degrees of freedom. As recognized by Zurek [1, 4], these effective equations may induce a preferred set of robust states in the Hilbert space of the subsystem. The latter are robust in the sense that they stay pure for a relatively long time, whereas their superpositions get mixed rapidly. In the case of the soccer ball, these robust states would be sharply localized states, moving on the classical trajectories. The term *pointer states* has also been coined [1, 4] for such states, which is due to their role in models for quantum measurement. While the basic ideas behind this superselection or *decoherence process* seem to be settled, it still remains an open problem to understand the emergence, the dynamics, and the main properties of the pointer states for microscopic realistic environments.

Several strategies have been proposed so far for determining the pointer basis given the environmental coupling. In [5] the suggestion was made to sort the pure states in the Hilbert space according to their linear entropy production rate. The pointer states are then identified with the states having minimal loss of purity. Similar results are obtained by the approach of [6–8] which is based on a time evolution equation whose solitonic solutions are identified with the pointer states. So far, this concept has been applied to the damped harmonic oscillator by Gisin and Rigo [7, 8] and to a free quantum particle coupled linearly to a bath

of harmonic oscillators by Diosi and Kiefer [6, 8]. Here, the solitonic solutions of the corresponding nonlinear equation are coherent states and Gaussian wave packets, respectively. Moreover, the decoherence to Gaussian pointer states was proved to be generic for linear coupling models [9].

All of the above studies were restricted to harmonic oscillator baths and linear couplings. The goal of this thesis is to understand the emergence and dynamics of pointer states for more realistic, non-perturbative models. More specifically, our aim is to explain the quantum-to-classical transition for systems which interaction with their environment in terms of individual scattering events.

To archive this goal, we focus on the so-called *quantum linear Boltzmann equation* (QLBE) proposed by Hornberger and Vacchini in [10–12]. It is the quantum counterpart of the classical linear Boltzmann equation, which describes how the motion of a classical test particle is affected by elastic collisions with an ideal, stationary background gas. The derivation of the QLBE is based on the monitoring approach [11, 13] which admits the treatment of the interactions with a background gas in a non-perturbative manner.

A limiting gas arises when the Brownian particle is much heavier than the particles of the background gas. In this limit, the QLBE simplifies, giving a model called *collisional decoherence*. This master equation has first been suggested by Gallis and Fleming [14] and was derived in its final form by Hornberger and Sipe [15]. Notably, experiments with interfering fullerene molecules display a reduction of interference visibility in agreement with this theory [16–20].

1.1 Overview of the results

The thesis is divided into two parts. First, we present a complete picture of the quantum-to-classical transition exhibited by the collisional decoherence model. The second part is devoted to the numerical solution of the QLBE.

Pointer states of collisional decoherence As mentioned above, the authors in [6–8] discuss a nonlinear equation, whose solitonic solutions yield ‘candidate’ pointer states. Here we apply this approach to the one-dimensional version of collisional decoherence, giving a nonlinear integro-differential equation. We show that it exhibits exponentially localized solitonic wave functions, which move according to the classical equations of motion. Using the underlying symmetry it is shown that these solitons are related via translation and boost operators. This admits to prove that these ‘candidate’ pointer states form an overcomplete basis.

To gain deeper insight into the emergence and dynamics of pointer states, we relate the nonlinear equation to a specific quantum trajectory method, the *orthogonal unraveling* [21, 22]. This stochastic process on the one hand provides the statistical weights of the pointer basis, and on the other hand presents an efficient way of solving master equations which possess pointer states. Moreover, it allows us to prove that the above solitons are indeed the pointer states of collisional decoherence.

As a further step, extensions of the above theory to the three-dimensional problem are studied, which yields in particular an expression for the spatial extension of the pointer states in a realistic scenario. The latter is proportional to the mean free path of the gaseous environment, in case of weakly interacting or

thin gases. In the limit of a strongly interacting or dense gas, on the other hand, it is bounded by the scale of the thermal wave length. This result allows us to estimate the coherence length of interacting gases.

While the above results are derived within the framework of decoherence theory, they can also be applied to dynamic reduction models which propose a modification of the Schrödinger equation by means of nonlinear and stochastic terms. In fact, the observational consequences of the Ghirardi-Rimini-Weber spontaneous localization model [23, 24] are equivalent to the ones of collisional decoherence, since they are described by the same master equation [25]. The present work therefore applies to the Ghirardi-Rimini-Weber model. In particular, it provides the corresponding pointer basis.

Unraveling the QLBE Collisional decoherence applies to situations where the tracer particle is much heavier than the gas molecules, such that there is no appreciable energy exchange. It is therefore not suitable for the description of long-time effects, such as dissipation or thermalization. To study the full interplay between coherence and decoherence on the one hand, and relaxation processes on the other hand, we analyze the solutions of the QLBE in the second part of the thesis.

Due to the complexity of the QLBE, it is in general not analytically tractable. Breuer and Vacchini have therefore suggested [26] a stochastic algorithm, which admits an efficient numerical solution of the QLBE in terms of a Monte Carlo wave function method [27–29]. However, their treatment is restricted to a simplified version of the QLBE and to specific initial states, which are superpositions of at most two momentum eigenstates.

We expand the algorithm of Breuer and Vacchini to the full QLBE and to arbitrary initial states, such as spatially localized wave packets. By using realistic, microscopically derived scattering amplitudes, several physical processes are simulated: the loss of momentum and spatial coherences, the formation of interference patterns, relaxation and thermalization, and the transition from quantum dispersion to classical diffusion. The accuracy of the simulations is checked by a variety of consistency tests, based on limiting forms of the QLBE. In particular, this admits to verify the analytical predictions made in [10–12].

1.2 Structure of the thesis

Chapter 2 gives a general introduction to the concept of open quantum systems. This includes in particular a discussion of the Markov assumption, as well as the ensuing Lindblad form. The reader who is already familiar with this topic may as well skip this chapter. As a next step, several exemplary master equations, which are used throughout the thesis as models for open quantum system, are presented in **Chapter 3**, including the Caldeira-Leggett equation and collisional decoherence. In **Chapter 4**, we briefly review the notion of pointer states, and we summarize the method for determining the pointer states discussed in [6–8].

This method is then applied to collisional decoherence in **Chapter 5**, which provides a set of solitonic states to be regarded as ‘candidate’ pointer states. It is shown that these solitons form an overcomplete basis of exponentially localized states, and we give an expression for their spatial extension. Moreover, we

demonstrate that these ‘candidate’ pointer states move on the classical phase space trajectories if they are sufficiently localized, and we study extensions of the formalism to three dimensions.

The remaining part of the thesis applies quantum stochastic processes. To introduce this concept a variety of results from the classical theory of Markovian processes are required. **Chapter 6** therefore presents a survey of classical stochastic processes. The reader who is already familiar with this subject may as well skip this chapter. **Chapter 7** then introduces the theory of quantum trajectories, including quantum state diffusion, the Monte Carlo wave function method and the orthogonal unraveling. The latter is then applied to collisional decoherence in **Chapter 8**, which allows us to show that the ‘candidate’ states are indeed pointer states in the sense of the definition given in Chapter 4. Furthermore, we use the orthogonal unraveling to show that the statistical weights of the pointer states are given by the overlap with the initial state.

The last two chapters are devoted to the numerical solution of the full QLBE. In **Chapter 9**, the QLBE is reviewed in its basis independent operator form, and the various limiting forms of the QLBE are summarized. We then develop a stochastic algorithm which admits an efficient solution of the QLBE. The numerical results of this algorithm are summarized in **Chapter 10**.

Chapter 2

Concepts of open quantum systems

An open quantum system [29,30] consists of a quantum system S , which interacts with the so-called environment E , another quantum system; the corresponding Hilbert spaces are denoted by \mathcal{H}_S and \mathcal{H}_E . Crucially, the environment E is assumed to have a large number of degrees of freedom, which is much greater than the one of S . The combined system, denoted by SE, is typically assumed to be closed, such that it follows unitary dynamics; its associated Hilbert space is given by the tensor product space $\mathcal{H}_{SE} = \mathcal{H}_E \otimes \mathcal{H}_S$. Figure 2.1 shows a schematic picture of the combined system. As an example, one might think of an atom which interacts with an ideal gas environment or an electromagnetic field mode coupled to a thermal bath of harmonic oscillators.

In Sect. 2.1, we briefly review the notion of density operators, which form the physically allowed states ρ_S of S . Their temporal evolution, which is induced by the unitary dynamics of SE, is discussed in Sect. 2.2.

2.1 Density operators

The observable properties of a quantum system (be it open or closed) are completely determined by a positive operator ρ with trace one, i.e.

$$\rho \geq 0, \quad (2.1)$$

$$\text{Tr}(\rho) = 1, \quad (2.2)$$

acting on the corresponding Hilbert space \mathcal{H} [29,31]. Since the operator ρ , which is called *density operator* or *density matrix*, is positive, it is also Hermitian,

$$\rho^\dagger = \rho. \quad (2.3)$$

This implies that ρ can be written in terms of its spectral decomposition as

$$\rho = \sum_i p_i |\psi_i\rangle\langle\psi_i|, \quad p_i \geq 0, \quad \sum_i p_i = 1, \quad (2.4)$$

where the p_i 's denote the eigenvalues of ρ and the $|\psi_i\rangle$'s are the corresponding eigenvectors. The relevance of the density operator ρ is that it gives the probabilities of measurement outcomes for an observable \mathbf{A} , with spectral resolution

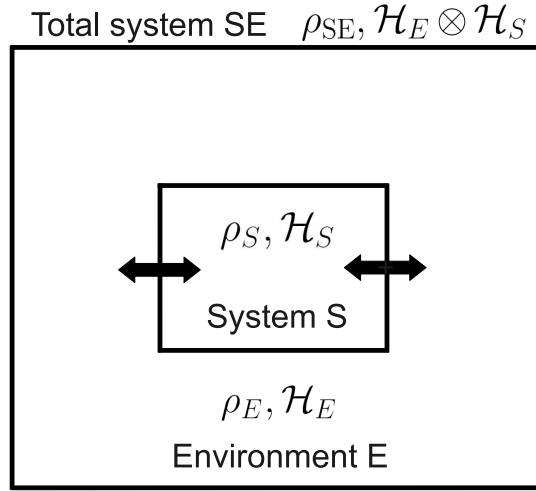


Figure 2.1: Schematic picture of an open quantum system S, which interacts with a thermal reservoir E. The combined system SE is assumed to be closed.

$A = \sum_i a_i |a_i\rangle\langle a_i|$, by means of the Born rule

$$\text{Prob}(a_i) = \text{Tr}(|a_i\rangle\langle a_i|\rho). \quad (2.5)$$

In particular, this admits the prediction of expectation values:

$$\begin{aligned} \langle A \rangle &= \sum_i a_i \text{Prob}(a_i) \\ &= \text{Tr}(\rho A). \end{aligned} \quad (2.6)$$

2.1.1 Pure versus mixed states

Crucially, the set of density operators $\mathcal{S}(\mathcal{H})$ is convex, that is

$$\lambda\rho_1 + (1 - \lambda)\rho_2 \in \mathcal{S}(\mathcal{H}), \quad \text{if } \rho_1, \rho_2 \in \mathcal{S}(\mathcal{H}) \text{ and } \lambda \in [0, 1]. \quad (2.7)$$

A state ρ of $\mathcal{S}(\mathcal{H})$ is called *mixed* if it can be written as $\lambda\rho_1 + (1 - \lambda)\rho_2$, where $0 < \lambda < 1$ and ρ_1 is different from ρ_2 . Otherwise, the state is called *pure*. The pure states are therefore the extreme points of the convex set $\mathcal{S}(\mathcal{H})$, and they form rank one projections,

$$\begin{aligned} \rho_{\text{pure}} &= P \\ &\equiv |\psi\rangle\langle\psi|, \quad \text{with } |\psi\rangle \in \mathcal{H}. \end{aligned}$$

In particular, this implies that a state is pure if and only if

$$\rho^2 = \rho. \quad (2.8)$$

A measure for the purity of states is the von Neumann entropy,

$$S_N(\rho) = -\text{Tr}(\rho \ln \rho). \quad (2.9)$$

$$= -\sum_i p_i \ln p_i, \quad (2.10)$$

which is equal to the Shannon entropy [31] of the eigenvalue distribution p_i . It vanishes if and only if the state is pure, that is $S_N(\mathbf{P}) = 0$, and it takes on its maximum value $S_N(\rho) = \ln d$ for the maximally mixed state $\rho = \mathbb{1}/d$, if \mathcal{H} is finite-dimensional with $d = \dim(\mathcal{H})$.

As an alternative measure for the purity of states, it is sometimes useful to consider the linear entropy,

$$S_{\text{lin}}(\rho) = 1 - \text{Tr}(\rho^2), \quad (2.11)$$

which has the upper and lower bounds $0 \leq S_{\text{lin}}(\rho) \leq 1 - 1/d$, if $d < \infty$. Similar to the von Neumann entropy, it attains its extreme values for the pure and the maximally mixed state.

2.1.2 Ensemble interpretation

The spectral decomposition (2.4) admits an interpretation of the mixed state ρ by means of a statistical ensemble $\{p_i, |\psi_i\rangle\}$ of systems, where p_i is the proportion of the ensemble being in the pure state $|\psi_i\rangle$. Conversely, the state ρ can be obtained by realizing the pure state ensemble $\{p_i, |\psi_i\rangle\}$.

However, this interpretation has to be taken with care, since the convex decomposition (2.4) is not unique. In fact, other partitions $\{q_i, |\varphi_i\rangle\}$, defined as

$$\sqrt{q_i}|\varphi_i\rangle = \sum_j U_{ij}\sqrt{p_j}|\psi_j\rangle, \quad \text{with} \quad \sum_j U_{ij}^\dagger U_{jk} = \delta_{ik}, \quad (2.12)$$

can be constructed, which represent the same mixed state $\rho = \sum_i p_i |\psi_i\rangle\langle\psi_i| = \sum_i q_i |\varphi_i\rangle\langle\varphi_i|$ [32]. Since the observable properties, that is the expectation values (2.6), are determined solely by the density matrix ρ , it is not possible to determine which particular partition is realized. Thus, it must be avoided to draw conclusions using a particular ensemble, which go beyond the predictions obtained from ρ . In fact, such a reasoning may lead to wrong conclusions known as the ‘‘partition ensemble fallacies’’ [33].

2.1.3 The reduced density operator

Perhaps the most important application of the density operator is the description of subsystems, such as the open system shown in Fig. 2.1, of a composite quantum system. Such a description is provided by the *reduced density operator*. Suppose the state ρ_{SE} of the combined system is known, then the reduced state of the open system S is given by

$$\begin{aligned} \rho_S &= \sum_i \langle i_E | \rho_{\text{SE}} | i_E \rangle \\ &\equiv \text{Tr}_E(\rho_{\text{SE}}), \end{aligned} \quad (2.13)$$

where the operator map $\text{Tr}_E(\cdot)$ denotes the *partial trace* over the environment E and $\{|i_E\rangle\}$ is a basis of \mathcal{H}_E . This choice is made so as to ensure that the reduced density operator ρ_S gives the correct results for the expectation values of local observables $\mathbf{A} = \mathbf{A}_S \otimes \mathbb{1}$. In other words, the definition (2.13) assures that [31]

$$\text{Tr}_{\text{SE}}(\rho_{\text{SE}} \mathbf{A}_S \otimes \mathbb{1}) = \text{Tr}_S(\rho_S \mathbf{A}_S). \quad (2.14)$$

As an example, let us assume that SE is a pair of two-level systems, prepared in a Bell state,

$$\rho_{SE} = \frac{1}{2}(|00\rangle + |11\rangle)(\langle 00| + \langle 11|). \quad (2.15)$$

Tracing out the environment according to (2.13), it follows that the open system S is in a maximally mixed state,

$$\begin{aligned} \rho_S &= \frac{1}{2}(|0\rangle\langle 0| + |1\rangle\langle 1|) \\ &= \frac{1}{2}\mathbb{1}. \end{aligned} \quad (2.16)$$

Remarkably, even though there is complete knowledge about the total system, since it is in a pure state, the open subsystem is maximally mixed, such that we are completely ignorant about local measurements. This property, which is due to the fact that the total system is in an entangled state, shows that the concept of mixed states arises naturally in open systems.

2.1.4 Matrix elements of the density operator

In order to handle the density operator, it is useful to represent ρ in terms of an orthonormal basis $\{|n\rangle\}$ of \mathcal{H} ,

$$\rho = \sum_{m,n} \rho_{mn} |m\rangle\langle n|, \quad \text{with } \rho_{mn} = \langle m|\rho|n\rangle. \quad (2.17)$$

The diagonal elements $0 \leq \rho_{nn} \leq 1$ of the corresponding matrix are called *populations*, since they present the probabilities that, in a measurement, the system is found in one of the basis states,

$$\rho_{nn} = \text{Tr}(|n\rangle\langle n|\rho). \quad (2.18)$$

On the other hand, the non-diagonal elements $\rho_{mn} = \rho_{nm}^*$, $m \neq n$, are called *coherences*, since they are responsible for interference effects between the different basis states. They are bounded from above by the geometric mean of the populations, i.e.

$$|\rho_{mn}|^2 \leq \rho_{mm} \rho_{nn}, \quad (2.19)$$

a relation that holds for any positive matrix [34].

Later these concepts are applied to infinite-dimensional systems, where in particular the one-dimensional motion of a single particle is considered. A basis of the associated Hilbert space is obtained, for instance, by the position eigenbasis $\{|x\rangle|x \in \mathbb{R}\}$, forming an uncountable set of improper eigenstates of the position operator x . A state ρ can be represented in this basis by means of a two-dimensional function $\rho(x, x') \equiv \langle x|\rho|x'\rangle$,

$$\rho = \int dx dx' \rho(x, x') |x\rangle\langle x'|. \quad (2.20)$$

Similarly to the finite-dimensional case, the populations $\rho(x, x)$ are probability densities, i.e. $\rho(x, x) \geq 0$ and $\int dx \rho(x, x) = 1$, providing the probability,

$$\text{Prob}(x \in [x_1, x_2]) = \int_{x_1}^{x_2} dx \rho(x, x), \quad (2.21)$$

that the particle is found in the interval $[x_1, x_2]$. On the other hand, the coherences $\rho(x, x') = \rho^*(x', x)$, $x \neq x'$, are responsible for spatial interference effects. As in finite dimensions, they are bounded from above by the geometric mean of the populations, i.e.

$$|\rho(x, x')|^2 \leq \rho(x, x) \rho(x', x'), \quad (2.22)$$

which can be shown using the positivity of ρ . To this end, one considers projections $\langle \theta | \rho | \theta \rangle \geq 0$ onto states of the form $|\theta\rangle = \cos(\theta) |x\rangle + e^{i\varphi} \sin(\theta) |x'\rangle$, with $\varphi = \arg[\rho(x, x')]$.

2.2 Dynamics of open quantum systems

2.2.1 Dynamical maps

Since the total system SE is assumed to be closed, it evolves unitarily,

$$\rho_{\text{SE}}(t) = \mathbf{U}_t \rho_{\text{SE}}(0) \mathbf{U}_t^\dagger, \quad (2.23)$$

where the propagator \mathbf{U}_t is generated by the Hamiltonian \mathbf{H}_{SE} of the total system, that is $\mathbf{U}_t = \exp(-i\mathbf{H}_{\text{SE}} t/\hbar)$. The latter may be taken to be of the form

$$\mathbf{H}_{\text{SE}} = \mathbf{H}_S \otimes \mathbf{I}_E + \mathbf{I}_S \otimes \mathbf{H}_E + \mathbf{H}_I, \quad (2.24)$$

where \mathbf{H}_S denotes the Hamiltonian of the open system S , \mathbf{H}_E is the free Hamiltonian of the environment E , and \mathbf{H}_I denotes the interaction Hamiltonian. The induced dynamics of the open system S is obtained by taking the partial trace over the environment,

$$\rho_S(t) = \text{Tr}_E \left(\mathbf{U}_t \rho_{\text{SE}}(0) \mathbf{U}_t^\dagger \right). \quad (2.25)$$

In order to simplify this relation, let us assume that the state of the total system ρ_{SE} is initially uncorrelated, i.e. $\rho_{\text{SE}}(0) = \rho_S(0) \otimes \rho_E(0)$. This allows one to formulate the temporal evolution of S in terms of a one-parameter family of maps, called *dynamical map*, from the space $\mathcal{S}(\mathcal{H}_S)$ of density matrices of the open system onto itself,

$$\mathcal{E}_t : \rho_S(0) \mapsto \rho_S(t) = \text{Tr}_E \left(\mathbf{U}_t \rho_S(0) \otimes \rho_E(0) \mathbf{U}_t^\dagger \right), \quad \text{with } t \in \mathbb{R}_0^+. \quad (2.26)$$

Crucially, the dynamical map \mathcal{E}_t is in general non-unitary (due to the interaction term \mathbf{H}_I). As a consequence, one encounters in open systems a variety of dynamical features, such as decoherence and thermalization, that are not observed in closed quantum systems.

In quantum information theory, one is typically interested in the input and output state of a quantum device, such that one considers the map \mathcal{E}_t at a particular point in time $t = T$ only. This map \mathcal{E}_T is in the literature referred to as *quantum operation* or *quantum channel*.

Kraus representation Dynamical maps can be represented completely in terms of operators acting on the open system's Hilbert space [29, 31]. To derive this representation, which is known as the *Kraus representation* or *operator-sum representation*, consider the spectral resolution of the initial state of the environment $\rho_E(0)$,

$$\rho_E(0) = \sum_i e_i |e_i\rangle\langle e_i|, \quad e_i \geq 0, \quad \sum_i e_i = 1. \quad (2.27)$$

Plugging (2.27) into the dynamical map (2.26) gives

$$\mathcal{E}_t(\rho_S(0)) = \sum_{i,j} \mathbf{E}_{ij}(t) \rho_S(0) \mathbf{E}_{ij}^\dagger(t), \quad (2.28)$$

where the *Kraus operators* $\mathbf{E}_{ij}(t)$, acting on \mathcal{H}_S , read as

$$\mathbf{E}_{ij}(t) = \sqrt{e_i} \langle e_i | \mathbf{U}_t | e_j \rangle. \quad (2.29)$$

Moreover, from the completeness of the basis $\{|e_i\rangle\}$ and the unitarity of \mathbf{U}_t , one obtains the completeness relation

$$\sum_{i,j} \mathbf{E}_{ij}^\dagger(t) \mathbf{E}_{ij}(t) = \mathbf{I}_S. \quad (2.30)$$

Due to the construction of $\mathbf{E}_{ij}(t)$, Eq. (2.29), the number N of required Kraus operators is limited by the dimension of the open system's Hilbert space, $N \leq \dim(\mathcal{H}_S)^2$, in finite-dimensional systems; in case of an infinite-dimensional Hilbert space, i and j label a countable set.

Properties of dynamical maps Using the operator-sum representation, one can deduce the basic properties of a dynamical map \mathcal{E}_t . One finds that it is (a) *trace-preserving*

$$\text{Tr}(\mathcal{E}_t(\rho_S(0))) = \text{Tr}\left(\rho_S(0) \sum_{i,j} \mathbf{E}_{ij}^\dagger(t) \mathbf{E}_{ij}(t)\right) = 1, \quad (2.31)$$

and (b) *convex-linear*, meaning that

$$\mathcal{E}_t\left(\sum_i p_i \rho_i\right) = \sum_i p_i \mathcal{E}_t(\rho_i), \quad \text{if } p_i \geq 0. \quad (2.32)$$

Moreover, \mathcal{E}_t is (c) *completely positive*, that is, trivial extensions of \mathcal{E}_t ,

$$\mathcal{E}_t \otimes \mathbf{I}_E : \rho_{SE}(0) = \sum_l \mathbf{A}_l \otimes \mathbf{B}_l \mapsto \rho_{SE}(t) = \sum_l \mathcal{E}_t(\mathbf{A}_l) \otimes \mathbf{B}_l, \quad (2.33)$$

map positive operators $\rho_{SE}(0) \in \mathcal{S}(\mathcal{H}_{SE})$ to positive operators $\rho_{SE}(t) \in \mathcal{S}(\mathcal{H}_{SE})$. This can be verified as follows:

$$\begin{aligned} \langle \psi | \mathcal{E}_t \otimes \mathbf{I}_E(\rho_{SE}) | \psi \rangle &= \sum_{i,j} \langle \psi | \mathbf{E}_{ij} \otimes \mathbf{I}_E \rho_{SE} \mathbf{E}_{ij}^\dagger \otimes \mathbf{I}_E | \psi \rangle \\ &= \sum_{i,j} \langle \varphi_{ij} | \rho_{SE} | \varphi_{ij} \rangle \\ &\geq 0, \end{aligned} \quad (2.34)$$

with $\rho_{SE} \geq 0$, $|\psi\rangle \in \mathcal{H}_{SE}$ and $|\varphi_{ij}\rangle \equiv \mathbf{E}_{ij}^\dagger \otimes \mathbf{I}_E |\psi\rangle \in \mathcal{H}_{SE}$.

Axiomatic approach One can take an approach to open quantum systems which is in some sense complementary to the ideas described above. To this end, one defines a dynamical map \mathcal{E}_t as a one-parameter family of maps

$$\mathcal{E}_t : \rho_S(0) \mapsto \rho_S(t), \quad \text{with } t \in \mathbb{R}_0^+, \quad (2.35)$$

satisfying the minimal set of requirements posed by the laws of quantum mechanics, that is it must be (a) trace-preserving, (b) convex-linear and (c) completely positive. From this definition one can then derive the representation given by Eq. (2.26).

The axioms (a) to (c) are required for the following reasons.

- a) $\mathcal{E}_t(\rho_S)$ is a density operator and hence has trace one for all times t .
- b) Suppose the state ρ_i is prepared initially with probability p_i ; then the state at time $t = T$ is given by $\mathcal{E}_T(\rho_i)$ with probability p_i . On the other hand, in the ensemble average, the initial state is $\sum_i p_i \rho_i$, while the image under the map \mathcal{E}_T reads as $\mathcal{E}_T(\sum_i p_i \rho_i)$. This implies that \mathcal{E}_t must be convex-linear.
- c) The open system S is a subsystem of the closed system SE. Apparently, \mathcal{E}_t can be extended to SE by multiplication with the identity operator $\mathcal{E}_t \otimes \mathbb{I}$. The image of this extended map must be a density operator, and hence has to be positive.

In finite-dimensional systems, the representation (2.26) is guaranteed by *Stinespring's dilation theorem* [35], which says that if $\mathcal{E}_T : \mathcal{S}(\mathcal{H}_S) \rightarrow \mathcal{S}(\mathcal{H}_S)$ is a map between states on a finite-dimensional Hilbert space \mathcal{H}_S , satisfying the conditions (a)-(c), then there exists a Hilbert space \mathcal{H}_E and a unitary operation \mathbf{U}_T on $\mathcal{H}_S \otimes \mathcal{H}_E$ such that

$$\mathcal{E}_T(\rho_S) = \text{Tr}_E \left(\mathbf{U}_T \rho_S \otimes |0_E\rangle\langle 0_E| \mathbf{U}_T^\dagger \right), \quad \text{for all } \rho_S \in \mathcal{S}(\mathcal{H}_S). \quad (2.36)$$

Here the ancilla space \mathcal{H}_E can be chosen such that $\dim(\mathcal{H}_E) \leq \dim(\mathcal{H}_S)^2$.

Quantum dynamical semigroups A variety of open quantum systems encountered in practice exhibit the so-called *Markov property*; a detailed introduction of this assumption is given below. To anticipate, a dynamical map is said to fulfill the Markov property if it satisfies the relation

$$\mathcal{E}_t(\mathcal{E}_s(\rho_S)) = \mathcal{E}_{t+s}(\rho_S), \quad \text{for all } \rho_S \in \mathcal{S}(\mathcal{H}_S). \quad (2.37)$$

Such a one-parameter family of maps \mathcal{E}_t is by definition closed under the binary operation $\mathcal{E}_t \bullet \mathcal{E}_s(\rho) = \mathcal{E}_t(\mathcal{E}_s(\rho))$, which implies that a dynamical map \mathcal{E}_t satisfying the Markov property forms a semigroup. Note that such a *quantum dynamical semigroup* (QDS) [36] does in general not form a regular group since the inverse element \mathcal{E}_t^{-1} is not necessarily part of the semigroup (open system dynamics is in general irreversible).

Under certain mathematical constraints [37], one can write a QDS in exponential form,

$$\mathcal{E}_t = \exp(\mathcal{L}t), \quad (2.38)$$

where \mathcal{L} , the *generator* of the QDS, is called *Liouville* super-operator. As we shall see below, this generator is of a particular form known as *Lindblad form*, which is enforced by the requirement that \mathcal{E}_t is trace-preserving, convex-linear and completely positive.

2.2.2 Master equations in Lindblad form

As in other areas of science, it is convenient to formulate the dynamics of S in terms of a differential equation. To this end, let us evaluate the time derivative of $\rho_S(t)$ using the dynamical map \mathcal{E}_t , which formally yields

$$\begin{aligned}\dot{\rho}_t &= \lim_{dt \rightarrow 0} \frac{\rho_{t+dt} - \rho_t}{dt} \\ &= \lim_{dt \rightarrow 0} \frac{\mathcal{E}_{t+dt}(\rho_0) - \mathcal{E}_t(\rho_0)}{dt} \equiv \mathcal{K}_t \rho_0,\end{aligned}\quad (2.39)$$

where we dropped the subscript S for brevity, i.e. $\rho_t \equiv \rho_S(t)$. Here \mathcal{K}_t is a super-operator, that is a map from the space $\mathcal{S}(\mathcal{H}_S)$ of density matrices into itself. Equation (2.39) shows that the evolution equation of an open quantum system is in general non-local in time. An interpretation of this dependence on the system's past is that the environment has a memory that stores information about the evolution of the system. This information may then flow from the environment back to the system, such that the change of ρ_t depends on its own history. However, one may typically neglect memory effects if environmental correlation times are much smaller than the characteristic time scale of the system evolution. Under this condition, one may assume that the change of ρ_t depends on the current state only. This is the so-called *Markov assumption* or *Markov property*. It admits to describe the temporal evolution in terms of a local differential equation,

$$\dot{\rho}_t = \mathcal{L}\rho_t,\quad (2.40)$$

generated by a time independent Liouville super-operator \mathcal{L} . Such an equation is called *quantum Master equation*, since it leads to a classical Master equation [38] for the populations, if expressed in an orthonormal basis.

Before the general form of the Liouvillian \mathcal{L} can be stated, a more formal definition of the Markov assumption and the corresponding quantum Markov process is needed. To this end, we first introduce the notion of a classical Markov process, and then deduce the definition of its quantum counterpart.

Classical Markov processes A classical Markov process [38] is a stochastic process, that is a one-parameter family of random variables X_t , $t \in \mathbb{R}_0^+$, whose conditional probability distribution is determined entirely by the most recent observation, meaning that

$$\text{Prob}(X_{t_{n+1}} | X_{t_n}, X_{t_{n-1}}, \dots, X_{t_1}) = \text{Prob}(X_{t_{n+1}} | X_{t_n}),\quad (2.41)$$

for ordered times $t_{n+1} \geq t_n \geq \dots \geq t_1$.

Quantum Markov processes This motivates the following definition of quantum Markov processes. Let us suppose that the observable \mathbf{X} ,

$$\mathbf{X} = \sum_i X_i |X_i\rangle \langle X_i|,\quad (2.42)$$

will be measured at time t_{n+1} . Then a quantum Markov process is a one-parameter family of density operators ρ_t , $t \in \mathbb{R}_0^+$, which leads to a conditional

probability distribution for the measurement outcomes of \mathbf{X} that is determined entirely by the most recent state, which means that

$$\text{Prob}(X_i | \rho_{t_n}, \rho_{t_{n-1}}, \dots, \rho_{t_1}) = \text{Prob}(X_i | \rho_{t_n}), \quad (2.43)$$

with time ordering $t_{n+1} \geq t_n \geq \dots \geq t_1$.

Using the dynamical map \mathcal{E}_t , one can rewrite Eq. (2.43) as

$$\begin{aligned} & \text{Tr} \{ |X_i\rangle \langle X_i| \mathcal{E}_{(t_{n+1}, t_n)} (\mathcal{E}_{(t_n, t_{n-1})} (\dots \mathcal{E}_{(t_1, t_0)} (\rho_0))) \} \\ &= \text{Tr} \{ |X_i\rangle \langle X_i| \mathcal{E}_{(t_{n+1}, t_n)} (\mathcal{E}_{(t_n, t_0)} (\rho_0)) \}. \end{aligned} \quad (2.44)$$

This implies that

$$\mathcal{E}_{(t_n, t_{n-1})} (\dots \mathcal{E}_{(t_1, t_0)} (\rho_0)) = \mathcal{E}_{(t_n, t_0)} (\rho_0), \quad (2.45)$$

which agrees with the semigroup assumption (2.37). We conclude that a quantum process is Markov if the corresponding dynamical map forms a quantum dynamical semigroup, characterized by condition (2.37).

Lindblad form Using the Markov assumption (2.37), one can reformulate the time derivative (2.39) as a time-local equation of motion for the state ρ_t

$$\begin{aligned} \dot{\rho}_t &= \lim_{dt \rightarrow 0} \frac{\mathcal{E}_{t+dt}(\rho_0) - \mathcal{E}_t(\rho_0)}{dt} \\ &= \lim_{dt \rightarrow 0} \frac{\mathcal{E}_{dt}(\rho_t) - \rho_t}{dt} \equiv \mathcal{L}\rho_t. \end{aligned} \quad (2.46)$$

Upon inserting the Kraus representation (2.28) for $\mathcal{E}_{dt}(\rho_t)$ and using the conservation of the trace, $\text{Tr}(\mathcal{L}\rho_t) = 0$, one obtains the so-called *Lindblad form* [29, 39],

$$\mathcal{L}\rho = \frac{1}{i\hbar} [\mathbf{H}, \rho] + \sum_{k=1}^N \gamma_k \left(\mathbf{L}_k \rho \mathbf{L}_k^\dagger - \frac{1}{2} \mathbf{L}_k^\dagger \mathbf{L}_k \rho - \frac{1}{2} \rho \mathbf{L}_k^\dagger \mathbf{L}_k \right), \quad (2.47)$$

with $N \leq \dim(\mathcal{H}_S)^2 - 1$, if \mathcal{H}_S is finite-dimensional. The first summand represents the unitary part of the dynamics generated by the Hermitian operator \mathbf{H} . It is not necessarily equal to \mathbf{H}_S , the Hamiltonian of S , which shows that the energy levels of the system may be shifted due to the interaction with the environment (a famous example for such an energy shift is the Lamb shift, caused by the interaction of the hydrogen's electron with the electromagnetic vacuum). The non-unitary part is characterized by the in general non-Hermitian operators \mathbf{L}_k known as *Lindblad operators* or *jump operators* (a name motivated by the quantum trajectory approach introduced below), and the positive rates γ_k . The latter have a dimension of inverse time, provided the \mathbf{L}_k 's are taken to be dimensionless.

The expression (2.47) was derived in 1976 by Gorini, Kossakowski and Sudarshan [40], and independently by Lindblad [37]. The former proved that (2.47) defines the most general generator of a QDS in finite-dimensional systems, while the latter showed that (2.47) is valid also for infinite-dimensional systems provided the generator is bounded and the index k is allowed to run over a countable set. In many applications, though, the generator \mathcal{L} is unbounded; this is for instance the case if the Lindblad operators are proportional to the position- or momentum operator. Unfortunately, in this case, there is no theorem giving the most general

structure of the generator. However, it turns out that all known examples of master equations describing Markovian systems are either of Lindblad form, or can be cast into it by slight modifications. In some of these examples, though, one encounters an uncountable set of Lindblad operators, such that (2.47) takes the form

$$\mathcal{L}\rho = \frac{1}{i\hbar} [\mathbf{H}, \rho] + \int d\mathbf{q} \gamma_{\mathbf{q}} \left(\mathbf{L}_{\mathbf{q}} \rho \mathbf{L}_{\mathbf{q}}^\dagger - \frac{1}{2} \mathbf{L}_{\mathbf{q}}^\dagger \mathbf{L}_{\mathbf{q}} \rho - \frac{1}{2} \rho \mathbf{L}_{\mathbf{q}}^\dagger \mathbf{L}_{\mathbf{q}} \right), \quad (2.48)$$

where the measure has the meaning of a rate density. This representation may also be convenient in cases where the generator is bounded (an example is collisional decoherence, which is studied below).

Non-uniqueness of the Lindblad operators Importantly, the generator \mathcal{L} does not uniquely fix the Lindblad operators $\mathbf{L}_{\mathbf{q}}$ and the Hamiltonian \mathbf{H} . This is due to the fact that the master equation (2.48) is invariant under certain transformations. As an example, let us consider the ‘Fourier transform’ of the Lindblad operators,

$$\sqrt{\gamma_{\mathbf{q}}} \mathbf{L}_{\mathbf{q}} \rightarrow \sqrt{\gamma'_{\mathbf{q}}} \mathbf{L}'_{\mathbf{q}} = \frac{1}{(2\pi)^{3/2}} \int d\mathbf{k} e^{i\mathbf{q}\mathbf{k}} \sqrt{\gamma_{\mathbf{k}}} \mathbf{L}_{\mathbf{k}}, \quad (2.49)$$

which will be used in Sect. 3.5.2 to reveal the similarity of collisional decoherence and the Ghirardi-Rimini-Weber model. The invariance of the generator (2.48) under (2.49) can be seen easily:

$$\begin{aligned} \mathcal{L}'\rho &= \frac{1}{i\hbar} [\mathbf{H}, \rho] + \int d\mathbf{k} d\mathbf{l} \frac{1}{(2\pi)^3} \int d\mathbf{q} e^{i\mathbf{q}(\mathbf{k}-\mathbf{l})} \sqrt{\gamma_{\mathbf{k}} \gamma_{\mathbf{l}}} \left(\mathbf{L}_{\mathbf{k}} \rho \mathbf{L}_{\mathbf{l}}^\dagger - \frac{1}{2} \mathbf{L}_{\mathbf{l}}^\dagger \mathbf{L}_{\mathbf{k}} \rho - \frac{1}{2} \rho \mathbf{L}_{\mathbf{l}}^\dagger \mathbf{L}_{\mathbf{k}} \right) \\ &= \frac{1}{i\hbar} [\mathbf{H}, \rho] + \int d\mathbf{k} d\mathbf{l} \delta^3(\mathbf{k}-\mathbf{l}) \sqrt{\gamma_{\mathbf{k}} \gamma_{\mathbf{l}}} \left(\mathbf{L}_{\mathbf{k}} \rho \mathbf{L}_{\mathbf{l}}^\dagger - \frac{1}{2} \mathbf{L}_{\mathbf{l}}^\dagger \mathbf{L}_{\mathbf{k}} \rho - \frac{1}{2} \rho \mathbf{L}_{\mathbf{l}}^\dagger \mathbf{L}_{\mathbf{k}} \right) \\ &= \mathcal{L}\rho. \end{aligned} \quad (2.50)$$

Another type of invariance transformations are inhomogeneous ones where a complex multiple $z_{\mathbf{q}}$ of the identity \mathbf{I} is added,

$$\mathbf{L}_{\mathbf{q}} \rightarrow \mathbf{L}'_{\mathbf{q}} = \mathbf{L}_{\mathbf{q}} + z_{\mathbf{q}} \mathbf{I}. \quad (2.51)$$

In this case, also the Hamiltonian must be transformed as

$$\mathbf{H} \rightarrow \mathbf{H}' = \mathbf{H} - \frac{i\hbar}{2} \int d\mathbf{q} \gamma_{\mathbf{q}} \left(z_{\mathbf{q}}^* \mathbf{L}_{\mathbf{q}} - z_{\mathbf{q}} \mathbf{L}_{\mathbf{q}}^\dagger \right), \quad (2.52)$$

in order to assure the invariance of the master equation (2.48). Like above, the latter can be demonstrated easily,

$$\begin{aligned} \mathcal{L}'\rho &= \frac{1}{i\hbar} \left[\mathbf{H} - \frac{i\hbar}{2} \int d\mathbf{q} \gamma_{\mathbf{q}} \left(z_{\mathbf{q}}^* \mathbf{L}_{\mathbf{q}} - z_{\mathbf{q}} \mathbf{L}_{\mathbf{q}}^\dagger \right), \rho \right] \\ &+ \int d\mathbf{q} \gamma_{\mathbf{q}} \left\{ (\mathbf{L}_{\mathbf{q}} + z_{\mathbf{q}}) \rho \left(\mathbf{L}_{\mathbf{q}}^\dagger + z_{\mathbf{q}}^* \right) - \frac{1}{2} \left(\mathbf{L}_{\mathbf{q}}^\dagger + z_{\mathbf{q}}^* \right) (\mathbf{L}_{\mathbf{q}} + z_{\mathbf{q}}) \rho \right. \\ &\left. - \frac{1}{2} \rho \left(\mathbf{L}_{\mathbf{q}}^\dagger + z_{\mathbf{q}}^* \right) (\mathbf{L}_{\mathbf{q}} + z_{\mathbf{q}}) \right\}. \end{aligned} \quad (2.53)$$

By expanding the terms on the right-hand side of the expression above, one obtains

$$\begin{aligned}
\mathcal{L}'\rho &= \frac{1}{i\hbar} [\mathbf{H}, \rho] - \frac{1}{2} \int d\mathbf{q} \gamma_{\mathbf{q}} \left(z_{\mathbf{q}}^* [\mathbf{L}_{\mathbf{q}}, \rho] - z_{\mathbf{q}} [\mathbf{L}_{\mathbf{q}}^\dagger, \rho] \right) \\
&+ \int d\mathbf{q} \gamma_{\mathbf{q}} \left(\mathbf{L}_{\mathbf{q}} \rho \mathbf{L}_{\mathbf{q}}^\dagger - \frac{1}{2} \mathbf{L}_{\mathbf{q}}^\dagger \mathbf{L}_{\mathbf{q}} \rho - \frac{1}{2} \rho \mathbf{L}_{\mathbf{q}}^\dagger \mathbf{L}_{\mathbf{q}} \right) \\
&+ \int d\mathbf{q} \gamma_{\mathbf{q}} \left(z_{\mathbf{q}}^* \mathbf{L}_{\mathbf{q}} \rho + z_{\mathbf{q}} \rho \mathbf{L}_{\mathbf{q}}^\dagger - \frac{1}{2} z_{\mathbf{q}} \mathbf{L}_{\mathbf{q}}^\dagger \rho - \frac{1}{2} z_{\mathbf{q}}^* \mathbf{L}_{\mathbf{q}} \rho - \frac{1}{2} z_{\mathbf{q}} \rho \mathbf{L}_{\mathbf{q}}^\dagger - \frac{1}{2} z_{\mathbf{q}}^* \rho \mathbf{L}_{\mathbf{q}} \right) \\
&= \mathcal{L}\rho.
\end{aligned} \tag{2.54}$$

Similar invariance transformations exist, if there is a finite number of jump operators, such that the master equation is of the form (2.47). In this case, the generator is invariant under linear combinations of Lindblad operators, with weights given by elements of a left unitary matrix,

$$\sqrt{\gamma_k} \mathbf{L}_k \rightarrow \sqrt{\gamma'_k} \mathbf{L}'_k = \sum_l U_{kl} \sqrt{\gamma_l} \mathbf{L}_l, \quad \text{with} \quad \sum_k U_{ik}^\dagger U_{kj} = \delta_{ij}. \tag{2.55}$$

Moreover, the generator (2.47) is invariant under the inhomogeneous transformations shown in Eqs. (2.51) and (2.52), although the integral in (2.52) must be replaced by a sum over the Lindblad operators.

Translation-covariant master equations The structure of the generator (2.48) can be further specified if the open system S is invariant under spatial translations. This is expected to hold for a free particle (that is a system that is not subject to any external potential) which is surrounded by a homogeneous medium forming the environment. In the main part of this thesis we consider models (collisional decoherence and the quantum linear Boltzmann equation) which are of this type.

To define translational-invariance, let us express $\dot{\rho}$ in position representation

$$\dot{\rho}(x, x'; \rho(y, y')) \equiv \langle x | \mathcal{L} \left(\int dy dy' \rho(y, y') |y\rangle \langle y'| \right) |x'\rangle. \tag{2.56}$$

In this representation, $\dot{\rho}$ depends on the position coordinates x, x' and on the density $\rho(y, y')$. To be invariant under spatial translations, it must satisfy

$$\dot{\rho}(x - z, x' - z; \rho(y - z, y' - z)) = \dot{\rho}(x, x'; \rho(y, y')), \tag{2.57}$$

for all spatial translations z . As one can check easily, this condition is equivalent with requiring that \mathcal{L} commutes with the translation operator, that is

$$\mathcal{L} \left(e^{-ix\mathbf{p}/\hbar} \rho e^{ix\mathbf{p}/\hbar} \right) = e^{-ix\mathbf{p}/\hbar} \mathcal{L}(\rho) e^{ix\mathbf{p}/\hbar}, \tag{2.58}$$

where \mathbf{p} denotes the momentum operator. \mathcal{L} is then said to be *translation-covariant*.

Under this condition, and provided the generator is bounded, it takes the form [41–45]

$$\begin{aligned}
\mathcal{L}\rho &= \frac{1}{i\hbar} [\mathbf{H}(\mathbf{p}), \rho] + \int d\mathbf{q} \sum_k \gamma_k(\mathbf{q}) \left(e^{i\mathbf{q}x/\hbar} \mathbf{L}_k(\mathbf{p}; \mathbf{q}) \rho \mathbf{L}_k^\dagger(\mathbf{p}; \mathbf{q}) e^{-i\mathbf{q}x/\hbar} \right. \\
&\quad \left. - \frac{1}{2} \mathbf{L}_k^\dagger(\mathbf{p}; \mathbf{q}) \mathbf{L}_k(\mathbf{p}; \mathbf{q}) \rho - \frac{1}{2} \rho \mathbf{L}_k^\dagger(\mathbf{p}; \mathbf{q}) \mathbf{L}_k(\mathbf{p}; \mathbf{q}) \right),
\end{aligned} \tag{2.59}$$

where \mathbf{q} has the dimension of momentum, $L_k(\mathbf{p}; \mathbf{q})$ are arbitrary functions of the momentum observable, and $H(\mathbf{p})$ is a Hamiltonian that depends on the momentum operator \mathbf{p} only.

The structure of the generator (2.59) can be interpreted as follows. The unitary operator $e^{i\mathbf{q}\mathbf{x}/\hbar}$ effects a transfer of momentum \mathbf{q} to the system, as follows from the relation

$$\langle \mathbf{p} | e^{i\mathbf{q}\mathbf{x}/\hbar} \rho e^{-i\mathbf{q}\mathbf{x}/\hbar} | \mathbf{p} \rangle = \langle \mathbf{p} - \mathbf{q} | \rho | \mathbf{p} - \mathbf{q} \rangle. \quad (2.60)$$

Crucially, the rate of this momentum transfer depends in general on the momentum of the system, which is due to the dependence of the functions $L_k(\mathbf{p}; \mathbf{q})$ on the system's momentum operator \mathbf{p} . In this way, effects like dissipation and relaxation are incorporated into the description.

Collisional decoherence If one is interested in effects, such as decoherence, which occur on a time scale that is much shorter than the relaxation time, then one can neglect the \mathbf{p} -dependence of the functions $L_k(\mathbf{p}; \mathbf{q})$, such that they become \mathbb{C} -numbers instead of operators. The generator (2.59) then takes the form

$$\mathcal{L}\rho = \frac{1}{i\hbar} [H(\mathbf{p}), \rho] + \gamma \int d\mathbf{q} G(\mathbf{q}) \left(e^{i\mathbf{q}\mathbf{x}/\hbar} \rho e^{-i\mathbf{q}\mathbf{x}/\hbar} - \rho \right), \quad (2.61)$$

with rate $\gamma G(\mathbf{q}) \equiv \sum_k \gamma_k(\mathbf{q}) |L_k(\mathbf{q})|^2$. Since $\gamma G(\mathbf{q}) \geq 0$, one can choose the dimensionless function $G(\mathbf{q})$ to be positive and normalized, i.e. $G(\mathbf{q}) \geq 0$ and $\int d\mathbf{q} G(\mathbf{q}) = 1$, such that it forms a probability density, providing the probability

$$\text{Prob}(\mathbf{q} \in V) = \int_V d\mathbf{q}' G(\mathbf{q}'), \quad (2.62)$$

that the momentum transfer \mathbf{q} lies within a certain region V .

The model (2.61) is introduced and analyzed in more detail in the next Chapter. We shall find that it describes the loss of spatial coherence due to collisions of the system with the background gas. It is therefore called *collisional decoherence*.

Chapter 3

Exemplary master equations and their microscopic derivations

We shall now discuss different methods which allow the derivation of the Lindblad operators based on microscopic considerations. Thereby, several exemplary master equations are introduced, which are used throughout the thesis as models for open quantum systems. The discussion is based on the treatments in [29,39].

3.1 The weak coupling formulation

The most widely used method for determining quantum master equations is the weak coupling approach. It permits the derivation of the generator (2.47) from the underlying total Hamiltonian (2.24). The starting point is the von Neumann equation expressed in the interaction picture

$$\frac{d}{dt}\tilde{\rho}_{\text{SE}}(t) = \frac{1}{i\hbar} \left[\tilde{\mathbf{H}}_I(t), \tilde{\rho}_{\text{SE}}(t) \right], \quad (3.1)$$

where the use of the interaction picture is denoted by the tilde

$$\tilde{\rho}_{\text{SE}}(t) = e^{i\mathbf{H}_0 t/\hbar} \rho_{\text{SE}} e^{-i\mathbf{H}_0 t/\hbar}, \quad (3.2)$$

$$\tilde{\mathbf{H}}_I(t) = e^{i\mathbf{H}_0 t/\hbar} \mathbf{H}_I e^{-i\mathbf{H}_0 t/\hbar}. \quad (3.3)$$

Here, $\mathbf{H}_0 = \mathbf{H}_S \otimes \mathbf{1}_E + \mathbf{1}_S \otimes \mathbf{H}_E$ denotes the sum of the free Hamiltonians. Next, the von Neumann equation is reformulated in its integral form

$$\tilde{\rho}_{\text{SE}}(t) = \tilde{\rho}_{\text{SE}}(0) + \frac{1}{i\hbar} \int_0^t ds \left[\tilde{\mathbf{H}}_I(s), \tilde{\rho}_{\text{SE}}(s) \right]. \quad (3.4)$$

Upon inserting the integral form back into the von Neumann equation (3.1) and taking the trace over the environment one obtains

$$\frac{d}{dt}\tilde{\rho}_S(t) = - \int_0^t ds \text{Tr}_E \left[\tilde{\mathbf{H}}_I(t), \left[\tilde{\mathbf{H}}_I(s), \tilde{\rho}_{\text{SE}}(s) \right] \right], \quad (3.5)$$

assuming that $\text{Tr}_E \left[\tilde{\mathbf{H}}_I(t), \tilde{\rho}_{\text{SE}}(0) \right] = 0$. This equation is still exact, although it is not particularly helpful as it stands, since it is neither closed nor local in time. In order to make it feasible, one introduces two kinds of approximations,

together known as the *Born-Markov approximation*. First, one assumes that the interaction Hamiltonian \mathbf{H}_I is sufficiently weak and the environment is reasonably large such that the changes of the state of the environment are small and the total state remains approximately in a product state,

$$\rho_{SE}(t) \simeq \rho_S(t) \otimes \rho_E. \quad (3.6)$$

This yields a closed integro-differential equation for the reduced state of S

$$\frac{d}{dt} \tilde{\rho}_S(t) = - \int_0^t ds \text{Tr}_E \left[\tilde{\mathbf{H}}_I(t), \left[\tilde{\mathbf{H}}_I(s), \tilde{\rho}_S(s) \otimes \tilde{\rho}_E \right] \right]. \quad (3.7)$$

Second, it is assumed that the system obeys the Markov property, so that one is allowed to recast the above equation into a time-local master equation, which gives

$$\frac{d}{dt} \tilde{\rho}(t) = - \int_0^\infty ds \text{Tr}_E \left[\tilde{\mathbf{H}}_I(t), \left[\tilde{\mathbf{H}}_I(t-s), \tilde{\rho}(t) \otimes \tilde{\rho}_E \right] \right], \quad (3.8)$$

with $\tilde{\rho}(t) \equiv \tilde{\rho}_S(t)$. Since we have performed two rather strong approximations, it is not guaranteed that the above master equation, which is known as the *Redfield equation*, is completely positive. To cast it into Lindblad form, one needs a further approximation known as the *rotating wave approximation*, which is applicable if the system Hamiltonian $\mathbf{H}_S = \sum_i \varepsilon_i |\varepsilon_i\rangle \langle \varepsilon_i|$ has a discrete non-degenerate spectrum $\{\varepsilon_i\}$. To this end, let us decompose the interaction Hamiltonian using an operator basis of the total Hilbert space which gives

$$\tilde{\mathbf{H}}_I(t) = \sum_k \tilde{\mathbf{A}}_k(t) \otimes \tilde{\mathbf{B}}_k(t). \quad (3.9)$$

Turning back to the Schrödinger picture, the system operators \mathbf{A}_k can be further decomposed using the eigenbasis of \mathbf{H}_S ,

$$\mathbf{A}_k = \sum_\omega \mathbf{A}_k(\omega), \quad (3.10)$$

where the operators $\mathbf{A}_k(\omega)$ are the contributions with equal energy spacings $\hbar\omega = \varepsilon' - \varepsilon$,

$$\mathbf{A}_k(\omega) = \sum_{\varepsilon' - \varepsilon = \hbar\omega} |\varepsilon\rangle \langle \varepsilon | \mathbf{A}_k | \varepsilon' \rangle \langle \varepsilon'|. \quad (3.11)$$

Due to this construction, the operators \mathbf{A}_k exhibit a simple time dependence when expressed in the interaction picture

$$\tilde{\mathbf{A}}_k(t) = \sum_\omega e^{i\omega t} \mathbf{A}_k(\omega). \quad (3.12)$$

Upon inserting (3.12) and (3.9) into (3.8), one obtains an equation whose summands are proportional to the phase factors $e^{i(\omega - \omega')t}$. By time-averaging this expression, one finds that the fast oscillating terms, i.e. summands that are proportional to $e^{i(\omega - \omega')t}$ with $\omega \neq \omega'$, can be neglected; this is the so-called rotating wave approximation. The resulting master equation has Lindblad form [29, 39]

$$\begin{aligned} \frac{d}{dt} \tilde{\rho}(t) = & \sum_{kl\omega} \gamma_{kl}(\omega) \left(\mathbf{A}_l(\omega) \tilde{\rho}(t) \mathbf{A}_k^\dagger(\omega) \right. \\ & \left. - \frac{1}{2} \mathbf{A}_k^\dagger(\omega) \mathbf{A}_l(\omega) \tilde{\rho}(t) - \frac{1}{2} \tilde{\rho}(t) \mathbf{A}_k^\dagger(\omega) \mathbf{A}_l(\omega) \right), \end{aligned} \quad (3.13)$$

where the positive matrix $\gamma_{kl}(\omega)$ is given by the Fourier transform of the bath correlation functions

$$\gamma_{kl}(\omega) = \frac{1}{\hbar^2} \int_{-\infty}^{\infty} dt e^{i\omega t} \langle \tilde{\mathbf{B}}_k(t) \tilde{\mathbf{B}}_l(0) \rangle_{\rho_E}. \quad (3.14)$$

3.2 The damped harmonic oscillator

As an application of the weak coupling approach let us now discuss the damped harmonic oscillator, which will be used in Chapter 4 to motivate the definition of pointer states. The model consists of a harmonic oscillator S , with frequency ω_0 , which is linearly coupled to a bath of harmonic oscillators E . This bath is characterized by a density of modes $g(\omega)$, and it is assumed to be in a thermal state,

$$\rho_E = \frac{1}{\mathcal{Z}} \exp\left(-\frac{\mathbf{H}_E}{k_B T}\right), \quad \text{with } \mathcal{Z} = \text{Tr} \left[\exp\left(-\frac{\mathbf{H}_E}{k_B T}\right) \right]. \quad (3.15)$$

The Hamiltonians of this model read as

$$\mathbf{H}_S = \hbar\omega_0 \mathbf{a}^\dagger \mathbf{a}, \quad (3.16)$$

$$\mathbf{H}_E = \int_0^\infty d\omega g(\omega) \hbar\omega \mathbf{b}^\dagger(\omega) \mathbf{b}(\omega), \quad (3.17)$$

$$\mathbf{H}_I = \int_0^\infty d\omega g(\omega) \hbar \left[\kappa^*(\omega) \mathbf{a} \mathbf{b}^\dagger(\omega) + \kappa(\omega) \mathbf{a}^\dagger \mathbf{b}(\omega) \right], \quad (3.18)$$

with ladder operators \mathbf{a} and $\mathbf{b}(\omega)$ and a frequency dependent coupling constant $\kappa(\omega)$. Applying the weak coupling approach Eqs. (3.13) and (3.14) to the system above, one finds the master equation of the damped harmonic oscillator [46]

$$\begin{aligned} \frac{d}{dt} \rho &= -i\omega_0 \left[\mathbf{a}^\dagger \mathbf{a}, \rho \right] + \gamma (\bar{n} + 1) \left(\mathbf{a} \rho \mathbf{a}^\dagger - \frac{1}{2} \mathbf{a}^\dagger \mathbf{a} \rho - \frac{1}{2} \rho \mathbf{a}^\dagger \mathbf{a} \right) \\ &\quad + \gamma \bar{n} \left(\mathbf{a}^\dagger \rho \mathbf{a} - \frac{1}{2} \mathbf{a} \mathbf{a}^\dagger \rho - \frac{1}{2} \rho \mathbf{a} \mathbf{a}^\dagger \right), \end{aligned} \quad (3.19)$$

with damping constant $\gamma \equiv 2\pi g(\omega_0) |\kappa(\omega_0)|^2$ and the mean occupation number

$$\bar{n} \equiv \bar{n}(\omega_0, T) = \text{Tr}_E \left[\rho_E \mathbf{b}^\dagger(\omega_0) \mathbf{b}(\omega_0) \right]. \quad (3.20)$$

Below the zero temperature limit of (3.19), $T \rightarrow 0$, is considered. Since the mean occupation number vanishes at zero temperature, that is $\bar{n}(\omega_0, T \rightarrow 0) = 0$, the corresponding master equation reads as

$$\frac{d}{dt} \rho = -i\omega_0 \left[\mathbf{a}^\dagger \mathbf{a}, \rho \right] + \gamma \left(\mathbf{a} \rho \mathbf{a}^\dagger - \frac{1}{2} \mathbf{a}^\dagger \mathbf{a} \rho - \frac{1}{2} \rho \mathbf{a}^\dagger \mathbf{a} \right). \quad (3.21)$$

In conclusion, the damped harmonic oscillator coupled to a zero temperature bath is described by a master equation in Lindblad form defined by the standard Hamiltonian $\mathbf{H} = \hbar\omega_0 \mathbf{a}^\dagger \mathbf{a}$, and a single Lindblad operator $\mathbf{L} = \mathbf{a}$, with associated rate γ .

3.3 The Caldeira-Leggett equation

Another paradigm of open quantum systems is the so-called *Caldeira-Leggett model* [47] describing the frictional quantum dynamics of a Brownian particle. The model considers a Brownian particle S of mass m with coordinate x , which moves in a potential $V(x)$. Like in the case of the damped harmonic oscillator, the environment E consists of a bath of harmonic oscillators with frequencies ω and masses $m(\omega)$. The bath is characterized by a density of modes $g(\omega)$, and it is assumed to be in a thermal state, see Eq. (3.15). The form of the interaction between system and environment is such that the position operator x of the Brownian particle couples linearly to the positions $x(\omega)$,

$$x(\omega) = \left(\frac{\hbar}{2m(\omega)\omega} \right)^{1/2} \left[\mathbf{b}(\omega) + \mathbf{b}^\dagger(\omega) \right], \quad (3.22)$$

of the oscillators in the environment. Accordingly, the Hamiltonians of the model are given by

$$H_S = \frac{\mathbf{p}^2}{2m} + V(x), \quad (3.23)$$

$$H_E = \int_0^\infty d\omega g(\omega) \hbar \omega \mathbf{b}^\dagger(\omega) \mathbf{b}(\omega), \quad (3.24)$$

$$H_I = -x \int_0^\infty d\omega g(\omega) \kappa(\omega) x(\omega), \quad (3.25)$$

with frequency dependent coupling constant $\kappa(\omega)$.

Remarkably, the reduced dynamics of the Brownian particle S generated by the above Hamiltonians can be solved in closed form [47] for all choices of $g(\omega)$ and $\kappa(\omega)$. In this thesis, though, a specific case is considered, namely the *weak-coupling* and *high-temperature limit*. In this regime, the evolution equation has almost Lindblad form [47]

$$\frac{d}{dt}\rho = \frac{1}{i\hbar} [H_S, \rho] + \frac{\gamma}{i\hbar} [x, \mathbf{p}\rho + \rho\mathbf{p}] - \frac{4\pi\gamma}{\Lambda_{\text{th}}^2} [x, [x, \rho]], \quad (3.26)$$

with Λ_{th} the *thermal de Broglie wavelength*,

$$\Lambda_{\text{th}}^2 \equiv \frac{2\pi\hbar^2}{mk_B T}. \quad (3.27)$$

The above equation is referred to as *Caldeira-Leggett master equation*.

It should be mentioned that we consider here a Brownian particle in one spatial dimension. The extension to three dimensions is obtained easily, by summing over the different coordinates on the right-hand side of Eq. (3.26).

3.3.1 Sketch of the derivation

Originally, the Caldeira-Leggett model was solved using the path integral approach, or more specifically the Feynman-Vernon influence functional technique [48]. Here a less sophisticated approach [29] is discussed, which applies specifically to the weak-coupling and high-temperature limit. In this case, the Born-Markov approximation may be applied, so that one can take the Redfield equation (3.8) as

starting point. However one cannot proceed further along the lines of Section 3.1, since the rotating wave approximation (RWA) is not applicable to the Caldeira-Leggett model. In fact, the RWA requires that the system Hamiltonian H_S has a discrete spectrum, so that the system dynamics is given by $t_S = |\omega - \omega'|^{-1}$, with $|\omega - \omega'|$ a typical energy spacing; the RWA can be applied if t_S is small compared to the relaxation time. However, the Hamiltonian of the Caldeira-Leggett model has a continuous energy spectrum, and one therefore needs an alternative approximation scheme.

To this end, one makes specific assumptions on the *spectral density*

$$J(\omega) \equiv g(\omega) \frac{|\kappa(\omega)|^2}{2m(\omega)\omega}. \quad (3.28)$$

In order to obtain *Ohmic damping*, which means frequency independent damping with the rate γ , one requires the spectral density to be proportional to the frequency for small ω ,

$$J(\omega) = \frac{2m\gamma}{\pi}\omega, \quad \text{for } \omega \rightarrow 0. \quad (3.29)$$

Furthermore, to assure that the integral appearing in (3.8) is convergent, one introduces a high-frequency cutoff Ω , such that $J(\omega) = 0$ for $\omega > \Omega$. A candidate for a spectral density which satisfies the above properties is the so-called *Ohmic spectral density with a Lorentz-Drude cutoff function*

$$J(\omega) = \frac{2m\gamma}{\pi}\omega \frac{\Omega^2}{\Omega^2 + \omega^2}. \quad (3.30)$$

As a further condition one requires that the system evolution is slow compared to the bath correlation time. If ω_0 denotes a typical frequency of the system evolution, then the time scale of the system dynamics can be estimated as $t_S = \omega_0^{-1}$. On the other hand, the bath correlation time $t_B = \nu_1^{-1}$ can be assessed by means of the *first Matsubara frequency* $\nu_1 \equiv 2\pi k_B T / \hbar$. The condition of slow system dynamics therefore reads as

$$\hbar\omega_0 \ll 2\pi k_B T. \quad (3.31)$$

As a further condition, it is assumed that the temperature is high, in the sense that

$$k_B T \geq \hbar\Omega. \quad (3.32)$$

Using these conditions together with the spectral density shown in (3.30), one can convert the Redfield equation (3.8) into the Caldeira-Leggett master equation (3.26). It should be mentioned that the latter can also be obtained with spectral densities other than the one in Eq. (3.30), as long as they are linear for small ω and zero for $\omega > \Omega$.

3.3.2 Extension to Lindblad form

Since the Caldeira-Leggett equation (3.26) cannot be cast in Lindblad form, it is not a completely positive master equation. As a matter of fact, it may violate the positivity of certain initial states, such as wave packets with a width less than

the thermal de Broglie wavelength Λ_{th} [49]. One might therefore ask whether the Caldeira-Leggett equation (3.26) can be brought into Lindblad form, without substantially modifying the dynamics. It turns out that this can be done by adding a further double commutator to the right-hand side of (3.26)

$$\begin{aligned} \frac{d}{dt}\rho &= \frac{1}{i\hbar} [\mathbf{H}_S, \rho] + \frac{\gamma}{i\hbar} [\mathbf{x}, \mathbf{p}\rho + \rho\mathbf{p}] - \frac{4\pi\gamma}{\Lambda_{\text{th}}^2} [\mathbf{x}, [\mathbf{x}, \rho]] \\ &\quad - \lambda \frac{\gamma\Lambda_{\text{th}}^2}{16\pi\hbar^2} [\mathbf{p}, [\mathbf{p}, \rho]]. \end{aligned} \quad (3.33)$$

This equation can be brought into Lindblad form (2.47), provided that the dimensionless parameter λ satisfies the condition $\lambda \geq 1$ [29, 49]. A *minimally invasive* modification is therefore obtained with the parameter $\lambda = 1$. The corresponding Lindblad operator reads as

$$\mathbf{L} = \frac{\sqrt{8\pi}}{\Lambda_{\text{th}}}\mathbf{x} + i\frac{\Lambda_{\text{th}}}{\sqrt{8\pi}\hbar}\mathbf{p}, \quad (3.34)$$

and the associated rate is given by γ . This can be verified by a lengthy, but straightforward calculation, which makes use of the canonical commutation relation, $[\mathbf{x}, \mathbf{p}] = i\hbar$.

It should be mentioned that the importance of the Lindblad form goes beyond the conservation of positivity: it admits to solve the master equation in terms of quantum trajectories. A detailed introduction to this topic is given in Chapter 7.

3.3.3 Relaxation

The Caldeira-Leggett equation is a model for quantum Brownian motion and, as such, it should capture relaxation processes. To see this, let us evaluate the time evolution of the mean kinetic energy,

$$\langle \mathbb{T}(t) \rangle = \text{Tr}(\rho_t \mathbb{T}), \quad \text{with } \mathbb{T} \equiv \frac{\mathbf{p}^2}{2m}, \quad (3.35)$$

for a free particle with $\mathbf{H}_S = \mathbf{p}^2/2m$. We therefore take the time derivative of the above expression and use the Caldeira-Leggett equation (3.26), which yields

$$\begin{aligned} \frac{d}{dt}\langle \mathbb{T}(t) \rangle &= \text{Tr}(\dot{\rho}_t \mathbb{T}) \\ &= \frac{\gamma}{i2m\hbar} \text{Tr}([\mathbf{x}, \mathbf{p}\rho + \rho\mathbf{p}] \mathbf{p}^2) - \text{Tr}\left(\frac{4\pi\gamma}{2m\Lambda_{\text{th}}^2} [\mathbf{x}, [\mathbf{x}, \rho]] \mathbf{p}^2\right). \end{aligned} \quad (3.36)$$

Upon using the canonical commutation relation, one obtains [29]

$$\frac{d}{dt}\langle \mathbb{T}(t) \rangle = -4\gamma\langle \mathbb{T}(t) \rangle + 2\gamma k_B T, \quad (3.37)$$

which is solved by the expression

$$\langle \mathbb{T}(t) \rangle = \frac{k_B T}{2} + \left(\langle \mathbb{T}(0) \rangle - \frac{k_B T}{2} \right) e^{-4\gamma t}. \quad (3.38)$$

In conclusion, the mean kinetic energy of the Brownian particle approaches the thermal energy $E_{\text{th}} = k_B T/2$ on a relaxation time scale set by the rate γ ¹.

¹In the three-dimensional case one obtains a similar result with $E_{\text{th}} = 3k_B T/2$.

Note that this also holds if one takes the Lindblad form of the Caldeira-Leggett equation (3.33) instead of (3.26).

In addition, one can show [50] that both versions of the Caldeira-Leggett equation, (3.26) and (3.33), exhibit the correct thermal state as stationary solutions. This holds for free particles as well as for quadratic potentials. The Caldeira-Leggett model thus accurately describes the long-time behavior of a Brownian particle.

3.3.4 Decoherence

Our next aim is to discuss the short-time dynamics induced by the Caldeira-Leggett equation (3.26). This regime is characterized by an interplay of coherent phenomena on the one hand, and decoherence, i.e. the loss of coherence, on the other hand, while concepts with a classical analog such as relaxation or thermalization do not yet play a role. To analyze the short-time dynamics, let us consider a simplified version of the Caldeira-Leggett equation

$$\frac{d}{dt}\rho = \frac{1}{i\hbar} [\mathbf{H}_S, \rho] - \frac{4\pi\gamma}{\Lambda_{\text{th}}^2} [\mathbf{x}, [\mathbf{x}, \rho]] , \quad (3.39)$$

which we shall refer to as the *linear coupling model* from now on. This simplification may be justified for sufficiently small Λ_{th} (that is, in the high-temperature limit) where the dominant terms in the Caldeira-Leggett equation are the unitary part and the double commutator. It should be mentioned that the above model, and in particular its role in decoherence, has been studied extensively in the literature [2, 3, 51].

Crucially, this model leads to localization in position space, that is to a loss of spatial coherence, as can be seen by switching to the interaction picture,

$$\tilde{\rho} = e^{i\mathbf{H}_S t/\hbar} \rho e^{-i\mathbf{H}_S t/\hbar} , \quad (3.40)$$

and the position representation, $\rho(x, x') \equiv \langle x | \rho | x' \rangle$, discussed in Section 2.1.4. The resulting evolution equation reads as

$$\partial_t \tilde{\rho}_t(x, x') = -\frac{4\pi\gamma}{\Lambda_{\text{th}}^2} (x - x')^2 \tilde{\rho}_t(x, x') , \quad (3.41)$$

where we included the time argument for clarity. This implies that the populations are unaffected by the incoherent part of (3.39), while the coherences decay exponentially

$$\tilde{\rho}_t(x, x') = e^{-F(x-x')t} \tilde{\rho}_0(x, x') , \quad (3.42)$$

with

$$F(x - x') = \frac{4\pi\gamma}{\Lambda_{\text{th}}^2} (x - x')^2 . \quad (3.43)$$

The decay rate of the spatial coherences is thus characterized by a *localization rate* $F(s) \geq 0$ which grows with the square of the distance $|x - x'|$. A comparison with the relaxation rate γ ,

$$\frac{F(x - x')}{\gamma} = 4\pi \frac{(x - x')^2}{\Lambda_{\text{th}}^2} , \quad (3.44)$$

reveals that the decoherence rate is much greater than the relaxation rate γ , provided the distance is large on the quantum scale set by the thermal de Broglie wavelength Λ_{th} . This holds in particular if the separation is macroscopic.

Let us point out that the localization rate $F(s)$ grows above all bounds if $s \rightarrow \infty$. However, this is in contrast to observations made in experiments with interfering fullerene molecules [16]. Here it was found that the localization rate saturates for large distances s at the average collision rate γ_{coll} , that is $F(s \rightarrow \infty) = \gamma_{\text{coll}}$. This is a physically intuitive result: if the separation is macroscopic, one collision should be sufficient to reveal the particles ‘which path’ information, so that one expects the decoherence rate to be given by γ_{coll} . We conclude that linear coupling models may lead to incorrect results when studying decoherence phenomena.

However, it turns out that this problem can be resolved if one goes beyond linear coupling models by treating the environmental coupling in a non-perturbative fashion. An approach which admits the incorporation of nonlinear couplings is presented in the following section.

3.4 The monitoring approach

Let us now discuss an alternative method for the derivation of master equations based on microscopic considerations. This so-called *monitoring approach* is quite different in nature than the weak coupling formulation used in the treatment of the damped harmonic oscillator or the Caldeira-Leggett model. It is *not* based on the total Hamiltonian \mathbf{H}_{SE} of the combined system, which permits to treat the environmental coupling in a non-perturbative fashion, i.e. it is not necessary to assume that the interaction Hamiltonian \mathbf{H}_I is weak. Moreover, one can incorporate the Markov assumption right from the outset, in contrast to the weak coupling approach where it was introduced artificially in Eq. (3.8). The method is the basis for the derivation of the quantum linear Boltzmann equation and the collisional decoherence model, both of which will be used throughout the thesis.

The approach is applicable whenever the interaction with the environment can reasonably be described in terms of individual two-particle interaction events or collisions. A prototype for such a scenario is the interaction of a Brownian particle with an ideal gas environment. The Markov assumption can here naturally be introduced by disregarding the change of the environment state after each collision.

A combination of scattering theory and the concept of generalized and continuous measurements then admits the derivation of a general expression of the master equation [13, 39]

$$\begin{aligned} \frac{d}{dt}\rho &= \frac{1}{i\hbar} [\mathbf{H}_S, \rho] + \frac{i}{2} \text{Tr}_E \left(\left[\mathbf{T} + \mathbf{T}^\dagger, \Gamma^{1/2} [\rho \otimes \rho_E] \Gamma^{1/2} \right] \right) \\ &\quad + \text{Tr}_E \left(\mathbf{T} \Gamma^{1/2} [\rho \otimes \rho_E] \Gamma^{1/2} \mathbf{T}^\dagger \right) \\ &\quad - \frac{1}{2} \text{Tr}_E \left(\Gamma^{1/2} \mathbf{T}^\dagger \mathbf{T} \Gamma^{1/2} [\rho \otimes \rho_E] \right) \\ &\quad - \frac{1}{2} \text{Tr}_E \left([\rho \otimes \rho_E] \Gamma^{1/2} \mathbf{T}^\dagger \mathbf{T} \Gamma^{1/2} \right), \end{aligned} \quad (3.45)$$

with ρ_E the reduced single-particle state of the environment. The operator \mathbf{T} is the nontrivial part of the two-particle S -matrix $\mathbf{S} = \mathbf{I} + i\mathbf{T}$ describing the effect of

a collision between system and environmental particle [52]. The rate of collisions is described by the positive operator Γ , which gives the probability that a collision occurs in a small time interval Δt ,

$$\text{Prob}(\text{coll}; \Delta t) = \Delta t \text{Tr}(\Gamma [\rho \otimes \rho_E]) . \quad (3.46)$$

3.5 Collisional decoherence

The application of the monitoring approach to the motion of a quantum test particle in an ideal gas environment yields the so-called *quantum linear Boltzmann equation* (QLBE) [10–12]. A detailed introduction of this equation is given in Chapter 9. For now, let us consider the limiting case where the Brownian particle is much heavier than the particles of the background gas, such that there is no appreciable energy exchange during a collision. In this limit, the QLBE simplifies a lot, giving a model called *collisional decoherence*. This model has been first discussed by Gallis and Fleming [14] and was derived in its final form by Hornberger and Sipe [15]. The corresponding master equation has Lindblad form (2.48), where the jump operators are momentum kick operators, $L_{\mathbf{q}} = e^{i\mathbf{q}\mathbf{x}/\hbar}$ (with position operator \mathbf{x}), and the rate is given by $\gamma_{\mathbf{q}} = \gamma G(\mathbf{q})$. The continuous label \mathbf{q} has the meaning of a momentum transfer experienced by the test particle with $G(\mathbf{q}) \geq 0$ the corresponding distribution, $\int d\mathbf{q} G(\mathbf{q}) = 1$; γ is the collision rate of the gas environment. The master equation thus reads

$$\frac{d}{dt}\rho = \frac{1}{i\hbar} [H_S, \rho] + \gamma \int d\mathbf{q} G(\mathbf{q}) \left(e^{i\mathbf{q}\mathbf{x}/\hbar} \rho e^{-i\mathbf{q}\mathbf{x}/\hbar} - \rho \right) . \quad (3.47)$$

This equation is already familiar from Sect. 2.2.2, Eq. (2.61), where the short-time limit of translation-covariant master equations was discussed.

Note that the authors in [14, 15] have presented explicit expressions for the distribution $G(\mathbf{q})$ and the rate γ , relating them to the relevant microscopic quantities; these formulas are shown below in Eqs. (3.52) to (3.53).

Spatial Localization As in the linear coupling model, collisional decoherence leads to localization in position space, that is to a loss of spatial coherence, as can be seen by switching to the interaction picture, $\tilde{\rho} = e^{iH_S t/\hbar} \rho e^{-iH_S t/\hbar}$, and the position representation,

$$\begin{aligned} \frac{d}{dt} \langle \mathbf{x} | \tilde{\rho} | \mathbf{x}' \rangle &= \gamma \int d\mathbf{q} G(\mathbf{q}) \left(\langle \mathbf{x} | e^{i\mathbf{q}\mathbf{x}/\hbar} \tilde{\rho} e^{-i\mathbf{q}\mathbf{x}/\hbar} | \mathbf{x}' \rangle - \langle \mathbf{x} | \tilde{\rho} | \mathbf{x}' \rangle \right) \\ &= \gamma \int d\mathbf{q} G(\mathbf{q}) \left(e^{i\mathbf{q}(\mathbf{x}-\mathbf{x}')/\hbar} - 1 \right) \langle \mathbf{x} | \tilde{\rho} | \mathbf{x}' \rangle . \end{aligned} \quad (3.48)$$

One thus finds an exponential decay of the spatial coherences,

$$\tilde{\rho}_t(\mathbf{x}, \mathbf{x}') = e^{-F(\mathbf{x}-\mathbf{x}')t} \tilde{\rho}_0(\mathbf{x}, \mathbf{x}') , \quad (3.49)$$

with a decay rate given by the localization rate $F(\mathbf{s}) \geq 0$. The latter is related to the momentum transfer distribution $G(\mathbf{q})$ by

$$F(\mathbf{s}) = \gamma \left[1 - \int d\mathbf{q} G(\mathbf{q}) \exp\left(\frac{i}{\hbar} \mathbf{q}\mathbf{s}\right) \right] . \quad (3.50)$$

By performing a Fourier inversion of (3.50), one obtains an expression, which admits to calculate the momentum transfer distribution from the localization function,

$$G(\mathbf{q}) = \frac{1}{(2\pi\hbar)^3} \int d\mathbf{s} \exp\left(\frac{i}{\hbar}\mathbf{q}\mathbf{s}\right) \left[1 - \frac{F(\mathbf{s})}{\gamma}\right]. \quad (3.51)$$

Since the Fourier transform of the distribution $G(\mathbf{q})$ tends to zero for large distances $s \equiv |\mathbf{s}|$, the localization rate saturates for large s at the maximum value given by the average collision rate γ , $F(s \rightarrow \infty) = \gamma$, which can be interpreted as the limit where one collision is sufficient to reveal the particles ‘which path’ information. Collisional decoherence therefore yields the expected behavior in the limit of large distances. According to Sect. 3.3.4, this behavior is in sharp contrast to linear models, where the localization rate grows quadratically, and thus approaches infinity in the limit of a large separation s .

3.5.1 Relation to microscopic quantities

Since collisional decoherence can be derived from a scattering description of the interaction between the quantum test particle S and the background gas, it is possible to express the localization rate in terms of the relevant microscopic quantities. These are the velocity distribution $\mu(v)$ of the background gas, its density n_{gas} , and the elastic scattering amplitude $f(\mathbf{p}_f, \mathbf{p}_i)$. The latter describes the effect of a collision between S and a bath particle E , with \mathbf{p}_i and \mathbf{p}_f the initial and final momentum of E , respectively. Assuming isotropic scattering, such that $f(\mathbf{p}_f, \mathbf{p}_i) = f(\cos(\mathbf{p}_f, \mathbf{p}_i); E_{\text{kin}} = p_i^2/2m)$, the localization functions reads as [15, 39]

$$F(\mathbf{s}) = \gamma - 2\pi n_{\text{gas}} \int_0^\infty dv \mu(v) v \int_{-1}^1 d\cos\theta |f(\cos\theta; E_{\text{kin}})|^2 \times \text{sinc}\left[2\sin\left(\frac{\theta}{2}\right) \frac{mv|\mathbf{s}|}{\hbar}\right], \quad (3.52)$$

with m the mass of a bath particle and θ the scattering angle. This admits in particular to calculate the momentum transfer distribution by means of Eq. (3.51). The average collision rate γ can also be determined from microscopic quantities by the thermal average

$$\gamma = \int_0^\infty dv \mu(v) n_{\text{gas}} v \sigma_{\text{tot}}(mv), \quad (3.53)$$

where σ_{tot} is the total cross section, $\sigma_{\text{tot}}(p) = 2\pi \int_{-1}^1 d\cos\theta |f(\cos\theta; p^2/2m)|^2$. Typically one assumes that the background gas is in thermal equilibrium, so that the velocity distribution is given by the Boltzmann distribution

$$\mu(v) = 4\pi \left(\frac{m}{2\pi k_B T}\right)^{3/2} v^2 \exp\left(-\frac{mv^2}{2k_B T}\right). \quad (3.54)$$

The localization rate shown in Eq. (3.52) has the behavior which was already predicted in the paragraph on spatial localization (see above). In the limit $s \rightarrow 0$, the sinc function approaches unity and the angular integral in (3.52) yields the

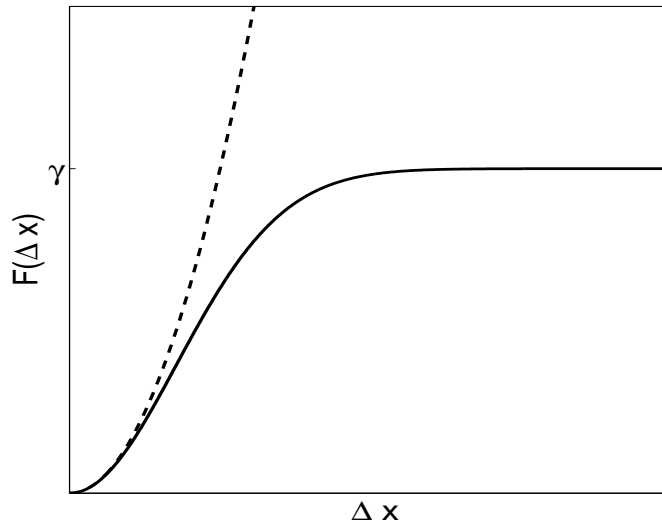


Figure 3.1: Sketch of the localization rate (3.52) as a function of the spatial separation Δx . The solid line, which gives the prediction of collisional decoherence, saturates at the average collision rate γ . The dashed line shows for comparison the quadratic behavior (3.43) which is predicted by the Caldeira-Leggett model. This demonstrates that collisional decoherence gives a more accurate description of decoherence than linear coupling models.

total cross section σ_{tot} , which implies that the localization rate vanishes. For small distances s , one may expand the sinc function to second order in s , so that $F(\mathbf{s})$ has the quadratic dependence predicted by the linear coupling model, see Eq. (3.44). In the limit of large distances, $s \rightarrow \infty$, the sinc function vanishes and the localization rate tends to the average collision rate γ , see Figure 3.1. As mentioned above, this result agrees with observations made in molecular interference experiments in the presence of various background gases [16].

3.5.2 Dynamic reduction models

Collisional decoherence is intimately connected with the so-called *Ghirardi-Rimini-Weber (GRW) spontaneous localization model* [23,24]. To see this, we give a short review of the basic ideas of quantum mechanics with spontaneous localization. This will show that the interpretation of the GRW model is completely different from the one underlying conventional quantum mechanics (and collisional decoherence). However, it will become apparent that both models, collisional decoherence and GRW, lead to the same observational consequences, since they are both described by the same master equation [25].

Quantum mechanics with spontaneous localization is a unified framework that captures both, the quantum properties of microscopic systems and the classical properties of macroscopic objects. To this end, it suggests a modification of the Schrödinger equation by means of nonlinear and stochastic terms which lead to a localization of the wave function. The rate, which is associated to these stochastic terms, grows linearly with the particle number, such that macroscopic bodies get localized while microscopic objects may be delocalized in position space.

Crucially, these extra terms are assumed to be part of the fundamental laws of quantum mechanics, they are not meant to be induced by an environmental coupling as it is the case in decoherence theory. It should also be stressed that the localizations affect directly the wave function, not only the statistical operator. In contrast to standard quantum mechanics, GRW assign an objective, i.e. observer independent, meaning to the wave function.

The stochastic process Let us now discuss in more detail the stochastic process experienced by the wave function $|\psi\rangle$ of a single particle. Here the wave function evolution has a deterministic part given by the usual Schrödinger equation, which is interrupted by random jumps. The latter are effected by Hermitian operators $\mathbf{L}_{\mathbf{y}}$,

$$|\psi\rangle \rightarrow |\psi'\rangle = \frac{\mathbf{L}_{\mathbf{y}}|\psi\rangle}{\|\mathbf{L}_{\mathbf{y}}|\psi\rangle\|}, \quad (3.55)$$

which cause a Gaussian-shaped localization at point \mathbf{y} ,

$$\mathbf{L}_{\mathbf{y}} = \frac{1}{(2\pi\sigma^2)^{3/4}} \exp\left(-\frac{(\mathbf{x} - \mathbf{y})^2}{4\sigma^2}\right), \quad \text{with } \int d\mathbf{y} \mathbf{L}_{\mathbf{y}}^2 = 1. \quad (3.56)$$

Here \mathbf{x} denotes the position operator. The jumps occur with the rate

$$r_{\mathbf{y}} = \|\mathbf{L}_{\mathbf{y}}|\psi\rangle\|^2, \quad (3.57)$$

ensuring that reductions are more likely to occur where the probability to find a particle is greater, according to conventional quantum mechanics.

The corresponding master equation This stochastic process implies that the evolution of the density matrix is described by a master equation in Lindblad form [23, 24]

$$\frac{d}{dt}\rho = \frac{1}{i\hbar} [\mathbf{H}_S, \rho] + \gamma \left(\int d\mathbf{y} \mathbf{L}_{\mathbf{y}} \rho \mathbf{L}_{\mathbf{y}} - \rho \right), \quad (3.58)$$

with rate γ and Lindblad operators $\mathbf{L}_{\mathbf{y}}$. The latter are however not uniquely fixed by the master equation (3.58), see Sect. 2.2.2. A master equation in Lindblad form is invariant under certain transformations of the Lindblad operators, such as a Fourier transform,

$$\sqrt{\gamma_{\mathbf{y}}} \mathbf{L}_{\mathbf{y}} \rightarrow \sqrt{\gamma'_{\mathbf{q}}} \mathbf{L}'_{\mathbf{q}} = \frac{1}{(2\pi\hbar)^{3/2}} \int d\mathbf{y} e^{i\mathbf{q}\mathbf{y}/\hbar} \sqrt{\gamma_{\mathbf{y}}} \mathbf{L}_{\mathbf{y}}. \quad (3.59)$$

Note that this equation agrees with Eq. (2.49) apart from the \hbar , which accounts for the fact that the variables \mathbf{y} and \mathbf{q} have the dimension of position and momentum, respectively. Upon applying this transformation to the Lindblad operators (3.56), one finds an alternative set of operators and rates,

$$\mathbf{L}'_{\mathbf{q}} = \exp\left(\frac{i}{\hbar} \mathbf{q}\mathbf{x}\right), \quad (3.60)$$

$$\gamma'_{\mathbf{q}} = \gamma \left(\frac{2\sigma^2}{\alpha\pi\hbar^2} \right)^{3/2} \exp\left(-\frac{2\mathbf{q}^2\sigma^2}{\hbar^2}\right). \quad (3.61)$$

Remarkably, these are the Lindblad operators of collisional decoherence, where the associated momentum transfer distribution $G(\mathbf{q}) \equiv \gamma'_{\mathbf{q}}/\gamma$ is a Gaussian with standard deviation $\sigma_G = \hbar/2\sigma$. In summary, both models, collisional decoherence and GRW, are described by the same master equation, provided the momentum transfer distribution $G(\mathbf{q})$ assumed in collisional decoherence is a Gaussian distribution [25].

Chapter 4

The pointer basis

The discussion so far was mainly focused on the characterization of dynamical equations governing the temporal evolution of Markovian open quantum systems. From now on, the characteristic features of the corresponding solutions are discussed. It turns out that there are typically two types of processes taking place on completely different time scales. On a short time scale one observes the loss of quantum coherence, called *decoherence*, which leads to the appearance of classical properties. Once the system behaves effectively classical, it may exhibit the whole range of features known from open classical systems, such as diffusion, dissipation and the relaxation to thermal equilibrium. However, these effects occur on a time scale which is typically much greater than the one it takes to lose quantum coherence. In the following chapters, solely the decoherence process is considered, the combined treatment of both decoherence and relaxation will be analyzed from Chapter 9 onwards.

What is typically observed in the decoherence process, exhibited by the short-time solutions of master equations, is the superselection of certain *robust states* in the corresponding Hilbert space. These so-called *pointer states*, which usually form a basis, are distinguished by the feature that they remain pure for a relatively long time, whereas their superpositions get mixed on a short time scale. This effective superselection therefore explains the absence of coherent phenomena in systems, such as macroscopic objects, which are sufficiently strongly coupled to their surroundings. Apart from that, one finds that, at least in realistic models, these robust states are localized wave packets moving according to the classical equations of motion, thus explaining the transition from quantum- to classical dynamics.

The name *pointer state* was coined in [1] due to its relevance for the physical description of a measurement apparatus. A measurement device which probes an observable $\mathbf{A} = \sum_{\alpha} \alpha \mathbf{P}_{\alpha}$ is constructed such that macroscopically distinct positions of the pointer or indicator are obtained for the different eigenstates \mathbf{P}_{α} of \mathbf{A} . For a quantum system initially prepared in an eigenstate of \mathbf{A} the read-out will display the corresponding eigenvalue with certainty provided these pointer states remain pure during the time evolution. On the other hand, if the quantum system is prepared in a superposition of eigenstates of \mathbf{A} , described by the state ρ_0 , one expects the pointer not to end up in a superposition of different read-out states, but rather to be at a definite position, though probabilistically, with probabilities p_{α} given by the Born rule, $p_{\alpha} = \text{Tr}(\rho_0 \mathbf{P}_{\alpha})$.

In Sect. 4.1, the prototype of an open quantum system, the damped harmonic

oscillator, is studied. This facilitates the induction of a general definition of pointer states, which will be provided in Sect. 4.2. Two different methods that admit the prediction of the pointer states, given a particular model of the open system, are summarized in Sects. 4.3 and 4.4.

4.1 The damed harmonic oscillator

In Section 3.2, a model for the damped harmonic oscillator coupled linearly to a zero temperature harmonic oscillator bath was introduced. According to Eq. (3.21), its evolution can be described by a master equation in Lindblad form defined by the standard Hamiltonian $\mathbf{H} = \hbar\omega\mathbf{a}^\dagger\mathbf{a}$, and a single Lindblad operator $\mathbf{L} = \mathbf{a}$, with associated rate γ . For convenience, let us write this master equation as

$$\frac{d}{dt}\rho_t = \gamma\mathbf{a}\rho_t\mathbf{a}^\dagger - \gamma_+\mathbf{a}^\dagger\mathbf{a}\rho_t - \gamma_-\rho_t\mathbf{a}^\dagger\mathbf{a} \equiv \mathcal{L}\rho_t, \quad (4.1)$$

with $\gamma_+ \equiv \gamma/2 + i\omega$ and $\gamma_- \equiv \gamma/2 - i\omega$. To start with, let us consider as initial state a coherent state [53]

$$\begin{aligned} \rho_0 &= |\alpha_0\rangle\langle\alpha_0| \\ &= e^{-|\alpha_0|^2} \exp(\alpha_0\mathbf{a}^\dagger) |0\rangle\langle 0| \exp(\alpha_0^*\mathbf{a}), \end{aligned} \quad (4.2)$$

which satisfies $\mathbf{a}|\alpha_0\rangle = \alpha_0|\alpha_0\rangle$, with $\alpha_0 \in \mathbb{C}$. The solution of (4.1) is then given by

$$\rho_t = |\alpha_t\rangle\langle\alpha_t|, \quad \text{with } \alpha_t = \alpha_0 \exp(-\gamma_+t), \quad (4.3)$$

which can easily be verified:

$$\begin{aligned} \frac{d}{dt}|\alpha_t\rangle\langle\alpha_t| &= \gamma|\alpha_t|^2|\alpha_t\rangle\langle\alpha_t| - \gamma_+\alpha_t\mathbf{a}^\dagger|\alpha_t\rangle\langle\alpha_t| - \gamma_-\alpha_t^*|\alpha_t\rangle\langle\alpha_t|\mathbf{a} \\ &= \mathcal{L}(|\alpha_t\rangle\langle\alpha_t|). \end{aligned} \quad (4.4)$$

This shows that the coherent states are robust in the sense that they are pure state solutions of the damped harmonic oscillator. According to Eq. (4.3), they spiral in phase space towards the origin, approaching the ground state for large times. Energy is therefore dissipated,

$$\langle\alpha_t|\mathbf{H}|\alpha_t\rangle = e^{-\gamma t}\langle\alpha_0|\mathbf{H}|\alpha_0\rangle, \quad (4.5)$$

on a relaxation time scale $t_{\text{rel}} = \gamma^{-1}$ determined by the rate γ .

Superposition of coherent states As a next step, let us consider as initial state a superposition of two quasi-orthogonal coherent states

$$|\psi_0\rangle = c_1|\alpha_0\rangle + c_2|\beta_0\rangle, \quad \text{with } |\alpha_0 - \beta_0|^2 \gg 1, \quad (4.6)$$

so that the corresponding density operator reads as

$$\rho_0 = |c_1|^2|\alpha_0\rangle\langle\alpha_0| + |c_2|^2|\beta_0\rangle\langle\beta_0| + c_1c_2^*|\alpha_0\rangle\langle\beta_0| + c_1^*c_2|\beta_0\rangle\langle\alpha_0|. \quad (4.7)$$

It is then easy to show that the master equation is solved by the expression [29,39]

$$\rho_t = |c_1|^2 |\alpha_t\rangle\langle\alpha_t| + |c_2|^2 |\beta_t\rangle\langle\beta_t| + c_1 c_2^* D_t |\alpha_t\rangle\langle\beta_t| + c_1^* c_2 D_t |\beta_t\rangle\langle\alpha_t|,$$

where the coherent ‘basis’ states have the same time dependence as in (4.3) and the coherences decay as

$$D_t = \exp\left(\left[-\frac{1}{2}|\alpha_0 - \beta_0|^2 + i\text{Im}(\alpha_0\beta_0^*)\right](1 - e^{-\gamma t})\right). \quad (4.8)$$

For times which are short compared to the relaxation time t_{rel} , one thus finds an exponential decay of the coherences

$$|D_t| = \exp\left(-\frac{\gamma}{2}|\alpha_0 - \beta_0|^2 t\right), \quad \text{for } t \ll \gamma^{-2}. \quad (4.9)$$

Assuming quasi-orthogonal coherent states, the time scale of this decay, that is the decoherence time t_{dec} , is much shorter than the relaxation time t_{rel} ,

$$t_{\text{dec}} = \frac{2t_{\text{rel}}}{|\alpha_0 - \beta_0|^2} \ll t_{\text{rel}}. \quad (4.10)$$

To conclude, any coherent state remains pure during the damped time evolution, while any superposition of distinct coherent states decays rapidly into a mixture

$$\rho_t \simeq |c_1|^2 |\alpha_t\rangle\langle\alpha_t| + |c_2|^2 |\beta_t\rangle\langle\beta_t|, \quad \text{if } t \gg t_{\text{dec}}. \quad (4.11)$$

Moreover, one finds that the statistical weights of this mixture are determined by the initial overlaps $|c_1|^2 = |\langle\alpha_0|\psi_0\rangle|^2$ and $|c_2|^2 = |\langle\beta_0|\psi_0\rangle|^2$. Due to this property, the coherent states are to be identified with the pointer states of the damped harmonic oscillator.

It should be mentioned that the quadratic dependence of the decoherence rate on the distance between the coherent states has been confirmed in a series of microwave cavity QED experiments at ENS in Paris [54,55]. Here the superposition state (4.6) was prepared in one of the field modes through the interaction of this cavity mode with a single Rydberg atom.

4.2 Definition of pointer states

The above observation serves as the starting point for the following definition of the pointer states for an open quantum system evolving according to a Lindblad master equation $\partial_t \rho = \mathcal{L}\rho$. We say that the system exhibits a pointer basis if its dynamics exhibits a separation of time scales, distinguished by a fast decoherence time t_{dec} , such that for any time much greater than t_{dec} , the evolved state is well approximated by a mixture of uniquely defined pure states $\mathbf{P}_\alpha = |\pi_\alpha\rangle\langle\pi_\alpha|$ which are independent of the initial state ρ_0 ,

$$e^{\mathcal{L}t} \rho_0 \simeq \int d\alpha \text{Prob}(\alpha|\rho_0) \mathbf{P}_\alpha(t), \quad \text{if } t \gg t_{\text{dec}}, \quad (4.12)$$

with $\text{Prob}(\alpha|\rho_0) \geq 0$ and $\int d\alpha \text{Prob}(\alpha|\rho_0) = 1$. Following the above example, one further demands that for initial states ρ_0 , which are superpositions of mutually orthogonal pointer states \mathbf{P}_β , the probability distribution $\text{Prob}(\alpha|\rho_0) = \sum_\beta w_\beta \delta(\alpha - \beta)$ is given by the initial projections

$$w_\beta = \text{Tr}(\rho_0 \mathbf{P}_\beta(0)). \quad (4.13)$$

The pointer states P_α initially form an (often overcomplete) basis, and they may evolve in time, though slowly compared to t_{dec} . Note that in (4.12) we assume a continuous set of pointer states; in case of a discrete set, the integral in (4.12) must be replaced by a sum.

The above definition shows that the importance of pointer states goes beyond the physics of measurement devices and the quantum-to-classical transition since they are also a practical tool for the solution of master equations. Knowing the pointer states P_α , their time evolution $P_\alpha(t)$, and the associated probability distribution $\text{Prob}(\alpha|\rho_0)$, one can immediately specify the solution of the master equation for any initial state and times greater than the decoherence time. Since the decoherence time is generically much shorter than the system and dissipation time scales of the pointer state motion, this allows one to capture a large part of the system evolution without solving the master equation.

4.3 The predictability sieve

The most widely used method for obtaining pointer states P_α , given the environmental coupling, is the so-called “predictability sieve” introduced by Zurek in [4,5,56]. In order to explain this approach, recall from Sect. 2.1.1, Eq. (2.11), that the linear entropy, $S_{\text{lin}}(\rho) = 1 - \text{Tr}(\rho^2)$, provides a convenient measure for the purity of states. It is therefore natural to measure robustness in terms of the linear entropy production rate,

$$\dot{S}_{\text{lin}}(\rho) = -2\text{Tr}[\rho\mathcal{L}(\rho)]. \quad (4.14)$$

This suggests identifying pointer states as the least entropy-producing states, i.e.

$$P_\alpha = \arg \min_{\mathbf{P}} \dot{S}_{\text{lin}}(\mathbf{P}), \quad (4.15)$$

where the optimization is with respect to pure states (since the pointer states are pure according to their definition in Eq. (4.12)) and the label α indicates that in general the minimum is not unique but gives a whole set. This optimization procedure is called “predictability sieve”, because it filters out the most predictable states.

As a first example, let us consider the damped harmonic oscillator. Recall from Sect. 4.1, that we have already identified coherent states $|\alpha\rangle$ as pure state solutions of the corresponding master equation, that is $\dot{S}_{\text{lin}}(|\alpha\rangle\langle\alpha|) = 0$. Thus, they provide solutions of the optimization problem (4.15).

Linear coupling model As a second example, let us consider the linear coupling model introduced in Sect. 3.3.4. It describes the decoherence dynamics exhibited by a quantum Brownian particle and it can be derived from the Hamiltonian of a particle which is linearly coupled to a bath of harmonic oscillators. Its evolution is obtained by a master equation in Lindblad form,

$$\frac{d}{dt}\rho_t = \frac{1}{i\hbar} [H_S, \rho_t] - \Lambda [x, [x, \rho_t]], \quad (4.16)$$

where $\Lambda \equiv 4\pi\gamma/\Lambda_{\text{th}}^2$ denotes the decoherence rate. The corresponding entropy production rate is determined by the spatial width of the state

$$\begin{aligned} \dot{S}_{\text{lin}}(\mathbf{P}) &= 2\Lambda\text{Tr}(\mathbf{P}^2\mathbf{x}^2 - \mathbf{P}\mathbf{x}\mathbf{P}\mathbf{x}) \\ &= 2\Lambda(\langle\mathbf{x}^2\rangle - \langle\mathbf{x}\rangle^2), \end{aligned} \quad (4.17)$$

so that position eigenstates $|x\rangle$ are the candidate pointer states obtained by the predictability sieve (4.15). However, localized states disperse quickly. An initially peaked wave packet will therefore rapidly spread in space, implying that the entropy production rate becomes large after a short time. It has therefore been suggested in [4, 5] to replace the time-local predictability sieve (4.15) by a time-integrated expression,

$$P_\alpha = \arg \min_P \int_0^\infty dt (S_{\text{lin}}(P; t) - 1). \quad (4.18)$$

Here $S_{\text{lin}}(P; t)$ denotes the time-dependent linear entropy, which results from an initial state P , that is

$$S_{\text{lin}}(P; t) = -2\text{Tr} [\rho_t \mathcal{L}(\rho_t)], \quad \text{with } \rho_t = e^{\mathcal{L}t} P. \quad (4.19)$$

As shown in [3], this function can be evaluated analytically

$$S_{\text{lin}}(\psi_\sigma; t) = 1 - \left(\frac{3m^2}{4\Lambda^2 \hbar^2 t^4 + 2\Lambda \hbar^2 \sigma^{-2} t^3 + 24\Lambda m^2 \sigma^2 t + 3m^2} \right)^{1/2}, \quad (4.20)$$

assuming Gaussian initial wave packets $\psi_\sigma(x)$ with variance σ^2 . A numerical optimization of the time-integrated linear entropy (4.18) then yields an optimal width [3]

$$\sigma_{\text{opt}} \simeq 0.5 \left(\frac{\hbar}{\Lambda m} \right)^{1/4}. \quad (4.21)$$

The candidate pointer states predicted by the time-integrated predictability sieve are therefore localized wave packets with a spatial extension σ_{opt} .

Disadvantages In spite of its conceptual clearness, the predictability sieve has several drawbacks. First of all, one has to solve a complicated optimization problem, in particular if the system is infinite-dimensional. In the latter case, it is usually necessary to restrict the set of states to a particular class of test functions, such as Gaussian wave packets. A numerical optimization routine may then yield a certain parameter, such as the width, but it does not provide the precise shape of the wave packets (see the example above). Furthermore, the predictability sieve does not yield the time evolution and the probability distribution of the pointer states. Both of them are needed in order to obtain the full solution (4.12) of the master equation.

4.4 Nonlinear equation for pointer states

A method which circumvents the disadvantages described above was proposed in [6–8]. Here the pointer states are obtained as the fixed points or solitons of a certain nonlinear equation.

4.4.1 Pointer states of pure dephasing

Let us illustrate this method by means of a two level system, subject to a *dephasing* environment. The corresponding master equation in interaction picture,

$$\partial_t \rho_t = \gamma (\sigma_z \rho_t \sigma_z - \rho_t), \quad (4.22)$$

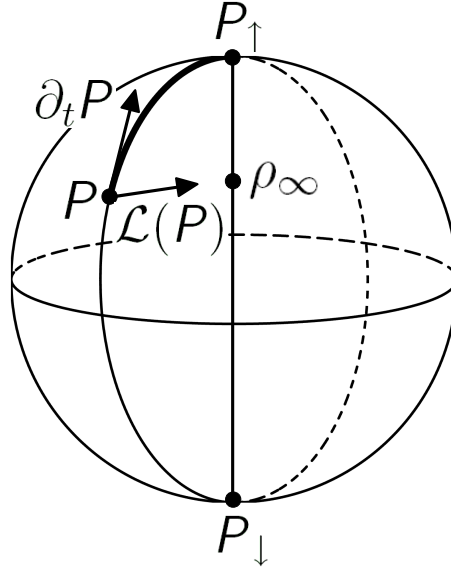


Figure 4.1: Bloch representation of a two level system subject to pure dephasing, as described by (4.22). As $t \rightarrow \infty$, the initial state $\rho_0 = P$ is projected onto the z-axis, implying that the poles (P_\uparrow and P_\downarrow) are the pointer states. The thick line indicates a trajectory within the set of pure states which connects the initial state to a nearby pointer state (the north pole). The infinitesimal increments of this trajectory has minimal distance from $\mathcal{L}(P)$ among all evolutions which generate pure state trajectories.

is characterized by the Lindblad jump operator $L = \sigma_z$ and the rate $\gamma > 0$. In order to solve this equation, use the so-called *Bloch representation*.

Bloch representation The density operator ρ of a two level system can be represented by a point in the unit sphere,

$$\rho = \frac{1}{2} (I + \mathbf{a} \cdot \boldsymbol{\sigma}), \quad \text{with } |\mathbf{a}| \leq 1, \quad (4.23)$$

where $\mathbf{a} = \text{Tr}(\boldsymbol{\sigma}\rho)$ is the Bloch vector and $\boldsymbol{\sigma} = (\sigma_x, \sigma_y, \sigma_z)$ denote the Pauli matrices. The pure states P form the surface $\{\mathbf{a} : |\mathbf{a}| = 1\}$ of the Bloch sphere, while mixed states lie in the interior.

Upon inserting the Bloch representation (4.23) into (4.22), one obtains a set of differential equations for the components of the Bloch vector

$$(\dot{a}_x, \dot{a}_y, \dot{a}_z) = (-2\gamma a_x, -2\gamma a_y, 0), \quad (4.24)$$

whose solution reads as

$$\mathbf{a}(t) = (e^{-2\gamma t} a_x(0), e^{-2\gamma t} a_y(0), a_z(0)). \quad (4.25)$$

Hence, the surface of the Bloch sphere is projected onto the z-axis in the course of the dephasing process. This implies that the decohered state $\mathbf{a}(\infty) = (0, 0, a_z(0))$ is a mixture of the eigenstates of σ_z (denoted by $P_\downarrow = |\downarrow\rangle\langle\downarrow|$ and $P_\uparrow = |\uparrow\rangle\langle\uparrow|$ respectively),

$$\rho_\infty = \text{Tr}[P_\uparrow \rho_0] P_\uparrow + \text{Tr}[P_\downarrow \rho_0] P_\downarrow. \quad (4.26)$$

The comparison with (4.12) shows that the north and the south pole of the Bloch sphere (corresponding to \mathbf{P}_\downarrow and \mathbf{P}_\uparrow) form the pointer basis of the pure dephasing process.

Since the solution of the master equation will not be at hand in general, one requires a method which yields the pointer states without the knowledge of ρ_t . To motivate this, notice that the north pole of the Bloch sphere is the asymptotic end point of the trajectory illustrated by the thick line in Fig. 4.1. This trajectory is generated by an equation of motion with the following properties. (i) It preserves the purity of pure initial states, meaning that an initial state which lies on the Bloch sphere remains on the surface. (ii) It is expected to be nonlinear because it must distinguish pointer states from their superpositions. (iii) The generated trajectory follows the exact solution of the master equation as closely as possible. In order to find such an equation of motion for $\mathbf{a}(t)$, it is suggestive to minimize the distance of the initial increments,

$$\min_{\partial_t \mathbf{a}} |\mathcal{L}(\mathbf{a}) - \partial_t \mathbf{a}|^2, \quad \text{with } \mathbf{a} \cdot \partial_t \mathbf{a} = 0. \quad (4.27)$$

Here, \mathcal{L} denotes the generator of the master equation (4.22) in Bloch representation and $\partial_t \mathbf{a}$ is subject to the condition $\mathbf{a} \cdot \partial_t \mathbf{a} = 0$ which ensures that the generated trajectory remains on the surface of the Bloch sphere. Using spherical coordinates for \mathbf{a} (and choosing the coordinate system such that the azimuth of \mathbf{a} vanishes, that is $\varphi = 0$) one can reformulate (4.27) as

$$\min_{\dot{\theta}, \dot{\varphi}} \left[\left(2\gamma \sin \theta + \dot{\theta} \cos \theta \right)^2 + \left(\dot{\varphi}^2 + \dot{\theta}^2 \right) \sin^2 \theta \right], \quad (4.28)$$

where it is used that $\dot{r} = 0$ due to the constraint $\mathbf{a} \cdot \partial_t \mathbf{a} = 0$. Since the function in (4.28) is quadratic in $\dot{\theta}$ and $\dot{\varphi}$, one can easily find its minimum by derivation, which yields

$$\left(\dot{r}, \dot{\varphi}, \dot{\theta} \right) = \left(0, 0, -\gamma \sin(2\theta) \right). \quad (4.29)$$

Because the sine is positive for $\theta \in (0, \pi/2)$, the solutions of these equations tend asymptotically towards a pointer state of the system, see Fig. 4.1. The equator of the Bloch sphere forms a set of unstable fixed points of (4.29).

4.4.2 General Markovian master equations

Let us now generalize the above argument to general Markovian master equations $\partial_t \rho = \mathcal{L}\rho$. To this end, let us replace the Euclidean norm in (4.27) by an appropriate operator norm. A common choice is the Hilbert-Schmidt norm $\|\mathbf{A}\|_{\text{HS}}^2 \equiv \text{Tr}(\mathbf{A}^\dagger \mathbf{A})$, which applies to arbitrary operators \mathbf{A} in \mathcal{H} . Accordingly, the generalization of (4.27) to higher dimensional systems reads

$$\min_{\partial_t \mathbf{P}} \|\mathcal{L}(\mathbf{P}) - \partial_t \mathbf{P}\|_{\text{HS}}^2, \quad (4.30)$$

where the minimization is with respect to all evolution equations $\partial_t \mathbf{P} = f(\mathbf{P})$ which propagate \mathbf{P} within the set of pure states, such that $\mathbf{P}_t^2 = \mathbf{P}_t$. In order to find the structure of this class of equations, let us write the evolution equation in completely general terms as

$$\partial_t |\psi\rangle = (\mathbf{A}_\psi + \mathbf{B}_\psi) |\psi\rangle, \quad (4.31)$$

where $\mathbf{A}_\psi = \mathbf{A}_\psi^\dagger$ and $\mathbf{B}_\psi = -\mathbf{B}_\psi^\dagger$ are ψ -dependent, Hermitian and anti-Hermitian mappings. This form can be further restricted using the conservation of norm

$$\begin{aligned} 0 &= \partial_t \|\psi\|^2 \\ &= (\partial_t \langle \psi |) |\psi\rangle + \langle \psi | \partial_t |\psi\rangle \\ &= 2\langle \psi | \mathbf{A}_\psi | \psi\rangle. \end{aligned} \quad (4.32)$$

To assure that \mathbf{A}_ψ has a vanishing expectation value, replace it as

$$\mathbf{A}_\psi \rightarrow \mathbf{A}_\psi - \langle \psi | \mathbf{A}_\psi | \psi\rangle. \quad (4.33)$$

In conclusion, norm-preserving evolution equations for state vectors $|\psi\rangle$ are of the form

$$\partial_t |\psi\rangle = (\mathbf{A}_\psi - \langle \psi | \mathbf{A}_\psi | \psi\rangle + \mathbf{B}_\psi) |\psi\rangle. \quad (4.34)$$

This implies that the equation of motion for the projector $\mathbf{P} = |\psi\rangle\langle\psi|$ is given by

$$\begin{aligned} \partial_t \mathbf{P} &= (\partial_t |\psi\rangle) \langle\psi| + |\psi\rangle \partial_t \langle\psi| \\ &= [\mathbf{P}, [\mathbf{P}, \mathbf{A}_\mathbf{P}]] + [\mathbf{B}_\mathbf{P}, \mathbf{P}] \\ &= [\mathbf{P}, [\mathbf{P}, \mathbf{A}_\mathbf{P} + [\mathbf{B}_\mathbf{P}, \mathbf{P}]]]. \end{aligned} \quad (4.35)$$

This expression can be further simplified, by introducing the Hermitian operator $\mathbf{X}_\mathbf{P} := \mathbf{A}_\mathbf{P} + [\mathbf{B}_\mathbf{P}, \mathbf{P}]$, which finally yields

$$\partial_t \mathbf{P} = [\mathbf{P}, [\mathbf{P}, \mathbf{X}_\mathbf{P}]]. \quad (4.36)$$

Note that any nonlinear trace and purity preserving evolution equation must have this structure.

We are now in the position to reformulate the optimization problem (4.30) in a more convenient form

$$\min_{\mathbf{X}_\mathbf{P}} \|\mathcal{L}(\mathbf{P}) - [\mathbf{P}, [\mathbf{P}, \mathbf{X}_\mathbf{P}]]\|_{\text{HS}}^2. \quad (4.37)$$

In order to solve it, let us rewrite the expression in Eq. (4.37) as

$$\begin{aligned} \|\mathcal{L}(\mathbf{P}) - \partial_t \mathbf{P}\|_{\text{HS}}^2 &= \text{Tr} \left[(\mathcal{L}(\mathbf{P}) - [\mathbf{P}, [\mathbf{P}, \mathbf{X}_\mathbf{P}]] \right)^2 \\ &= \text{Tr} \left[\mathcal{L}(\mathbf{P})^2 - 2 \left(\mathcal{L}(\mathbf{P})^2 \mathbf{P} - (\mathcal{L}(\mathbf{P}) \mathbf{P})^2 \right) \right. \\ &\quad \left. + 2 \text{Tr} \left[(\mathcal{L}(\mathbf{P}) - \mathbf{X}_\mathbf{P})^2 \mathbf{P} - [(\mathcal{L}(\mathbf{P}) - \mathbf{X}_\mathbf{P}) \mathbf{P}]^2 \right] \right]. \end{aligned} \quad (4.38)$$

Here the first summand is independent of $\mathbf{X}_\mathbf{P}$, whereas the second one can be rephrased as

$$2 \text{Tr} \left[\mathbf{Y}_\mathbf{P}^2 \mathbf{P} - (\mathbf{Y}_\mathbf{P} \mathbf{P})^2 \right] = 2 \left(\langle \mathbf{Y}_\mathbf{P}^2 \rangle - \langle \mathbf{Y}_\mathbf{P} \rangle^2 \right), \quad (4.39)$$

with the definition $\mathbf{Y}_\mathbf{P} := \mathcal{L}(\mathbf{P}) - \mathbf{X}_\mathbf{P}$, $\mathbf{Y}_\mathbf{P}^\dagger = \mathbf{Y}_\mathbf{P}$. The variance in (4.39) is minimal whenever the mapping $\mathbf{Y}_\mathbf{P}$ admits $|\psi\rangle$ as an eigenstate, $\mathbf{Y}_\mathbf{P} \mathbf{P} = \lambda \mathbf{P}$. This implies that the solution of (4.37) meets the condition

$$\mathbf{X}_{\min} \mathbf{P} = (\mathcal{L}(\mathbf{P}) - \lambda) \mathbf{P}. \quad (4.40)$$

The right-hand side of (4.36) therefore reads

$$\begin{aligned} [\mathbf{P}, [\mathbf{P}, \mathbf{X}_{\min}]] &= \mathbf{P}\mathcal{L}(\mathbf{P}) + \mathcal{L}(\mathbf{P})\mathbf{P} - 2\mathbf{P}\mathcal{L}(\mathbf{P})\mathbf{P} \\ &= [\mathbf{P}, [\mathbf{P}, \mathcal{L}(\mathbf{P})]]. \end{aligned} \quad (4.41)$$

To conclude, the generalization of (4.29) reads as [6–8]

$$\partial_t \mathbf{P} = [\mathbf{P}, [\mathbf{P}, \mathcal{L}(\mathbf{P})]]. \quad (4.42)$$

Motivated by the example in Sect. 4.4.1, one is let to conjecture that the asymptotic solutions of (4.42) provide the pointer states in more complex systems as well.

State vector representation In practical applications, it is more convenient to work with the vector representation of (4.42) rather than with the projector equation itself. The former is given by

$$\partial_t |\psi\rangle = (\mathcal{L}(\mathbf{P}_\psi) - \langle \psi | \mathcal{L}(\mathbf{P}_\psi) | \psi \rangle) |\psi\rangle, \quad (4.43)$$

with $\mathbf{P}_\psi \equiv |\psi\rangle\langle\psi|$. It is straightforward to show that Eq. (4.43) implies the projector equation (4.42)

$$\begin{aligned} \partial_t \mathbf{P} &= (\mathcal{L}(\mathbf{P}_\psi) - \langle \mathcal{L}(\mathbf{P}_\psi) \rangle) |\psi\rangle\langle\psi| + |\psi\rangle\langle\psi| (\mathcal{L}(\mathbf{P}_\psi) - \langle \mathcal{L}(\mathbf{P}_\psi) \rangle) \\ &= \mathcal{L}(\mathbf{P}_\psi) \mathbf{P}_\psi + \mathbf{P}_\psi \mathcal{L}(\mathbf{P}_\psi) - 2|\psi\rangle\langle\psi| \mathcal{L}(\mathbf{P}_\psi) |\psi\rangle\langle\psi| \\ &= [\mathbf{P}, [\mathbf{P}, \mathcal{L}(\mathbf{P})]]. \end{aligned} \quad (4.44)$$

If one takes the Lindblad form for the generator in (4.43), the equation reads

$$\begin{aligned} \partial_t |\psi\rangle &= \frac{1}{i\hbar} (\mathbf{H} - \langle \mathbf{H} \rangle) |\psi\rangle \\ &\quad + \int d\mathbf{q} \gamma_{\mathbf{q}} \left[\langle \mathbf{L}_{\mathbf{q}}^\dagger \rangle (\mathbf{L}_{\mathbf{q}} - \langle \mathbf{L}_{\mathbf{q}} \rangle) - \frac{1}{2} (\mathbf{L}_{\mathbf{q}}^\dagger \mathbf{L}_{\mathbf{q}} - \langle \mathbf{L}_{\mathbf{q}}^\dagger \mathbf{L}_{\mathbf{q}} \rangle) \right] |\psi\rangle, \end{aligned} \quad (4.45)$$

where the expectation values are with respect to $|\psi\rangle$. Note that the energy expectation $\langle \mathbf{H} \rangle$ is disregarded in the following, since it contributes only an additional phase.

Quantum trajectories and the nonlinear equation It will be important in subsequent chapters that Eq. (4.45) is known also in another context: it corresponds to the deterministic part of a specific quantum trajectory method called *orthogonal unraveling*. As we will demonstrate in Chapter 8, one can use this specific unraveling to prove for a particular model that the asymptotic solutions of (4.45) indeed provide the pointer states. Moreover, it allows one to calculate the probability distribution $\text{Prob}(\alpha|\rho_0)$ of the pointer states, with ρ_0 the initial state.

4.4.3 Pointer states of the damped harmonic oscillator

As a first application of the nonlinear equation (4.45), let us consider again the damped harmonic oscillator introduced in Sect. 3.2. It is described by the Hamiltonian $\mathbf{H} = \hbar\omega \mathbf{a}^\dagger \mathbf{a}$ and the single Lindblad operator $\mathbf{L} = \mathbf{a}$, implying that Eq. (4.45) becomes

$$\partial_t |\psi\rangle = -i\omega \mathbf{a}^\dagger \mathbf{a} |\psi\rangle + \gamma \left[\langle \mathbf{a}^\dagger \rangle (\mathbf{a} - \langle \mathbf{a} \rangle) - \frac{1}{2} (\mathbf{a}^\dagger \mathbf{a} - \langle \mathbf{a}^\dagger \mathbf{a} \rangle) \right] |\psi\rangle. \quad (4.46)$$

It is known already from Sect. 4.1 that coherent states $|\alpha\rangle$ constitute the pointer states of this model, suggesting the ansatz $|\psi\rangle = |\alpha\rangle$. Since coherent states are eigenstates of \mathbf{a} , the first term of the non-unitary part in (4.46) vanishes, leading to the equation

$$\partial_t|\alpha\rangle = \left(\frac{\gamma}{2}|\alpha|^2 - \gamma_+\alpha\mathbf{a}^\dagger\right)|\alpha\rangle, \quad (4.47)$$

with $\gamma_+ \equiv \gamma/2 + i\omega$. It can be verified easily that this equation is solved by

$$|\alpha_t\rangle = e^{-|\alpha_t|^2/2}e^{\alpha_t\mathbf{a}^\dagger}|0\rangle, \quad (4.48)$$

with $\alpha_t = \alpha_0 \exp(-\gamma_+t)$. This shows that coherent states are indeed the predicted pointer states, consistent with the explicit solution of the master equation (4.1). Moreover, we find that the nonlinear equation provides the correct time evolution for the pointer states, agreeing with the result obtained in Sect. 4.1, Eq. (4.3).

Additional condition Surprisingly, the nonlinear equation (4.46) is also solved by energy eigenstates $|n\rangle$ of the isolated oscillator. These states are eigenvectors of the ‘number operator’ $\mathbf{n} \equiv \mathbf{a}^\dagger\mathbf{a}$, which implies that the second term of the non-unitary part in (4.46) vanishes. The first term is also zero, since

$$\langle n|\mathbf{a}^\dagger|n\rangle = \sqrt{n+1}\langle n|n+1\rangle = 0. \quad (4.49)$$

Therefore, Equation (4.46) exhibits solutions of the form

$$|n_t\rangle = e^{-i\omega n t}|n\rangle. \quad (4.50)$$

Energy eigenstates, however, are very fragile quantum states, since their entropy production rate grows linearly with the occupation number n

$$\begin{aligned} \dot{S}_{\text{lin}}(|n\rangle\langle n|) &= -2\gamma \left(\langle n|\mathbf{a}|n\rangle\langle n|\mathbf{a}^\dagger|n\rangle - \langle n|\mathbf{a}^\dagger\mathbf{a}|n\rangle \right) \\ &= 2\gamma n, \end{aligned} \quad (4.51)$$

and they do therefore not match with the definition of pointer states (4.12) or (4.15).

This shows that the fixed points \mathbf{P} of the nonlinear equation (4.45) are not necessarily pointer states. In fact, one needs a further condition: the entropy production rate $\dot{S}_{\text{lin}}(\mathbf{P})$ of the asymptotic solutions \mathbf{P} of the nonlinear equation (4.45) must be small. The reason for this additional condition will become clear in Chapter 8 when studying the orthogonal unraveling mentioned above.

4.4.4 Pointer states of the linear coupling model

As a second application of the nonlinear equation (4.45), let us study the linear coupling model, see Sect. 3.3.4, which describes the decoherence dynamics of a quantum Brownian particle. It is characterized by the Hamiltonian $\mathbf{H} = \mathbf{p}^2/2m$ and the single Lindblad operator $\mathbf{L} = \sqrt{2\Lambda/\gamma}\mathbf{x}$, implying that Eq. (4.45) becomes

$$\partial_t|\psi\rangle = \frac{\mathbf{p}^2}{i\hbar 2m}|\psi\rangle - \Lambda \left[(\mathbf{x} - \langle \mathbf{x} \rangle)^2 - \sigma^2 \right] |\psi\rangle, \quad (4.52)$$

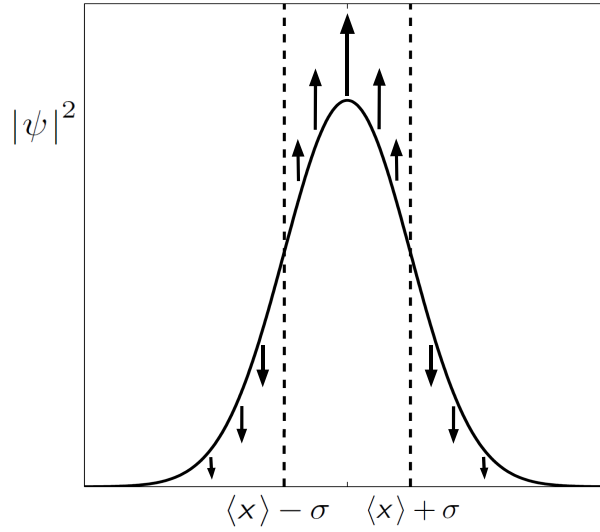


Figure 4.2: Localization induced by the incoherent part of the nonlinear equation (4.53). The centered parts of the wave function $\psi(x)$, which lie within one sigma of the mean $\langle x \rangle$, get amplified, i.e. $\partial_t \psi > 0$, whereas the tails get damped, that is $\partial_t \psi < 0$.

with variance $\sigma^2 \equiv \langle x^2 \rangle - \langle x \rangle^2$. This equation is most conveniently studied in position representation, which yields [6, 39, 57]

$$\partial_t \psi_t(x) = \frac{i\hbar}{2m} \partial_x^2 \psi_t(x) - \Lambda \left[(x - \langle x_t \rangle)^2 - \sigma_t^2 \right] \psi_t(x), \quad (4.53)$$

where we included the time arguments for clarity.

The two summands in (4.53) have counteractive effects on the dynamics of the wave function: the coherent term leads to its dispersion, whereas the second, incoherent summand tends to localize the solution. In order to explain this localization, note that the centered parts of the wave function, which lie within a one-sigma interval around the mean, $|x - \langle x \rangle| < \sigma$, get amplified, i.e. $\partial_t \psi > 0$, whereas the tails of the wave function, where $|x - \langle x \rangle| > \sigma$, get damped, i.e. $\partial_t \psi < 0$. This effect is visualized in Figure 4.2. As a consequence of these competing contributions, one expects solitonic solutions where both effects are in equilibrium, so that the state moves with fixed shape and constant velocity. As discussed above and already in [6, 57], these solitons are candidates for the pointer states of the linear coupling model.

Indeed, the nonlinear equation (4.53) exhibits Gaussian solitonic solutions of the form [6, 57]

$$\pi_t(x) = \mathcal{N} \exp \left(-\frac{1-i}{4\sigma^2} [x - \langle x_t \rangle]^2 + \frac{i}{\hbar} [x - \langle x_t \rangle] \langle p \rangle + i\phi_t \right), \quad (4.54)$$

which move with constant momentum $\langle p \rangle$,

$$\langle x_t \rangle = \frac{\langle p \rangle}{m} t + \langle x_0 \rangle. \quad (4.55)$$

Here \mathcal{N} denotes the normalization constant and ϕ_t is a linear function in time, given by

$$\phi_t = \left(\frac{\langle \mathbf{p} \rangle^2}{2\hbar m} - \frac{\hbar}{4m\sigma^2} \right) t + \phi_0. \quad (4.56)$$

Crucially, the Gaussian solitons move with a fixed width, which is given by the expression [6, 39, 57]

$$\sigma = \frac{1}{\sqrt{2}} \left(\frac{\hbar}{m\Lambda} \right)^{1/4} = \frac{1}{\sqrt{2}} \left(\frac{\hbar\Lambda_{\text{th}}^2}{4\pi\gamma} \right)^{1/4}. \quad (4.57)$$

We note that this width tends to zero in the limit of large temperature T or large coupling constant γ , that is $\sigma(T \rightarrow \infty) = 0$ or $\sigma(\gamma \rightarrow \infty) = 0$. This implies that the pointer states of the linear coupling model are localized in the limiting regime where classical behavior is expected. It should also be mentioned that this result for the soliton width agrees (apart from a factor of $1/\sqrt{2}$) with the prediction of the time-integrated predictability sieve, see Sect. 4.3, Eq. (4.21). This indicates that the two approaches are of similar type.

In order to verify that (4.54) presents a solution of (4.53), let us evaluate its time and position derivative, which yields

$$\begin{aligned} \partial_t \pi_t(x) - \frac{i\hbar}{2m} \partial_x^2 \pi_t(x) &= \left(i\partial_t \phi_t - \frac{i\langle \mathbf{p} \rangle^2}{2\hbar m} + \frac{i\hbar}{4m\sigma^2} \right. \\ &\quad \left. - \frac{\hbar}{4m\sigma^4} ([x - \langle \mathbf{x}_t \rangle^2] - \sigma^2) \right) \pi_t(x), \end{aligned} \quad (4.58)$$

where the ballistic motion (4.55) is used. The complex part of the right-hand side vanishes if the phase ϕ_t exhibits the time dependence shown in Eq. (4.56). The above equation then simplifies, giving

$$\partial_t \pi_t(x) - \frac{i\hbar}{2m} \partial_x^2 \pi_t(x) = -\frac{\hbar}{4m\sigma^4} ([x - \langle \mathbf{x}_t \rangle^2] - \sigma^2) \pi_t(x). \quad (4.59)$$

This dynamical equation coincides with the nonlinear equation (4.53), provided the width is given by Eq. (4.57). This shows that the Gaussian soliton (4.54) moves according to Eq. (4.53), if it satisfies the conditions (4.55), (4.56) and (4.57). We conclude that the linear coupling model (4.16) exhibits Gaussian pointer states.

General linear coupling models Recall from Sect. 3.3 that the linear coupling model (4.16) is based on the Caldeira-Leggett equation (3.26), which was derived in [47] assuming the high-temperature limit (3.32) and Ohmic spectral densities (3.29). A more general result was obtained by Hu, Paz and Zhang [58], where a master equation is derived for the reduced state of a free quantum system linearly coupled to a heat bath at arbitrary temperature, with arbitrary spectral density. It was proved rigorously in [9] that this master equation leads to the complete, finite time decoherence in the Gaussian basis. This shows that the decoherence to Gaussian pointer states is a generic feature of linear coupling models. Note, however, that linear models may lead to incorrect results when studying decoherence phenomena, see Sect. 3.3.4.

Chapter 5

Pointer states of collisional decoherence

In the previous chapter, a nonlinear equation was discussed whose solitonic solutions are supposed to provide the pointer states for a given open quantum system. It was applied to several examples including the damped harmonic oscillator and a free quantum particle coupled linearly to a bath of harmonic oscillators. There, the solitonic solutions of the corresponding nonlinear equation are coherent states and Gaussian wave packets, respectively [6, 57]. In the following, we go beyond linear coupling models by applying the formalism to the one-dimensional version of collisional decoherence, which provides a realistic description of the decoherence process generated by an ideal gas environment, see Sect. 3.5.

In Sect. 5.1, we derive the corresponding nonlinear equation and present its numerical solution. The properties of the obtained solitonic solutions are analyzed in Sect. 5.2. A discussion of their temporal evolution in the presence of an external potential follows in Sect. 5.3.

5.1 Determining the pointer states of collisional decoherence

Collisional decoherence is described by a master equation in Lindblad form (3.47), where the jump operators are momentum kick operators, $\mathbf{L}_{\mathbf{q}} = e^{i\mathbf{q}\mathbf{x}/\hbar}$, and the rate is given by $\gamma_{\mathbf{q}} = \gamma G(\mathbf{q})$, see Sect. 3.5. For simplicity, let us treat the one-dimensional case in the following, where the momentum vector \mathbf{q} is replaced by the one-dimensional momentum q . Assuming a free particle and the Lindblad operators shown above, the nonlinear equation (4.45) becomes

$$\partial_t |\psi\rangle = \frac{\mathbf{p}^2}{i\hbar 2m} |\psi\rangle + \gamma \int_{-\infty}^{\infty} dq G(q) \langle e^{-iqx/\hbar} \rangle \left(e^{iqx/\hbar} - \langle e^{iqx/\hbar} \rangle \right) |\psi\rangle, \quad (5.1)$$

where it is used that the second term of the non-unitary part in (4.45) vanishes, due to the unitarity of the jump operators \mathbf{L}_q . This equation is most conveniently studied in position representation, which gives

$$\begin{aligned} \partial_t \psi(x) &= \frac{i\hbar}{2m} \partial_x^2 \psi(x) + \gamma \psi(x) \int_{-\infty}^{\infty} dq G(q) \int_{-\infty}^{\infty} dy |\psi(y)|^2 e^{-iqy/\hbar} \\ &\quad \times \left(e^{iqx/\hbar} - \int_{-\infty}^{\infty} dz |\psi(z)|^2 e^{iqz/\hbar} \right). \end{aligned} \quad (5.2)$$

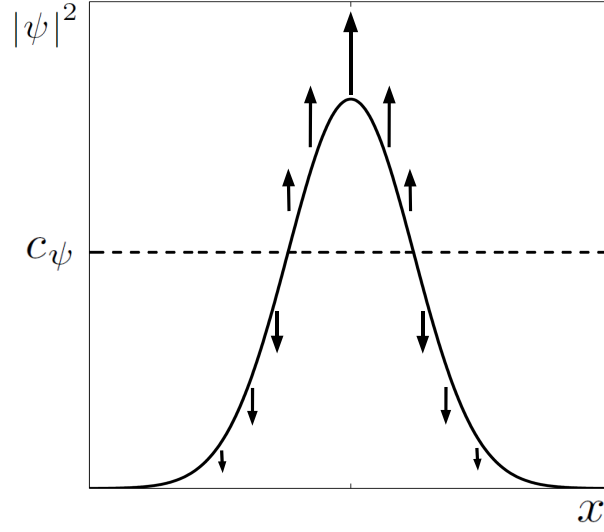


Figure 5.1: Simplified picture of the localization induced by the incoherent part of the nonlinear equation (5.5), in the limit of a broad distribution where $|\psi|^2 * \hat{G} \simeq |\psi|^2$. This assumption implies that the centered parts of the wave function $\psi(x)$, where $|\psi|^2$ exceeds the constant c_ψ , get amplified, i.e. $\partial_t \psi > 0$, whereas the tails get damped, i.e. $\partial_t \psi < 0$. The ψ -dependent constant c_ψ is given by the double integral $c_\psi = \int dy |\psi|^2(y) (|\psi|^2 * \hat{G})(y)$.

Upon interchanging the integrals in this equation, one finds

$$\begin{aligned} \partial_t \psi(x) &= \frac{i\hbar}{2m} \partial_x^2 \psi(x) + \gamma \psi(x) \left(\int_{-\infty}^{\infty} dy |\psi(y)|^2 \int_{-\infty}^{\infty} dq G(q) e^{iq(x-y)/\hbar} \right. \\ &\quad \left. - \int_{-\infty}^{\infty} dy |\psi(y)|^2 \int_{-\infty}^{\infty} dz |\psi(z)|^2 \int_{-\infty}^{\infty} dq G(q) e^{iq(z-y)/\hbar} \right). \end{aligned} \quad (5.3)$$

This expression can be simplified by defining the Fourier transform of $G(q)$, that is $\hat{G}(x) \equiv \int_{-\infty}^{\infty} dq G(q) \exp(iqx/\hbar)$, which yields

$$\begin{aligned} \partial_t \psi(x) &= \frac{i\hbar}{2m} \partial_x^2 \psi(x) + \gamma \psi(x) \left(\int_{-\infty}^{\infty} dy |\psi(y)|^2 \hat{G}(x-y) \right. \\ &\quad \left. - \int_{-\infty}^{\infty} dy |\psi(y)|^2 \int_{-\infty}^{\infty} dz |\psi(z)|^2 \hat{G}(z-y) \right) \\ &= \frac{i\hbar}{2m} \partial_x^2 \psi(x) + \gamma \psi(x) \left(|\psi|^2 * \hat{G}(x) \right. \\ &\quad \left. - \int_{-\infty}^{\infty} dy |\psi(y)|^2 (|\psi|^2 * \hat{G})(y) \right). \end{aligned} \quad (5.4)$$

Here, $g * h(x) \equiv \int_{-\infty}^{\infty} dy g(y) h(x-y)$ denotes the convolution of g and h . We conclude that the application of the nonlinear equation (4.45) to collisional decoherence yields an integro-differential equation of the form

$$\partial_t \psi_t(x) = \frac{i\hbar}{2m} \partial_x^2 \psi_t(x) + \psi_t(x) \Lambda [|\psi_t|^2](x), \quad (5.5)$$

$$\Lambda [|\psi_t|^2](x) = \gamma \left(|\psi_t|^2 * \hat{G}(x) - \int_{-\infty}^{\infty} dy |\psi_t|^2(y) (|\psi_t|^2 * \hat{G})(y) \right), \quad (5.6)$$

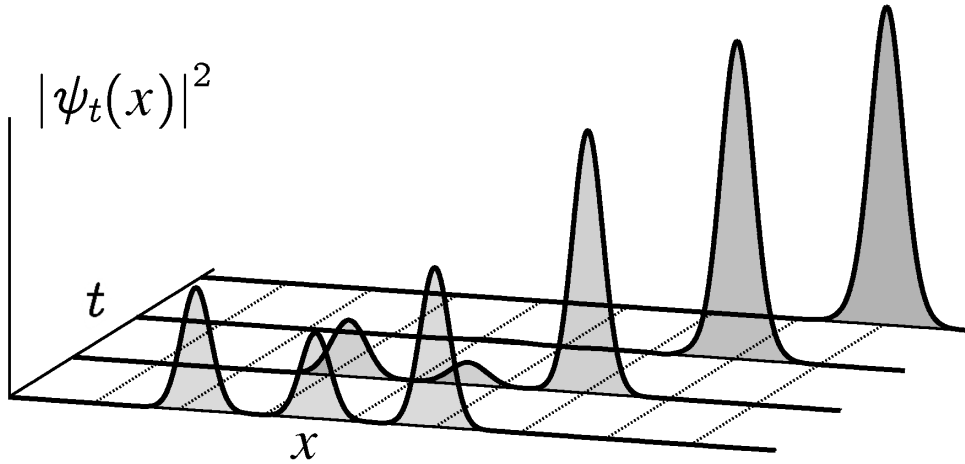


Figure 5.2: The nonlinear equation (5.14) drives any initial state $|\psi_0\rangle$ (here a superposition of wave packets traveling to the right) into a localized soliton $|\pi_t\rangle$ that moves with fixed envelope and constant velocity. These solitonic solutions form an overcomplete set, the pointer basis of collisional decoherence.

where the time argument is included for clarity.

The two summands in (5.5) have counteractive effects on the temporal evolution of the wave function: the coherent term leads to its dispersion, whereas the second, incoherent summand tends to localize the solution. In order to explain this localization, note that the second summand in (5.6) is independent of x . This implies that the centered parts of the wave function, where the convolution $|\psi_t|^2 * \hat{G}(x)$ exceeds the constant term in (5.6), get amplified, i.e. $\partial_t \psi_t > 0$, whereas the tails of the wave function get damped, i.e. $\partial_t \psi_t < 0$, see Fig. 5.1. (Note that this differs from the localization mechanism discussed in Fig. 4.2.) As a consequence of these competing effects, solutions of (5.5) evolve towards solitonic states $\pi_t(x)$ where both effects are in equilibrium, so that the state moves with fixed shape and constant velocity, that is $|\pi_t(x)| = |\pi_0(x - vt)|$. As discussed above, these solitons are candidates for the pointer states of collisional decoherence.

Dimensionless form Let us now reformulate Eq. (5.5) in dimensionless form. To this end, we use the dimensionless variables

$$y \equiv \frac{\sigma_G}{\hbar} x \quad \text{and} \quad \tau \equiv \gamma t, \quad (5.7)$$

to define the dimensionless wave function

$$\varphi_\tau(y) \equiv \sqrt{\frac{\hbar}{\sigma_G}} \psi_{\tau/\gamma} \left(\frac{\hbar}{\sigma_G} y \right), \quad (5.8)$$

with a momentum scale σ_G (whose meaning will become clear soon). This implies that the original wave function can be written as

$$\psi_t(x) = \sqrt{\frac{\sigma_G}{\hbar}} \varphi_{\gamma t} \left(\frac{\sigma_G}{\hbar} x \right), \quad (5.9)$$

whereas the derivative and the differential transform as

$$\partial_x = \frac{\sigma_G}{\hbar} \partial_y \quad \text{and} \quad dx = \frac{\hbar}{\sigma_G} dy. \quad (5.10)$$

Upon inserting Eqs. (5.9) and (5.10) into the nonlinear equation (5.5), one obtains

$$\begin{aligned} \partial_\tau \varphi_\tau(y) = & \frac{i\hbar}{2m\gamma} \left(\frac{\sigma_G}{\hbar} \right)^2 \partial_y^2 \varphi_\tau(y) + \varphi_\tau(y) \left(\int dy' |\varphi_\tau(y')|^2 \hat{G} \left(\frac{\hbar}{\sigma_G} [y - y'] \right) \right. \\ & \left. - \int \int dy' dy'' |\varphi_\tau(y')|^2 |\varphi_\tau(y'')|^2 \hat{G} \left(\frac{\hbar}{\sigma_G} [y - y'] \right) \right), \end{aligned} \quad (5.11)$$

where we dropped the integral boundaries for brevity. This expression can be further simplified assuming the momentum transfer distribution $G(q)$ to be a centered Gaussian with variance σ_G^2 ,

$$G(q) = \frac{1}{\sqrt{2\pi}\sigma_G} \exp\left(-\frac{q^2}{2\sigma_G^2}\right), \quad (5.12)$$

which implies that

$$\hat{G}(x) = \exp\left(-\frac{\sigma_G^2}{2\hbar^2} x^2\right) = \exp\left(-\frac{y^2}{2}\right). \quad (5.13)$$

Finally, by inserting (5.13) into (5.11), one obtains a nonlinear evolution equation which depends only on the single dimensionless parameter $\kappa \equiv \sigma_G^2 / (m\hbar\gamma)$,

$$\begin{aligned} \partial_\tau \varphi_\tau(y) = & -\frac{\kappa}{2i} \partial_y^2 \varphi_\tau(y) + \varphi_\tau(y) \int_{-\infty}^{\infty} dy' |\varphi_\tau(y')|^2 \\ & \times \left(e^{-(y-y')^2/2} - \int_{-\infty}^{\infty} dy'' |\varphi_\tau(y'')|^2 e^{-(y'-y'')^2/2} \right). \end{aligned} \quad (5.14)$$

It should be mentioned that, under the assumption of a normal momentum transfer distribution $G(q)$, the master equation of collisional decoherence is equivalent with the one of the Ghirardi-Rimini-Weber model, see Sect. 3.5.2.

Numerical solution Figures 5.2 and 5.3 show numerical solutions of (5.14) computed with the so-called *split operator FFT method* [59,60]. In Fig. 5.2, we choose as the initial state a superposition of three localized states $\phi_{1,2,3}$ travelling to the right, $\psi_0(x) = c_1\phi_1(x) + c_2\phi_2(x) + c_3\phi_3(x)$. The initial state in Fig. 5.3, on the other hand, is a superposition of two counter-propagating localized states $\phi_{4,5}$, $\psi_0(x) = c_4\phi_4(x) + c_5\phi_5(x)$. As expected from the above discussion, the (modulus of the) solution converges to a soliton, in both cases. Moreover, it is found that the soliton inherits its initial position and momentum expectation value from that localized component ϕ_i of the initial state which has the greatest weight c_i , $|c_i| > |c_{j \neq i}|$. Similar observations are found for various other initial states.

5.2 Properties of the solitons

Let us proceed to characterize the solitonic solutions of (5.5). In Sect. 5.2.1, the consequences of the conservation of probability on the phase of the solitons are analyzed, allowing us to predict the asymptotic shape of the solitons in Sect. 5.2.2. In Sect. 5.2.3 we estimate the spatial extension of the solitons, followed by the proof that they form a basis of the Hilbert space in Sect. 5.2.4.

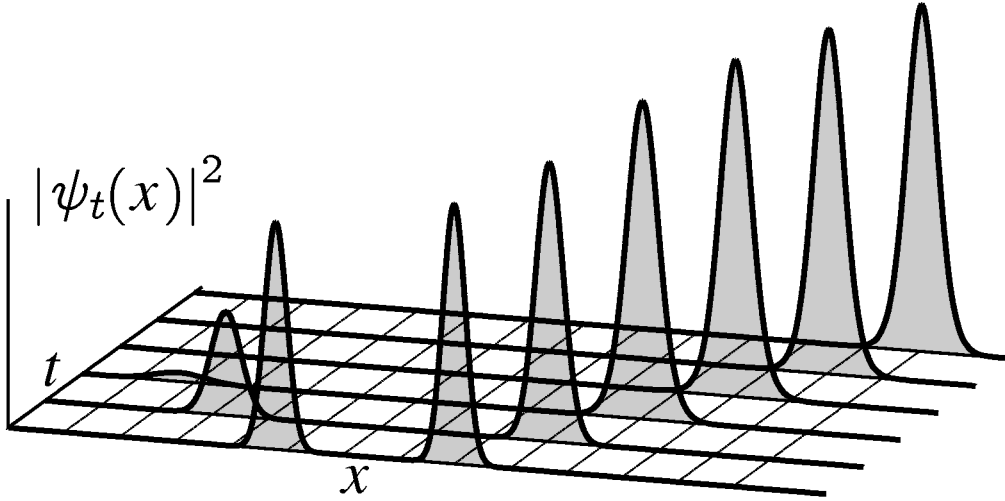


Figure 5.3: Similar scenario as in Figure 5.2, but with a different initial state. The latter is a superposition of two counter-propagating localized states. The picture shows that the soliton inherits its initial position and momentum expectation value from that localized component of the initial state which has the greatest weight.

5.2.1 Consequences of the continuity equation

As observed in the previous section, the nonlinear equation (5.5) exhibits solitonic solutions $\pi_t(x)$ in the sense that the modulus of $\pi_t(x)$ moves with constants shape and velocity, i.e.

$$\pi_t(x) = f(x - vt) e^{ig(x,t)}, \quad (5.15)$$

with $f \geq 0$ and g real. In this section, the general structure of the phase $g(x, t)$ is analyzed, which will be relevant subsequently. The time derivative of a solution $|\psi_t(x)|^2$ of (5.5), yields the continuity equation for $\psi_t(x)$,

$$\partial_t |\psi_t(x)|^2 = -\frac{\hbar}{m} \partial_x \text{Im}(\psi_t^* \partial_x \psi_t) + 2|\psi_t(x)|^2 \Lambda[|\psi_t|^2](x). \quad (5.16)$$

Plugging the solitonic form (5.15) into (5.16), gives

$$\begin{aligned} & -2\Lambda[f^2](x - vt) - v\partial_x \log f^2(x - vt) \\ & = -\frac{\hbar}{m} [\partial_x^2 g(x, t) + \partial_x g(x, t) \partial_x \log f^2(x - vt)]. \end{aligned} \quad (5.17)$$

Here it is used that $\Lambda[f_t^2](x) = \Lambda[f^2](x - vt)$, which follows from $f_t(x) = f(x - vt)$. The time dependence of the left hand side of (5.17) corresponds to a spatial shift. Thus, also the right-hand side of (5.17) must exhibit such a simple time dependence, which implies that

$$-v\partial_x r(x, t) = \partial_t r(x, t), \quad (5.18)$$

where $r(x, t)$ denotes the right-hand side of (5.17). It follows that

$$\begin{aligned} & -v\partial_x^3 g(x, t) - v\partial_x^2 g(x, t) \partial_x \log f^2(x - vt) \\ & = \partial_t \partial_x^2 g(x, t) + \partial_t \partial_x g(x, t) \partial_x \log f^2(x - vt). \end{aligned} \quad (5.19)$$

Since this equation must hold for all x, v and t , we may assume that the equality holds already for the summands, so that

$$-v\partial_x^2 g(x, t) = \partial_t [\partial_x g(x, t)]. \quad (5.20)$$

Therefore, the temporal and spatial dependence of the phase has the general structure

$$g(x, t) = \phi(x - vt) + \chi(t), \quad (5.21)$$

with unknown functions ϕ and χ .

5.2.2 Asymptotic form of the solitons

To explore the tails of the solitonic states $\pi_t(x)$ let us consider the form of (5.5) for asymptotically large positions. For this purpose, note that the convolution $|\psi_t|^2 * \hat{G}(x)$ vanishes in the limit $|x| \rightarrow \infty$. It follows that Eq. (5.5) becomes

$$\partial_t \psi_t(x) \sim -\frac{\hbar}{2mi} \partial_x^2 \psi_t(x) - \gamma a_\psi \psi_t(x), \quad \text{for } |x| \rightarrow \infty, \quad (5.22)$$

with

$$a_\psi \equiv \int_{-\infty}^{\infty} dy |\psi_t|^2(y) \left(|\psi_t|^2 * \hat{G} \right)(y), \quad (5.23)$$

a ψ -dependent, positive constant. Inserting the solitonic form (5.15) into (5.22) yields

$$\begin{aligned} i\partial_t g(x, t) f(x - vt) &= i\frac{\hbar}{2m} \left[\partial_x^2 f(x - vt) - f(x - vt) (\partial_x g(x, t))^2 \right] \\ &\quad + v f(x - vt) - \frac{\hbar}{m} [\partial_x f(x - vt) \partial_x g(x, t) \\ &\quad + f(x - vt) \partial_x^2 g(x, t)] - \gamma a_\psi f(x - vt). \end{aligned} \quad (5.24)$$

Using (5.21), we find that both $\partial_x g(x, t)$ and $\partial_x^2 g(x, t)$ are only a function of $x_t = x - vt$, and accordingly, that also the left hand side of (5.24) must be a function of x_t . It follows that $\chi(t)$ is at most linear in t (that is $\chi(t) = \chi_1 t + \chi_0$, with unknown constants χ_0 and χ_1). Regarding the real and imaginary part of (5.24) separately, one obtains two coupled (second order) differential equations

$$v\partial_x f - \gamma a_\psi f = \frac{\hbar}{m} \left(\partial_x f \partial_x \phi + \frac{1}{2} f \partial_x^2 \phi \right), \quad (5.25)$$

$$(\chi_1 - v\partial_x \phi) f = \frac{\hbar}{2m} \left(\partial_x^2 f - f [\partial_x \phi]^2 \right), \quad (5.26)$$

where $f \equiv f(x - vt)$ and $\phi \equiv \phi(x - vt)$. This set of equations has two unique solutions

$$f(x) = e^{\pm k|x|}, \quad (5.27)$$

$$\phi(x) = \mp \text{sgn}(x) \frac{m}{\hbar} \left(v + \frac{\gamma a_\psi}{k} \right) x, \quad (5.28)$$

where the constant $k > 0$ depends on the boundary condition for (5.25) (which can be determined only by solving the full nonlinear equation (5.5)). The solution

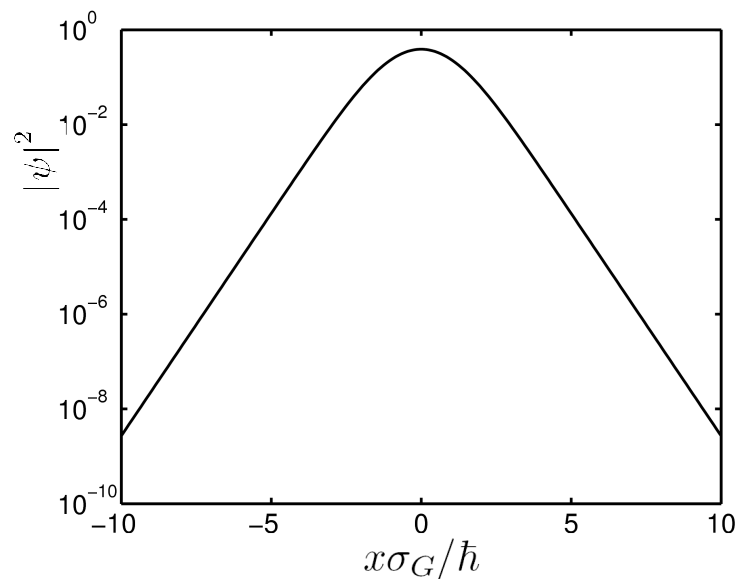


Figure 5.4: Semi-logarithmic plot of the numerical solitonic solution of (5.14). The graph clearly demonstrates that the pointer states have exponential tails.

with the positive exponent in (5.27) is irrelevant, since it is not normalizable. Figure 5.4 confirms that the tails of the numerically obtained solitonic solutions of (5.14) are in agreement with the functional form (5.27); they are straight lines in the semi-logarithmic plot. This shows that, unlike in linear models [9] where the pointer states are Gaussian, the pointer states of collisional decoherence are exponentially localized.

5.2.3 Size of the solitons

An important characteristic of the pointer states is their spatial extension. As explained in Sect. 5.4, the latter can be related to the experimentally accessible one-particle coherence length of a thermal gas. We will determine the pointer width in this section, and apply the result later, when studying the dynamics of pointer states in an external potential.

As a first step, consider the standard deviation $\tilde{\sigma}_\pi$ of the numerically obtained dimensionless solitonic solution $|\tilde{\pi}(y)|^2$ of (5.14) as a function of the dimensionless parameter $\kappa = \sigma_G^2 / (\gamma m \hbar)$. As shown by the solid line in Fig. 5.5, the size $\tilde{\sigma}_\pi$ increases linearly with κ over a wide range of this parameter.

This observation can be reproduced by a simplified model which has the practical advantage that it can be applied to more involved situations, such as 3D gases with a microscopically realistic localization rate F , see Sect. 5.4. The idea of the model goes as follows: the ideal gas environment consists of particles which collide with the system at a rate γ . At each collision, the ambient particles gain position information, so that the wave function becomes spatially localized to a length scale ℓ_{loc} determined by the localization rate F , see Eq. (3.50). After the scattering event, the particle disperses freely, until it becomes localized again by a subsequent collision. The approximate pointer width σ_π is then obtained by averaging the time-dependent width of the wave function over the waiting-time

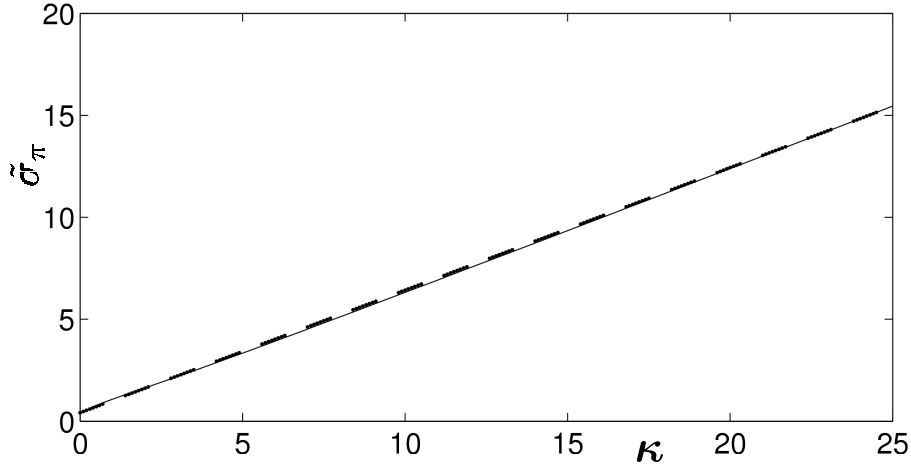


Figure 5.5: Spatial extension of the solitonic solution of (5.14) as a function of the dimensionless parameter $\kappa = \sigma_G^2 / (\gamma m \hbar)$. The solid line represents the numerical solution of (5.14). The result of the localization model (5.36) with parameter $a_{\text{loc}} = 0.42$ is given by the dashed line.

distribution of a Poisson process.

More specifically, it is assumed that the length scale ℓ_{loc} is characterized by the free parameter

$$a'_{\text{loc}} = \frac{F(\ell_{\text{loc}})}{F(\infty)}. \quad (5.29)$$

To evaluate this expression, we take the momentum transfer distribution $G(q)$ to be a centered Gaussian with variance σ_G^2 , see Eq. (5.12), which yields

$$F(x) = \gamma \left[1 - \exp\left(-\frac{\sigma_G^2}{2\hbar^2} x^2\right) \right], \quad (5.30)$$

where the definition of F (3.50) and the expression (5.13) is used. It follows that the characteristic length scale ℓ_{loc} can be expressed as

$$\ell_{\text{loc}} = \frac{a_{\text{loc}} \hbar}{\sigma_G}, \quad (5.31)$$

with $a_{\text{loc}}^2 \equiv -2 \log(1 - a'_{\text{loc}})$. The free dispersion after the collision yields the time-dependent size

$$\sigma_\pi^2(t) = \left(\frac{\hbar t}{2m\ell_{\text{loc}}} \right)^2 + \ell_{\text{loc}}^2. \quad (5.32)$$

Upon averaging over the waiting-time distribution $\text{Prob}(t) = \gamma e^{-\gamma t}$, one obtains

$$\sigma_\pi \equiv \int_0^\infty d\tau \text{Prob}(\tau) \frac{1}{\tau} \int_0^\tau dt \sigma_\pi(t). \quad (5.33)$$

$$\simeq \ell_{\text{loc}} + \frac{\hbar}{4m\gamma\ell_{\text{loc}}}, \quad (5.34)$$

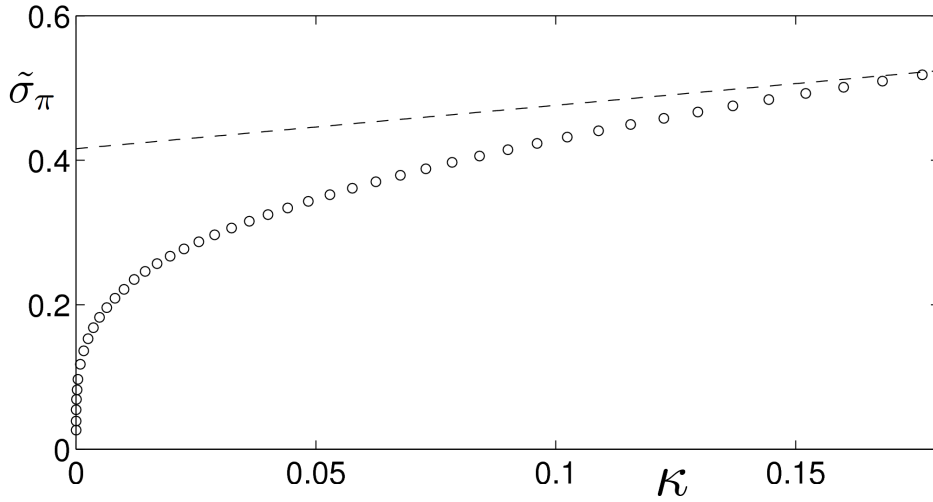


Figure 5.6: Similar to Fig. 5.5, but for small κ 's. The circles represent the numerical solution of (5.14) and the result of the localization model (5.36) with parameter $a_{\text{loc}} = 0.42$ is given by the dashed line. The plot indicates that the solitonic width tends to zero (5.14) for $\kappa \rightarrow 0$.

where we use a linearization of $\sigma_\pi(t)$ in the second line. Finally, by inserting the expression for the localization length scale (5.31), we find

$$\sigma_\pi = a_{\text{loc}} \frac{\hbar}{\sigma_G} + \frac{\sigma_G}{4a_{\text{loc}}m\gamma}. \quad (5.35)$$

The dimensionless version of (5.35) reads

$$\begin{aligned} \tilde{\sigma}_\pi &\equiv \frac{\sigma_\pi \sigma_G}{\hbar} \\ &= a_{\text{loc}} + \frac{1}{4a_{\text{loc}}} \kappa. \end{aligned} \quad (5.36)$$

The dashed line in Figure 5.5 shows the fit of (5.36) to the numerical solution of (5.14), as represented by the solid line. This fit yields a value of $a_{\text{loc}} \simeq 0.4$.

Limit $\kappa \rightarrow 0$ It should be mentioned that the localization model leads to incorrect results for small values of κ . This is visualized in Fig. 5.6, which shows the dimensionless width $\tilde{\sigma}_\pi$ as a function of κ in the regime $\kappa \in [0, 0.2]$. Here the circles were obtained from the numerical solution of (5.14), while the dashed line shows the prediction of the localization model.

Figure 5.6 indicates that the numerical result tends to zero for small κ 's. This behaviour can be explained by writing Eq. (5.14) as

$$\begin{aligned} \partial_\tau |\varphi_\tau(y)|^2 &= 2 |\varphi_\tau(y)|^2 \left(\int_{-\infty}^{\infty} dy' |\varphi_\tau(y')|^2 e^{-(y-y')/2} \right. \\ &\quad \left. - \int_{\mathbb{R}^2} dy' dy'' |\varphi_\tau(y')|^2 |\varphi_\tau(y'')|^2 e^{-(y'-y'')/2} \right), \quad \text{for } \kappa \rightarrow 0. \end{aligned} \quad (5.37)$$

This equation has delta functions, $|\pi_\tau(y)|^2 = \delta(y - y_0)$, as stationary solutions (meaning that $\partial_\tau |\pi_\tau(y)|^2 = 0$), which implies that the solitonic size vanishes for $\kappa = 0$.

The localization model, on the other hand, predicts a finite solitonic width $\sigma_\pi = \ell_{\text{loc}}$ for $\kappa = 0$. To explain this, recall that the model assumes that the wave function gets localized to the localization length scale ℓ_{loc} at each collision. Thus, in the limit of infinitely large collision rates ($\gamma \rightarrow \infty$ or $\kappa \rightarrow 0$) the width is equal to the characteristic length scale, $\sigma_\pi = \ell_{\text{loc}}$. It follows that the localization model is not reliable in this regime.

5.2.4 Completeness of the soliton basis

Our next aim is to show that the solitonic solutions of (5.5), which are interpreted as the pointer states of collisional decoherence, form an overcomplete basis. For this purpose, we first present a general method to construct a manifold of solutions of (4.42) given a specific one. It relies on the symmetry properties of the corresponding master equation. Since collisional decoherence exhibits Galilean (that is translation and boost) invariance, it is then easy to show that the pointer states of this model form an overcomplete basis.

Suppose there is a family of unitary operators U_t , satisfying

$$U_t \mathcal{D}(\rho) U_t^\dagger = \mathcal{D}(U_t \rho U_t^\dagger), \quad (5.38)$$

$$\partial_t U_t = \frac{1}{i\hbar} [H, U_t], \quad (5.39)$$

where \mathcal{D} denotes the incoherent part of the master equation, $\mathcal{L}(\rho) \equiv [H, \rho] / (i\hbar) + \mathcal{D}(\rho)$. Then, given a solution P_t of the nonlinear equation (4.42), also $U_t P_t U_t^\dagger$ constitutes a solution of (4.42).

This can be verified easily:

$$\begin{aligned} \left[U P U^\dagger, \left[U P U^\dagger, \mathcal{L}(U P U^\dagger) \right] \right] &= \frac{1}{i\hbar} \left(H U P U^\dagger - U P U^\dagger H \right) + U [P, [P, \mathcal{D}(P)]] U^\dagger \\ &= \frac{1}{i\hbar} (H U P U^\dagger - U P U^\dagger H + U H P U^\dagger - U H P U^\dagger \\ &\quad + U P H U^\dagger - U P H U^\dagger) + U [P, [P, \mathcal{D}(P)]] U^\dagger, \end{aligned} \quad (5.40)$$

where the time argument is dropped for brevity. Here, the first equality makes use of (5.38) and the unitarity of U . The above expression can be further simplified using the relation $[H, P] = [P, [P, [H, P]]]$, which yields

$$\begin{aligned} &\left[U P U^\dagger, \left[U P U^\dagger, \mathcal{L}(U P U^\dagger) \right] \right] \\ &= \frac{1}{i\hbar} [H, U] P U^\dagger + U \left[P, \left[P, \frac{1}{i\hbar} [H, P] + \mathcal{D}(P) \right] \right] U^\dagger - \frac{1}{i\hbar} U P [U^\dagger, H] \\ &= \partial_t (U P U^\dagger), \end{aligned} \quad (5.41)$$

where (4.42) and (5.39) is used in the third line.

Let us now apply this to the Galilean invariance of collisional decoherence; the latter being described by the master equation (3.47). We will see that the phase space translations

$$U_t \equiv T_{s,u} = \exp\left(\frac{i}{\hbar} [u_t x - s_t p]\right), \quad (5.42)$$

satisfy the symmetry conditions (5.38) and (5.39) provided the time dependence of s_t and u_t has the particular form

$$s_t = u_0 t/m + s_0, \quad (5.43)$$

$$u_t = u_0. \quad (5.44)$$

The latter enact a phase space translation in accordance with the free shearing motion.

Let us first verify condition (5.38):

$$\begin{aligned} \mathbb{T}_{s,u} \mathcal{D}(\rho) \mathbb{T}_{s,u}^\dagger &= \gamma \int_{-\infty}^{\infty} dq G(q) \mathbb{T}_{s,u} e^{iqx/\hbar} \rho e^{-iqx/\hbar} \mathbb{T}_{s,u}^\dagger - \gamma \mathbb{T}_{s,u} \rho \mathbb{T}_{s,u}^\dagger \\ &= \gamma \int_{-\infty}^{\infty} dq G(q) \mathbb{T}_{s,u} e^{iqx/\hbar} \mathbb{T}_{s,u}^\dagger \mathbb{T}_{s,u} \rho \mathbb{T}_{s,u}^\dagger \mathbb{T}_{s,u} e^{-iqx/\hbar} \mathbb{T}_{s,u}^\dagger \\ &\quad - \gamma \mathbb{T}_{s,u} \rho \mathbb{T}_{s,u}^\dagger. \end{aligned} \quad (5.45)$$

Since phase space translation operators satisfy $\mathbb{T}_{s,u} f(x) \mathbb{T}_{s,u}^\dagger = f(x-s)$ for any function f , one finds

$$\begin{aligned} \mathbb{T}_{s,u} \mathcal{D}(\rho) \mathbb{T}_{s,u}^\dagger &= \gamma \int_{-\infty}^{\infty} dq G(q) e^{iq(x-s)/\hbar} \mathbb{T}_{s,u} \rho \mathbb{T}_{s,u}^\dagger e^{-iq(x-s)/\hbar} - \gamma \mathbb{T}_{s,u} \rho \mathbb{T}_{s,u}^\dagger \\ &= \mathcal{D}(\mathbb{T}_{s,u} \rho \mathbb{T}_{s,u}^\dagger), \end{aligned} \quad (5.46)$$

which confirms condition (5.38). In order to verify (5.39), use the Campbell-Hausdorff formula to rewrite the translation operator (5.42) as

$$\begin{aligned} \mathbb{T}_{s,u} &= \exp\left(\frac{i}{\hbar} u_t x\right) \exp\left(-\frac{i}{\hbar} s_t p\right) \exp\left(-\frac{1}{2} \left[\frac{i}{\hbar} u_t x, -\frac{i}{\hbar} s_t p\right]\right) \\ &= \exp\left(\frac{i}{\hbar} u_t x\right) \exp\left(-\frac{i}{\hbar} s_t p\right) \exp\left(-\frac{i}{2\hbar} s_t u_t\right). \end{aligned} \quad (5.47)$$

The time derivative thus yields

$$\begin{aligned} \partial_t \mathbb{T}_{s,u} &= \frac{i}{\hbar} \left(\dot{u}_t \mathbb{T}_{s,u} - \dot{s}_t \mathbb{T}_{s,u} p - \frac{1}{2} (\dot{u}_t s_t + \dot{s}_t u_t) \mathbb{T}_{s,u} \right) \\ &= \frac{i}{\hbar} \left(-\frac{u_t}{m} \mathbb{T}_{s,u} p - \frac{u_t^2}{2m} \mathbb{T}_{s,u} \right) \\ &= \frac{1}{i\hbar} \left[\frac{p^2}{2m}, \mathbb{T}_{s,u} \right], \end{aligned} \quad (5.48)$$

where the shearing transformation (5.43) and (5.44) is required in the second line. This confirms (5.39) for $H = p^2/2m$.

In conclusion, the nonlinear equation (5.5) exhibits a family of solitonic solutions $P_\Gamma = \mathbb{T}_{s,u} P \mathbb{T}_{s,u}^\dagger$, parameterized by the phase space coordinate $\Gamma = (s_0, u_0)$. In order to verify that this family forms an overcomplete basis, let us consider a specific class of phase space representations. According to [61], any Hilbert-Schmidt operator A can be represented as

$$A = \int d\Gamma A(\Gamma) \mathbb{T}_{s,u} Q \mathbb{T}_{s,u}^\dagger, \quad (5.49)$$

provided \mathbf{Q} is a trace-class operator, meaning that

$$0 < \text{Tr} \left(\sqrt{\mathbf{Q}^\dagger \mathbf{Q}} \right) < \infty. \quad (5.50)$$

Here, $\int d\Gamma \cdot$ denotes a phase space integral and $A(\Gamma)$ is a function of the phase space coordinate Γ . Choosing for \mathbf{A} the identity \mathbf{I} , and for \mathbf{Q} the solitonic solution $\mathbf{P}_{0,0}$ of (5.5) with vanishing position and momentum expectations, one obtains a resolution of the identity in terms of the solitons $\mathbf{P}_\Gamma = \mathbf{T}_{s,u} \mathbf{P}_{0,0} \mathbf{T}_{s,u}^\dagger$,

$$\mathbf{I} = \int d\Gamma I(\Gamma) \mathbf{P}_\Gamma. \quad (5.51)$$

This demonstrates that the pointer states of collisional decoherence form an over-complete basis.

5.3 Dynamics in an external potential

So far, we have characterized the solitonic solutions of the nonlinear equation (5.5) which applies in the absence of an external force. If an additional potential is present the corresponding nonlinear equation contains an additional term $V(x)/(i\hbar)$ on the right-hand side of (5.5). The numerical treatment shows that the solutions still converge to localized wave packets, which, however, change their shape and velocity in the course of the evolution. It is found that the center of these wave packets moves on the corresponding classical phase space trajectory in the case of large collision rates. We first summarize our numerical findings and then proceed with an analytic explanation.

Figure 5.7 shows the position and momentum expectation values of the numerical solution of the nonlinear equation, in case of an anharmonic external potential of the form

$$V(x) = ax^4 - bx^2, \quad \text{with } a, b > 0, \quad (5.52)$$

starting from an Gaussian initial state. The panel on the left hand side of Fig. 5.7 was obtained in the limit of a vanishing collision rate γ (i.e. $\kappa \rightarrow \infty$), which turns (5.14) into the Schrödinger equation. The solution therefore disperses, and the solid line shows a typical evolution of the phase space expectation values. The dashed line, on the other hand, gives the classical trajectory of the phase space point where the initial state is localized. The result for a large collision rate γ (or small κ) is shown on the right-hand side of Fig. 5.7. Here, the initial state turns rapidly into a soliton whose expectation values move on the corresponding classical trajectory. This illustrates that the time evolution turns from quantum to classical dynamics with increasing collision rate γ (decreasing κ). Similar observations were made with various other potentials.

In order to explain the numerical observation, first consider a particle in a linear potential $V(x) = \alpha x$. The corresponding nonlinear equation reads as

$$\begin{aligned} \partial_t \psi_t(x) + \frac{\hbar}{2mi} \partial_x^2 \psi_t(x) &= \frac{1}{i\hbar} \alpha x \psi_t(x) + \gamma \psi_t(x) \left(|\psi_t|^2 * \tilde{G}(x) \right. \\ &\quad \left. - \int_{-\infty}^{\infty} dy |\psi_t|^2(y) \left(|\psi_t|^2 * \hat{G} \right)(y) \right). \end{aligned} \quad (5.53)$$

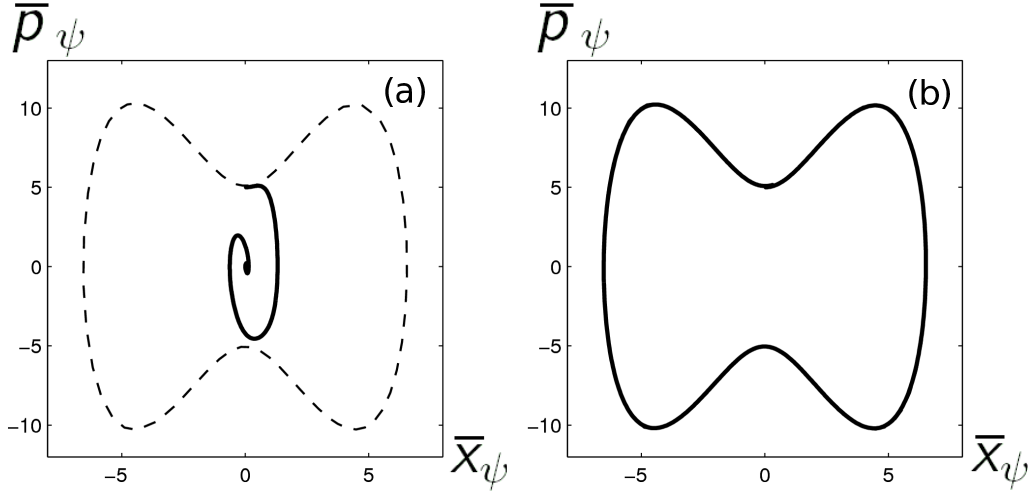


Figure 5.7: Time evolution of pointer states in an anharmonic potential (solid line). The dashed line shows the corresponding classical phase space trajectory. (a) The collision rate γ vanishes leading to dispersive quantum dynamics. (b) The collision rate γ is large, so that the dynamics of the pointer state is indistinguishable from the classical trajectory.

As discussed in Sect. 5.2.1, Eqs. (5.15) and (5.21), the field-free version of this equation ($\alpha = 0$) exhibits uniformly moving solitonic solutions of the form

$$\psi_t(x) = f(x - vt) \exp(i[\phi(x - vt) + \chi(t)]) . \quad (5.54)$$

This implies that (5.53) has solitonic solutions of the form

$$\psi_t(x) = f(x - x_t) \exp(ig(x - x_t, t)) , \quad (5.55)$$

$$g(x, t) = \phi(x) + \chi'(t) - \frac{\alpha}{\hbar} tx , \quad (5.56)$$

which are uniformly *accelerated*, $x_t = vt - \alpha t^2/2m$. The time-dependent phase $\chi'(t)$ in (5.56) is given by the expression

$$\chi'(t) = \chi(t) - \frac{2\alpha}{\hbar} \int_0^t d\tau x_\tau . \quad (5.57)$$

In order to verify this statement, we evaluate the left-hand side of (5.53) with the ansatz given by (5.55). This yields

$$\begin{aligned} \partial_t \psi_t(x) + \frac{\hbar}{2mi} \partial_x^2 \psi_t(x) &= e^{ig} \left(\frac{\alpha}{i\hbar} x f + i f \partial_t \chi'(t) + \frac{2\alpha}{\hbar} i x_t f - v (\partial_x f + i f \partial_x \phi) \right. \\ &\quad \left. + \frac{\hbar}{m} \left(\partial_x f \partial_x \phi - \frac{i}{2} \partial_x^2 f + \frac{i}{2} f (\partial_x \phi)^2 + \frac{1}{2} f \partial_x^2 \phi \right) \right) , \end{aligned} \quad (5.58)$$

with $g \equiv g(x - x_t, t)$, $f \equiv f(x - x_t)$ and $\phi \equiv \phi(x - x_t)$. The expression can be further simplified by noting that the free soliton (5.54) is a solution of the

field-free version of (5.53), implying that

$$\begin{aligned} \gamma f \Lambda [f^2] (x) &= i f \partial_t \chi (t) - v (\partial_x f + i f \partial_x \phi) \\ &\quad + \frac{\hbar}{m} \left(\partial_x f \partial_x \phi - \frac{i}{2} \partial_x^2 f + \frac{i}{2} f (\partial_x \phi)^2 + \frac{1}{2} f \partial_x^2 \phi \right), \end{aligned} \quad (5.59)$$

with $\Lambda [f^2] (x)$ defined in (5.6). Using (5.58), (5.59) and the definition of $\chi' (t)$, see Eq. (5.57), one finds that

$$\partial_t \psi_t (x) + \frac{\hbar}{2mi} \partial_x^2 \psi_t (x) = \frac{1}{i\hbar} \alpha x \psi_t (x) + \gamma \psi_t (x) \Lambda [|\psi_t|^2] (x), \quad (5.60)$$

which confirms that $\psi_t (x)$ evolves according to (5.53).

We conclude that in a linear potential the pointer states have the same shape as in the field-free case and they are uniformly accelerated like a classical particle. For general potentials, this implies that the pointer states follow the corresponding classical motion, provided the spatial width of the solitons is sufficiently small, so that the linearization of the potential is justified over their spatial extension. Since the size of the pointer states decreases with the collision rate (see Section 5.2.3), the pointer states must exhibit classical dynamics in the limit of large collision rates.

5.4 Extensions to 3D

The above results apply to the one-dimensional motion of a tracer particle in a gaseous environment. Clearly, the connection of these results to realistic experiments requires their extension to the three-dimensional situation. The nonlinear equation (5.5) itself is trivially extended to 3D, though their numerical treatment is then more difficult. However, the localization model introduced in Sect. 5.2.3 allows one to directly estimate the 3D pointer width. As we shall see below, the latter admits the derivation of the coherence length of an interacting gas. Using the microscopic definition of the localization rate F (3.52), one can tailor this method to all kinds of realistic interacting gases (specified by the velocity distribution $\mu (v)$, its density n_{gas} and the elastic scattering amplitude $f (\mathbf{p}_f, \mathbf{p}_i)$).

Let us illustrate this method for the case of *s-wave hard-sphere scattering* [62] off a thermal gas with Maxwell-Boltzmann velocity distribution (3.54). Here the scattering length [52] is equal to the radius R of the particles, so that the scattering amplitude is independent of the scattering angle θ and the energy of the incoming particles E_{kin} , that is [62]

$$|f (\cos \theta; E_{\text{kin}})|^2 = R^2. \quad (5.61)$$

We shall first estimate the characteristic length scale ℓ_{loc} for this particular setting, see Sect. 5.4.1. This allows us to derive the 3D pointer width in Sect. 5.4.2. The determination of the coherence length follows in Sect. 5.4.3.

5.4.1 Estimation of the localization length scale

According to Eq. (5.29), the localization length scale ℓ_{loc} is characterized by the free parameter $a'_{\text{loc}} = F (\ell_{\text{loc}}) / F (\infty)$, with F the localization rate (3.52). Equa-

tions (5.29), (3.52) and (5.61) together with $F(\infty) = \gamma$ imply that

$$\gamma a'_{\text{loc}} = \gamma - 2\pi n_{\text{gas}} R^2 \int_0^\infty dv \mu(v) v \int_{-1}^1 d \cos \theta \text{sinc} \left[2 \sin \left(\frac{\theta}{2} \right) \frac{mv}{\hbar} \ell_{\text{loc}} \right]. \quad (5.62)$$

The integral on the right-hand side can easily be evaluated [63], which gives

$$\begin{aligned} \gamma (1 - a'_{\text{loc}}) &= 4\pi n_{\text{gas}} R^2 \int_0^\infty dv \mu(v) v \text{sinc}^2 \left(\frac{mv}{\hbar} \ell_{\text{loc}} \right) \\ &\equiv 4\pi n_{\text{gas}} R^2 \langle v \text{sinc}^2 (mv \ell_{\text{loc}} / \hbar) \rangle_{\text{th}}, \end{aligned} \quad (5.63)$$

with $\langle \cdot \rangle_{\text{th}}$ the thermal average.

To evaluate Eq. (5.63), let us first calculate the average collision rate γ using Eq. (3.53). Since the scattering amplitude is constant (5.61), the total cross section reads as

$$\sigma_{\text{tot}}(mv) = 4\pi R^2. \quad (5.64)$$

By combining Eqs. (3.53) and (5.64), we find

$$\begin{aligned} \gamma &= 4\pi n_{\text{gas}} R^2 \int_0^\infty dv \mu(v) v \\ &\equiv 4\pi n_{\text{gas}} R^2 \langle v \rangle_{\text{th}}. \end{aligned} \quad (5.65)$$

The mean velocity $\langle v \rangle_{\text{th}}$ is easily obtained by using the Maxwell-Boltzmann distribution (3.54), which yields

$$\langle v \rangle_{\text{th}} = \sqrt{\frac{8kT}{\pi m}} = \frac{4\hbar}{\Lambda_{\text{th}} m}, \quad (5.66)$$

a result that can also be found in standard textbooks, such as [64]. The average collision rate therefore reads

$$\gamma = 16\pi n_{\text{gas}} R^2 \hbar (\Lambda_{\text{th}} m)^{-1}. \quad (5.67)$$

As a next step, let us estimate the thermal average on the right-hand side of Eq. (5.63). Upon inserting the Maxwell Boltzmann distribution (3.54), one obtains

$$\begin{aligned} &\langle v \text{sinc}^2 (mv \ell_{\text{loc}} / \hbar) \rangle_{\text{th}} \quad (5.68) \\ &= 4\pi \left(\frac{m}{2\pi kT} \right)^{3/2} \left(\frac{\hbar}{m \ell_{\text{loc}}} \right)^2 \int_0^\infty dv v \exp \left(-\frac{mv^2}{2kT} \right) \sin^2 \left(\frac{mv \ell_{\text{loc}}}{\hbar} \right). \end{aligned}$$

By introducing the dimensionless quantities $x^2 \equiv mv^2 / (2kT)$ and $\xi_{\text{loc}} \equiv \ell_{\text{loc}} / \Lambda_{\text{th}}$, Eq. (5.68) becomes

$$\langle v \text{sinc}^2 (mv \ell_{\text{loc}} / \hbar) \rangle_{\text{th}} = \frac{2\Lambda_{\text{th}} \hbar}{\pi m \ell_{\text{loc}}^2} \int_0^\infty dx x e^{-x^2} \sin^2 (2\sqrt{\pi} x \xi_{\text{loc}}). \quad (5.69)$$

The integral on the right-hand side of this equation can be evaluated analytically [63], which yields

$$\langle v \text{sinc}^2 (mv \ell_{\text{loc}} / \hbar) \rangle_{\text{th}} = \frac{\hbar \Lambda_{\text{th}} \xi_{\text{loc}}}{m \ell_{\text{loc}}^2} \exp(-4\pi \xi_{\text{loc}}^2) \text{erfi}(2\sqrt{\pi} \xi_{\text{loc}}). \quad (5.70)$$

Here $\operatorname{erfi}(\cdot)$ denotes the *imaginary error function*, which is defined as

$$\operatorname{erfi}(z) \equiv -i \operatorname{erf}(iz). \quad (5.71)$$

Finally, by combining Eqs. (5.63), (5.67) and (5.70), we find an analytic expression for the characteristic length scale,

$$\xi_{\text{loc}} = \frac{1}{4(1 - a'_{\text{loc}})} \exp(-4\pi\xi_{\text{loc}}^2) \operatorname{erfi}(2\sqrt{\pi}\xi_{\text{loc}}). \quad (5.72)$$

Using the definition of a'_{loc} this equation becomes

$$\xi_{\text{loc}} = \frac{1}{4} \exp\left(\frac{a_{\text{loc}}^2}{2} - 4\pi\xi_{\text{loc}}^2\right) \operatorname{erfi}(2\sqrt{\pi}\xi_{\text{loc}}). \quad (5.73)$$

The numerical solution of this relation yields $\xi_{\text{loc}} \simeq 0.1$ if we assume $a_{\text{loc}} \simeq 0.4$ as in Sect. 5.2.3.

5.4.2 Estimation of the pointer size

As you may recall from Sect. 5.2.3, the localization model assumes that scattering events occurring with rate γ localize the wave function to the length scale ℓ_{loc} , while it disperses freely between the collisions. Averaging the wave function width over the waiting-time distribution of a Poissonian process then yields Eq. (5.34), a relation between ℓ_{loc} and the pointer state position spread σ_π . By combining Eqs. (5.34) and (5.67) together with $\ell_{\text{loc}} = \xi_{\text{loc}}\Lambda_{\text{th}}$ one obtains an expression for the 3D pointer width,

$$\sigma_\pi = \xi_{\text{loc}}\Lambda_{\text{th}} + \frac{1}{4\xi_{\text{loc}}16\pi n_{\text{gas}}R^2}, \quad (5.74)$$

which connects σ_π with the microscopic details of the open system. This formula can be further simplified by introducing the mean free path [64]

$$\ell_{\text{free}} = \frac{1}{n_{\text{gas}}\sigma_{\text{tot}}} = \frac{1}{n_{\text{gas}}4\pi R^2}, \quad (5.75)$$

which yields

$$\sigma_\pi = \xi_{\text{loc}}\Lambda_{\text{th}} + \frac{\ell_{\text{free}}}{16\xi_{\text{loc}}}. \quad (5.76)$$

For a weakly interacting or thin gas, the pointer state width is thus essentially determined by the mean free path, that is

$$\sigma_\pi = \frac{1}{16\xi_{\text{loc}}}\ell_{\text{free}}, \quad \text{for } \Lambda_{\text{th}} \ll \ell_{\text{free}}. \quad (5.77)$$

In the limit of a strongly interacting or dense gas, on the other hand, it is bounded by the scale of the thermal wave length, meaning that

$$\sigma_\pi = \xi_{\text{loc}}\Lambda_{\text{th}}, \quad \text{for } \Lambda_{\text{th}} \gg \ell_{\text{free}}. \quad (5.78)$$

5.4.3 Determining the coherence length

Let us now use the above results to access the coherence length Λ_{coh} of a self-interacting gas. The latter is defined [3] by the decay of the position off-diagonal elements of the reduced single particle gas state ρ_{gas} ,

$$\langle \mathbf{r} | \rho_{\text{gas}} | \mathbf{r}' \rangle \propto \exp \left(-\pi \frac{|\mathbf{r} - \mathbf{r}'|^2}{\Lambda_{\text{coh}}^2} \right). \quad (5.79)$$

To characterize the thermal state of a particle in presence of the interacting gas, we use the definition of the pointer basis (4.12), and take the pointer states momenta to be Maxwell distributed, that is

$$\mu(\mathbf{p}) = \frac{1}{(2\pi mkT)^{3/2}} \exp \left(-\frac{|\mathbf{p}|^2}{2mkT} \right). \quad (5.80)$$

Moreover, we let the particles be confined to the region $\Omega \subset \mathbb{R}^3$, which yields

$$\rho_{\text{gas}} = \frac{1}{\Omega} \int_{\Omega} \int_{\mathbb{R}^3} d\mathbf{x} d\mathbf{p} \mu(\mathbf{p}) |\pi_{\mathbf{x}, \mathbf{p}}\rangle \langle \pi_{\mathbf{x}, \mathbf{p}}|, \quad (5.81)$$

with $|\pi_{\mathbf{x}, \mathbf{p}}\rangle$ the corresponding pointer states; here \mathbf{x} and \mathbf{p} denote the mean position and velocity of $|\pi_{\mathbf{x}, \mathbf{p}}\rangle$, respectively. To evaluate the position representation of (5.81), assume the pointer states to be coherent states [65],

$$\langle \mathbf{r} | \pi_{\mathbf{x}, \mathbf{p}} \rangle = \frac{1}{(2\pi\sigma_{\pi}^2)^{3/4}} \exp \left(-\frac{|\mathbf{r} - \mathbf{x}|^2}{4\sigma_{\pi}^2} + \frac{i}{\hbar} \mathbf{p} \cdot \mathbf{r} \right), \quad (5.82)$$

where the position spread is given by (5.76). The matrix elements of the pointer states thus read as

$$\begin{aligned} & \langle \mathbf{r} | \pi_{\mathbf{x}, \mathbf{p}} \rangle \langle \pi_{\mathbf{x}, \mathbf{p}} | \mathbf{r}' \rangle \\ &= \frac{1}{(2\pi)^{3/2} \sigma_{\pi}} \exp \left(-\frac{1}{4\sigma_{\pi}^2} \left[|\mathbf{r} - \mathbf{x}|^2 + |\mathbf{r}' - \mathbf{x}|^2 \right] + \frac{i}{\hbar} \mathbf{p} \cdot [\mathbf{r} - \mathbf{r}'] \right). \end{aligned} \quad (5.83)$$

This implies that the position representation of the reduced gas state, $\rho_{\text{gas}}(\mathbf{r}, \mathbf{r}') \equiv \langle \mathbf{r} | \rho_{\text{gas}} | \mathbf{r}' \rangle$, is given by

$$\begin{aligned} \rho_{\text{gas}}(\mathbf{r}, \mathbf{r}') &= \frac{1}{(2\pi)^{3/2} \sigma_{\pi} \Omega} \int_{\Omega} d\mathbf{x} \exp \left(-\frac{1}{4\sigma_{\pi}^2} \left[|\mathbf{r} - \mathbf{x}|^2 + |\mathbf{r}' - \mathbf{x}|^2 \right] \right) \\ &\quad \times \int_{\mathbb{R}^3} d\mathbf{p} \mu(\mathbf{p}) \exp \left(\frac{i}{\hbar} \mathbf{p} \cdot [\mathbf{r} - \mathbf{r}'] \right). \end{aligned} \quad (5.84)$$

The Fourier transform of the Maxwell distribution can easily be evaluated, which yields

$$\begin{aligned} \rho_{\text{gas}}(\mathbf{r}, \mathbf{r}') &= \frac{1}{(2\pi)^{3/2} \sigma_{\pi} \Omega} \exp \left(-\pi \frac{|\mathbf{r} - \mathbf{r}'|^2}{\Lambda_{\text{th}}^2} \right) \\ &\quad \times \int_{\Omega} d\mathbf{x} \exp \left(-\frac{1}{4\sigma_{\pi}^2} \left[|\mathbf{r} - \mathbf{x}|^2 + |\mathbf{r}' - \mathbf{x}|^2 \right] \right). \end{aligned} \quad (5.85)$$

To evaluate the position integral, consider the limit $\Omega \rightarrow \mathbb{R}^3$, which gives

$$\begin{aligned} & \int_{\Omega} d\mathbf{x} \exp\left(-\frac{1}{4\sigma_{\pi}^2} \left[|\mathbf{r} - \mathbf{x}|^2 + |\mathbf{r}' - \mathbf{x}|^2\right]\right) \\ &= (2\pi\sigma_{\pi}^2)^{3/2} \exp\left(-\frac{|\mathbf{r} - \mathbf{r}'|^2}{8\sigma_{\pi}^2}\right), \quad \text{for } \Omega \rightarrow \mathbb{R}^3. \end{aligned} \quad (5.86)$$

The position representation of the reduced single particle gas state therefore reads

$$\rho_{\text{gas}}(\mathbf{r}, \mathbf{r}') = \frac{1}{\Omega} \exp\left(-\pi |\mathbf{r} - \mathbf{r}'|^2 \left[\frac{1}{\Lambda_{\text{th}}^2} + \frac{1}{8\pi\sigma_{\pi}^2}\right]\right). \quad (5.87)$$

Finally, by comparing this equation with the definition of the coherence length (5.79), we find

$$\frac{1}{\Lambda_{\text{coh}}^2} = \frac{1}{\Lambda_{\text{th}}^2} + \frac{1}{8\pi\sigma_{\pi}^2}. \quad (5.88)$$

The square of the coherence length is therefore determined by the harmonic mean of Λ_{th}^2 and $8\pi\sigma_{\pi}^2$. This intuitive result shows that the ideal coherence length, $\Lambda_{\text{coh}}(\ell_{\text{free}} \rightarrow \infty) = \Lambda_{\text{th}}$, is reduced by the interactions in the gas. Since σ_{π} is a function of the mean free path ℓ_{free} and the thermal wave length Λ_{th} , see Eq. (5.76), we have thus a means of computing the coherence length Λ_{coh} from the microscopic parameters.

Outlook The coherence length is a quantity that is in principle measurable in interference experiments [66, 67]. Equation (5.88) should therefore admit the experimental verification of the formalism used in this chapter. A detailed elaboration of such experimental tests, however, remains open for future investigations.

Another possible application of Eq. (5.88) (or of similar equations, that are derived from more realistic scattering amplitudes) is the prediction of the critical temperature of phase transitions, such as the Bose-Einstein condensation of interacting Bose systems. A textbook argument states that the condensation occurs whenever the coherence length Λ_{coh} is close to the mean particle distance $d \simeq 1/n_{\text{gas}}$. While this argument is typically used in the context of ideal Bose gases, it has also been applied in some articles [68, 69] to determine the critical temperature of interacting systems. Since Eq. (5.88) describes the temperature dependence of the coherence length of interacting gases, it might be applicable to such scenarios.

Chapter 6

Classical stochastic processes

Thus far, we have been concerned with the derivation of ‘candidate’ pointer states as the solitonic solutions of a nonlinear equation, and we have studied their properties and dynamics. Since our goal is to show that these states have all properties of a pointer basis, we proceed to relate this nonlinear equation to the deterministic parts of a class of stochastic processes in the space of pure quantum states. These processes, or “unravelings”, are designed such that their ensemble mean reproduces the solution of the master equation. Using this connection to the solution of the master equation, a complete picture of the emergence of the pointer basis will be obtained. In particular, this admits to show that the solitons mentioned above are genuine pointer states P_α in the sense of definition (4.12), and it allows one to calculate the probability distribution $\text{Prob}(\alpha|\rho_0)$ of the pointer states (with ρ_0 the initial state).

The concept of quantum stochastic processes is based on a variety of results from the classical theory of stochastic processes. We shall therefore give a survey of classical stochastic processes in this chapter; this discussion is based on the treatments in [29, 38, 70]. The introduction of quantum stochastic processes is postponed to the next chapter, such that readers familiar with classical stochastic processes may as well skip the present chapter.

6.1 Classical Markov processes

In many applications of dynamical systems, from Brownian motion to derivative pricing, one must account for sources of noise that make the time evolution probabilistic. A means of incorporating this randomness into the mathematical description of the dynamics is provided by the concept of *stochastic processes*. Technically speaking, a stochastic process is a one-parameter family of (possibly multivariate) random variables, \mathbf{X}_t , $t \in \mathbb{R}_0^+$. According to Kolmogorov’s existence theorem [71], it is completely characterized by the *family of finite joint probability distributions*

$$p(\mathbf{x}_1, t_1) , \tag{6.1}$$

$$p(\mathbf{x}_2, t_2; \mathbf{x}_1, t_1) , \tag{6.2}$$

$$\vdots$$

$$p(\mathbf{x}_n, t_n; \dots; \mathbf{x}_1, t_1) , \tag{6.3}$$

with \mathbf{x}_i a realization of \mathbf{X}_t at time $t = t_i$.

The complexity of this hierarchy of distributions can be reduced tremendously by applying the Markov assumption motivated in Sect. 2.2.2. The latter requires the conditional probability to be determined entirely by the most recent observation,

$$p(\mathbf{x}_n, t_n | \mathbf{x}_{n-1}, t_{n-1}; \dots; \mathbf{x}_1, t_1) = p(\mathbf{x}_n, t_n | \mathbf{x}_{n-1}, t_{n-1}), \quad (6.4)$$

where the times satisfy the ordering $t_n \geq t_{n-1} \geq \dots \geq t_1$. Under this assumption, one can construct the complete family of distributions by means of the propagator $p(\mathbf{x}_2, t_2 | \mathbf{x}_1, t_1)$ and the initial distribution $p(\mathbf{x}_0, t_0)$.

$$\begin{aligned} p(\mathbf{x}_n, t_n; \dots; \mathbf{x}_1, t_1) &= p(\mathbf{x}_n, t_n | \mathbf{x}_{n-1}, t_{n-1}) p(\mathbf{x}_{n-1}, t_{n-1} | \mathbf{x}_{n-2}, t_{n-2}) \dots \\ &\dots p(\mathbf{x}_1, t_1 | \mathbf{x}_0, t_0) p(\mathbf{x}_0, t_0). \end{aligned} \quad (6.5)$$

A characterization of the set of all Markov processes is obtained using the so-called *Chapman-Kolmogorov equation*. In order to derive this equation, let us consider the three-point distribution of a Markov process

$$p(\mathbf{x}_3, t_3; \mathbf{x}_2, t_2; \mathbf{x}_1, t_1) = p(\mathbf{x}_3, t_3 | \mathbf{x}_2, t_2) p(\mathbf{x}_2, t_2 | \mathbf{x}_1, t_1) p(\mathbf{x}_1, t_1). \quad (6.6)$$

Upon integrating over \mathbf{x}_2 , one obtains

$$p(\mathbf{x}_3, t_3; \mathbf{x}_1, t_1) = p(\mathbf{x}_1, t_1) \int d\mathbf{x}_2 p(\mathbf{x}_3, t_3 | \mathbf{x}_2, t_2) p(\mathbf{x}_2, t_2 | \mathbf{x}_1, t_1), \quad (6.7)$$

which immediately yields the Chapman-Kolmogorov equation in integral form

$$\begin{aligned} p(\mathbf{x}_3, t_3 | \mathbf{x}_1, t_1) &\equiv \frac{p(\mathbf{x}_3, t_3; \mathbf{x}_1, t_1)}{p(\mathbf{x}_1, t_1)} \\ &= \int d\mathbf{x}_2 p(\mathbf{x}_3, t_3 | \mathbf{x}_2, t_2) p(\mathbf{x}_2, t_2 | \mathbf{x}_1, t_1). \end{aligned} \quad (6.8)$$

The classification of Markov processes amounts to the classification of the solutions of this integral equation. For this purpose, it is useful to rewrite the Chapman-Kolmogorov equation in its differential form. Under rather weak conditions, one obtains the differential form of Eq. (6.8) [29, 38],

$$\begin{aligned} \partial_t p(\mathbf{x}, t | \mathbf{x}_0, t_0) &= - \sum_i \frac{\partial}{\partial x_i} [A_i(\mathbf{x}, t) p(\mathbf{x}, t | \mathbf{x}_0, t_0)] \\ &\quad + \sum_{i,j} \frac{1}{2} \frac{\partial^2}{\partial x_i \partial x_j} [B_{ij}(\mathbf{x}, t) p(\mathbf{x}, t | \mathbf{x}_0, t_0)] \\ &\quad + \int d\mathbf{y} [W(\mathbf{x} | \mathbf{y}, t) p(\mathbf{y}, t | \mathbf{x}_0, t_0) - W(\mathbf{y} | \mathbf{x}, t) p(\mathbf{x}, t | \mathbf{x}_0, t_0)], \end{aligned} \quad (6.9)$$

with positive semi-definite matrices $\mathbf{A}(\mathbf{x}, t)$, $\mathbf{B}(\mathbf{x}, t)$ and the non-negative rate $W(\mathbf{x} | \mathbf{y}, t)$.

The different summands on the right-hand side of (6.9) give rise to completely different types of solutions. In case that $\mathbf{B}(\mathbf{x}, t)$ and $W(\mathbf{x} | \mathbf{y}, t)$ vanish, one ends up with the *Liouville equation*,

$$\partial_t p(\mathbf{x}, t | \mathbf{x}_0, t_0) = - \sum_i \frac{\partial}{\partial x_i} [A_i(\mathbf{x}, t) p(\mathbf{x}, t | \mathbf{x}_0, t_0)], \quad (6.10)$$

so that the process is deterministic. Here $\mathbf{A}(\mathbf{x}, t)$ is known as the drift vector. If the second summand is also present, one obtains the *Fokker-Planck equation*

$$\begin{aligned} \partial_t p(\mathbf{x}, t | \mathbf{x}_0, t_0) &= - \sum_i \frac{\partial}{\partial x_i} [A_i(\mathbf{x}, t) p(\mathbf{x}, t | \mathbf{x}_0, t_0)] \\ &\quad + \sum_{i,j} \frac{1}{2} \frac{\partial^2}{\partial x_i \partial x_j} [B_{ij}(\mathbf{x}, t) p(\mathbf{x}, t | \mathbf{x}_0, t_0)] , \end{aligned} \quad (6.11)$$

which describes diffusion processes; $\mathbf{B}(\mathbf{x}, t)$ is referred to as the diffusion matrix. As we shall see below, realizations of the corresponding process are continuous but not differentiable.

A further class of processes arises when the rate $W(\mathbf{x} | \mathbf{y}, t)$ is non-zero and the diffusion matrix vanishes, implying that the differential Chapman-Kolmogorov equation (6.9) becomes

$$\begin{aligned} \partial_t p(\mathbf{x}, t | \mathbf{x}_0, t_0) &= - \sum_i \frac{\partial}{\partial x_i} [A_i(\mathbf{x}, t) p(\mathbf{x}, t | \mathbf{x}_0, t_0)] \\ &\quad + \int d\mathbf{y} [W(\mathbf{x} | \mathbf{y}, t) p(\mathbf{y}, t | \mathbf{x}_0, t_0) - W(\mathbf{y} | \mathbf{x}, t) p(\mathbf{x}, t | \mathbf{x}_0, t_0)] . \end{aligned} \quad (6.12)$$

This is the so-called *Liouville master equation*. It has an intuitive physical interpretation as a balance equation for the rate of change of the probability density. The first term in the second line of (6.12) describes the rate of increase of the probability density at \mathbf{x} due to jumps from other states \mathbf{y} into \mathbf{x} . The second term in the second line of (6.12) is the rate for the loss of probability due to jumps occurring out of the state \mathbf{x} . Thus, this equation describes piecewise deterministic processes, whose realizations consist of smooth deterministic parts which are interrupted by random jumps. The latter occur with a rate determined by the *jump rate* $W(\mathbf{x} | \mathbf{y}, t)$.

Needless to say, a general Markov process will consist of both diffusion and jump processes. Still, it is reasonable to treat them individually, since the formalisms used for their solutions are different. Let us therefore first discuss diffusion processes in Sect. 6.2 and then treat jump processes in Sect. 6.3.

As a final point, note that Eqs. (6.9) to (6.12) are valid also for the one-point probability density $p(\mathbf{x}, t)$, since the latter is obtained from the propagator by the integral

$$p(\mathbf{x}, t) = \int d\mathbf{x}_0 p(\mathbf{x}, t | \mathbf{x}_0, t) p(\mathbf{x}_0, t) . \quad (6.13)$$

However, the propagator is required for a complete specification of the process by means of Eq. (6.5).

6.2 Diffusion processes

As mentioned above, a diffusion process is a stochastic process described by the Fokker-Planck equation (6.11). Of course, the latter can be solved by standard numerical techniques such as finite element and finite difference methods [72]. However, let us follow here a different approach which relies on *stochastic differential equations* (SDEs). The idea is to consider an ensemble of sample paths

$\mathbf{x}_\alpha(t)$, $\alpha \in \{1, \dots, N\}$, such that upon averaging one recovers all expectation values of the process,

$$\mathbb{E}[f(\mathbf{X}_t)] = \frac{1}{N} \sum_{\alpha=1}^N f(\mathbf{x}_\alpha(t)), \quad (6.14)$$

with f an arbitrary function of \mathbf{X}_t . The ensemble of trajectories $\mathbf{x}_\alpha(t)$ is obtained as the solution of a SDE, that is, a differential equation where one or more of the terms are given by a stochastic process. In case of diffusion, these stochastic terms are proportional to the increments of the so-called *Wiener process*, which is the fundamental diffusion process corresponding to a unit diffusion matrix $B_{ij} = \delta_{ij}$ and a vanishing drift term. As such the Wiener process is the building block for the construction of all diffusion processes.

We shall therefore first define the Wiener process in Sect. 6.2.1. The following section is devoted to *stochastic integration*, that is to integration with respect to the Wiener process. This allows us to introduce the notion of stochastic differential equations in Sect. 6.2.3.

6.2.1 Wiener process

The Wiener process \mathbf{W}_t is a diffusion process with vanishing drift vector $\mathbf{A} = 0$ and diffusion matrix $\mathbf{B} = \mathbf{I}$, i.e. it is described by the diffusion equation

$$\partial_t p(\mathbf{w}, t | \mathbf{w}_0, t_0) = \frac{1}{2} \sum_i \frac{\partial^2}{\partial w_i^2} p(\mathbf{w}, t | \mathbf{w}_0, t_0). \quad (6.15)$$

Furthermore, it is assumed to be peaked at the origin initially, $p(\mathbf{w}, 0) = \delta(\mathbf{w})$. By definition the multivariate Wiener process

$$\mathbf{W}(t) = [W_1(t), W_2(t), \dots, W_n(t)], \quad (6.16)$$

is composed of n statistically independent one-dimensional processes $W_i(t)$, allowing us to restrict the following discussion to one-dimensional processes.

The solution of (6.15) is obtained [38] by transforming (6.15) into an algebraic equation in Fourier space, which yields the Gaussian distribution

$$p(w, t | w_0, t_0) = \frac{1}{\sqrt{2\pi(t-t_0)}} \exp\left(-\frac{(w-w_0)^2}{2(t-t_0)}\right). \quad (6.17)$$

Hence, the variance of the process grows linearly with time, as expected from a diffusion process.

The sample paths of the Wiener process are continuous but not differentiable, since one can show [38] from (6.17) that the probability for the difference quotient to be larger than an arbitrary threshold k converges to unity, i.e.

$$\lim_{h \rightarrow 0} \text{Prob}\left(\frac{w(t+h) - w(t)}{h} > k\right) = 1. \quad (6.18)$$

Hence, the derivative is almost certainly infinite at all times.

Increments of the Wiener process The SDE corresponding to a diffusion process involves the increments $dW(t) = W(t+dt) - W(t)$ of the Wiener process. An important property of these increments, which is used in many proofs concerning SDEs, is their statistical independence,

$$p(dW_n; dW_{n-1}; \dots; dW_1) = p(dW_n)p(dW_{n-1}) \dots p(dW_1), \quad (6.19)$$

with $dW_i = W(t_i + dt) - W(t_i)$. To see this, let us use the Markov property of W_t , which yields

$$\begin{aligned} p(w_n, t_n; w_{n-1}, t_{n-1}; \dots; w_0, 0) &= \prod_{i=0}^{n-1} p(w_{i+1}, t_{i+1} | w_i, t_i) p(w_0, 0) \quad (6.20) \\ &= \prod_{i=0}^{n-1} \frac{\delta(w_0)}{\sqrt{2\pi(t_{i+1} - t_i)}} \exp\left(-\frac{(w_{i+1} - w_i)^2}{2(t_{i+1} - t_i)}\right). \end{aligned}$$

It follows that the increments $\Delta w_i \equiv w_i - w_{i-1}$ are distributed as

$$p(\Delta w_n; \Delta w_{n-1}; \dots; \Delta w_1; w_0) = \prod_{i=1}^n \frac{\delta(w_0)}{\sqrt{2\pi\Delta t_i}} \exp\left(-\frac{(\Delta w_i)^2}{2\Delta t_i}\right), \quad (6.21)$$

with $\Delta t_i \equiv t_i - t_{i-1}$. This confirms the statistical independence (6.19) of the increments Δw_i , and it shows that the variance of the increments is linear in Δt ,

$$\text{Var}[\Delta W] = \Delta t. \quad (6.22)$$

6.2.2 Stochastic integration

In the next section we shall find a representation of the sample paths $\mathbf{x}_\alpha(t)$ of diffusion processes in terms of stochastic differential equations of the form

$$\frac{d\mathbf{x}(t)}{dt} = \mathbf{a}(\mathbf{x}, t) + \mathbf{b}(\mathbf{x}, t) \frac{d\mathbf{W}(t)}{dt}. \quad (6.23)$$

However, this equation is not well-defined as it stands, since the Wiener process is not differentiable, see Eq. (6.18). To make sense of (6.23) one must consider the corresponding integral equation

$$\mathbf{x}(t) = \mathbf{x}(0) + \int_{t_0}^t \mathbf{a}(\mathbf{x}, t) dt + \int_{t_0}^t \mathbf{b}(\mathbf{x}, t) d\mathbf{W}(t), \quad (6.24)$$

which can be defined in a strict mathematical sense by introducing the concept of a stochastic integral as in the third term of (6.24). The naming ‘stochastic integral’ is due to the fact that the increments of the Wiener process form a stochastic process, implying that the value of the corresponding integral is described by a stochastic process. Needless to say, since the Wiener process is highly irregular, these stochastic integrals have properties which are quite different from the ones known from ordinary integrals (which applies even more so to the associated stochastic differential calculus). A survey of the relevant definitions and major results is given in the following.

For ease of notation, we denote from now on both stochastic processes \mathbf{X}_t and sample paths $\mathbf{x}_\alpha(t)$ in lowercase. This notation is typically used in physics literature, such as the textbook by Gardiner [38].

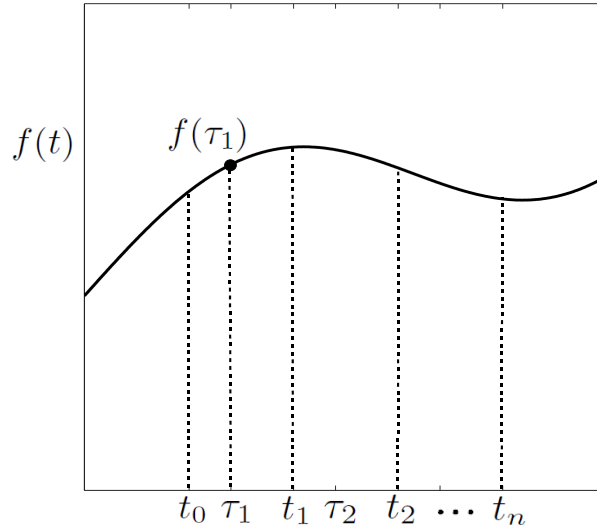


Figure 6.1: Definition of the stochastic integral of a function $f(t) \equiv f[x(t), t]$.

Definition of stochastic integrals Consider a real function $f[x(t), t]$ of time and of a stochastic process $x(t)$ as drawn in Fig. 6.1 and let $W(t)$ be the Wiener process. Strictly speaking, $f[x(t), t]$ must be *non-anticipating*, that is $f[x(t), t]$ must be statistically independent from $W(s) - W(t)$ for all $s > t$. One defines the integral $\int_{t_0}^t f[x(t'), t'] dW(t')$ similar to a Riemann integral. To this end, consider a partitioning of the interval $[t_0, t_n = t]$ into subintervals

$$[t_0, t_1], [t_1, t_2], \dots, [t_{n-1}, t_n], \quad (6.25)$$

and a set of intermediate points τ_i , with $t_{i-1} \leq \tau_i < t_i$, as depicted in Fig. 6.1. The stochastic integral is then defined as the limit of the Riemann sum

$$\int_{t_0}^t f[x(t'), t'] dW(t') := \lim_{n \rightarrow \infty} \sum_{i=1}^n f[x(\tau_i), \tau_i] [W(t_i) - W(t_{i-1})]. \quad (6.26)$$

Here $x = \lim_{n \rightarrow \infty} x_n$ is understood as the *mean square limit*, that is

$$\lim_{n \rightarrow \infty} \mathbb{E} [(x - x_n)^2] = 0. \quad (6.27)$$

Remarkably, though, the value of the above integral depends on the particular choice of the supporting points τ_i , which can be seen in the following example.

Example Let us make the choice $f[x(t), t] = W(t)$. The expectation value of the corresponding Riemann sum S_n yields

$$\begin{aligned} \mathbb{E}[S_n] &\equiv \mathbb{E} \left[\sum_i W(\tau_i) (W(t_i) - W(t_{i-1})) \right] \\ &= \sum_i [\min(\tau_i, t_i) - \min(\tau_i, t_{i-1})] \\ &= \sum_i (\tau_i - t_{i-1}), \end{aligned} \quad (6.28)$$

where it is used that $\mathbb{E}[W(s)W(t)] = \min(s, t)$, see Ref. [29, page 26]. If one chooses for the intermediate points

$$\tau_i = \alpha t_i + (1 - \alpha) t_{i-1}, \quad \text{with } 0 \leq \alpha < 1, \quad (6.29)$$

then

$$\mathbb{E}[S_n] = \sum_{i=1}^n \alpha (t_i - t_{i-1}) = \alpha (t - t_0). \quad (6.30)$$

Thus, the mean value of the stochastic integral with integrand $f[x(t), t] = W(t)$ can be anything between zero and $(t - t_0)$, depending on the choice of the intermediate points.

Definition of the Ito stochastic integral The most important choices for the parameter α , see Eq. (6.29), are

- $\alpha = 0$, defining the Ito stochastic integral, and
- $\alpha = 1/2$, defining the Stratonovich stochastic integral.

Let us first treat the Ito integral and postpone the discussion of the Stratonovich integral to Sect. 6.2.3. To repeat, the Ito integral reads as

$$I \int_{t_0}^t f[x(t'), t'] dW(t') := \lim_{n \rightarrow \infty} \sum_{i=1}^n f[x(t_{i-1}), t_{i-1}] [W(t_i) - W(t_{i-1})]. \quad (6.31)$$

This definition is particularly suitable for mathematical proofs, since the two factors $f[x(t_{i-1}), t_{i-1}]$ and $[W(t_i) - W(t_{i-1})]$ appearing in (6.31) are statistically independent. Using this property one can show that [38]

$$\begin{aligned} I \int_{t_0}^t f[x(t'), t'] [dW(t')]^{2+N} &= \int_{t_0}^t f[x(t'), t'] dt', \quad \text{if } N = 0 \quad (6.32) \\ &= 0, \quad \text{if } N > 0. \quad (6.33) \end{aligned}$$

Similarly, it can be shown that [38]

$$\begin{aligned} &I \int_{t_0}^t f[x(t'), t'] dt' dW(t') \\ &:= \lim_{n \rightarrow \infty} \sum_{i=1}^n f[x(t_{i-1}), t_{i-1}] [W(t_i) - W(t_{i-1})] [t_i - t_{i-1}] \\ &= 0 \end{aligned} \quad (6.34)$$

Since the increment $dW(t)$ only occurs under integrals, one simply writes

$$dW^2(t) = dt, \quad (6.35)$$

$$dW^{2+N}(t) = 0, \quad \text{if } N > 0, \quad (6.36)$$

$$dW(t) dt = 0. \quad (6.37)$$

These relations form the backbone of the *Ito calculus*, by which we mean the calculus associated to Ito integrals and the corresponding Ito SDEs. In contrast

to ordinary calculus, it implies that terms quadratic in dW are significant, while higher order terms may be neglected. This is important in particular when dealing with Taylor expansions.

In the multivariate case, the corresponding rules read as

$$dW_i(t) dW_j(t) = \delta_{ij} dt, \quad (6.38)$$

$$dW_i^{2+N}(t) = 0, \quad \text{if } N > 0, \quad (6.39)$$

$$dW_i(t) dt = 0, \quad (6.40)$$

where it is used that the different components of a multivariate Wiener process are statistically independent.

6.2.3 Stochastic differential equations (SDEs)

A random process \mathbf{x}_t is said to obey the SDE (6.23) if it satisfies the stochastic integral (6.24). Though, the latter is not uniquely defined, since it depends on the particular choice of the intermediate points τ_i . It is therefore necessary to specify the stochastic integral, in order to define the corresponding SDE. To make this clear, let us define the Ito SDE.

A stochastic process \mathbf{x}_t obeys an Ito SDE written as

$$d\mathbf{x}(t) = \mathbf{a}(\mathbf{x}, t) dt + \mathbf{b}(\mathbf{x}, t) d\mathbf{W}(t), \quad (6.41)$$

if for all t and t_0 we have

$$\mathbf{x}(t) = \mathbf{x}(0) + \int_{t_0}^t \mathbf{a}(\mathbf{x}, t') dt' + I \int_{t_0}^t \mathbf{b}(\mathbf{x}, t') d\mathbf{W}(t'). \quad (6.42)$$

Ito's formula As a first result concerning Ito SDEs let us consider a change of variables from $x(t)$ to $f[x(t), t]$, where the one-dimensional process $x(t)$ is assumed to satisfy the Ito SDE (6.41). To see what differential equation f obeys one expands f in a Taylor series in x and t , and uses the Ito rules (6.35) and (6.36),

$$\begin{aligned} df[x, t] &= \partial_x f dx + \partial_t f dt + \frac{1}{2} \partial_x^2 f dx^2 \\ &= \left(\partial_t f + a \partial_x f + \frac{1}{2} b^2 \partial_x^2 f \right) dt + b \partial_x f dW, \end{aligned} \quad (6.43)$$

with the abbreviations $f \equiv f[x(t), t]$, $a \equiv a[x(t), t]$, $b \equiv b[x(t), t]$, $W \equiv W(t)$ and $x \equiv x(t)$. This famous result is known as *Ito's formula* or *Ito's lemma*. It is the stochastic calculus counterpart of the chain rule in ordinary calculus. The result for the multivariate case can be found for instance in [38].

SDEs and the Fokker-Planck equation Our next aim is to show that SDEs of the form (6.41) generate diffusion processes. To this end, let us demonstrate that the associated propagator $p(\mathbf{x}, t; \mathbf{x}_0, t_0)$ obeys the Fokker-Planck equation (6.11). In particular, this reveals the relation between the matrices $\mathbf{a}(\mathbf{x}, t)$ and $\mathbf{b}(\mathbf{x}, t)$ specifying the Ito SDE, and the drift and diffusion matrices $\mathbf{A}(\mathbf{x}, t)$, $\mathbf{B}(\mathbf{x}, t)$ of the Fokker-Planck equation.

To start with, let us consider the time derivative of the expectation value of an arbitrary function $f(x(t))$,

$$\partial_t \mathbb{E}[f(x(t))] = \frac{\mathbb{E}[df(x(t))]}{dt}, \quad (6.44)$$

where the one-dimensional process $x(t)$ is assumed to satisfy the Ito SDE (6.41). Applying Ito's formula (6.43) and using $\mathbb{E}[dW] = 0$, one obtains

$$\partial_t \mathbb{E}[f] = \mathbb{E}\left[a\partial_x f + \frac{1}{2}b^2\partial_x^2 f\right], \quad (6.45)$$

with $f \equiv f(x(t))$, $a \equiv a[x(t), t]$, and $b \equiv b[x(t), t]$. Alternatively, one can represent the process in terms of its conditional probability density $p \equiv p(x, t; x_0, t_0)$, which yields

$$\partial_t \mathbb{E}[f] = \int dx f(x) \partial_t p. \quad (6.46)$$

On the other hand, we find from (6.45) that

$$\begin{aligned} \partial_t \mathbb{E}[f] &= \int dx \left(a\partial_x f + \frac{1}{2}b^2\partial_x^2 f\right) p \\ &= \int dx f(x) \left(-\partial_x[ap] + \frac{1}{2}\partial_x^2[b^2p]\right), \end{aligned} \quad (6.47)$$

where integration by parts was used in the second line. Since $f(x)$ is arbitrary, one may assume that the integrands of (6.46) and (6.47) are equal,

$$\begin{aligned} \partial_t p(x, t; x_0, t_0) &= -\partial_x[a(x, t)p(x, t; x_0, t_0)] \\ &\quad + \frac{1}{2}\partial_x^2[b(x, t)^2 p(x, t; x_0, t_0)]. \end{aligned} \quad (6.48)$$

It follows that the Ito process $x(t)$ is governed by a Fokker-Planck equation with drift coefficient $a(x, t)$ and diffusion coefficient $b^2(x, t)$.

A similar reasoning can be used to treat the multivariate scenario [38]. One then finds that a process $\mathbf{x}(t)$ obeying the Ito SDE (6.41) is described by a Fokker-Planck equation (6.11) with drift vector $\mathbf{a}(\mathbf{x}, t)$ and diffusion matrix

$$\mathbf{B}(\mathbf{x}, t) = \mathbf{b}(\mathbf{x}, t) \mathbf{b}^T(\mathbf{x}, t). \quad (6.49)$$

Surprisingly, this shows that the same Fokker-Planck equation arises if one considers a transformed Ito SDE

$$d\mathbf{x}(t) = \mathbf{a}(\mathbf{x}, t) dt + \mathbf{b}(\mathbf{x}, t) \mathbf{O}(t) d\mathbf{W}(t), \quad (6.50)$$

provided $\mathbf{O}(t)$ is orthogonal, $\mathbf{O}(t) \mathbf{O}^T(t) = \mathbf{I}$. The increments $d\mathbf{V} = \mathbf{O}d\mathbf{W}$ of this process are also increments of a Wiener process, since, as a linear combination of Gaussian variables $d\mathbf{W}$, they are Gaussian distributed, and they have the same correlation matrix as the Wiener process.

$$\begin{aligned} \langle dV_i dV_j \rangle &= \sum_{k,l} O_{ik} O_{jl} \langle dW_k dW_l \rangle \\ &= \sum_k O_{ik} O_{jk} dt = \delta_{ij} dt. \end{aligned} \quad (6.51)$$

This implies that the ensemble of trajectories, generated by (6.50), is identical with the one generated by (6.41).

Stratonovich's stochastic differential equation The definition of the Ito integral gives rise to a stochastic calculus quite different from the ordinary one, as can be seen by Ito's formula (6.43). An obvious question is whether one can choose the intermediate points τ_i in the definition of the stochastic integral (6.26) such that the corresponding calculus coincides with the ordinary one. It turns out that this can be done by choosing the τ_i 's as the midpoints of the intervals $[t_{i-1}, t_i]$, which yields the so-called Stratonovich integral. To be more precise, Stratonovich [73] defined the stochastic integral of a function $f[\mathbf{x}(t), t]$, which depends on both $\mathbf{x}(t)$ and t , as

$$\begin{aligned} & \int_{t_0}^t f[\mathbf{x}(t), t] \circ dW(t') \\ & := \lim_{n \rightarrow \infty} \sum_{i=1}^n f\left[\frac{\mathbf{x}(t_i) - \mathbf{x}(t_{i-1})}{2}, t_{i-1}\right] [W(t_i) - W(t_{i-1})]. \end{aligned} \quad (6.52)$$

Thus, only the dependence on the process variable $x(t)$ is averaged. It is shown below that this particular choice leads to ordinary calculus. It should be noted that the usage of Stratonovich's definition is indicated by the symbol \circ .

Having specified the stochastic integral, one can define the corresponding SDE: a stochastic process \mathbf{x}_t obeys a Stratonovich SDE written as

$$d\mathbf{x}(t) = \boldsymbol{\alpha}(\mathbf{x}, t) dt + \boldsymbol{\beta}(\mathbf{x}, t) \circ d\mathbf{W}(t), \quad (6.53)$$

if for all t and t_0 we have

$$\mathbf{x}(t) = \mathbf{x}(0) + \int_{t_0}^t \boldsymbol{\alpha}(\mathbf{x}, t') dt' + \int_{t_0}^t \boldsymbol{\beta}(\mathbf{x}, t') \circ d\mathbf{W}(t'). \quad (6.54)$$

Connection between Ito and Stratonovich SDEs Our next aim is to show that the SDE (6.53) is equivalent to an appropriate Ito SDE. For simplicity, let us treat the one-dimensional case; the multivariate case can be dealt with analogously [38]. To start with, let us consider a discretized version of the Stratonovich SDE,

$$\Delta x = \alpha(x_i, t_i) \Delta t + \beta\left(\frac{x_{i+1} - x_i}{2}, t_i\right) \circ \Delta W, \quad (6.55)$$

obtained by taking a mesh of points t_i such that $t_i < t_{i+1}$. Here we used the abbreviations $x_i \equiv x(t_i)$, $\Delta x \equiv x_{i+1} - x_i$ and $\Delta t \equiv t_{i+1} - t_i$. By using a first-order expansion of β , one obtains

$$\Delta x = \alpha(x_i, t_i) \Delta t + \beta(x_i, t_i) \Delta W + \frac{1}{2} \partial_x \beta(x_i, t_i) \Delta x \Delta W. \quad (6.56)$$

Now, substitute the right-hand side of the above equation for the Δx contained in the last term, and use the Ito rules (6.35) to (6.37). This yields the expression

$$\Delta x = \left[\alpha(x_i, t_i) + \frac{1}{2} \partial_x \beta(x_i, t_i) \beta(x_i, t_i) \right] \Delta t + \beta(x_i, t_i) \Delta W, \quad (6.57)$$

which is a discretized version of the Ito SDE

$$dx = \left[\alpha(x, t) + \frac{1}{2} \partial_x \beta(x, t) \beta(x, t) \right] dt + \beta(x, t) dW. \quad (6.58)$$

In conclusion, the one-dimensional version of the Stratonovich SDE (6.53) is equivalent to the Ito SDE (6.58). Conversely, the Ito SDE

$$dx = a(x, t) dt + b(x, t) dW, \quad (6.59)$$

is equivalent to the Stratonovich SDE

$$dx = \left[a(x, t) - \frac{1}{2} b(x, t) \partial_x b(x, t) \right] dt + b(x, t) \circ dW. \quad (6.60)$$

Moreover, from Eqs. (6.55) and (6.56), one obtains the expression

$$\beta \circ dW = \beta dW + \frac{1}{2} d\beta dW, \quad (6.61)$$

which gives a relation between Stratonovich and Ito differentials. This relation is used in the next chapter, where a quantum Stratonovich SDE is derived from its Ito counterpart.

Change of variables Let us use the above results to show that the rule for a change of variables in Stratonovich's SDE is the same as in ordinary calculus. For this purpose, consider a function $f[x(t)]$ of a one-dimensional process $x(t)$ which obeys the Stratonovich SDE

$$dx = \alpha(x, t) dt + \beta(x, t) \circ dW. \quad (6.62)$$

The corresponding Ito SDE is given by Eq. (6.58). By applying Ito's formula (6.43) to Eq. (6.58), we find a formula for the increments of f :

$$df = \left(\left[\alpha + \frac{1}{2} \beta \partial_x \beta \right] \partial_x f + \frac{1}{2} \beta^2 \partial_x^2 f \right) dt + \beta \partial_x f dW, \quad (6.63)$$

with $f \equiv f[x(t)]$, $\alpha \equiv \alpha(x, t)$ and $\beta \equiv \beta(x, t)$. Now, apply Eq. (6.61), which yields an expression for the last term of (6.63)

$$\beta \partial_x f dW = \beta \partial_x f \circ dW - \frac{1}{2} [\partial_x \beta \partial_x f + \beta \partial_x^2 f] dx dW. \quad (6.64)$$

Upon inserting (6.58) into (6.64), and using the Ito rules (6.35) to (6.37), one finds

$$\beta \partial_x f dW = \beta \partial_x f \circ dW - \frac{1}{2} [\partial_x \beta \partial_x f + \beta \partial_x^2 f] \beta dt. \quad (6.65)$$

Finally, by plugging (6.65) into (6.63), we obtain the chain rule of the Stratonovich calculus,

$$df = \partial_x f (\alpha dt + \beta \circ dW) = \partial_x f dx. \quad (6.66)$$

Indeed, this result agrees with the ordinary chain rule.

Example: geometric Brownian motion As an application of stochastic calculus, let us consider *geometric Brownian motion*. This is a stochastic process in which the logarithm of the random variable follows a Brownian motion. The corresponding Ito SDE reads as

$$dx = \mu x dt + \sigma x dW(t). \quad (6.67)$$

This SDE is used in finance as the standard model for the description of stock-price dynamics. In particular, it is the asset-price model applied in the famous Black-Scholes theory [74]. First, let us solve this equation using Ito calculus, then we repeat this computation by means of Stratonovich calculus.

To start with, make a change of variables

$$f(x) = \log x. \quad (6.68)$$

By applying Ito's formula (6.43), one obtains an Ito SDE for f :

$$df = \left(\mu - \frac{1}{2}\sigma^2 \right) dt + \sigma dW(t). \quad (6.69)$$

This SDE can easily be integrated giving

$$f(t) = f(0) + \left(\mu - \frac{1}{2}\sigma^2 \right) t + \sigma W(t), \quad (6.70)$$

where it is used that $t_0 = 0$ and $W(0) = 0$. The solution of (6.67) therefore reads

$$x(t) = x_0 \exp \left(\left[\mu - \frac{1}{2}\sigma^2 \right] t + \sigma W(t) \right). \quad (6.71)$$

Equation (6.70) shows that the logarithm of $x(t)$ follows a Brownian motion.

To demonstrate the application of the Stratonovich calculus, let us repeat this computation within the Stratonovich picture. By applying Eqs. (6.59) and (6.60) to the Ito SDE (6.67), one obtains the Stratonovich SDE of geometric Brownian motion,

$$dx = \left(\mu - \frac{1}{2}\sigma^2 \right) x dt + \sigma x \circ dW(t). \quad (6.72)$$

The corresponding SDE for $f = \log x$ is found using the ordinary chain rule (6.66),

$$df = \left(\mu - \frac{1}{2}\sigma^2 \right) dt + \sigma \circ dW(t). \quad (6.73)$$

The integral of this SDE yields the same result as the corresponding Ito SDE (6.69), since there is no dependence on $x(t)$ in (6.73). This implies that the solution of (6.72) is given by Eq. (6.71).

Ito versus Stratonovich calculus As a last point it is worthwhile to discuss which stochastic calculus one should choose in a given circumstance. First of all, it should be mentioned that the Ito integral as defined in (6.31) has the favourable property that it forms a so-called *martingale*. This is the name for a stochastic

process x_t that has no tendency to rise or fall, such that its conditional expectation satisfies the relation

$$\mathbb{E}(x_t | x_s; s \in [a, b]) = x_b. \quad (6.74)$$

Mathematicians have derived a variety of theorems on martingales [75]; the mathematical literature is therefore almost entirely concerned with Ito integrals. (Another reason may be that Ito SDEs appear typically in finance applications [70].)

In physics applications, though, it is the Stratonovich SDE which is obtained most naturally. This can be understood, by considering the Langevin-like equation

$$dx = a(x, t) dt + b(x, t) \xi_{\tau_c}(t) dt, \quad (6.75)$$

which turns up frequently in physics. Here $\xi_{\tau_c}(t)$ is a rapidly varying noise term which exhibits some finite correlation time $\tau_c > 0$. In order to obtain a mathematically tractable form, one typically considers the white noise limit, $\tau_c \rightarrow 0$, of this SDE. As discussed in [38, 76], the Langevin-like equation then becomes a Stratonovich SDE with the same coefficients, that is, it yields

$$\begin{aligned} dx &= \lim_{\tau_c \rightarrow 0} [a(x, t) dt + b(x, t) \xi_{\tau_c}(t) dt] \\ &= a(x, t) dt + b(x, t) \circ dW. \end{aligned} \quad (6.76)$$

It is thus the Stratonovich form, which is obtained by taking the white noise limit of a ‘‘colored Langevin equation’’.

6.3 Piecewise deterministic processes (PDPs)

The remaining part of this chapter is devoted to piecewise deterministic Markov processes. These are stochastic processes which can be described by a Liouville master equation (6.12). In the following the corresponding SDEs are presented. These kind of SDEs can easily be implemented in many applications by means of Monte Carlo methods [72].

The Poisson process serves as the fundamental process for the construction of jump processes in the same way as the Wiener process is the basic building block for diffusion processes. Let us therefore first define the Poisson process in Sect. 6.3.1 and then introduce the stochastic calculus for piecewise deterministic Markov processes in Sect. 6.3.2.

6.3.1 Poisson process

The Poisson process is a stochastic process where discrete events occur continuously and independently of one another with a time-dependent rate $\gamma(t)$, e.g. raindrops arriving at a given surface of unit area. The time-dependent random variable $x(t)$ associated to the process counts the number of events $N(t)$ that have occurred up to time t , i.e. $x(t) = N(t)$. The process is therefore integer-valued. In addition, it is a one-step process, meaning that only jumps from n to $n + 1$ are possible (since the probability for two independent events occurring exactly at the same time vanishes).

Accordingly, the master equation of the Poisson process reads

$$\partial_t p(n, t | n_0, t_0) = \gamma(t) p(n - 1, t | n_0, t_0) - \gamma(t) p(n, t | n_0, t_0), \quad (6.77)$$

where the initial condition $P(n, 0) = \delta_{n,0}$ is usually assumed. A solution of this equation is obtained [29] using the characteristic function of the propagator, which yields the Poisson distribution

$$p(n, t | n_0, t_0) = \frac{[\mu(t, t_0)]^{n-n_0}}{(n-n_0)!} e^{-\mu(t, t_0)}. \quad (6.78)$$

Here $\mu(t, t_0) \equiv \int_{t_0}^t d\tau \gamma(\tau)$ denotes the integrated jump rate. Similarly, the one-point distribution $p(n, t)$ is found to be Poisson distributed

$$p(n, t) = \frac{[\mu(t, 0)]^n}{n!} e^{-\mu(t, 0)}, \quad (6.79)$$

with mean and variance given by

$$\mathbb{E}[N(t)] = \text{Var}[N(t)] = \mu(t, 0). \quad (6.80)$$

A special case arises when the rate $\gamma(t)$ is time-independent, $\gamma(t) \equiv \gamma$, such that the integrated jump rate reads $\mu(t, 0) = \gamma t$. The process is then called *homogeneous*, while the general case, where $\gamma(t)$ has a non-trivial time-dependence, is referred to as *inhomogeneous Poisson process*.

An important characteristic of the Poisson process are the *inter-arrival times* τ_i which elapse between two successive events. These times are independent random variables and, in the case of the homogeneous process, they are exponentially distributed [29], $p(\tau_i) = \gamma \exp(-\gamma\tau_i)$. The corresponding *arrival times* are

$$s_n = \sum_{k=1}^n \tau_k, \quad (6.81)$$

that is s_n is the time of the n th jump or event.

Increments of the Poisson process The SDE associated to a PDP involves the increments $dN(t) = N(t+dt) - N(t)$ of the Poisson process. An important feature of these increments is their statistical independence,

$$p(dN_m; dN_{m-1}; \dots; dN_1) = p(dN_m) p(dN_{m-1}) \dots p(dN_1), \quad (6.82)$$

with $dN_i = N(t_i + dt) - N(t_i)$. To see this, let us use the Markov property of the process N_t ,

$$\begin{aligned} p(n_m, t_m; n_{m-1}, t_{m-1}; \dots; n_0, 0) &= \prod_{i=0}^{m-1} p(n_{i+1}, t_{i+1} | n_i, t_i) p(n_0, 0) \\ &= \prod_{i=0}^{m-1} \frac{\mu(t_{i+1}, t_i)^{(n_{i+1}-n_i)}}{(n_{i+1}-n_i)!} e^{-\mu(t_{i+1}, t_i)} \delta_{n_0, 0}. \end{aligned} \quad (6.83)$$

It follows that the increments $\Delta n_i = n_i - n_{i-1}$ are distributed as

$$p(\Delta n_m; \Delta n_{m-1}; \dots; \Delta n_1, n_0) = \prod_{i=0}^m \frac{\mu(t + \Delta t_i, t)^{\Delta n_i}}{\Delta n_i!} e^{-\mu(t + \Delta t_i, t)} \delta_{n_0, 0}, \quad (6.84)$$

with $\Delta t_i = t_i - t_{i-1}$. This confirms the statistical independence (6.82) of the increments and it shows that the expectation of the increments is given by

$$\begin{aligned} \mathbb{E}[\Delta N(t)] &= \mu(t + \Delta t, t) \\ &= \gamma(t) \Delta t, \quad \text{if } \Delta t \rightarrow 0. \end{aligned} \quad (6.85)$$

Note that, in contrast to the Wiener increments, one has to specify the rate $\gamma(t)$ in order to uniquely fix the distribution of the Poisson increments.

6.3.2 Stochastic calculus for PDPs

Our next aim is to use the increments of the Poisson process in order to construct SDEs for PDPs. For simplicity, the one-dimensional case is treated in the following; however, we allow various types of jumps to occur, that is we consider SDEs of the form

$$dx = a(x, t) dt + \sum_i b_i(x, t) dN_i(t), \quad (6.86)$$

where the $N_i(t)$'s are statistically independent inhomogeneous Poisson processes with rates $\gamma_i(t)$. A stochastic process X_t is said to satisfy the SDE (6.86) if it obeys the corresponding integral equation

$$x(t) = x(0) + \int_0^t a(x, t) dt + \sum_i \int_0^t b_i(x, t) dN_i(t). \quad (6.87)$$

Stochastic integrals for PDPs To give a meaning to the integral appearing in Eq. (6.87), we must define stochastic integrals of the form $\int_0^t f[x(t'), t'] dN(t')$, where $f[x(t), t]$ is a real function of time and of a stochastic process $x(t)$ and $N(t)$ is a Poisson process. Moreover, $f[x(t), t]$ must be *non-anticipating*, that is $f[x(t), t]$ must be statistically independent from $N(s) - N(t)$ for all $s > t$. In contrast to the diffusive case, there is a 'natural' partition of the time interval $[0, t]$ in terms of the arrival times s_i , see Eq. (6.81),

$$[0, s_1], [s_1, s_2], \dots, [s_{n-1}, s_n], [s_n, t]. \quad (6.88)$$

For vanishing drift, $a(x, t) = 0$, one expects the process to be constant in the intermediate times (s_{i-1}, s_i) , while at the jump times $t = s_i$ one has $\Delta x = f[x(s_i), s_i]$. Accordingly, one defines the stochastic integral of a PDP as [70]

$$\int_0^t f[x(t'), t'] dN(t') = \sum_{i=1}^n f[x(s_i), s_i] \Delta N_i. \quad (6.89)$$

Here $\Delta N_i = 1$, since the Poisson process is a one-step process.

Note that, in contrast to the diffusive case, the definition of the stochastic integral is *non-ambiguous*. Thus, there is only one type of stochastic calculus for PDPs, which is called the *Ito calculus for PDPs* [29, 70].

As a first example, let us derive the Ito rules for PDPs. To this end, consider an integral of the form $\int_0^t f[x(t'), t'] dN(t')^2$. Using the above definition, we find

$$\begin{aligned} \int_0^t f[x(t'), t'] dN(t')^2 &= \sum_{i=1}^n f[x(s_i), s_i] (\Delta N_i)^2 \\ &= \sum_{i=1}^n f[x(s_i), s_i] \Delta N_i \\ &= \int_0^t f[x(t'), t'] dN(t'). \end{aligned} \quad (6.90)$$

Since the increment $dN(t)$ only occurs under integrals, one may write

$$dN(t)^2 = dN(t). \quad (6.91)$$

This formula is the PDP counterpart of the diffusive Ito rules (6.35) to (6.37). It shows that $dN(t)$ is either zero or one, implying that the stochastic terms of (6.86) do not get small as $dt \rightarrow 0$. In particular, this is important when dealing with Taylor expansions, where all orders of $dN(t)$ are relevant.

In the multiple jump case, where several statistically independent Poisson processes take place in parallel, the Ito rules read as

$$dN_i(t) dN_j(t) = \delta_{ij} dN_i(t). \quad (6.92)$$

Ito's formula for PDPs Later we need the chain rule for PDPs. Let us therefore consider a function $f[x(t)]$ of the process variable $x(t)$; the latter is assumed to satisfy the SDE (6.86). One would like to obtain a SDE for the increments

$$df[x(t)] \equiv f(x + a(x, t) dt + dJ) - f(x), \quad (6.93)$$

of the function f , with $dJ \equiv \sum_i b_i(x, t) dN_i(t)$. To this end, expand (6.93) to first order in the drift term and keep the jump term to all orders, which yields

$$df[x(t)] = \partial_x f(x) a(x, t) dt + f(x + dJ) - f(x). \quad (6.94)$$

This result is known as *Ito's formula for PDPs* [70]. Note that a further expansion of (6.94) to a finite order in dJ is not permissible, since the jump term may have finite size according to the Ito rule (6.91).

SDEs and the Liouville master equation Let us now construct a SDE which generates a PDP x_t whose propagator $p(x, t|x_0, t_0)$ satisfies the Liouville master equation (6.12). To this end, one should design the stochastic part of the SDE such that jumps from $x(t)$ to z occur with a rate $W(z|x(t))$. One therefore needs a continuous set of jump processes $dN_z(t)$ in the SDE (6.86). The sum \sum_i in (6.86) must accordingly be replaced by an integral $\int dz$, such that (6.86) reads

$$dx = a(x, t) dt + \int dz b_z(x, t) dN_z(t). \quad (6.95)$$

In addition, the Ito rule (6.92) must be replaced by its continuous counterpart

$$dN_x(t) dN_y(t) = \delta(x - y) dN_x(t). \quad (6.96)$$

Since the stochastic term describes jumps from $x(t)$ to z , it is suggestive to make the choice $b_z(x, t) = z - x(t)$, implying that (6.95) becomes

$$dx = a(x, t) dt + \int dz [z - x(t)] dN_z(t). \quad (6.97)$$

Furthermore, since the rate of jumps from $x(t)$ to z is given by $W(z|x(t))$, we set

$$\mathbb{E}[dN_z(t)] = W(z|x(t)) dt. \quad (6.98)$$

Let us now check that Eqs. (6.97) and (6.98) lead to the correct dynamical behavior as predicted by the Liouville master equation (6.12). To start with, let us consider the time derivative of the expectation value of an arbitrary function $f(x(t))$,

$$\partial_t \mathbb{E}[f(x(t))] = \frac{\mathbb{E}[df(x(t))]}{dt}, \quad (6.99)$$

where the one-dimensional process $x(t)$ is assumed to satisfy the SDE (6.97). Applying Ito's formula (6.94), one obtains

$$\partial_t \mathbb{E}[f] = \mathbb{E}[a \partial_x f + f(x + dJ) - f(x)], \quad (6.100)$$

with $dJ = \int dz [z - x(t)] dN_z(t)$, $f \equiv f(x(t))$ and $a \equiv a(x, t)$. An approximation of this expression by a finite Taylor expansion is not allowed, since the jump term dJ is not necessarily infinitesimal small. One may however perform an infinite Taylor expansion

$$\begin{aligned} \mathbb{E}[f(x + dJ) - f(x)] &= \mathbb{E}\left[\sum_{k=1}^{\infty} \frac{(dJ)^k}{k!} \partial_x^{(k)} f(x)\right] \\ &= \mathbb{E}\left[\sum_{k=1}^{\infty} \frac{1}{k!} \partial_x^{(k)} f(x) \int dz (z - x)^k dN_z(t)\right] \\ &= \mathbb{E}\left[\int dz (f(z) - f(x)) dN_z(t)\right], \end{aligned} \quad (6.101)$$

where the Ito rule (6.96) is used in the second line. Upon using the expectation value (6.98), one obtains

$$\partial_t \mathbb{E}[f] = \mathbb{E}\left[a \partial_x f + \int dz [f(z) - f(x)] W(z|x)\right]. \quad (6.102)$$

Alternatively, one can represent the process in terms of its conditional probability density $p \equiv p(x, t; x_0, t_0)$, which yields

$$\partial_t \mathbb{E}[f] = \int dx f(x) \partial_t p. \quad (6.103)$$

On the other hand, we find from (6.102) that

$$\begin{aligned} \partial_t \mathbb{E}[f] &= \int dx \left(a \partial_x f + \int dz (f(z) - f(x)) W(z|x) \right) p(x, t|x_0, t_0) \\ &= \int dx f(x) \left(-\partial_x [a(x) p(x, t|x_0, t_0)] \right. \\ &\quad \left. + \int dz [W(x|z) p(z, t|x_0, t_0) - W(z|x) p(x, t|x_0, t_0)] \right). \end{aligned} \quad (6.104)$$

Here integration by parts is used in the second line, and the variables x and z are interchanged in the third line.

Since $f(x)$ is arbitrary, one may assume that the integrands of (6.103) and (6.104) are equal,

$$\begin{aligned} \partial_t p(x, t; x_0, t_0) &= -\partial_x [a(x, t) p(x, t; x_0, t_0)] \\ &+ \int dz [W(x|z) p(z, t|x_0, t_0) - W(z|x) p(x, t|x_0, t_0)]. \end{aligned} \quad (6.105)$$

It follows that Eqs. (6.97) and (6.98) lead to the correct dynamical behavior as predicted by the Liouville master equation (6.12) with a drift coefficient $A(x, t) = a(x, t)$.

Chapter 7

Quantum trajectories

7.1 The quantum Markov process

Having introduced the notion of classical Markovian stochastic processes in the previous chapter, we are now in the position to deal with its quantum counterpart. As explained above, classical Markovian processes \mathbf{X}_t are characterized by means of the Chapman-Kolmogorov equation (6.8). Solutions of this equation were obtained in terms of an appropriate stochastic differential equation,

$$\partial_t \mathbf{x} = \mathbf{a}(\mathbf{x}) + \mathbf{noise}(\mathbf{x}), \quad (7.1)$$

which admits the generation of random trajectories $\{\mathbf{x}_\alpha(t) | \mathbf{x}_\alpha(t) \in \mathbb{R}^n\}$, with $\alpha = 1 \dots N$. Upon averaging one recovers all kinds of expectation values of the process,

$$\mathbb{E}[f(\mathbf{X}_t)] \simeq \frac{1}{N} \sum_{\alpha=1}^N f(\mathbf{x}_\alpha(t)), \quad (7.2)$$

with f an arbitrary function of \mathbf{X}_t .

Similarly, quantum Markovian processes ρ_t are characterized by master equations in Lindblad form (2.47), see Sect. 2.2.2. Solutions of the latter may be obtained [21, 27–29, 77–80] by means of a suitable quantum stochastic differential equation (quantum SDE),

$$\partial_t |\psi\rangle = |a(\psi)\rangle + |\mathbf{noise}(\psi)\rangle, \quad (7.3)$$

allowing one to generate random samples of pure state trajectories $\{|\psi_\alpha(t)\rangle\}$, $|\psi_\alpha(t)\rangle$ in \mathcal{H} , called *quantum trajectories* [77]. The ensemble average admits to calculate different expectation values $\langle \mathbf{A} \rangle \equiv \text{Tr}(\rho_t \mathbf{A})$,

$$\langle \mathbf{A} \rangle \simeq \frac{1}{N} \sum_{\alpha=1}^N \langle \psi_\alpha(t) | \mathbf{A} | \psi_\alpha(t) \rangle, \quad (7.4)$$

with \mathbf{A} an arbitrary observable. Moreover, the evolution of the density matrix $\rho_t \equiv e^{\mathcal{L}t} \rho_0$ can be evaluated by averaging over the corresponding projectors $\mathbf{P}_\alpha(t) \equiv |\psi_\alpha(t)\rangle \langle \psi_\alpha(t)|$,

$$\rho_t = \frac{1}{N} \sum_{\alpha=1}^N \mathbf{P}_\alpha(t). \quad (7.5)$$

Any stochastic process in the Hilbert space of pure quantum states is called an *unraveling* of the master equation $\partial_t \rho = \mathcal{L}\rho$ [77], if it satisfies the relations (7.4) and (7.5).

As the reader may recall from the previous chapter, there are different classes of classical stochastic processes. These processes may be either diffusive or piecewise deterministic. In the first case, one has a noise term in (7.1) which is proportional to the time derivative of the Wiener process $\mathbf{W}(t)$, i.e.

$$d\mathbf{x} = \mathbf{a}(\mathbf{x}) dt + \mathbf{b}(\mathbf{x}) d\mathbf{W}, \quad (7.6)$$

so that the sample paths are continuous but non-differentiable. In the second case, the noise term is proportional to the time derivative of the Poisson process $\mathbf{N}(t)$,

$$d\mathbf{x} = \mathbf{a}'(\mathbf{x}) dt + \mathbf{b}'(\mathbf{x}) d\mathbf{N}, \quad (7.7)$$

implying that the sample paths consist of smooth deterministic parts which are interrupted by random jumps. Similarly, also the unravelings of a quantum master equation may be either diffusive [78–80], with quantum SDE

$$|d\psi\rangle = |a(\psi)\rangle dt + \sum_i |b_i(\psi)\rangle dW_i, \quad (7.8)$$

or piecewise deterministic [27–29],

$$|d\psi\rangle = |a'(\psi)\rangle dt + \sum_i |b'_i(\psi)\rangle dN_i. \quad (7.9)$$

Note, however, that there is a crucial difference between classical- and quantum Markov processes. In the classical case, unequal SDEs correspond to different probability densities $p(\mathbf{x}, t)$. For instance, the Ito SDE (6.41) is equivalent to the Fokker-Planck equation (6.11), while the piecewise deterministic SDE (6.97) corresponds to the Liouville master equation (6.12). The associated time-dependent probability densities are therefore different in these two cases.

In the quantum mechanical setting, though, different quantum SDEs may lead to the same time-dependent density operator ρ_t [28, 29]. This is due to the fact that the convex decompositions of the density matrix,

$$\rho_t = \sum_{\alpha} p_{\alpha}(t) |\psi_{\alpha}(t)\rangle \langle \psi_{\alpha}(t)|, \quad (7.10)$$

are not unique, see Sect. 2.1.2. In fact, other ensembles $\{q_{\alpha}(t), |\varphi_{\alpha}(t)\rangle\}$ may lead to the same evolution

$$\rho_t = \sum_{\alpha} q_{\alpha}(t) |\varphi_{\alpha}(t)\rangle \langle \varphi_{\alpha}(t)|. \quad (7.11)$$

Hence, the quantum SDEs which generate $\{p_{\alpha}(t), |\psi_{\alpha}(t)\rangle\}$ and $\{q_{\alpha}(t), |\varphi_{\alpha}(t)\rangle\}$ are different, even though they are associated to the same master equation. This implies that the unravelings of a given master equation are not unique. Moreover, they are physically indistinguishable, since the observable properties are determined solely by the density matrix.

It should be mentioned that one may assign a physical meaning to specific quantum SDEs (and to the corresponding quantum trajectories) if the environment of the system is continuously monitored by a complete measurement [29, 77, 81]. Then the system evolves stochastically, always in a pure state, so that individual quantum trajectories are indeed realized in such a setting. In this thesis, though, such scenarios are not considered, and hence different unravelings of a given master equation are assumed to be physically indistinguishable.

The purpose of this chapter is to give an overview of quantum SDEs which generate unravelings. In Sect. 7.2, diffusive unravelings (7.8) are discussed. In particular, explicit expressions for the drift and the noise terms $|a(\psi)\rangle$ and $|b_i(t)\rangle$ are derived, relating them to the Lindblad operators L_i of the master equation. A similar treatment of piecewise deterministic unravelings is presented in Sect. 7.3.

7.2 Diffusive unravelings

A diffusive unraveling of a master equation $\dot{\rho} = \mathcal{L}\rho$ is a stochastic process of pure quantum states $\mathbf{P}(t)$, generated by a quantum SDE of the form (7.8), whose ensemble mean satisfies $\mathbb{E}[\mathbf{P}(t)] = e^{\mathcal{L}t}\mathbf{P}(0)$. It was developed by Gisin and Percival in [78] where it was called *quantum-state diffusion*.

We shall first give a formal definition of diffusive quantum SDEs. An explicit expression for the drift and diffusion terms of the Ito quantum SDE is evaluated in Section 7.2.1. The derivation of the corresponding quantum SDE in Stratonovich form follows in Section 7.2.2.

Complex-valued Wiener processes It was found in [78] that the Wiener process appearing in (7.8) must be multivariate and complex-valued in order to provide an unraveling. A *multivariate complex-valued Wiener process* $\mathbf{W}(t)$ is a stochastic process of the form [78, 82]

$$\begin{aligned} \mathbf{W}(t) &\equiv [W_1(t), W_2(t), \dots, W_n(t)] \\ &\equiv [U_1(t) + iV_1(t), U_2(t) + iV_2(t), \dots, U_n(t) + iV_n(t)], \end{aligned} \quad (7.12)$$

where $U_i(t)$ and $V_j(t)$ are independent real-valued Wiener processes.

The increments of the components $U_i(t)$ and $V_j(t)$ satisfy the Ito rules

$$2dU_i dU_j = \delta_{ij}dt, \quad (7.13)$$

$$2dV_i dV_j = \delta_{ij}dt, \quad (7.14)$$

$$dU_i dV_j = 0, \quad (7.15)$$

where the Ito rules (6.38) for real-valued Wiener processes are used in the first and the second line, and the third line is due to the statistical independence of the dU_i 's and the dV_j 's. The factor 2 in Eqs. (7.13) and (7.14) was included for notational convenience. Accordingly, the Ito rules for the complex-valued Wiener process read as

$$dW_i dW_j = dU_i dU_j - dV_i dV_j = 0, \quad (7.16)$$

$$dW_i^* dW_j = dU_i dU_j + dV_i dV_j = \delta_{ij}dt. \quad (7.17)$$

Quantum stochastic integrals Recall from Section 6.2.3 that classical SDEs are defined in terms of the corresponding integral equations. Similarly, let us define quantum SDEs by means of the corresponding quantum stochastic integral equations. To do so, one first has to define quantum stochastic integrals of the form $\int_{t_0}^t |f[\psi(t); t]\rangle dW(t)$.

Let $|f[\psi(t); t]\rangle \in \mathcal{H}$ be an arbitrary non-anticipating vector-valued function that depends on the state $\psi(t) \equiv |\psi(t)\rangle$ and on time t , and let $W(t)$ be a complex-valued Wiener process. To define the stochastic integral, consider a partitioning of the interval $[t_0, t_n = t]$ into subintervals

$$[t_0, t_1], [t_1, t_2], \dots, [t_{n-1}, t_n]. \quad (7.18)$$

We define the quantum Ito stochastic integral of $|f[\psi(t); t]\rangle$ as the limit

$$\begin{aligned} \int_{t_0}^t |f[\psi(t'); t']\rangle dW(t') &= \lim_{n \rightarrow \infty} \sum_{i=1}^n |f[\psi(t_{i-1}); t_{i-1}]\rangle \\ &\quad \times [W(t_i) - W(t_{i-1})], \end{aligned} \quad (7.19)$$

where $X = \lim_{n \rightarrow \infty} X_n$ is understood as the mean square limit, see Eq. (6.27). Similarly, the quantum Stratonovich integral is defined as

$$\begin{aligned} &\int_{t_0}^t |f[\psi(t'); t']\rangle \circ dW(t') \\ &= \lim_{n \rightarrow \infty} \sum_{i=1}^n |f\left[\frac{\psi(t_i) + \psi(t_{i-1})}{2}; t_{i-1}\right]\rangle [W(t_i) - W(t_{i-1})]. \end{aligned} \quad (7.20)$$

Quantum stochastic differential equations (quantum SDEs)

Having defined the complex-valued Wiener process $W(t)$ and the Ito and Stratonovich quantum stochastic integrals, we are now in the position to define quantum SDEs.

A stochastic process of pure quantum states $|\psi_t\rangle \in \mathcal{H}$ obeys an Ito quantum SDE written as

$$|d\psi_t\rangle = |a(\psi_t; t)\rangle dt + \sum_i |b_i(\psi_t; t)\rangle dW_i(t), \quad (7.21)$$

if for all t and t_0 one has

$$|\psi_t\rangle = |\psi_{t_0}\rangle + \int_{t_0}^t |a(\psi_\tau; \tau)\rangle d\tau + \sum_i \int_{t_0}^t |b_i(\psi_\tau; \tau)\rangle dW_i(\tau). \quad (7.22)$$

Analogously, $|\psi_t\rangle \in \mathcal{H}$ satisfies a Stratonovich quantum SDE

$$|d\psi_t\rangle = |\alpha(\psi_t; t)\rangle dt + \sum_i |\beta_i(\psi_t; t)\rangle \circ dW_i(t), \quad (7.23)$$

if for all t and t_0 we have

$$|\psi_t\rangle = |\psi_{t_0}\rangle + \int_{t_0}^t |\alpha(\psi_\tau; \tau)\rangle d\tau + \sum_i \int_{t_0}^t |\beta_i(\psi_\tau; \tau)\rangle \circ dW_i(\tau). \quad (7.24)$$

Conservation of normalization One usually requires a quantum SDE to be norm-preserving, meaning that $\|\psi_t\| = 1$ for all times t . This implies that the fluctuations induced by the noise term must be orthogonal to that state [78],

$$\langle \psi_t | b_j \rangle = 0, \quad (7.25)$$

with $|b_j\rangle \equiv |b_j(\psi_t; t)\rangle$. To see this, consider the differential of $\|\psi_t\|^2$ and use the Ito rule (7.17),

$$\begin{aligned} d\|\psi_t\|^2 &= \langle d\psi_t | \psi_t \rangle + \langle \psi_t | d\psi_t \rangle + \langle d\psi_t | d\psi_t \rangle \\ &= \langle a | \psi_t \rangle dt + \sum_i \langle b_i | \psi_t \rangle dW_i^* + \langle \psi_t | a \rangle dt \\ &\quad + \sum_i \langle \psi_t | b_i \rangle dW_i + \sum_i \langle b_i | b_i \rangle dt. \end{aligned} \quad (7.26)$$

Upon multiplying Eq. (7.26) with the Wiener increment dW_j^* , one obtains [78]

$$d\|\psi_t\|^2 dW_i^* = \langle \psi_t | b_j \rangle dt, \quad (7.27)$$

where Eqs. (7.16), (7.17) and (6.40) are used. In order to preserve the normalization of $|\psi_t\rangle$, the differential $d\|\psi_t\|^2$ vanishes, which implies Eq. (7.25) since $dt \neq 0$.

7.2.1 Derivation of the drift and diffusion terms

In the following we shall determine the drift and diffusion vectors $|a\rangle \equiv |a(\psi_t; t)\rangle$ and $|b_i\rangle \equiv |b_i(\psi_t; t)\rangle$, such that the Ito quantum SDE (7.21) provides an unraveling of the master equation (2.47). This derivation is based on the original proposal of quantum-state diffusion [78].

To start with, we assume that the initial state is pure $\rho = |\psi\rangle\langle\psi|$. The quantum SDE (7.21) implies that ρ evolves as [78]

$$\begin{aligned} \partial_t \rho &= \frac{1}{dt} \mathbb{E} [|d\psi\rangle\langle\psi| + |\psi\rangle\langle d\psi| + |d\psi\rangle\langle d\psi|] \\ &= |a\rangle\langle\psi| + |\psi\rangle\langle a| + \sum_i |b_i\rangle\langle b_i|, \end{aligned} \quad (7.28)$$

where the Ito rule (7.17) and the expectation $\mathbb{E}[dW] = 0$ was used. On the other hand, one demands that ρ evolves according to the master equation (2.47), [78]

$$|a\rangle\langle\psi| + |\psi\rangle\langle a| + \sum_i |b_i\rangle\langle b_i| = \mathcal{L}(|\psi\rangle\langle\psi|), \quad (7.29)$$

where $\mathcal{L}(\rho)$ has Lindblad form. This relation is used below to determine the drift and diffusion vectors.

Notice that Eq. (7.29) guarantees [78] that also mixed initial states

$$\rho = \sum_\alpha p_\alpha |\psi_\alpha\rangle\langle\psi_\alpha|, \quad (7.30)$$

evolve according to the master equation (2.47). For, due to the linearity of \mathcal{L} , one finds

$$\begin{aligned} d\rho &= \mathbb{E} \left[\sum_i p_\alpha (|d\psi_\alpha\rangle\langle\psi_\alpha| + |\psi_\alpha\rangle\langle d\psi_\alpha| + |d\psi_\alpha\rangle\langle d\psi_\alpha|) \right] \\ &= \sum_i p_\alpha \mathcal{L} (|\psi_\alpha\rangle\langle\psi_\alpha|) dt \\ &= \mathcal{L}(\rho) dt. \end{aligned} \quad (7.31)$$

Derivation of the noise terms The noise terms $|b_i\rangle$ can be determined by considering the component of $\partial_t \rho$ in the space orthogonal to $\mathbf{P} \equiv |\psi\rangle\langle\psi|$ [78]. To see this, multiply Eq. (7.29) with the projector $\mathbf{P}_\perp \equiv \mathbf{I} - |\psi\rangle\langle\psi|$, and use Eq. (7.25) [78]

$$\begin{aligned} &\mathbf{P}_\perp \mathcal{L}(\mathbf{P}) \mathbf{P}_\perp \\ &= (\mathbf{I} - |\psi\rangle\langle\psi|) \left(|a\rangle\langle\psi| + |\psi\rangle\langle a| + \sum_i |b_i\rangle\langle b_i| \right) (\mathbf{I} - |\psi\rangle\langle\psi|) \\ &= \sum_i |b_i\rangle\langle b_i|. \end{aligned} \quad (7.32)$$

Upon inserting the Lindblad form (2.47) of the generator $\mathcal{L}(\mathbf{P})$ in (7.32), one obtains after a short and straightforward calculation [78]

$$\sum_i |b_i\rangle\langle b_i| = \sum_i \gamma_i (\mathbf{I} - \mathbf{P}) \mathbf{L}_i \mathbf{P} \mathbf{L}_i (\mathbf{I} - \mathbf{P}). \quad (7.33)$$

This equation is satisfied for instance by the set of noise terms [78]

$$|b_i\rangle = \sqrt{\gamma_i} (\mathbf{L}_i - \langle \mathbf{L}_i \rangle) |\psi\rangle, \quad (7.34)$$

with the expectation values $\langle \mathbf{L}_i \rangle \equiv \langle \psi | \mathbf{L}_i | \psi \rangle$.

Derivation of the drift term To obtain the drift term of the diffusive unraveling, multiply Eq. (7.29) from the right-hand side with $|\psi\rangle$ [78].

$$\mathcal{L}(\mathbf{P}) |\psi\rangle = |\psi\rangle\langle a|\psi\rangle + |a\rangle. \quad (7.35)$$

Here it is used again that the noise is orthogonal to the state, see Eq. (7.25), which follows from the condition that the quantum SDE must be norm-preserving. Now multiply (7.35) from the left-hand side with $\langle\psi|$, which gives [78]

$$\langle\psi|\mathcal{L}(\mathbf{P})|\psi\rangle = 2\text{Re}(\langle a|\psi\rangle). \quad (7.36)$$

Equations (7.35) and (7.36) imply that [78]

$$|a\rangle = \mathcal{L}(\mathbf{P}) |\psi\rangle - \left(\frac{1}{2} \langle\psi|\mathcal{L}(\mathbf{P})|\psi\rangle + i c_\psi \right) |\psi\rangle, \quad (7.37)$$

with $c_\psi \equiv \text{Im}(\langle a|\psi\rangle)$. Upon inserting the Lindblad form (2.47) of the generator $\mathcal{L}(\mathbf{P})$ in (7.37), one obtains after a short and straightforward calculation

$$\begin{aligned} |a\rangle &= -\frac{i}{\hbar} (\mathbf{H} - \langle \mathbf{H} \rangle + \hbar c_\psi) |\psi\rangle \\ &\quad + \sum_i \gamma_i \left(\langle \mathbf{L}_i^\dagger \rangle \mathbf{L}_i - \frac{1}{2} \mathbf{L}_i^\dagger \mathbf{L}_i - \frac{1}{2} \langle \mathbf{L}_i^\dagger \rangle \langle \mathbf{L}_i \rangle \right) |\psi\rangle, \end{aligned} \quad (7.38)$$

where the expectation values are with respect to $|\psi\rangle$.

The ψ -dependent constant c_ψ contributes only an additional phase, and it is therefore chosen such that the quantum SDE agrees with the usual Schrödinger equation if the system is closed [78]. Thus, one makes the choice $c_\psi = \langle \mathbf{H} \rangle / \hbar$, which together with the noise term (7.34) yields [78–80]

$$\begin{aligned} |d\psi\rangle &= -\frac{i}{\hbar} \mathbf{H}|\psi\rangle dt + \sum_i \gamma_i \left(\langle \mathbf{L}_i^\dagger \rangle \mathbf{L}_i - \frac{1}{2} \mathbf{L}_i^\dagger \mathbf{L}_i - \frac{1}{2} \langle \mathbf{L}_i^\dagger \rangle \langle \mathbf{L}_i \rangle \right) |\psi\rangle dt \\ &\quad + \sum_i \sqrt{\gamma_i} (\mathbf{L}_i - \langle \mathbf{L}_i \rangle) |\psi\rangle dW_i. \end{aligned} \quad (7.39)$$

This represents the Ito quantum SDE of quantum-state diffusion.

Complete parameterization of diffusive unravelings The unraveling defined by the above Ito quantum SDE and the Ito rules (7.16) and (7.17) is not the only conceivable diffusive unraveling. In fact, others may be constructed by allowing correlations between the different components dW_i of the Wiener process. It was proved by Wiseman and Diosi in [83] that a complete parameterization of diffusive quantum trajectories is obtained by writing the Ito rules as

$$dW_i dW_j = u_{ij} dt, \quad (7.40)$$

$$dW_i^* dW_j = \delta_{ij} dt, \quad (7.41)$$

with u a complex symmetric matrix subject to the condition $\|u\|_2 \leq 1$ for the matrix two-norm. The latter is defined as the square root of the maximum eigenvalue of $u^\dagger u$.

7.2.2 Quantum Stratonovich SDEs

Let us now evaluate the Stratonovich quantum SDE associated to the Ito diffusive unraveling (7.39). To this end, recall that the classical relation between Stratonovich and Ito differentials is provided by Eq. (6.61). The corresponding relation for state vectors reads as ¹

$$|b_i(\psi)\rangle \circ dW_i = |b_i(\psi)\rangle dW_i + \frac{1}{2} |db_i(\psi)\rangle dW_i, \quad (7.42)$$

with $|db_i(\psi)\rangle \equiv |b_i(\psi + d\psi)\rangle - |b_i(\psi)\rangle$. By choosing the noise term (7.34), one obtains

$$\begin{aligned} |db_i(\psi)\rangle dW_i &= \sqrt{\gamma_i} (\mathbf{L}_i - [\langle \psi | + \langle d\psi |] \mathbf{L}_i [|\psi\rangle + |d\psi\rangle]) (|\psi\rangle + |d\psi\rangle) dW_i \\ &\quad - \sqrt{\gamma_i} (\mathbf{L}_i - \langle \psi | \mathbf{L}_i | \psi \rangle) |\psi\rangle dW_i, \end{aligned} \quad (7.43)$$

where $|d\psi\rangle$ is given by the Ito quantum SDE (7.39). Upon using the Ito rules (7.16) and (7.17), we find that the only non-vanishing term on the right-hand side of (7.43) is the one containing the factor $\langle d\psi | \mathbf{L}_i | \psi \rangle dW_i$. Thus,

$$\begin{aligned} |db_i(\psi)\rangle dW_i &= \sqrt{\gamma_i} \langle d\psi | \mathbf{L}_i | \psi \rangle |\psi\rangle dW_i \\ &= - \left(\langle \mathbf{L}_i^\dagger \mathbf{L}_i \rangle - \langle \mathbf{L}_i^\dagger \rangle \langle \mathbf{L}_i \rangle \right) |\psi\rangle dt, \end{aligned} \quad (7.44)$$

¹The proof of this relation is analogous to the classical one shown in Sect. 6.2.3. One merely has to replace the functions $\alpha(x, t)$, $\beta(x, t)$ and $x(t)$ by state vectors.

where we used (7.39) and the Ito rules $dW_i dt = 0$ and (7.17). It follows from Eqs. (7.39), (7.42) and (7.44) that the Stratonovich quantum SDE associated to Eq. (7.39) is given by [7, 57, 80]

$$\begin{aligned} |d\psi\rangle &= -\frac{i}{\hbar} \mathbf{H}|\psi\rangle dt + \sum_i \gamma_i \left(\frac{1}{2} \langle \mathbf{L}_i^\dagger \mathbf{L}_i \rangle - \frac{1}{2} \mathbf{L}_i^\dagger \mathbf{L}_i + \langle \mathbf{L}_i^\dagger \rangle \mathbf{L}_i - \langle \mathbf{L}_i^\dagger \rangle \langle \mathbf{L}_i \rangle \right) |\psi\rangle dt \\ &+ \sum_i \sqrt{\gamma_i} (\mathbf{L}_i - \langle \mathbf{L}_i \rangle) |\psi\rangle \circ dW_i. \end{aligned} \quad (7.45)$$

Notice that the drift term of this quantum SDE agrees with the nonlinear equation (4.45) whose asymptotic states are argued to provide the pointer states of the open system, see Chapter 4. For this reason, it is suggestive to use this particular unraveling in order to study the emergence and evolution of pointer states. This has indeed been done by Diosi and Kiefer [6] in the context of linear coupling models; the following chapter will comment on this in more detail.

7.3 Piecewise deterministic unravelings

A piecewise deterministic unraveling of a master equation $\partial_t \rho = \mathcal{L} \rho$ is a stochastic process $\mathbf{P}(t) = |\psi_t\rangle\langle\psi_t|$ in the Hilbert space of pure quantum states which is defined by a quantum SDE of the form (7.9), and whose ensemble mean satisfies $\mathbb{E}[\mathbf{P}(t)] = e^{\mathcal{L}t} \mathbf{P}(0)$. As discussed at the beginning of this chapter, these unravelings are not unique, meaning that there are infinitely many equations of the form (7.9), which generate the same time-dependent density matrix $\rho_t = \mathbb{E}[\mathbf{P}_t]$. The most widely used piecewise deterministic unraveling is the Monte Carlo method [27, 28]; here the quantum jumps are induced by the Lindblad operators \mathbf{L}_i , so that the noise terms read as

$$|b_i(\psi)\rangle = \frac{\mathbf{L}_i |\psi\rangle}{\|\mathbf{L}_i |\psi\rangle\|} - |\psi\rangle. \quad (7.46)$$

We start out with a formal definition of piecewise deterministic quantum SDEs. Then the Monte Carlo unraveling is derived (Sect. 7.3.1), and a strategy admitting the generation of other unravelings is presented (Sect. 7.3.2). This strategy is then used to determine the so-called *orthogonal unraveling*, which will be important in the next chapter when the emergence of pointer states is discussed.

Stochastic integrals of quantum jump processes Let $|f[\psi_t; t]\rangle \in \mathcal{H}$ be an arbitrary non-anticipating vector-valued function that depends on the state $\psi_t \equiv |\psi_t\rangle$ and on time t , and let $N(t)$ be a Poisson process with rate $r(t)$ and arrival times s_i . Then we define the quantum stochastic integral of $|f[\psi_t; t]\rangle$ as

$$\int_{t_0}^t |f[\psi_{t'}; t']\rangle dN(t') = \sum_{i=1}^n |f[\psi_{s_i}; s_i]\rangle \Delta N_i, \quad (7.47)$$

with $\Delta N_i = 1$ and n defined by the inequality $s_n < t < s_{n+1}$.

Piecewise deterministic quantum SDEs A stochastic process of pure quantum states $|\psi_t\rangle \in \mathcal{H}$ obeys a piecewise deterministic quantum SDE written as

$$|d\psi_t\rangle = |a(\psi_t; t)\rangle dt + \sum_i |b_i(\psi_t; t)\rangle dN_i(t), \quad (7.48)$$

if for all t and t_0 one has

$$|\psi_t\rangle = |\psi_0\rangle + \int_{t_0}^t d\tau |a(\psi_\tau; \tau)\rangle d\tau + \sum_i \int_{t_0}^t d\tau |b_i(\psi_\tau; \tau)\rangle dN_i(\tau). \quad (7.49)$$

Notice that one must specify the rates $r_i(t)$ of the Poisson processes $N_i(t)$, in order to uniquely define the quantum SDE (7.48).

7.3.1 Derivation of the Monte Carlo unraveling

Let us now derive the Monte Carlo unraveling, that is a quantum SDE of the form (7.48) with noise terms (7.46) and expectation value

$$\mathbb{E}[|\psi_t\rangle\langle\psi_t|] = e^{\mathcal{L}t}|\psi_0\rangle\langle\psi_0|, \quad (7.50)$$

where $|\psi_t\rangle$ are stochastic solutions of the quantum SDE and $|\psi_0\rangle$ is some arbitrary initial state. $\mathcal{L}(\cdot)$ denotes the generator (2.47) of a quantum dynamical semigroup. To achieve this task, one has to determine the drift term $|a\rangle \equiv |a(\psi_t; t)\rangle$ and the rates $r_i(t)$ of the Poisson processes involved in (7.48).

To start with, assume that the initial state is pure $\rho = |\psi\rangle\langle\psi|$. The general case follows from the linearity of the generator \mathcal{L} , as in Sect. 7.2.1, Eq. (7.31). The quantum SDE (7.48) implies that ρ evolves as

$$\begin{aligned} \partial_t \rho &= \frac{1}{dt} \mathbb{E}[|d\psi\rangle\langle\psi| + |\psi\rangle\langle d\psi| + |d\psi\rangle\langle d\psi|] \\ &= |a\rangle\langle\psi| + |\psi\rangle\langle a| \\ &\quad + \sum_i (|b_i\rangle\langle\psi| + |\psi\rangle\langle b_i| + |b_i\rangle\langle b_i|) r_i, \end{aligned} \quad (7.51)$$

where we used the Ito rule (6.92) and the relation $\mathbb{E}[dN_i] = r_i dt$ (see Eq. (6.85)). As a next step, notice that the quantum SDE should agree with the Schrödinger equation if the system is closed. It is therefore suggestive to make the ansatz

$$|a\rangle = -\frac{i}{\hbar} \mathbf{H}|\psi\rangle + |\tilde{a}\rangle, \quad (7.52)$$

with unknown state $|\tilde{a}\rangle$. By inserting the drift vector (7.52) and the noise terms (7.46) into Eq. (7.51), one obtains

$$\begin{aligned} \partial_t \rho &= -\frac{i}{\hbar} [\mathbf{H}, \mathbf{P}] + |\tilde{a}\rangle\langle\psi| + |\psi\rangle\langle\tilde{a}| \\ &\quad + \sum_i \left[\left(\frac{\mathbf{L}_i}{\mathcal{N}_i} - \mathbf{I} \right) \mathbf{P} + \mathbf{P} \left(\frac{\mathbf{L}_i^\dagger}{\mathcal{N}_i} - \mathbf{I} \right) + \left(\frac{\mathbf{L}_i}{\mathcal{N}_i} - \mathbf{I} \right) \mathbf{P} \left(\frac{\mathbf{L}_i^\dagger}{\mathcal{N}_i} - \mathbf{I} \right) \right] r_i \\ &= -\frac{i}{\hbar} [\mathbf{H}, \mathbf{P}] + |\tilde{a}\rangle\langle\psi| + |\psi\rangle\langle\tilde{a}| + \sum_i r_i \left(\frac{\mathbf{L}_i \mathbf{P} \mathbf{L}_i^\dagger}{\mathcal{N}_i^2} - \mathbf{P} \right), \end{aligned} \quad (7.53)$$

with normalization $\mathcal{N}_i \equiv \|\mathbf{L}_i|\psi\rangle\|$ and $\mathbf{P} \equiv |\psi\rangle\langle\psi|$. On the other hand, we demand that ρ evolves according to the master equation,

$$\partial_t \rho = -\frac{i}{\hbar} [\mathbf{H}, \mathbf{P}] + \sum_i \gamma_i \left(\mathbf{L}_i \mathbf{P} \mathbf{L}_i^\dagger - \frac{1}{2} \mathbf{L}_i^\dagger \mathbf{L}_i \mathbf{P} - \frac{1}{2} \mathbf{P} \mathbf{L}_i^\dagger \mathbf{L}_i \right). \quad (7.54)$$

A comparison of (7.53) and (7.54) suggests the ansatz

$$r_i = \gamma_i \mathcal{N}_i^2 = \gamma_i \langle \mathbf{L}_i^\dagger \mathbf{L}_i \rangle, \quad (7.55)$$

so that Eq. (7.53) becomes

$$\partial_t \rho = -\frac{i}{\hbar} [\mathbf{H}, \mathbf{P}] + |\tilde{a}\rangle\langle\psi| + |\psi\rangle\langle\tilde{a}| + \sum_i \gamma_i \left(\mathbf{L}_i \mathbf{P} \mathbf{L}_i^\dagger - \langle \mathbf{L}_i^\dagger \mathbf{L}_i \rangle \mathbf{P} \right). \quad (7.56)$$

From Eqs. (7.54) and (7.56) one finds an equation for the drift $|\tilde{a}\rangle$

$$\begin{aligned} & |\tilde{a}\rangle\langle\psi| + |\psi\rangle\langle\tilde{a}| \\ &= \sum_i \gamma_i \left(\langle \mathbf{L}_i^\dagger \mathbf{L}_i \rangle |\psi\rangle\langle\psi| - \frac{1}{2} \mathbf{L}_i^\dagger \mathbf{L}_i |\psi\rangle\langle\psi| - \frac{1}{2} |\psi\rangle\langle\psi| \mathbf{L}_i^\dagger \mathbf{L}_i \right), \end{aligned} \quad (7.57)$$

which is satisfied by the vector

$$|\tilde{a}\rangle = \sum_i \gamma_i \left(\frac{1}{2} \langle \mathbf{L}_i^\dagger \mathbf{L}_i \rangle - \frac{1}{2} \mathbf{L}_i^\dagger \mathbf{L}_i \right) |\psi\rangle. \quad (7.58)$$

Finally, by combining Eqs. (7.48), (7.52), (7.58) and (7.46), one finds that the Monte Carlo unraveling is described by the piecewise deterministic quantum SDE [27–29]

$$\begin{aligned} |d\psi_t\rangle &= -\frac{i}{\hbar} \mathbf{H} |\psi_t\rangle dt - \frac{1}{2} \sum_i \gamma_i \left(\mathbf{L}_i^\dagger \mathbf{L}_i - \langle \mathbf{L}_i^\dagger \mathbf{L}_i \rangle \right) |\psi_t\rangle dt \\ &+ \sum_i \left(\frac{\mathbf{L}_i |\psi_t\rangle}{\|\mathbf{L}_i |\psi_t\rangle\|} - |\psi_t\rangle \right) dN_i(t), \end{aligned} \quad (7.59)$$

where the Poisson increments satisfy the expectations [27–29]

$$\begin{aligned} \mathbb{E} [dN_i(t)] &= r_i(t) dt \\ &= \gamma_i \langle \mathbf{L}_i^\dagger \mathbf{L}_i \rangle dt. \end{aligned} \quad (7.60)$$

7.3.2 Derivation of the orthogonal unraveling

As may be recalled from Sect. 2.2.2, the Lindblad master equation $\dot{\rho} = \mathcal{L}(\rho)$ does not uniquely fix the Lindblad operators \mathbf{L}_i and the Hamiltonian \mathbf{H} . That is, there are certain transformations $\mathbf{L}_i \rightarrow \mathbf{L}'_i$ and $\mathbf{H} \rightarrow \mathbf{H}'$ which keep $\mathcal{L}(\rho)$ invariant. The idea suggested in [78] and [28] is to generate other unravelings, by inserting the transformed operators \mathbf{L}'_i and \mathbf{H}' into a known unraveling, such as the Monte Carlo quantum SDE (7.59).

For reasons which will become apparent shortly, let us consider the inhomogeneous transformations (2.51) and (2.52) with the particular choice

$$z_i = -\langle \mathbf{L}_i \rangle. \quad (7.61)$$

In this case the transformed Lindblad operators are given by

$$\mathbf{L}_i \rightarrow \mathbf{L}'_i = \mathbf{L}_i - \langle \mathbf{L}_i \rangle, \quad (7.62)$$

and the corresponding Hamiltonian reads as

$$\mathbf{H} \rightarrow \mathbf{H}' = \mathbf{H} - \frac{i\hbar}{2} \sum_i \gamma_i \left(\langle \mathbf{L}_i \rangle \mathbf{L}_i^\dagger - \langle \mathbf{L}_i^\dagger \rangle \mathbf{L}_i \right). \quad (7.63)$$

By inserting these operators into the quantum SDE (7.59), one obtains

$$\begin{aligned} |d\psi_t\rangle &= -\frac{i}{\hbar} \left[\mathbf{H} - \frac{i\hbar}{2} \sum_i \gamma_i \left(\langle \mathbf{L}_i \rangle \mathbf{L}_i^\dagger - \langle \mathbf{L}_i^\dagger \rangle \mathbf{L}_i \right) \right] |\psi_t\rangle dt \\ &\quad - \frac{1}{2} \sum_i \gamma_i \left[\left(\mathbf{L}_i^\dagger - \langle \mathbf{L}_i^\dagger \rangle \right) \left(\mathbf{L}_i - \langle \mathbf{L}_i \rangle \right) - \langle \mathbf{L}_i^\dagger \rangle \mathbf{L}_i + \langle \mathbf{L}_i^\dagger \rangle \langle \mathbf{L}_i \rangle \right] |\psi_t\rangle dt \\ &\quad + \sum_i \left(\frac{(\mathbf{L}_i - \langle \mathbf{L}_i \rangle) |\psi_t\rangle}{\|(\mathbf{L}_i - \langle \mathbf{L}_i \rangle) \psi_t\|} - |\psi_t\rangle \right) dN_i(t). \end{aligned} \quad (7.64)$$

Upon expanding Eq. (7.64), one obtains the quantum SDE of the orthogonal unraveling [22]

$$\begin{aligned} |d\psi_t\rangle &= -\frac{i}{\hbar} \mathbf{H} |\psi_t\rangle dt + \sum_i \gamma_i \left(\frac{1}{2} \langle \mathbf{L}_i^\dagger \rangle \mathbf{L}_i - \frac{1}{2} \mathbf{L}_i^\dagger \mathbf{L}_i + \langle \mathbf{L}_i^\dagger \rangle \mathbf{L}_i - \langle \mathbf{L}_i^\dagger \rangle \langle \mathbf{L}_i \rangle \right) |\psi_t\rangle dt \\ &\quad + \sum_i \left(\frac{(\mathbf{L}_i - \langle \mathbf{L}_i \rangle) |\psi_t\rangle}{\|(\mathbf{L}_i - \langle \mathbf{L}_i \rangle) \psi_t\|} - |\psi_t\rangle \right) dN_i(t), \end{aligned} \quad (7.65)$$

where the Poisson increments must now exhibit the expectation values

$$\begin{aligned} \mathbb{E}[dN_i(t)] &= \gamma_i \langle (\mathbf{L}_i^\dagger - \langle \mathbf{L}_i^\dagger \rangle) (\mathbf{L}_i - \langle \mathbf{L}_i \rangle) \rangle dt \\ &= \gamma_i \left(\langle \mathbf{L}_i^\dagger \rangle \mathbf{L}_i - \langle \mathbf{L}_i^\dagger \rangle \langle \mathbf{L}_i \rangle \right) dt. \end{aligned} \quad (7.66)$$

To our knowledge, this unraveling was first noted by Rigo and Gisin [22], although it has not been studied numerically so far.

Discussion of the sample paths The orthogonal unraveling has a number of remarkable properties. Crucially, the deterministic pieces of the sample paths of (7.65) are generated by the nonlinear equation (4.45), whose asymptotic states are supposed to provide the pointer states of the open system, see Chapter 4. For this reason, one may use this unraveling to study the emergence and dynamics of pointer states; a detailed explanation of this application is given in the next chapter.

The stochastic parts, on the other hand, consist of quantum jumps which occur with the rate

$$\begin{aligned} r_i(t) &= \frac{\mathbb{E}[dN_i(t)]}{dt} \\ &= \gamma_i \left(\langle \mathbf{L}_i^\dagger \rangle \mathbf{L}_i - \langle \mathbf{L}_i^\dagger \rangle \langle \mathbf{L}_i \rangle \right), \end{aligned} \quad (7.67)$$

and are caused by the nonlinear operators

$$\mathbf{J}_i = \frac{\mathbf{L}_i - \langle \mathbf{L}_i \rangle}{\sqrt{r_i}}. \quad (7.68)$$

This implies that the overlap $\langle \psi | \mathbf{J}_i | \psi \rangle$ vanishes,

$$\langle \psi | \mathbf{J}_i | \psi \rangle = \frac{1}{\sqrt{r_i}} \langle \psi | (\mathbf{L}_i - \langle \mathbf{L}_i \rangle) | \psi \rangle = 0, \quad (7.69)$$

which means that the states $|\psi_i\rangle = \mathbf{J}_i |\psi\rangle$ into which the system may jump are orthogonal to the original state $|\psi\rangle$. This justifies the naming ‘orthogonal unraveling’. Notice, however, that the states $|\psi_i\rangle$ are not necessarily mutually orthogonal.

Another quantity of interest, which will be needed below, is the total jump rate $r \equiv \sum_i r_i$. In the case of the orthogonal unraveling, it is determined by the linear entropy production rate \dot{S}_{lin} defined in Sect. 2.1.1, Eq. (2.11).

$$r(t) = \frac{1}{2} \dot{S}_{\text{lin}}(|\psi\rangle\langle\psi|). \quad (7.70)$$

This can be verified easily:

$$\begin{aligned} \dot{S}_{\text{lin}}(|\psi\rangle\langle\psi|) &= -2\langle \psi | \mathcal{L}(|\psi\rangle\langle\psi|) | \psi \rangle \\ &= 2 \sum_i \gamma_i \left(\langle \mathbf{L}_i^\dagger \mathbf{L}_i \rangle - \langle \mathbf{L}_i^\dagger \rangle \langle \mathbf{L}_i \rangle \right) = 2 \sum_i r_i. \end{aligned} \quad (7.71)$$

In the next chapter, we seek an unraveling whose quantum trajectories turn into pointer states asymptotically. This implies that the total jump rate of the asymptotic trajectories must tend to zero for such an unraveling. On the other hand, recall from Sect. 4.3, Eq. (4.15), that pointer states are distinguished by having the minimal linear entropy production rate in the Hilbert space. Since in the case of the orthogonal unraveling the total jump rate agrees with \dot{S}_{lin} (apart from a factor 2), the latter is a candidate for an unraveling whose quantum trajectories evolve into pointer states asymptotically; the following chapter will comment on this in more detail.

Diosi’s orthogonal unraveling A related unraveling, which is also referred to as the ‘orthogonal unraveling’, was introduced by Diosi [21, 84]. Here, the deterministic pieces of the evolution are as well generated by the nonlinear equation (4.45). However, the states $|\psi_i\rangle$ into which the system may jump are obtained differently, as the eigenvectors of the Hermitian operator

$$\mathbf{P}_\perp \mathcal{L}(\mathbf{P}) \mathbf{P}_\perp, \quad (7.72)$$

with $\mathbf{P}_\perp \equiv \mathbf{I} - |\psi\rangle\langle\psi|$ and $\mathbf{P} \equiv |\psi\rangle\langle\psi|$. As a consequence, these states are also *mutually* orthogonal (in finite dimensional systems). Since the orthogonal unraveling of [21, 84] requires the diagonalization of the operator (7.72), it is much more involved than the one defined by (7.65) and (7.66), which is why the latter is used in the subsequent chapter.

Continuous set of Lindblad operators Finally, we note that all of the relations presented in this chapter are also valid if there is an uncountable set of Lindblad operators, so that the master equation has the form (2.48). The discrete index i must then be replaced by a continuous label q , and the sums are substituted by integrals.

Chapter 8

Unraveling collisional decoherence

8.1 Pointer states and quantum trajectories

As shown in the preceding chapter, a given Lindblad master equation is completely equivalent to certain quantum stochastic differential equations (quantum SDEs). The latter should therefore encode information about the pointer states \mathbf{P}_α , if there are any. Moreover, it was found that there are infinitely many of those unravelings, all leading to the same physical predictions. This gives us the freedom to choose among the unravelings the ones most convenient for the analysis of pointer states. As we shall find in this chapter, these are the unravelings which generate directly the ensemble of pointer states, meaning that the corresponding quantum trajectories end up asymptotically in one of the \mathbf{P}_α 's.

To make this more concrete, let us recall the definition of pointer states given in Sect. 4.2. The set of pointer states $\mathbf{P}_\alpha(t)$ is essentially characterized by the fact that the evolved state $\rho_t = e^{\mathcal{L}t}\rho_0$ can be convex-decomposed for any initial state ρ_0 and for times greater than the decoherence time, $t \gg t_{\text{dec}}$, as ¹

$$\rho_t \simeq \sum_{\alpha} p_{\alpha} \mathbf{P}_{\alpha}(t) . \quad (8.1)$$

A natural further requirement is that the weights p_{α} are given by the *initial* projections

$$p_{\alpha} = \text{Tr}[\rho_0 \mathbf{P}_{\alpha}(0)] . \quad (8.2)$$

From this definition it becomes clear that an unraveling will produce the ensemble of pointer states if it generates for any initial state ρ_0 an ensemble of trajectories $\{\mathbf{P}_{\alpha}(t)\}$ which get independent of ρ_0 for large times. Then the ensemble mean has precisely the form shown in Eq. (8.1), so that the asymptotic states of the quantum trajectories are to be identified with the pointer states of the system. This implies that one may use the relative frequency of these states to estimate the probabilities p_{α} of the pointer states, and to verify whether Eq. (8.2) holds. Such an unraveling does therefore provide the complete information, that is $\{p_{\alpha}, \mathbf{P}_{\alpha}(t)\}$, about the decoherence process.

¹For clarity, the definition is given for a finite number of dimensions.

It still remains an open problem to give a complete list of unravelings which produce the pointer states of a master equation, if there are any. Clearly this is a challenging task, since it is not even known so far how to completely parameterize unravelings. Besides that, even the general proof that a particular unraveling generates pointer states remains open.

What can be done, however, is to give plausibility arguments that indicate why certain unravelings are supposed to do the job. This leads in particular to the diffusive and the orthogonal unraveling introduced in the previous chapter. One can then prove for particular models that these unravelings produce pointer states. To make this more precise, it is useful to discuss diffusive and piecewise deterministic unravelings separately.

Diffusive unravelings As was noted by Diosi in [6], a candidate for an unraveling with the above property is the diffusive unraveling described by the Ito quantum SDE (7.39). Expressed in the Stratonovich picture (7.45), its drift term agrees with the nonlinear equation (4.45) whose asymptotic states are supposed to provide the pointer states of the system, see Chapter 4. Of course, it is not clear whether this also holds in the presence of the diffusive noise terms contained in the quantum SDE (7.45).

It turns out, however, that this is indeed the case for the linear coupling model shown in Eq. (3.39). According to [6], the solutions of (7.45) tend for all initial states to the Gaussian solitons (4.54) with width (4.57). Once the trajectory has turned into a soliton, its position and momentum expectation values follow the classical motion Eq. (4.55) up to a small random diffusion [6].

Surprisingly, the above only holds for a specific diffusive unraveling where the noise terms are characterized by the Ito rules (7.16) and (7.17). Recall from Sect. 7.2.1 that diffusive unravelings are not unique. There is a certain freedom in the choice of the Ito rules, which is expressed in Eqs. (7.40) and (7.41).

It should be mentioned that the observations made in [6] hold for both the Ito and the Stratonovich picture, since the two are equivalent in the sense that the corresponding quantum SDEs (7.39) and (7.45) produce the same ensemble of quantum trajectories.

In summary, the diffusive unraveling described by the quantum SDE (7.39) and the Ito rules (7.16) and (7.17) produces asymptotically the ensemble of pointer states in the example of the linear coupling model. Nevertheless, we do not apply this diffusive unraveling in the following, since we are not aware of general criteria which guarantee that the quantum trajectories of the diffusive unraveling evolve into pointer states asymptotically.

Piecewise deterministic unravelings However, in the case of piecewise deterministic unravelings, one may formulate such criteria. These criteria will be crucial below, when we analyze the formation of pointer states in collisional decoherence. To start with, recall that we seek a piecewise deterministic unraveling which produces for any initial state P_0 an ensemble of P_0 -independent projectors $\{P_\alpha(t)\}$. Clearly, this is satisfied if

- 1) its deterministic part exhibits stable fixed points or solitons P_α ,
- 2) the associated total jump rate vanishes, $r(P_\alpha) = 0$.

In that case, the sample paths characterizing the process will end up in one of the states P_α , by all means. The conditions 1) and 2) therefore provide a sufficient condition for the P_α 's to be genuine pointer states.

A candidate for such an unraveling is the orthogonal unravelings discussed in Sect. 7.3.2, Eqs. (7.65) and (7.66). One may expect it to fulfill the above conditions, provided the system exhibits pointer states, for the following reasons.

- I) Its deterministic part is given by the nonlinear equation (4.45) whose asymptotic states are reasonable candidates for the pointer basis of the system, as discussed in detail in Chapter 4. Moreover, Equation (4.45) exhibits stable fixed points or solitons in all of the examples studied so far (namely, the damped harmonic oscillator, the linear coupling model and collisional decoherence). We therefore conjecture that this is a generic feature of Eq. (4.45).
- II) Its total jump rate is determined by the linear entropy production rate, see Eq. (7.70). Recall that the latter should be minimal for pointer states, as discussed in Sect. 4.3, Eq. (4.15). It is therefore reasonable to expect that the total jump rate of the asymptotic states vanishes or is at least much smaller than the typical rates.

Hence, there is strong evidence that the orthogonal unraveling generates the ensemble of pointer states, if the system exhibits classical properties.

8.2 Application to collisional decoherence

Now let us come back to the main theme of this thesis, namely to the emergence and dynamics of pointer states in the motion of a quantum test particle coupled to an ideal gas environment. Such a system is described by collisional decoherence, discussed in Sect. 3.5. We therefore apply the orthogonal unraveling defined by Eqs. (7.65) and (7.66) to collisional decoherence (3.47), by first evaluating the deterministic part of the quantum SDE (7.65) in Sect. 8.2.1 and then the stochastic one in Sect. 8.2.2. This allows us in particular to verify the conditions 1) and 2) mentioned in the previous section, so that we are able to identify the pointer states P_α of collisional decoherence.

8.2.1 Deterministic evolution

The deterministic part of the quantum SDE (7.65) corresponds to the nonlinear equation (4.45) derived in Sect. 4.4. Applying (4.45) to the case of collisional decoherence yields the soliton equation (5.5) discussed in Sect. 5.1. Let us now further simplify this equation, by considering initial states

$$\Psi_0(x) = \sum_{i=1}^N c_i(0) \phi_i(x, 0), \quad (8.3)$$

which are superpositions of non-overlapping wave functions $\phi_i(x, 0)$,

$$\phi_i(x, 0) \phi_{j \neq i}^*(x, 0) = 0. \quad (8.4)$$

The latter are assumed to be localized in the sense that

$$\sigma_{\phi_i}^2 < \frac{2\pi\hbar^2}{\sigma_G^2}, \quad (8.5)$$

where $\sigma_{\phi_i}^2$ and σ_G^2 denote the variances of the distributions $|\phi_i(x, 0)|^2$ and $G(q)$, respectively. Under this assumption, which will be justified at the end of this section, one can extract a system of evolution equations for the time evolution of the coefficients in (8.3),

$$\frac{d}{dt}c_i(t) = - \left(\sum_{j=1}^N F_{ij} |c_j(t)|^2 - \sum_{j,k=1}^N F_{jk} |c_j(t)|^2 |c_k(t)|^2 \right) c_i(t). \quad (8.6)$$

Here, the matrix $F_{ij} \equiv F(x_i - x_j)$ is obtained from the one-dimensional version of the localization rate (3.50), where the $x_i \equiv \langle x \rangle_{\phi_i}$ denote the mean positions of the constituent wave functions $\phi_i(x, t)$. The latter evolve according to

$$\begin{aligned} \partial_t \phi_i(x, t) &= -\frac{\hbar}{2mi} \partial_x^2 \phi_i(x, t) + \phi_i(x, t) \Lambda \left[|\phi_i|^2 \right](x, t) \\ &\quad + \phi_i(x, t) \sum_{j=1, j \neq i}^N |c_j(t)|^2 \tilde{\gamma}_{ij}(x, t), \end{aligned} \quad (8.7)$$

where Λ is defined in (5.6) and $\tilde{\gamma}_{ij}$ is a rate of the order of γ ,

$$\tilde{\gamma}_{ij}(x, t) \equiv |\phi_i|^2 * F(x, t) - |\phi_j|^2 * F(x, t) + F_{ij}. \quad (8.8)$$

Before verifying these evolution equations, let us discuss the consequences of the localization assumption (8.5). It is required to justify the approximation

$$\int_{-\infty}^{\infty} dx |\phi_i(x)|^2 e^{iqx/\hbar} \simeq e^{iqx_i/\hbar}, \quad (8.9)$$

for all q contributing appreciably to integrals weighted with the momentum transfer distribution $G(q)$; we comment on the validity of this approximation at the end of this section. Equation (8.9), in turn, implies

$$F_{jk} \simeq \int_{-\infty}^{\infty} dx |\phi_j(x)|^2 \left(|\phi_k|^2 * F \right)(x). \quad (8.10)$$

To see this, combine Eqs. (3.50) and (8.9) to obtain

$$\begin{aligned} F(x_j - x_k) &\simeq \gamma \left(1 - \int dq G(q) \int dx |\phi_j(x)|^2 e^{iqx/\hbar} \int dy |\phi_k(y)|^2 e^{-iqy/\hbar} \right) \\ &= \int dx |\phi_j(x)|^2 \int dy |\phi_k(y)|^2 \gamma \left(1 - \int dq G(q) e^{iq(x-y)/\hbar} \right) \\ &= \int dx |\phi_j(x)|^2 \int dy |\phi_k(y)|^2 F(x - y), \end{aligned} \quad (8.11)$$

which confirms Eq. (8.10). Furthermore, from the latter together with $F(0) = 0$ one can induce that

$$\int_{-\infty}^{\infty} dx |\phi_i(x)|^2 \left(|\phi_i|^2 * F \right)(x) \simeq 0. \quad (8.12)$$

Verification of the evolution equations Let us now verify that

$$\Psi_t(x) = \sum_{i=1}^N c_i(t) \phi_i(x, t), \quad (8.13)$$

with $c_i(t)$ and $\phi_i(x, t)$ solutions of (8.6) and (8.7), evolves according to (5.5). To this end, consider the time derivative of $\Psi_t(x)$, which gives

$$\begin{aligned} \partial_t \Psi &= \sum_{i=1}^N \left(\dot{c}_i \phi_i + c_i \dot{\phi}_i \right) \\ &= -\frac{\hbar}{2mi} \sum_{i=1}^N c_i \partial_x^2 \phi_i - \left(\sum_{i=1}^N c_i \phi_i \right) \left(\sum_{j=1}^N |c_j|^2 (|\phi_j|^2 * F) \right. \\ &\quad \left. - \sum_{j,k=1}^N |c_j|^2 |c_k|^2 F_{jk} \right) + \sum_{i=1}^N c_i \phi_i \left(\Lambda [|\phi_i|^2] + |\phi_i|^2 * F \right), \end{aligned} \quad (8.14)$$

where the arguments are dropped for brevity. In (8.14), we used (8.6)-(8.8), the fact that $F_{ii} = 0$, and the normalization condition $\sum_{i=1}^N |c_i|^2 = 1$. This expression can be further simplified, by noting that, due to the definition of Λ (5.6) and the relation (3.50), one has

$$\begin{aligned} \Lambda [|\phi_i|^2](x, t) &= \int_{-\infty}^{\infty} dx |\phi_i(x)|^2 (|\phi_i|^2 * F)(x) - (|\phi_i|^2 * F)(x, t) \\ &= -(|\phi_i|^2 * F)(x, t), \end{aligned} \quad (8.15)$$

where Eq. (8.12) was used in the second line. Equation (8.14) therefore turns into

$$\begin{aligned} \partial_t \Psi &= -\frac{\hbar}{2mi} \sum_{i=1}^N c_i \partial_x^2 \phi_i - \left(\sum_{i=1}^N c_i \phi_i \right) \\ &\quad \times \left(\sum_{j=1}^N |c_j|^2 (|\phi_j|^2 * F) - \sum_{j,k=1}^N |c_j|^2 |c_k|^2 F_{jk} \right). \end{aligned} \quad (8.16)$$

Now, replace F_{jk} in (8.16) by the right-hand side of (8.10), and use (8.4), which yields

$$\begin{aligned} \partial_t \Psi_t(x) &= -\frac{\hbar}{2mi} \partial_x^2 \Psi_t(x) - \Psi_t(x) [|\Psi_t|^2 * F(x) \\ &\quad - \int_{-\infty}^{\infty} dx |\Psi_t|^2(y) (|\Psi_t|^2 * F)(y)]. \end{aligned} \quad (8.17)$$

Finally, by using (3.50), one obtains

$$\begin{aligned} \partial_t \Psi_t(x) &= -\frac{\hbar}{2mi} \partial_x^2 \Psi_t \\ &\quad + \gamma \Psi_t(x) \left(|\Psi_t|^2 * \hat{G}(x) - \int_{-\infty}^{\infty} dy |\Psi_t|^2(y) (|\Psi_t|^2 * \hat{G})(y) \right), \end{aligned} \quad (8.18)$$

which confirms that $\Psi_t(x)$ evolves according to (5.5).

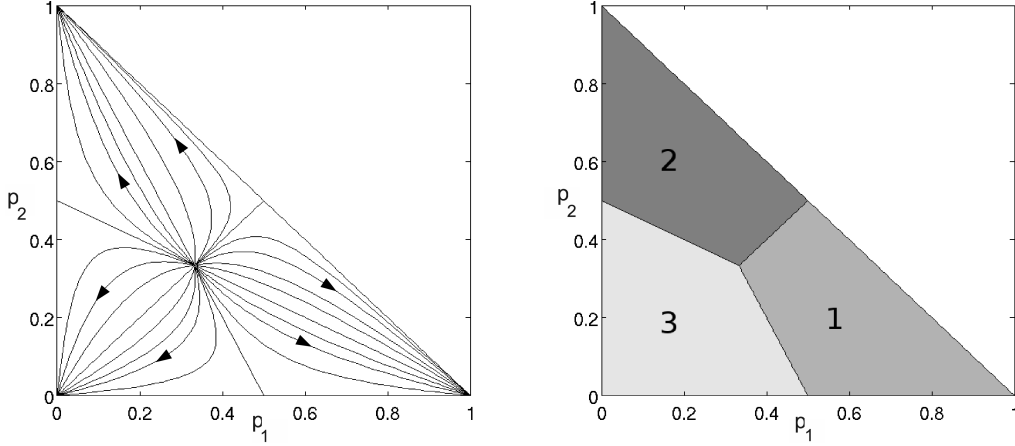


Figure 8.1: Numerical solution of (8.6) for $N = 3$. The x -axis gives $p_1 = |c_1|^2$ and the y -axis $p_2 = |c_2|^2$; $|c_3|^2$ is then fixed by normalization. Left: trajectories indicating the flow into the stable fixed points $|c_i| = \delta_{i,n}$, ($n = 1, 2, 3$). Right: regions of attraction of the stable fixed points; the area denoted with n is the region of attraction of the fixed point $|c_i| = \delta_{i,n}$.

Evolution of the coefficients Let us now discuss the time evolution of the coefficients according to Eq. (8.6). First consider situations where the wave packets $\phi_i(x)$ are sufficiently far apart so that the localization rate is saturated, meaning that

$$F_{ij} = \gamma(1 - \delta_{ij}). \quad (8.19)$$

Under this assumption, (8.6) reduces to the equation

$$\frac{d}{dt}c_i(t) = -\gamma \left(\sum_{j=1}^N |c_j(t)|^4 - |c_i(t)|^2 \right) c_i(t), \quad (8.20)$$

which was already studied in [85] in the context of a discrete model for quantum measurement. It is shown there that all stable fixed points of (8.20) have the form $|c_i| = \delta_{i,m}$, and that the particular fixed point $|c_i| = \delta_{i,m}$, with

$$m = \operatorname{argmax}_i \left(|c_i(0)|^2 \right), \quad (8.21)$$

is approached monotonically, i.e. the component with the largest initial weight wins. This behavior is visualized in Fig. 8.1 which was obtained by solving (8.20) numerically for the case $N = 3$. Here, the x - and the y -axis indicate the weights $p_1 = |c_1|^2$ and $p_2 = |c_2|^2$, respectively. The plot on the left-hand side shows various trajectories, illustrating in particular the fixed points. The plot on the right displays the regions of attraction of the stable fixed points $|c_i| = \delta_{i,n}$, in agreement with the criterion (8.21). For instance, area 1 highlights the region of attraction of the fixed point $|c_i| = \delta_{i,1}$.

Figure 8.2, on the other hand, depicts a situation where the wave packets $\phi_i(x)$ are located more closely so that the localization rate is unsaturated, that is

$$F_{ij} \neq \gamma(1 - \delta_{ij}). \quad (8.22)$$

Here, we choose $N = 3$ and non-equidistant position expectations,

$$(x_1, x_2, x_3) = \frac{\sigma_G}{\hbar} (1.4, 1.3, 0.8). \quad (8.23)$$

It is observed that similarly to the saturated case all stable fixed points of (8.6) have the form $|c_i| = \delta_{i,n}$. However, the regions of attraction are deformed so that criterion (8.21) is no longer valid, and the fixed points are not necessarily approached monotonically.

Proof of the fixed point stability To see that $|c_i| = \delta_{i,n}$ are *stable* fixed points of (8.6), assume that the coefficients are close by, in the sense that

$$|c_n(t)|^2 = 1 - \varepsilon(t), \quad (8.24)$$

$$|c_{j \neq n}(t)|^2 = O(\varepsilon(t)), \quad (8.25)$$

with $\varepsilon(0) \ll 1$. Now, let us consider the time evolution of $|c_n(t)|^2$ induced by (8.6),

$$\frac{d}{dt}|c_n|^2 = -2 \left(\sum_j F_{nj} |c_j|^2 - \sum_{j,k} F_{jk} |c_j|^2 |c_k|^2 \right) |c_n|^2. \quad (8.26)$$

Here the time arguments are dropped for brevity. By inserting Eq. (8.24), one obtains

$$\dot{\varepsilon} = 2 \left(\sum_j F_{nj} |c_j|^2 - \sum_{j,k} F_{jk} |c_j|^2 |c_k|^2 \right) (1 - \varepsilon), \quad (8.27)$$

which together with $F_{nn} = 0$ yields

$$\dot{\varepsilon} = 2 \sum_j F_{nj} |c_j|^2 - 2 \sum_k (F_{nk} + F_{kn}) (1 - \varepsilon)^2 |c_k|^2 + O(\varepsilon^2). \quad (8.28)$$

Since the localization rate $F(x)$ is a function of the distance $|x|$ only, see Eq. (3.52), F_{jk} is symmetric, $F_{jk} = F_{kj}$, so that

$$\dot{\varepsilon}(t) = - \sum_j F_{nj} |c_j(t)|^2 + O(\varepsilon^2) < 0, \quad (8.29)$$

and hence, $|c_i(t \rightarrow \infty)| = \delta_{i,n}$.

Evolution of the wave packets The knowledge of the fixed points of the coefficients allows us to discuss the asymptotic evolution of the initial state shown in Eq. (8.3). Since the coefficients c_j with $j \neq m$ tend to zero asymptotically, it follows that

$$|\psi(t \rightarrow \infty)\rangle = |\phi_m(t \rightarrow \infty)\rangle, \quad (8.30)$$

for a specific m (which is given by (8.21) in the saturated case). The asymptotic behavior of the wave packets $|\phi_m\rangle$ can, in turn, be predicted from Eq. (8.7). Since the $c_{j \neq m}$ vanish for large times, the coupling term given by the last summand in

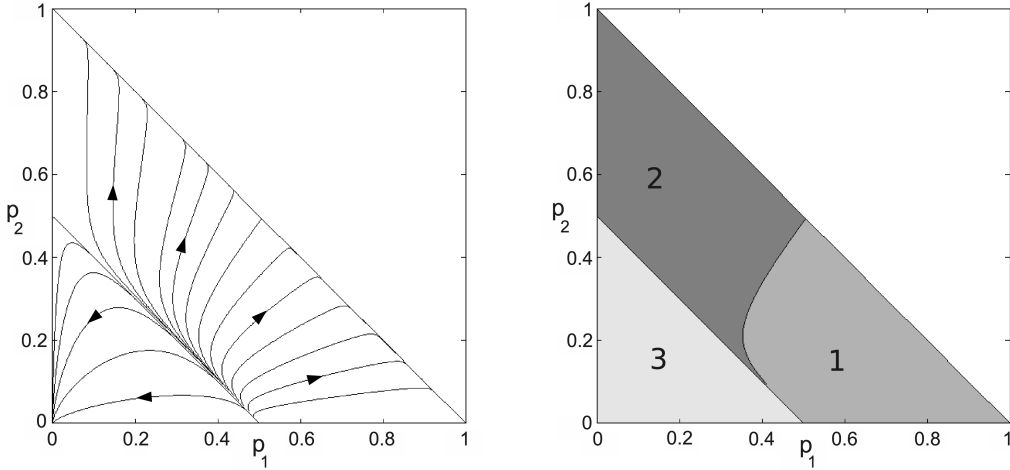


Figure 8.2: Similar to Fig. 8.1, but the wave packets $\phi_i(x)$ are positioned closer so that the localization rate is unsaturated, i.e. $F_{ij} \leq \gamma(1 - \delta_{ij})$. The stable fixed points are still of the form $|c_i| = \delta_{i,n}$, but they may be approached non-monotonically and the regions of attraction, shown on the right, are deformed compared to the saturated case.

(8.7) vanishes as well, implying that the time evolution (8.7) of $|\phi_m\rangle$ is asymptotically equal to the soliton equation (5.5). Therefore, in the absence of stochastic jumps, the state $|\Psi_0\rangle$ evolves into the solitonic solution $\pi_m(x)$ of (5.5) which is associated to the initial wave packets $|\phi_m(0)\rangle$.

It should be mentioned that Eqs. (8.6) and (8.7) for the coefficients c_i and the constituent wave packets ϕ_i are not completely decoupled, since (8.6) depends on the matrix $F_{ij} \equiv F(x_i - x_j)$ which contains the position expectations x_i of the wave packets ϕ_i . However, the position expectation follows the classical trajectory for sufficiently large κ 's, implying that (8.6) can be solved without knowing the solution of (8.7).

Discussion of the assumptions Let us now take a closer look at the validity of the assumption of small position variance (8.5), and the ensuing approximation (8.9). The former can be justified by our observation in Section 5.2.3, that the dimensionless pointer width $\sigma_\pi \sigma_G / \hbar$ is a function of the parameter $\kappa \equiv \sigma_G^2 / m \hbar \gamma$ only,

$$\sigma_\pi \frac{\sigma_G}{\hbar} = \frac{\kappa}{4a_{\text{loc}}} + a_{\text{loc}}, \quad \text{with } a_{\text{loc}} = 0.4. \quad (8.31)$$

Thus, for all $\kappa \ll 4a_{\text{loc}}^2 \simeq 1$ we find that the position variance σ_π^2 of a pointer state is one order of magnitude smaller than the reciprocal width of the momentum transfer distribution $G(q)$,

$$\sigma_\pi^2 \simeq a_{\text{loc}}^2 \frac{\hbar^2}{\sigma_G^2} \simeq 0.2 \frac{\hbar^2}{\sigma_G^2} < 2\pi \frac{\hbar^2}{\sigma_G^2}. \quad (8.32)$$

The above relation for the width of the pointer state is also sufficient to justify the approximation

$$\int dx e^{iqx/\hbar} |\pi(x)|^2 \simeq e^{iq\langle x \rangle \pi/\hbar}, \quad (8.33)$$

as we checked numerically, by using the solitonic solution of (6). The relative error is less than 2% for $q \in [-2\sigma_G, 2\sigma_G]$ and $\kappa \leq 10^{-3}$.

8.2.2 Stochastic part

Jump operators By inserting the Lindblad operator $L_q = \sqrt{\gamma G(q)} e^{iqx}$ into Eq. (7.68) one finds that the jump operator takes the form

$$J_q = \mathcal{N}_q \left(e^{iqx/\hbar} - \langle e^{iqx/\hbar} \rangle \right). \quad (8.34)$$

Here \mathcal{N}_q denotes the normalization

$$\mathcal{N}_q = \left(1 - |\langle e^{iqx/\hbar} \rangle|^2 \right)^{-1/2}. \quad (8.35)$$

Again consider states of the form (8.3) which are superpositions of non-overlapping (8.4) and localized (8.5) wave packets $\phi_i(x)$. Under this assumption, it follows that

$$\langle \phi_j | e^{iqx/\hbar} | \phi_k \rangle = \delta_{jk} e^{iqx_j/\hbar}, \quad (8.36)$$

so that one can evaluate the expectation value in (8.34)

$$\begin{aligned} \langle e^{iqx/\hbar} \rangle_\Psi &= \sum_{j,k} c_j^* c_k \langle \phi_j | e^{iqx/\hbar} | \phi_k \rangle \\ &= \sum_j |c_j|^2 e^{iqx_j/\hbar}. \end{aligned} \quad (8.37)$$

Accordingly, the state $\Psi_q(x) \equiv J_q \Psi(x)$ into which the system may jump takes the form

$$\Psi_q(x) = \mathcal{N}_q \left(e^{iqx/\hbar} - \sum_i |c_i|^2 e^{iqx_i/\hbar} \right) \sum_i c_i \phi_i(x). \quad (8.38)$$

Later we will choose the wave functions $\phi_i(x)$ to be solitons $\pi_i(x)$. Let us therefore assume that the ϕ_i 's form a basis, so that $\Psi_q(x)$ can be represented as $\Psi_q(x) = \sum_i c_i(q) \phi_i(x)$. Then the transformed coefficients $c_k(q)$ can be evaluated by the overlap $c_k(q) = \langle \phi_k | J_q | \Psi \rangle$. Using (8.4) and (8.9) this leads to the following expression for the redistribution of the coefficients due to an orthogonal jump

$$c_k(q) = \mathcal{N}_q \left(e^{iqx_k/\hbar} - \sum_{i=1}^N |c_i|^2 e^{iqx_i/\hbar} \right) c_k. \quad (8.39)$$

Jump rates Similarly, one can evaluate the rate (7.67) associated to the jump operator of collisional decoherence,

$$r_q = \gamma G(q) \left(1 - |\langle e^{iqx/\hbar} \rangle|^2 \right). \quad (8.40)$$

The above approximation (8.37) further simplifies this expression,

$$r_q = \gamma G(q) \left(1 - \sum_{j,k=1}^N |c_j|^2 |c_k|^2 e^{iq(x_j - x_k)/\hbar} \right). \quad (8.41)$$

One observes that this rate vanishes for the stable fixed points $|c_i| = \delta_{i,n}$. Thus, it is verified that states of the form (8.3) with $|c_i| = \delta_{i,n}$ satisfy the conditions 1) and 2) presented in Sect. 8.1. Recall that these conditions guarantee that the quantum trajectories of the orthogonal unraveling evolve into the pointer states. Since states with $|c_i| = \delta_{i,n}$ evolve asymptotically into solitonic solutions $\pi_t(x)$ of (5.5), it is thus evident that the latter represent the pointer states of collisional decoherence.

Non-ideal pointer states It should be mentioned that due to the finite pointer width (5.36) the *exact* expression for the jump rate (8.40) does not vanish identically, although it is very small compared to γ . For instance, the numerically obtained soliton displays a strongly suppressed total jump rate $r_{\text{tot}} = \int dq r_q$ of $r_{\text{tot}}/\gamma = 7 \times 10^{-3}$ for $\kappa = 10^{-3}$, while the superposition state decays with the rate $r_{\text{tot}} \cong \gamma$.

One requires from pointer states P_α satisfying definition (4.12) that the quantum trajectories of the orthogonal unraveling stay most of the time within the set of states $\{P_\alpha\}$, for times greater than the decoherence time. The jump rate r_{tot} of the solitons must therefore be small compared to the *contraction rates* γ_c . The latter characterize the times which are needed for the transformed states $P_{\alpha,q} \equiv J_q P_\alpha J_q^\dagger$ to return to solitons of the nonlinear equation (4.45). If the contraction rate is estimated by γ , that is by the localization rate in the saturated regime, we find that indeed $r_{\text{tot}} \ll \gamma_c$ for the numerically obtained soliton. Hence, the latter match with the definition of pointer states (4.12).

Stochastic differential equation (SDE) By combining Eqs. (8.6), (8.39) and (8.41), one finds a set of coupled SDEs for the stochastic evolution of the coefficients

$$\begin{aligned} dc_i(t) = & - \left(\sum_j F_{ij} |c_j(t)|^2 - \sum_{j,k} F_{jk} |c_j(t)|^2 |c_k(t)|^2 \right) c_i(t) dt \\ & + \int dq \left(\mathcal{N}_q \left[e^{iqx_i/\hbar} - \sum_j |c_j(t)|^2 e^{iqx_j/\hbar} \right] c_i(t) - c_i(t) \right) dN_q(t), \end{aligned} \quad (8.42)$$

where the Poisson increments satisfy the expectations $\mathbb{E}[dN_q] = r_q dt$. The original quantum SDE (7.65), which is defined in the infinite dimensional Hilbert space of the system, has therefore been reduced to a SDE in \mathbb{C}^N , demonstrating the efficiency of the orthogonal unraveling.

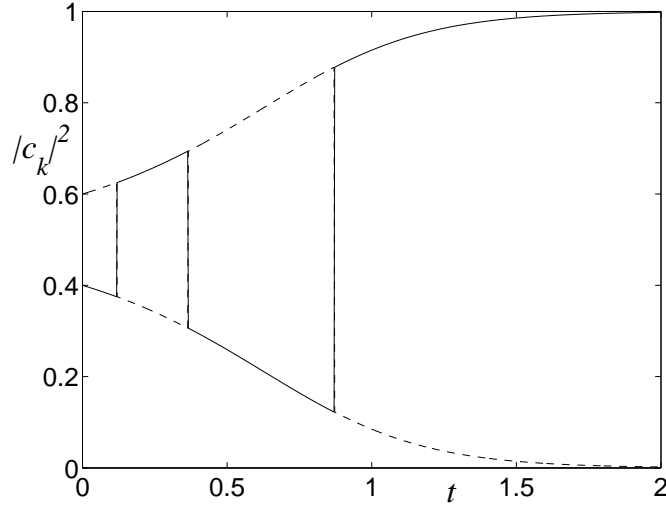


Figure 8.3: Quantum trajectory generated by (8.42) and (8.41) with $N = 2$. The solid line depicts the evolution of $|c_1(t)|^2$, while the dashed line shows $|c_2(t)|^2$. Since there is an odd number of jumps (three jumps in this example), the trajectory evolves into the fixed point $|c_i| = \delta_{i,1}$.

8.3 The statistical weights of the pointer states

The previous section showed that the orthogonal unraveling of an initial superposition state subject to collisional decoherence can be reduced to a stochastic process with respect to the corresponding coefficients. In particular, this applies to the case where the initial state is a superposition of pointer states,

$$|\Psi_0\rangle = \sum_{i=1}^N c_i |\pi_i(0)\rangle. \quad (8.43)$$

Thus one can now verify, by using the discrete process defined by the SDE (8.42) and the rate (8.41), that after decoherence the statistical weights of the pointer states are given by the overlap of the initial state with the initial pointer states, in agreement with Eq. (8.2). More specifically, this demonstrates that the initial state $\Psi_0(x)$ evolves into the mixture

$$\rho(x, x') = \sum_{i=1}^N p_i \pi_i(x) \pi_i^*(x'), \quad (8.44)$$

where the statistical weights are given by the overlap

$$p_i = |\langle \Psi_0 | \pi_i(x, 0) \rangle|^2. \quad (8.45)$$

First an analytic proof of the above for $N = 2$ is presented. The general case, $N > 2$, is then treated numerically in the following section.

8.3.1 Superposition of two localized states

Consider the expectation value for the coefficients after a jump, that is

$$\langle c_k(q) \rangle_G := \int_{-\infty}^{\infty} dq G(q) c_k(q), \quad k = 1, 2. \quad (8.46)$$

Upon inserting (8.39) one obtains

$$\begin{aligned}\langle c_1(q) \rangle_G &= \langle \mathcal{N}_q (e^{iqx_1/\hbar} - |c_1|^2 e^{iqx_1/\hbar} - |c_2|^2 e^{iqx_2/\hbar}) c_1 \rangle_G \\ &= \mathcal{N}' |c_2|^2 c_1,\end{aligned}\quad (8.47)$$

with the normalization constant $\mathcal{N}' = \langle \mathcal{N}_q (e^{iqx_1/\hbar} - e^{iqx_2/\hbar}) \rangle_G$. By using

$$\begin{aligned}1 &= |\langle c_1(q) \rangle_G|^2 + |\langle c_2(q) \rangle_G|^2 \\ &= \mathcal{N}'^2 |c_2|^4 |c_1|^2 + \mathcal{N}'^2 |c_1|^4 |c_2|^2 \\ &= \mathcal{N}'^2 |c_1 c_2|^2,\end{aligned}\quad (8.48)$$

one finds $|\mathcal{N}'| = 1/(|c_1 c_2|)$ which implies

$$|\langle c_1(q) \rangle_G| = |c_2|. \quad (8.49)$$

This shows that after a jump the moduli of the coefficients are simply interchanged. This property (which does not hold for $N > 2$) makes the stochastic process analytically tractable (because the dynamics is independent of the phases of the coefficients). Since the deterministic part (8.6) of the evolution is monotonic for $N = 2$, a trajectory starting from $|c_1(0)| < 1/2$ will end up in the state $|c_i(\infty)| = \delta_{i,1}$ if and only if an odd number of jumps occurs in the process. This is demonstrated in Fig. 8. Crucially, the jump rate $r_{\text{tot}}(t)$,

$$\begin{aligned}r_{\text{tot}}(t) &:= \int_{-\infty}^{\infty} dq r_q(t) \\ &= \sum_{j,k=1}^2 F(x_j - x_k) |c_j(t)|^2 |c_k(t)|^2 \\ &= 2F(x_1 - x_2) |c_1(t)|^2 |c_2(t)|^2,\end{aligned}\quad (8.50)$$

is unaffected by the jump (8.49) at all times, since it is invariant under interchanging the coefficients. Hence, the time dependence of the jump rate is identical for all trajectories, which, in turn, means that the number of jumps follows an inhomogeneous Poisson process. The probability for an odd number of jumps, which is equal to the statistical weight p_1 of the pointer state $\pi_1(x)$, can therefore be evaluated analytically by using Eq. (6.79),

$$\begin{aligned}\text{Prob}(\text{odd}) &= e^{-\mu(\infty)} \sum_{n=0}^{\infty} \frac{\mu(\infty)^{2n+1}}{(2n+1)!} \\ &= e^{-\mu(\infty)} \sinh[\mu(\infty)] \\ &= 1 - \frac{1}{2} e^{-2\mu(\infty)},\end{aligned}\quad (8.51)$$

with $\mu(t) = \int_0^t d\tau r_{\text{tot}}(\tau)$ the integrated jump rate. The latter can easily be evaluated by noting that (8.6) can be written for $N = 2$ as

$$2F(x_1 - x_2) |c_1(\tau)|^2 |c_2(\tau)|^2 = \frac{1}{2} \frac{d}{dt} \ln(1 - 2|c_1(\tau)|^2). \quad (8.52)$$

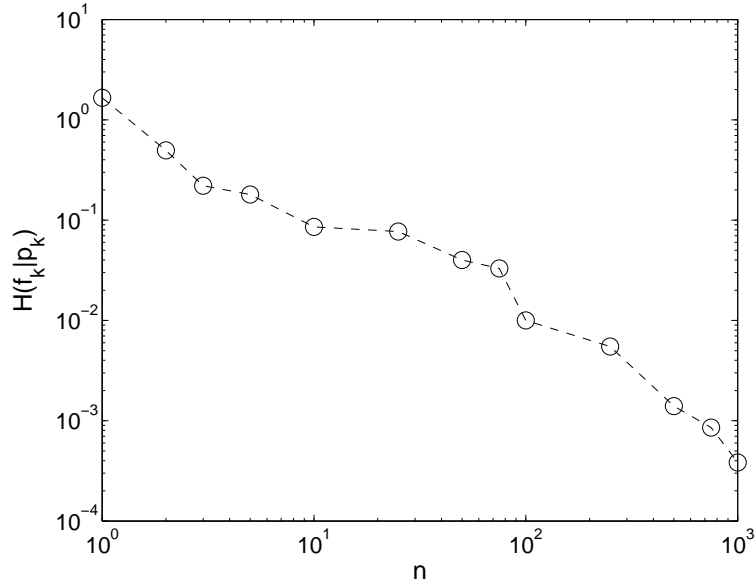


Figure 8.4: Relative entropy $H(f_k|p_k)$ of the numerically obtained distribution of pointer states f_k with respect to the expected distribution $p_k = |c_k|^2$ as a function of the number of trajectories n generated in the simulation. The plot indicates that the pointer states are distributed according to the initial overlap $|c_k|^2$.

By inserting this result into (8.50) one obtains the integrated jump rate:

$$\begin{aligned} \mu(\infty) &= \int_0^\infty d\tau \frac{1}{2} \frac{d}{dt} \ln(1 - 2|c_1(\tau)|^2) \\ &= -\frac{1}{2} \ln(1 - 2|c_1(0)|^2). \end{aligned} \quad (8.53)$$

Noting (8.51) we thus find the probability of an odd number of jumps

$$\text{Prob(odd)} = |c_1(0)|^2. \quad (8.54)$$

This finally confirms that the statistical weights of the pointer states are indeed given by the expected overlap (8.45).

8.3.2 Superposition of $N > 2$ localized states

The stochastic process is much more complicated if the initial superposition consists of more than two pointer states. Our numerical implementation of the stochastic process defined by the SDE (8.42) and the rate (8.41) is based on a Metropolis-Hastings algorithm [72] to draw the momentum transfer q in accordance with the rate (8.41), with $G(q)$ a Gaussian. Each of the generated trajectories ends asymptotically in one of the fixed points corresponding to a pointer state, and we thus obtain a numerical estimate of the statistical weights by means of the relative frequencies f_k , $1 \leq k \leq N$, of the asymptotic states.

Relative entropy To confirm the expected probability distribution $p_k = |c_k(0)|^2$, we evaluate the relative entropy

$$H(f_k|p_k) \equiv \sum_k p_k \ln \frac{p_k}{f_k}, \quad (8.55)$$

between these two distributions. Figure 9 shows the result for a random initial state with $N = 5$ as a function of the number of trajectories n , indicating convergence to zero. In addition, we found for 100 random initial states, with random $2 < N < 11$, based on 10^4 trajectories that the relative entropy was always less than 4×10^{-3} . This holds both for cases where the initial wave packets $\pi_i(x)$ are far apart such that the localization rate is saturated, $F(x_i - x_j) \simeq \gamma$, and for situations where the wave packets are located close together so that $F(x_i - x_j) < \gamma$. This is good evidence that the asymptotic trajectories are indeed distributed according to the expected overlap (8.45).

Chi square test As an alternative confirmation of the statistical weights, we performed a χ^2 -test. Similar to the treatment above, 100 random initial states $\{\Psi_i | 1 \leq i \leq 100\}$, with random $2 < N < 11$, were drawn by the simplex picking method [86]. For each random state, $n = 100$ trajectories were generated, each of which ends asymptotically in one of the pointer states. Using the observed relative frequencies f_k , $1 \leq k \leq N$, of the pointer states, we evaluate

$$\chi^2 = n \sum_{k=1}^N \frac{\left(f_k - |c_k(0)|^2\right)^2}{|c_k(0)|^2}, \quad (8.56)$$

for each random state. In order to verify that the pointer states are distributed according to $|c_k(0)|^2$, the set $\{\chi_i^2\}$ must be shown to be sampled from a χ^2 -distribution with $N - 1$ degrees of freedom. Comparing the set $\{\chi_i^2\}$ with the α -quantiles ² (denoted by Q_α) of the corresponding χ^2 -distribution, a typical run shows ten cases where $\chi_i^2 > Q_{0.9}$, one case where $\chi_i^2 > Q_{0.99}$, but not a single case where $\chi_i^2 > Q_{0.999}$, as one expects if the $\{\chi_i^2\}$ are χ^2 -distributed. Like above, this confirms statistically that the asymptotic trajectories are distributed according to the expected overlap (8.45)

²For instance, the 0.9 quantile is the value such that 90% of the samples lie below $Q_{0.9}$.

Chapter 9

Unraveling the quantum linear Boltzmann equation

The previous chapters have been concerned with the short-time dynamics induced by collisional decoherence. As discussed in Sect. 3.5, collisional decoherence describes the motion of a quantum test particle in an ideal gas environment, assuming the Brownian particle to be much heavier than the atoms or molecules of the background gas. The situation is much more involved when the tracer mass M is of the order of the gas mass m . In this case the Brownian particle experiences friction, so that the corresponding master equation must be able to describe the full interplay between decoherence and dissipation.

An example of such an equation is the Caldeira-Leggett equation (3.26), discussed in Sect. 3.3. However, this equation is applicable only if the interaction can be linearized and the particle state is close to a thermal one. Moreover, its derivation is not based on a microscopic description of the collisional interaction with the gas.

A Lindblad master equation which circumvents these downsides is the *quantum linear Boltzmann equation* QLBE, proposed in [10–12]. It is the quantum counterpart of the *classical linear Boltzmann equation* [87], which describes how the motion of a classical test particle is affected by elastic collisions with an ideal, stationary background gas. The derivation of the QLBE is based on the monitoring approach, discussed in Sect. 3.4, which admits the treatment of the interactions with the background gas in a non-perturbative manner. These interactions may therefore be strong and the tracer particle may be in a state which is far from equilibrium. A premise for the applicability of the monitoring approach is that three-particle collisions are sufficiently unlikely, and that subsequent collisions with the same gas particle are negligible within the relevant time scale. These conditions should be fulfilled for the case of an ideal gas in a stationary state. A further condition is that the interactions are short-ranged, such that the application of scattering theory is possible.

Due to the complexity of the QLBE, it is in general not analytically tractable. However, since the QLBE has Lindblad form, one may apply quantum trajectory methods, such as the Monte Carlo unraveling discussed in Sect. 7.3.1. The straightforward application would be computationally very intensive, especially if one is dealing with the three-dimensional version. Breuer and Vacchini have therefore suggested in [26] to exploit the translation-covariance of the QLBE to solve it efficiently. Their treatment is restricted to the Born approximation of the

QLBE and to simulations of specific initial states, which are superpositions of at most two momentum eigenstates.

The purpose of this chapter is to expand the algorithm of Breuer and Vacchini [26] to the full QLBE and to arbitrary initial states, such as spatially localized wave packets. The latter will allow us to analyze physical phenomena which are more apparent in position space, such as diffusion or decoherence in position. As a further extension of [26], we apply the algorithm to realistic, microscopically derived scattering amplitudes.

The structure of this chapter is as follows. Section 9.1 reviews the QLBE in its basis independent operator form. In Sect. 9.2, the various limiting forms of the QLBE are summarized, based on the treatments in [10, 12, 13]. In Sect. 9.3, we apply the Monte Carlo unraveling to the QLBE; as mentioned above, this treatment is an extension of the work presented in [12, 26]. The numerical results of this algorithm are summarized in the next chapter.

9.1 The quantum linear Boltzmann equation (QLBE)

The QLBE is a Markovian master equation for the reduced density operator ρ describing the evolution of a tracer particle in an ideal gas environment. It has Lindblad form, $\dot{\rho} = \mathcal{L}\rho$, with generator

$$\mathcal{L}\rho = \frac{1}{i\hbar} \left[\frac{\mathbf{P}^2}{2M} + \mathbf{H}_n(\mathbf{P}), \rho \right] + \mathcal{D}\rho. \quad (9.1)$$

Here $\mathbf{H}_n(\mathbf{P})$ describes the energy shift due to the interaction with the background gas; it will be neglected in the following, since it is typically small. The incoherent part of the interaction is accounted for by the superoperator \mathcal{D} , which can be expressed as [10–12]

$$\begin{aligned} \mathcal{D}\rho = & \int_{\mathbb{R}^3} d\mathbf{Q} \int_{\mathbf{Q}^\perp} d\mathbf{p} \left(e^{i\mathbf{Q}\cdot\mathbf{X}/\hbar} L(\mathbf{p}, \mathbf{P}, \mathbf{Q}) \rho L^\dagger(\mathbf{p}, \mathbf{P}, \mathbf{Q}) e^{-i\mathbf{Q}\cdot\mathbf{X}/\hbar} \right. \\ & \left. - \frac{1}{2} \left\{ \rho, L^\dagger(\mathbf{p}, \mathbf{P}, \mathbf{Q}) L(\mathbf{p}, \mathbf{P}, \mathbf{Q}) \right\} \right), \end{aligned} \quad (9.2)$$

with $\mathbf{X} = (X_1, X_2, X_3)$ and $\mathbf{P} = (P_1, P_2, P_3)$ the position and the momentum operator of the Brownian tracer particle and $\{\cdot, \cdot\}$ the anti-commutator. The integration variables are given by \mathbf{Q} , the momentum transfer experienced in a single collision, and \mathbf{p} , corresponding to the momentum of a gas particle. Notably, the \mathbf{p} -integration is over the plane \mathbf{Q}^\perp , which is perpendicular to \mathbf{Q} , that is $\mathbf{Q}^\perp = \{\mathbf{p} \in \mathbb{R}^3 | \mathbf{p} \cdot \mathbf{Q} = 0\}$.

The operator-valued function $L(\mathbf{p}, \mathbf{P}, \mathbf{Q})$ contains all the details of the collisional interaction with the gas; these are the gas density n_{gas} , the momentum distribution function $\mu(\mathbf{p})$ of the gas, and the elastic scattering amplitude $f(\mathbf{p}_f, \mathbf{p}_i)$. It is defined by [10–12]

$$\begin{aligned} L(\mathbf{p}, \mathbf{P}, \mathbf{Q}) = & \sqrt{\frac{n_{\text{gas}} m}{m_*^2 Q}} f \left(\text{rel}(\mathbf{p}_{\perp \mathbf{Q}}, \mathbf{P}_{\perp \mathbf{Q}}) - \frac{\mathbf{Q}}{2}, \text{rel}(\mathbf{p}_{\perp \mathbf{Q}}, \mathbf{P}_{\perp \mathbf{Q}}) + \frac{\mathbf{Q}}{2} \right) \\ & \times \sqrt{\mu \left(\mathbf{p}_{\perp \mathbf{Q}} + \frac{m}{m_*} \frac{\mathbf{Q}}{2} + \frac{m}{M} \mathbf{P}_{\parallel \mathbf{Q}} \right)}. \end{aligned} \quad (9.3)$$

Here $m_* \equiv mM/(m+M)$ is the reduced mass, $Q \equiv |\mathbf{Q}|$ gives the modulus of the momentum transfer \mathbf{Q} , and

$$\text{rel}(\mathbf{p}, \mathbf{P}) \equiv \frac{m_*}{m} \mathbf{p} - \frac{m_*}{M} \mathbf{P}, \quad (9.4)$$

defines relative momenta. The subscripts $\parallel \mathbf{Q}$ and $\perp \mathbf{Q}$ denote the component of a vector parallel and perpendicular to \mathbf{Q} , meaning that

$$\mathbf{P}_{\parallel \mathbf{Q}} = \frac{(\mathbf{P} \cdot \mathbf{Q}) \mathbf{Q}}{Q^2}, \quad (9.5)$$

$$\mathbf{P}_{\perp \mathbf{Q}} = \mathbf{P} - \mathbf{P}_{\parallel \mathbf{Q}}. \quad (9.6)$$

Notice that the QLBE described by Eqs. (9.1) and (9.2) has the general structure of a translation-covariant Lindblad master equation (2.59), as characterized by Holevo [41–45]. This feature will be important below, when applying the Monte Carlo unraveling to the QLBE.

9.2 Limiting forms

Suitable limiting procedures reduce the QLBE to other well-known evolution equations, whose solutions are (at least partly) understood. These connections allow us to interpret the numerical solutions of the QLBE in the next chapter. At the same time, the stochastic simulation technique of the full QLBE permits us to study the range of validity of these approximate evolution equations.

9.2.1 Classical linear Boltzmann equation (CLBE)

To establish the connection with the CLBE, one may switch to the interaction picture, $\tilde{\rho} = e^{i\mathbf{H}t/\hbar} \rho e^{-i\mathbf{H}t/\hbar}$ with $\mathbf{H} = \mathbf{P}^2/2M$, and consider the evolution of the diagonal elements $w(\mathbf{P}) \equiv \langle \mathbf{P} | \tilde{\rho} | \mathbf{P} \rangle$ in the momentum basis. As is shown in [10–12], the incoherent part of the QLBE, Eqs. (9.2) and (9.3), implies that

$$\partial_t w(\mathbf{P}) = \int d\mathbf{Q} [W(\mathbf{P} | \mathbf{P} - \mathbf{Q}) w(\mathbf{P} - \mathbf{Q}) - W(\mathbf{P} + \mathbf{Q} | \mathbf{P}) w(\mathbf{P})], \quad (9.7)$$

where the transition rates W are given by

$$\begin{aligned} W(\mathbf{P} + \mathbf{Q} | \mathbf{P}) &= \int_{\mathbf{Q}^\perp} d\mathbf{p} |L(\mathbf{p}, \mathbf{P}, \mathbf{Q})|^2 \\ &= \frac{n_{\text{gas}} m}{m_*^2 Q} \int_{\mathbf{Q}^\perp} d\mathbf{p} \mu \left(\mathbf{p}_{\perp \mathbf{Q}} + \frac{m}{m_*} \frac{\mathbf{Q}}{2} + \frac{m}{M} \mathbf{P}_{\parallel \mathbf{Q}} \right) \\ &\quad \times \sigma \left(\text{rel}(\mathbf{p}_{\perp \mathbf{Q}}, \mathbf{P}_{\perp \mathbf{Q}}) - \frac{Q}{2}, \text{rel}(\mathbf{p}_{\perp \mathbf{Q}}, \mathbf{P}_{\perp \mathbf{Q}}) + \frac{Q}{2} \right). \end{aligned} \quad (9.8)$$

Here $\sigma(\mathbf{p}_f, \mathbf{p}_i) \equiv |f(\mathbf{p}_f, \mathbf{p}_i)|^2$ denotes the quantum mechanically defined differential cross section.

According to [10–12], Eqs. (9.7) and (9.9) agree with the collisional part of the CLBE. A comparison with Eq. (6.9) shows that it has the structure of a classical Markovian master equation, with W the transition rates of the Markovian process.

In addition, it is argued in [12] that the solution of the QLBE gets asymptotically diagonal in momentum basis for any initial state ρ_0 , that is

$$\langle \mathbf{P} | e^{\mathcal{L}t} \rho_0 | \mathbf{P}' \rangle \rightarrow 0, \quad \text{for } t \rightarrow \infty \text{ and } \mathbf{P} \neq \mathbf{P}'. \quad (9.10)$$

It follows that the QLBE asymptotically approaches the CLBE for the population dynamics in momentum space. This connection will be important below, when analyzing the diffusive behavior exhibited by the numerical solution of the QLBE.

9.2.2 Pure collisional decoherence

The complexity of the QLBE reduces a lot, if one assumes the test particle to be much heavier than the gas molecules. For, taking m/M to zero the Lindblad operators in (9.2) no longer dependent on the momentum operator \mathbf{P} of the tracer particle, so that the \mathbf{p} -integration in (9.2) can be carried out [11, 12]. The QLBE then turns into the master equation of pure collisional decoherence defined by Eqs. (3.47), (3.51), (3.52) and (3.53).

As the reader may recall from Sect. 3.5, Eq. (3.49), collisional decoherence leads to an exponential decay of the spatial coherences. The corresponding decay rate, and its dependence on the spatial distance $s = |\mathbf{x} - \mathbf{x}'|$, is described by the localization rate $F(s)$, which can be determined from the relevant microscopic quantities by Eq. (3.52). This fact will allow us below to predict the decoherence dynamics exhibited by the numerical solution of the QLBE in the limit $M \gg m$.

9.2.3 Born approximation

Another simplification results when the interaction potential $V(\mathbf{x})$ is much weaker than the kinetic energy $E = p^2/2m$ (\mathbf{x} and \mathbf{p} denote relative coordinates). One may then replace the exact scattering amplitude f by its Born approximation f_B , which is determined by the Fourier transform of the interaction potential,

$$f_B(\mathbf{p}_f - \mathbf{p}_i) = -\frac{m_*}{2\pi\hbar^2} \int d\mathbf{x} V(\mathbf{x}) \exp\left(-i\frac{(\mathbf{p}_f - \mathbf{p}_i) \cdot \mathbf{x}}{\hbar}\right). \quad (9.11)$$

The approximated scattering amplitude therefore depends on the momentum transfer $\mathbf{p}_f - \mathbf{p}_i$ only, such that the f in (9.3) is not operator-valued anymore. Taking μ to be Maxwell-Boltzmann distributed, see Eq. (5.80), one may then perform the \mathbf{p} -integration in (9.2), such that the generator \mathcal{D} becomes [11, 12, 88, 89]

$$\begin{aligned} \mathcal{D}_B \rho &= \int d\mathbf{Q} \left(e^{i\mathbf{Q} \cdot \mathbf{x} / \hbar} L_B(\mathbf{P}, \mathbf{Q}) \rho L_B^\dagger(\mathbf{P}, \mathbf{Q}) e^{-i\mathbf{Q} \cdot \mathbf{x} / \hbar} \right. \\ &\quad \left. - \frac{1}{2} \left\{ \rho, L_B^\dagger(\mathbf{P}, \mathbf{Q}) L_B(\mathbf{P}, \mathbf{Q}) \right\} \right). \end{aligned} \quad (9.12)$$

Here the jump operators contain the functions $L_B(\mathbf{P}, \mathbf{Q})$, given by the expression [11, 12, 89]

$$\begin{aligned} L_B(\mathbf{P}, \mathbf{Q}) &= \left(\frac{\beta m}{2\pi} \right)^{1/4} \sqrt{\frac{n_{\text{gas}} \sigma_B(\mathbf{Q})}{m_*^2 Q}} \\ &\quad \times \exp\left(-\frac{\beta}{16mQ^2} \left[\left(1 + \frac{m}{M}\right) Q^2 + 2\frac{m}{M} \mathbf{P} \cdot \mathbf{Q} \right]^2\right), \end{aligned} \quad (9.13)$$

where $\sigma_B(\mathbf{Q}) \equiv |f_B(\mathbf{Q})|^2$ denotes the differential cross section in Born approximation and $\beta \equiv 1/kT$ is the inverse temperature.

The QLBE in Born approximation defined by Eqs. (9.12) and (9.13) was proposed by Vacchini in [88,89]. As mentioned in the introduction of this chapter, its solution may be obtained numerically by the stochastic algorithm proposed by Breuer and Vacchini [26].

9.2.4 Quantum Brownian limit

The *quantum Brownian* or *diffusive limit* applies when the Brownian state is close to thermal and the mass of the test particle is much greater than the gas particle mass [11,12]. The momentum transfer \mathbf{Q} is then small compared to the momentum of the tracer particle. As discussed in [90], this admits the expansion of the Lindblad operators in (9.2) up to second order in the position and momentum operators. According to [11,12], this expansion yields the Caldeira-Leggett equation in Lindblad form (3.33), with dimensionless parameter $\lambda = 1$. The QLBE therefore leads naturally to the minimally invasive modification of the original Caldeira-Leggett equation, see Sect. 3.3.2.

As a by-product, this derivation yields a microscopic expression for the relaxation rate appearing in the Caldeira-Leggett equation [12]

$$\gamma = n_{\text{gas}} \frac{8m}{3M} \sqrt{\frac{2\pi}{m\beta}} \int_0^\infty du u^5 e^{-u^2} \int_0^\pi d\theta \sin\theta (1 - \cos\theta) |f(\cos\theta, up_\beta)|^2. \quad (9.14)$$

Here it is assumed that the gas particle momenta are Maxwell-Boltzmann distributed, and that the scattering is isotropic such that f depends only on the scattering angle θ and the modulus of the momentum $p \equiv |\mathbf{p}_i| = |\mathbf{p}_f|$. The integration variable $u \equiv p/p_\beta$ denotes the momentum in dimensionless form and $p_\beta = \sqrt{2m/\beta}$ is the most probable momentum at temperature $T = 1/(k_B\beta)$.

9.3 Monte Carlo unraveling

To solve the QLBE we now employ the Monte Carlo wave function method [27–29]. In this framework, a pure initial state $|\psi(0)\rangle$ is propagated by a stochastic differential equation (SDE) to generate an ensemble of pure states $\{|\psi_\alpha(t)\rangle\}$, whose average yields the solution of the master equation,

$$\mathbb{E}[|\psi(t)\rangle\langle\psi(t)|] = e^{\mathcal{L}t}|\psi(0)\rangle\langle\psi(0)|. \quad (9.15)$$

As can be recalled from Sect. 7.3.1, Eq. (7.59), the corresponding SDE has the form

$$\begin{aligned} |d\psi_t\rangle &= -\frac{i}{\hbar} \mathbf{H}_{\text{eff}} |\psi_t\rangle dt + \frac{1}{2} \sum_i \gamma_i \|\mathbf{L}_i |\psi_t\rangle\|^2 |\psi_t\rangle dt \\ &+ \sum_i \left(\frac{\mathbf{L}_i |\psi_t\rangle}{\|\mathbf{L}_i |\psi_t\rangle\|} - |\psi_t\rangle \right) dN_i(t), \end{aligned} \quad (9.16)$$

where the non-Hermitian operator \mathbf{H}_{eff} denotes the effective Hamiltonian

$$\mathbf{H}_{\text{eff}} = \mathbf{H} - \frac{i\hbar}{2} \sum_i \gamma_i \mathbf{L}_i^\dagger \mathbf{L}_i. \quad (9.17)$$

The Poisson increments $dN_i(t)$ in Eq. (9.16) satisfy the Ito rules (6.92) and the expectation value (7.60), which can also be written as

$$\mathbb{E}[dN_i(t)] = \gamma_i \|L_i|\psi_t\rangle\|^2 dt. \quad (9.18)$$

In the following section, we will introduce an algorithm which is typically used for the implementation of the SDE (9.16); this discussion is based on the treatments in [29, 91]. The algorithm is then applied to unravel the QLBE in Sect. 9.3.2. As mentioned in the introduction, this result is an extension of the work presented in [12, 26].

9.3.1 The general algorithm

Suppose the state $|\psi_t\rangle$ was reached through a quantum jump at time t . Then, subsequently, the state follows a deterministic evolution generated by the nonlinear equation

$$\partial_t |\psi_t\rangle = -\frac{i}{\hbar} \mathbf{H}_{\text{eff}} |\psi_t\rangle + \frac{1}{2} \sum_i \gamma_i \|L_i|\psi_t\rangle\|^2 |\psi_t\rangle. \quad (9.19)$$

Its formal solution reads as [29]

$$|\psi_{t+\tau}\rangle = \frac{\exp(-i\mathbf{H}_{\text{eff}}\tau/\hbar) |\psi_t\rangle}{\|\exp(-i\mathbf{H}_{\text{eff}}\tau/\hbar) |\psi_t\rangle\|}, \quad (9.20)$$

which can be verified by computing the time derivative of $|\psi_{t+\tau}\rangle$ [29]. The probability for a jump to occur out of this state is characterized by the total jump rate

$$\Gamma(\psi_t) = \frac{1}{dt} \sum_i \mathbb{E}[dN_i(t)] = \sum_i \gamma_i \|L_i|\psi_t\rangle\|^2, \quad (9.21)$$

which admits to evaluate the corresponding *waiting time distribution* $W(\tau|\psi_t)$. The latter is the cumulative distribution function of the probability that a jump occurs in the time interval $[t, t + \tau]$. Since the quantum jumps follow a Poisson process, the waiting time distribution reads

$$W(\tau|\psi_t) = 1 - \text{Prob}(\text{no jump in } [t, t + \tau]) \quad (9.22)$$

$$= 1 - \exp\left(-\int_t^{t+\tau} dt' \Gamma(\psi_{t'})\right), \quad (9.23)$$

where we have used Eq. (6.79) in the second line. Using (9.20) and (9.21) it can be shown that this yields [29]

$$W(\tau|\psi_t) = 1 - \|\exp(-i\mathbf{H}_{\text{eff}}\tau/\hbar) |\psi_t\rangle\|^2. \quad (9.24)$$

A sample τ of this cumulative distribution function is obtained, for instance, by the inversion method, that is by solving the equation

$$\eta = \|\exp(-i\mathbf{H}_{\text{eff}}\tau/\hbar) |\psi_t\rangle\|^2, \quad (9.25)$$

where η is a random number drawn from the uniform distribution on $[0, 1]$.

Once this waiting time τ has elapsed, the state makes a jump, that is $|\psi_{t+\tau}\rangle$ is replaced by

$$|\psi_{t+\tau}\rangle \rightarrow \frac{\mathbf{L}_i |\psi_{t+\tau}\rangle}{\|\mathbf{L}_i |\psi_{t+\tau}\rangle\|}. \quad (9.26)$$

The index i of the corresponding jump operator is drawn from the probability distribution given by the ratio of the jump rate $\Gamma_i(\psi_{t+\tau}) = \mathbb{E}[dN_i(t+\tau)]/dt$ of the Poisson process $N_i(t)$ and the total jump rate $\Gamma(\psi_{t+\tau})$, that is

$$\begin{aligned} \text{Prob}(i|\psi_{t+\tau}) &= \frac{\Gamma_i(\psi_{t+\tau})}{\Gamma(\psi_{t+\tau})} \\ &= \frac{\gamma_i}{\Gamma(\psi_{t+\tau})} \|\mathbf{L}_i |\psi_{t+\tau}\rangle\|^2. \end{aligned} \quad (9.27)$$

9.3.2 Unraveling the QLBE

The Monte Carlo method is now applied to solve the QLBE, which is characterized by the two-parameter family of Lindblad operators $e^{i\mathbf{Q}\cdot\mathbf{X}/\hbar} \mathbf{L}(\mathbf{p}, \mathbf{P}, \mathbf{Q})$. The corresponding algorithm is obtained by replacing the index i with the continuous variables \mathbf{Q} and \mathbf{p} , and by substituting sums over i by integrals over these momenta, that is

$$\sum_i \rightarrow \int_{\mathbb{R}^3} d\mathbf{Q} \int_{\mathbf{Q}^\perp} d\mathbf{p}. \quad (9.28)$$

This procedure is straightforward; nevertheless, we repeat the main steps in the following, since these formulas are required for reference later on.

The stochastic differential equation The Monte Carlo unraveling of the QLBE is described by the SDE

$$\begin{aligned} |d\psi_t\rangle &= -\frac{i}{\hbar} \mathbf{H}_{\text{eff}} |\psi_t\rangle dt + \frac{1}{2} \int_{\mathbb{R}^3} d\mathbf{Q} \int_{\mathbf{Q}^\perp} d\mathbf{p} \|L(\mathbf{p}, \mathbf{P}, \mathbf{Q}) |\psi_t\rangle\|^2 |\psi_t\rangle dt \\ &+ \int_{\mathbb{R}^3} d\mathbf{Q} \int_{\mathbf{Q}^\perp} d\mathbf{p} \left(\frac{e^{i\mathbf{Q}\cdot\mathbf{X}/\hbar} L(\mathbf{p}, \mathbf{P}, \mathbf{Q}) |\psi_t\rangle}{\|L(\mathbf{p}, \mathbf{P}, \mathbf{Q}) |\psi_t\rangle\|} - |\psi_t\rangle \right) dN_{\mathbf{Q}, \mathbf{p}}(t), \end{aligned} \quad (9.29)$$

where the effective Hamiltonian has the form

$$\mathbf{H}_{\text{eff}} = \mathbf{H} - \frac{i\hbar}{2} \int_{\mathbb{R}^3} d\mathbf{Q} \int_{\mathbf{Q}^\perp} d\mathbf{p} \mathbf{L}^\dagger(\mathbf{p}, \mathbf{P}, \mathbf{Q}) \mathbf{L}(\mathbf{p}, \mathbf{P}, \mathbf{Q}). \quad (9.30)$$

The Poisson increments in (9.29) satisfy the expectation values

$$\mathbb{E}[dN_{\mathbf{Q}, \mathbf{p}}(t)] = \|L(\mathbf{p}, \mathbf{P}, \mathbf{Q}) |\psi_t\rangle\|^2 dt, \quad (9.31)$$

and the Poisson field

$$dN_{\mathbf{Q}, \mathbf{p}}(t) dN_{\mathbf{Q}', \mathbf{p}'}(t) = \delta^{(3)}(\mathbf{Q} - \mathbf{Q}') \delta^{(2)}(\mathbf{p}_{\perp \mathbf{Q}} - \mathbf{p}'_{\perp \mathbf{Q}}) dN_{\mathbf{Q}, \mathbf{p}}(t). \quad (9.32)$$

These rules are the continuous counterpart of the discrete set of equations (6.92).

The Monte Carlo algorithm The deterministic part of the Monte Carlo unraveling is generated by the nonlinear equation

$$\partial_t |\psi_t\rangle = -\frac{i}{\hbar} H_{\text{eff}} |\psi_t\rangle + \frac{1}{2} \int_{\mathbb{R}^3} d\mathbf{Q} \int_{\mathbf{Q}^\perp} d\mathbf{p} \|L(\mathbf{p}, \mathbf{P}, \mathbf{Q}) |\psi_t\rangle\|^2 |\psi_t\rangle, \quad (9.33)$$

whose formal solution is given by Eq. (9.20). The probability for a jump to occur out of this state is determined by the total jump rate

$$\Gamma(\psi_t) = \int_{\mathbb{R}^3} d\mathbf{Q} \int_{\mathbf{Q}^\perp} d\mathbf{p} \|L(\mathbf{p}, \mathbf{P}, \mathbf{Q}) |\psi_t\rangle\|^2, \quad (9.34)$$

which is associated to the waiting time distribution (9.24). An instance of a waiting time τ is obtained by the inversion method, that is by the solution of Eq. (9.25).

At time $t + \tau$, the state makes a jump, that is $|\psi_{t+\tau}\rangle$ is replaced as

$$|\psi(t + \tau)\rangle \rightarrow \frac{e^{i\mathbf{Q}\cdot\mathbf{X}/\hbar} L(\mathbf{p}, \mathbf{P}, \mathbf{Q}) |\psi_{t+\tau}\rangle}{\|L(\mathbf{p}, \mathbf{P}, \mathbf{Q}) |\psi_{t+\tau}\rangle\|}. \quad (9.35)$$

The momenta \mathbf{p} and \mathbf{Q} characterizing the above jump operator are drawn from the following probability density

$$\text{Prob}(\mathbf{p}, \mathbf{Q} | \psi_{t+\tau}) = \frac{1}{\Gamma(|\psi_{t+\tau}\rangle)} \|L(\mathbf{p}, \mathbf{P}, \mathbf{Q}) |\psi_{t+\tau}\rangle\|^2. \quad (9.36)$$

9.3.3 Unraveling the QLBE in the momentum basis

As suggested in [26], the implementation of the above algorithm is particularly simple when the initial state is a discrete superposition of a finite number of momentum eigenstates

$$|\psi(0)\rangle = \sum_{i=1}^N \alpha_i(0) |\mathbf{P}_i(0)\rangle, \quad \text{with} \quad \sum_{i=1}^N |\alpha_i(0)|^2 = 1. \quad (9.37)$$

Due to the translation-covariance of the QLBE, the Lindblad operators have the structure $e^{i\mathbf{Q}\cdot\mathbf{X}/\hbar} L(\mathbf{p}, \mathbf{P}, \mathbf{Q})$. This implies that the effective Hamiltonian is a function of the momentum operator only, so that the deterministic evolution affects solely the weights of the superposition, that is

$$|\psi(t)\rangle = \sum_{i=1}^N \alpha_i(t) |\mathbf{P}_i(0)\rangle. \quad (9.38)$$

The jumps, on the other hand, cause a translation of the momentum eigenstates and a redistribution of the weights,

$$e^{i\mathbf{Q}\cdot\mathbf{X}/\hbar} L(\mathbf{p}, \mathbf{P}, \mathbf{Q}) |\psi(t)\rangle = \sum_{i=1}^N \alpha'_i(t) |\mathbf{P}_i + \mathbf{Q}\rangle, \quad (9.39)$$

This shows that the quantum trajectory remains a superposition of N momentum eigenstates at all times. The stochastic process has therefore been reduced from an infinite dimensional unraveling to a stochastic process in the space of amplitudes α_i and momenta \mathbf{P}_i [12, 26].

It should be mentioned that the momentum eigenstates in (9.37) are assumed to be normalized with respect to a large volume Ω , so that they form a discrete basis $\langle \mathbf{P}_i | \mathbf{P}_j \rangle = \delta_{ij}$. Strictly speaking, the algorithm in Sect. 9.3.2 is not applicable to the continuous case, where the momentum eigenstates are improper. Practically, however, the states $|\mathbf{P}_i\rangle$ may be considered to discretize the continuous basis, assuming Ω to be sufficiently large.

Dimensionless variables It turns out to be convenient to work with the dimensionless variables

$$\mathbf{U} \equiv \frac{\mathbf{P}}{Mv_\beta}, \quad \mathbf{K} \equiv \frac{\mathbf{Q}}{m_*v_\beta}, \quad \mathbf{W} \equiv \frac{\mathbf{p}}{mv_\beta}, \quad (9.40)$$

with the scale given by the most probable velocity of the gas particles $v_\beta = \sqrt{2k_B T/m}$. Note that \mathbf{W} , being proportional to \mathbf{p} , lies in the plane perpendicular to \mathbf{K} . The quantum trajectories are then represented as

$$|\psi(t)\rangle = \sum_{i=1}^N \alpha_i(t) |\mathbf{U}_i(t)\rangle, \quad \text{with } \sum_{i=1}^N |\alpha_i(t)|^2 = 1. \quad (9.41)$$

Jump rate Before discussing the unraveling of the QLBE in more detail, let us evaluate the jump rate (9.34) for momentum eigenstates, $|\psi_t\rangle = |\mathbf{P}\rangle$. This quantity appears frequently in the algorithm described below.

By inserting $|\psi_t\rangle = |\mathbf{P}\rangle$ into Eq. (9.34), one obtains

$$\begin{aligned} \Gamma(\mathbf{P}) &= \int_{\mathbb{R}^3} d\mathbf{Q} \int_{\mathbf{Q}^\perp} d\mathbf{p} \|L(\mathbf{p}, \mathbf{P}, \mathbf{Q}) |\mathbf{P}\rangle\|^2 \\ &= \int_{\mathbb{R}^3} d\mathbf{Q} \int_{\mathbf{Q}^\perp} d\mathbf{p} |L(\mathbf{p}, \mathbf{P}, \mathbf{Q})|^2. \end{aligned} \quad (9.42)$$

Noting Eq. (9.8), one finds that the jump rate agrees with the total collision rate for a particle with momentum \mathbf{P} ,

$$\Gamma(\mathbf{P}) = \int d\mathbf{Q} W(\mathbf{P} + \mathbf{Q} | \mathbf{P}). \quad (9.43)$$

It follows that $\Gamma(\mathbf{P}) = \Gamma(P)$ is function of the modulus of \mathbf{P} only, since the collision rate must be independent of the orientation of \mathbf{P} for a homogeneous background gas.

Upon using the dimensionless quantities (9.40), Eq. (9.42) becomes

$$\Gamma(U) = m_* m v_\beta^2 \int_{\mathbb{R}^3} d\mathbf{K} \int_{\mathbf{K}^\perp} d\mathbf{W} |L(mv_\beta \mathbf{W}, Mv_\beta \mathbf{U}, m_* v_\beta \mathbf{K})|^2. \quad (9.44)$$

By inserting (9.3) for L and the Maxwell-Boltzmann distribution (5.80) for μ , one finds

$$\Gamma(U) = \int_{\mathbb{R}^3} d\mathbf{K} \int_{\mathbf{K}^\perp} d\mathbf{W} g(\mathbf{W}, \mathbf{U}, \mathbf{K}) p_{\sigma_K}(\mathbf{K}) p_{\sigma_W}(\mathbf{W}), \quad (9.45)$$

with

$$\begin{aligned} g(\mathbf{W}, \mathbf{U}, \mathbf{K}) &= 8\pi n_{\text{gas}} v_\beta \frac{1}{|\mathbf{K}|} \left| f\left(m_* v_\beta \left[\mathbf{R} - \frac{\mathbf{K}}{2}\right], m_* v_\beta \left[\mathbf{R} + \frac{\mathbf{K}}{2}\right]\right) \right|^2 \\ &\quad \times e^{-\mathbf{K} \cdot \mathbf{U}} e^{-U_{\parallel \mathbf{K}}^2}, \end{aligned} \quad (9.46)$$

and $\mathbf{R} \equiv \mathbf{W}_{\perp \mathbf{K}} - \mathbf{U}_{\perp \mathbf{K}}$. The densities $p_{\sigma_K}(\mathbf{K})$ and $p_{\sigma_W}(\mathbf{W})$ denote three- and two-dimensional normal distributions, respectively,

$$\begin{aligned} p_{\sigma_K}(\mathbf{K}) &= \frac{1}{(2\pi\sigma_K)^{3/2}} \exp\left(-\frac{\mathbf{K}^2}{2\sigma_K^2}\right), \\ p_{\sigma_W}(\mathbf{W}) &= \frac{1}{2\pi\sigma_W} \exp\left(-\frac{\mathbf{W}^2}{2\sigma_W^2}\right), \end{aligned} \quad (9.47)$$

with variances $\sigma_K = \sqrt{2}$ and $\sigma_W = 1/\sqrt{2}$.

The integral (9.45) can be solved numerically using a Monte Carlo method with importance sampling [72]. For this purpose, one draws n samples \mathbf{K}_i from the normal distribution $p_{\sigma_K}(\mathbf{K})$ and computes orthonormal vectors \mathbf{e}_{1i} and \mathbf{e}_{2i} which are orthogonal to \mathbf{K}_i , that is

$$\mathbf{e}_{1i} \cdot \mathbf{K}_i = 0, \quad \mathbf{e}_{2i} \cdot \mathbf{K}_i = 0, \quad \mathbf{e}_{1i} \cdot \mathbf{e}_{2i} = 0, \quad (9.48)$$

using the Gram-Schmidt method. As a next step, n further samples (u_i, v_i) are drawn from the two-dimensional Gaussian distribution p_{σ_W} , which admits to evaluate instances of scaled momentum vectors

$$\mathbf{W}_i = u_i \mathbf{e}_{1i} + v_i \mathbf{e}_{2i}. \quad (9.49)$$

The jump rate (9.45) is then approximated by the average

$$\Gamma(U) \simeq \frac{1}{n} \sum_{i=1}^n g(\mathbf{W}_i, U, \mathbf{K}_i). \quad (9.50)$$

The deterministic evolution Let us now discuss in more detail the unraveling of the QLBE in the momentum basis. To this end, suppose the state

$$|\psi(t)\rangle = \sum_{i=1}^N \alpha_i(t) |\mathbf{U}_i(t)\rangle, \quad (9.51)$$

was obtained through a quantum jump at time t . As mentioned above, the effective Hamiltonian (9.30) depends on the momentum operator only, such that the momenta \mathbf{U}_i stay constant during the deterministic evolution. The propagation of the state (9.51) with the non-Hermitian operator (9.30) thus yields

$$|\psi(t+\tau)\rangle = \sum_{i=1}^N \alpha_i(t+\tau) |\mathbf{U}_i(t)\rangle. \quad (9.52)$$

Here the weights have the form

$$\alpha_i(t+\tau) = \frac{1}{\mathcal{N}} \exp\left(-\frac{i}{2\hbar} M v_\beta \mathbf{U}_i^2 \tau\right) \exp\left(-\frac{\tau}{2} \Gamma(\mathbf{U}_i)\right) \alpha_i(t), \quad (9.53)$$

with the normalization

$$\mathcal{N}^2 = \sum_{i=1}^N |\alpha_i(t+\tau)|^2 = \sum_{i=1}^N |\alpha_i(t)|^2 \exp(-\tau \Gamma(\mathbf{U}_i)). \quad (9.54)$$

Drawing waiting times As a next step, let us evaluate the waiting times τ . For this purpose, consider the expression

$$\begin{aligned} & \|\exp(-i\mathbf{H}_{\text{eff}}\tau/\hbar)|\psi_t\rangle\|^2 \\ &= \sum_{i,j=1}^N \alpha_i^*(t) \alpha_j(t) \langle \mathbf{U}_i(t) | e^{i\mathbf{H}_{\text{eff}}^\dagger\tau/\hbar} e^{-i\mathbf{H}_{\text{eff}}\tau/\hbar} | \mathbf{U}_j(t) \rangle. \end{aligned} \quad (9.55)$$

By using the definition of \mathbf{H}_{eff} (9.30), the fact that the two summands in \mathbf{H}_{eff} commute, and the jump rate (9.44), this yields

$$\|\exp(-i\mathbf{H}_{\text{eff}}\tau/\hbar)|\psi_t\rangle\|^2 = \sum_{i=1}^N |\alpha_i(t)|^2 \exp(-\tau\Gamma(U_i)). \quad (9.56)$$

It follows from (9.25) that samples of the waiting times τ are obtained by solving the non-algebraic equation

$$\eta = \sum_{i=1}^N |\alpha_i(t)|^2 \exp(-\tau\Gamma(U_i)), \quad (9.57)$$

with η drawn from the uniform distribution on $[0, 1]$.

Drawing the momentum transfer To be able to carry out the quantum jumps, we have to determine the momenta \mathbf{K} and \mathbf{W} , which characterize the jump operator. These vectors are obtained by sampling from the probability distribution (9.36). Upon inserting states of the form (9.52), Eq. (9.36) becomes

$$\begin{aligned} \text{Prob}(\mathbf{W}, \mathbf{K}|\psi_{t+\tau}) &= \frac{\sum_{i=1}^N |\alpha_i(t+\tau)|^2 \Gamma(U_i)}{\sum_{j=1}^N |\alpha_j(t+\tau)|^2 \Gamma(U_j)} \frac{\|L(\mathbf{W}, \mathbf{U}_i, \mathbf{K})|\mathbf{U}_i\rangle\|^2}{\Gamma(U_i)} \\ &\equiv \sum_{i=1}^N p_i \text{Prob}(\mathbf{W}, \mathbf{K}|\mathbf{U}_i). \end{aligned} \quad (9.58)$$

This distribution is a mixture of the probabilities

$$p_i = \frac{|\alpha_i(t+\tau)|^2 \Gamma(U_i)}{\sum_{j=1}^N |\alpha_j(t+\tau)|^2 \Gamma(U_j)}, \quad (9.59)$$

and the probability densities

$$\begin{aligned} \text{Prob}(\mathbf{W}, \mathbf{K}|\mathbf{U}_i) &= \frac{\|L(\mathbf{W}, \mathbf{U}_i, \mathbf{K})|\mathbf{U}_i\rangle\|^2}{\Gamma(U_i)} \\ &= \frac{8\pi n_{\text{gas}} v_\beta}{\Gamma(U_i) |\mathbf{K}|} \left| f\left(m_* v_\beta \left[\mathbf{R} - \frac{\mathbf{K}}{2}\right], m_* v_\beta \left[\mathbf{R} + \frac{\mathbf{K}}{2}\right]\right) \right|^2 \\ &\quad \times \mu\left(m v_\beta \left[\mathbf{W}_{\perp\mathbf{K}} + \frac{\mathbf{K}}{2} + \mathbf{U}_{\parallel\mathbf{K}}\right]\right). \end{aligned} \quad (9.60)$$

In order to draw a sample from the mixture (9.59), one may proceed as follows [26]. First, an index i is drawn from the probabilities (9.59). Then, the momenta \mathbf{K} and \mathbf{W} are drawn from the probability distribution $\text{Prob}(\mathbf{W}, \mathbf{K}|\mathbf{U}_i)$ using a stochastic sampling method, such as the *Metropolis-Hastings algorithm* [72].

Application of the jump operators Having the momenta \mathbf{W} and \mathbf{K} at hand, one can now perform the quantum jump. According to Eq. (9.35), the state (9.52) is transformed as

$$\begin{aligned} |\psi(t+\tau)\rangle &\rightarrow \tilde{\mathcal{N}}^{-1} \exp\left(\frac{i}{\hbar} m v_\beta \mathbf{K} \cdot \mathbf{X}\right) L(\mathbf{W}, \mathbf{U}, \mathbf{K}) \sum_{i=1}^N \alpha_i(t+\tau) |\mathbf{U}_i(t)\rangle \\ &= \sum_{i=1}^N \tilde{\mathcal{N}}^{-1} L(\mathbf{W}, \mathbf{U}_i, \mathbf{K}) \alpha_i(t+\tau) |\mathbf{U}_i(t) + \frac{m_*}{M} \mathbf{K}\rangle, \end{aligned} \quad (9.61)$$

where the normalization $\tilde{\mathcal{N}}$ is determined by

$$\tilde{\mathcal{N}}^2 = \sum_{i=1}^N |L(\mathbf{W}, \mathbf{U}_i, \mathbf{K}) \alpha_i(t+\tau)|^2. \quad (9.62)$$

This shows that the momentum eigenstates are shifted

$$|\mathbf{U}_i\rangle \rightarrow |\mathbf{U}_i + \frac{m_*}{M} \mathbf{K}\rangle, \quad (9.63)$$

while the weights are redistributed as

$$\alpha_i(t+\tau) \rightarrow \alpha'_i(t+\tau) = x_i \alpha_i(t+\tau), \quad (9.64)$$

where the factors x_i are given by $x_i = \tilde{\mathcal{N}}^{-1} L(\mathbf{W}, \mathbf{U}_i, \mathbf{K})$. Upon using the explicit form of L (9.3), and by inserting the Maxwell-Boltzmann distribution (5.80), we find

$$\begin{aligned} x_i &= \frac{1}{\tilde{\mathcal{N}}} f\left(m_* v_\beta \left[\mathbf{R}_i - \frac{\mathbf{K}}{2}\right], m_* v_\beta \left[\mathbf{R}_i + \frac{\mathbf{K}}{2}\right]\right) \\ &\quad \times \exp\left(-\frac{1}{2} \left[\frac{\mathbf{K}}{2} + \mathbf{U}_{i\parallel\mathbf{K}}\right]^2\right) \end{aligned} \quad (9.65)$$

with relative momenta $\mathbf{R}_i = \mathbf{W}_{\perp\mathbf{K}} - \mathbf{U}_{i\perp\mathbf{K}}$.

Numerical analysis According to Eq. (9.63), the momentum eigenstates are all shifted with the same momentum \mathbf{K} in a quantum jump. This fact is very important for the numerical performance of the algorithm, since it implies that the time intensive Metropolis-Hastings algorithm must be applied only once for all $i \in \{1, \dots, N\}$. This suggests that the algorithm can be applied also to initial states which are superpositions of many momentum eigenstates.

This is substantiated by the numerical analysis depicted in the logarithmic plot of Figure 9.1. Here, the CPU time of the above algorithm was measured as a function of the number N of basis states involved in the initial superposition. For the latter, we choose the (arbitrary) state $|\psi(0)\rangle = \sum_{i=1}^N |\mathbf{U}_i\rangle / \sqrt{N}$, with $\mathbf{U}_i = (0, 0, i)$. The simulation is based on 10^2 quantum trajectories in each run. The curve shown in Fig. 9.1 is almost a straight line with a slope $a \simeq 1.1$. It follows that the CPU time grows almost linearly, $t \propto N^{1.1}$, with N .

We conclude that the Monte Carlo unraveling can be implemented for initial superposition states that are composed of a large number of momentum eigenstates (say, on the order of 10^2 to 10^3). This implies that one may choose localized initial states and consider scenarios where a particle crosses a slit or a grid. The following chapter presents numerical results obtained with such kind of states.

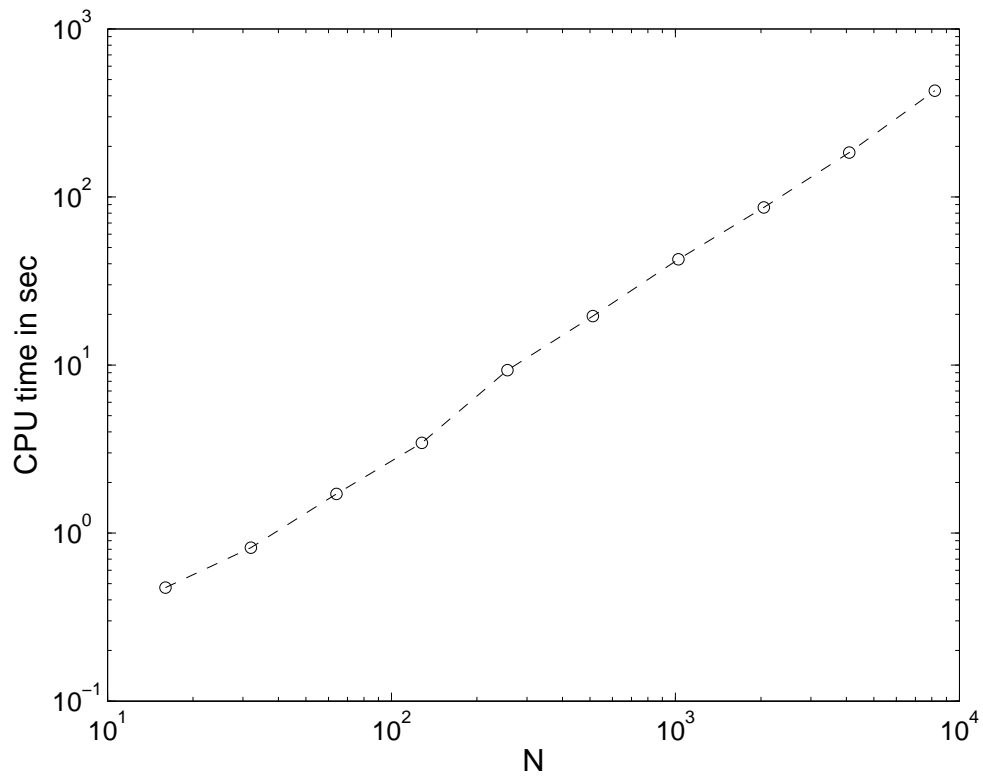


Figure 9.1: CPU time of the Monte Carlo unraveling as a function of the number N of basis states involved in the initial superposition. The curve is almost a straight line with slope $a \simeq 1.1$ in the logarithmic plot. It follows that the CPU time grows almost linearly with N , that is $t \propto N^{1.1}$.

Chapter 10

Numerical results

In the previous chapter an algorithm was developed which admits an efficient unraveling of the quantum linear Boltzmann equation (QLBE). In the following, let us apply this tool to simulate the dynamics of a test particle, affected by elastic collisions with an ideal, thermal background gas. The interaction will be described by two kinds of scenarios: s-wave hard-sphere scattering and a more realistic one, which results from a Gaussian interaction potential; an overview of these scattering amplitudes is given in Sect. 10.1.

In the first part of this chapter, the simulation of short-time effects is discussed. At first, initial states are chosen which are superpositions of two momentum eigenstates, and the loss of coherence in this basis is measured (Sect. 10.2). As a next step, superpositions of *spatially* localized wave packets are considered, such that decoherence in the position basis can be measured (Sect. 10.3). This admits in particular to extract the localization function introduced in Sect. 3.5. As a further application, counter-propagating localized initial states are considered, which leads to the formation of interference patterns (Sect. 10.4). In the course of the evolution, fringe visibility is lost, such that the interplay between coherence and decoherence can be demonstrated.

The second part of this chapter is devoted to long-time effects, which exhibit a classical counterpart. Section 10.5 studies energy and momentum relaxation, and the approach to thermal equilibrium. Then, in Sect. 10.6, spatially localized initial states are considered, and the variance of the populations is measured. Here, one observes a transition from quantum dispersion to classical diffusion.

As discussed in Sect. 9.2, the QLBE has several limiting forms, for some of which analytical solutions are known. Some of the simulations presented in this chapter correspond to situations where these limiting forms are expected to be valid. This admits to test the validity of our numerical results, and, on the other hand, to verify the limiting procedures discussed in Sect. 9.2. Other simulations presented in this chapter correspond to situations where the full QLBE is required, so that new physical regimes are entered which have not been understood so far. This includes in particular simulations of decoherence effects where the tracer mass is taken to be comparable to the gas particle mass.

10.1 Scattering amplitudes

Let us start with a description of the two kinds of elastic scattering amplitudes $f(\mathbf{p}_f, \mathbf{p}_i)$ used throughout this chapter.

10.1.1 s-wave hard-sphere scattering

In s-wave hard-sphere scattering [62], the particles are assumed to be hard spheres with radius R , such that the interaction potential $V(r)$ has the form

$$V(r) = \begin{cases} \infty, & \text{if } r \leq R, \\ 0, & \text{if } r > R, \end{cases} \quad (10.1)$$

with r the distance between the colliding particles. In addition, the energy of the incoming particles is assumed to be small, $pR \ll \hbar$, implying that the description can be restricted to the lowest partial wave contribution.

It is a textbook problem [62] to show that the scattering length [52] is in this case equal to the radius R of the particles, such that the scattering amplitude is independent of the scattering angle θ and the energy of the incoming particles E_{kin} , that is

$$|f(\cos \theta; E_{\text{kin}})|^2 = R^2. \quad (10.2)$$

Since this cross section is constant, one may perform the \mathbf{p} -integration in the QLBE (9.2), such that it agrees with the QLBE in Born approximation (9.12). The numerical results obtained with this interaction should therefore agree with the ones found by the stochastic algorithm of Breuer and Vacchini [26], providing a further test for the correctness of our algorithm.

Below, a variety of examples is presented, where the interaction is described by s-wave hard-sphere scattering. In these examples, the system of units is defined by setting $\hbar = 1$, $M = 1$ and $R = 1$; for the temperature we chose $k_B T = 1$ and the gas density is set to one, $n_{\text{gas}} = 1$.

An important ingredient for the implementation of the Monte Carlo unraveling is the jump rate $\Gamma(U)$ presented in Eq. (9.45). Figure 10.1 shows its numerical solution choosing the scattering amplitude (10.2). This plot is obtained using a Monte Carlo integration with importance sampling (9.50), where the number of steps is taken to be sufficiently large, $n = 10^5$. The jump rate is scaled with the characteristic rate

$$\Gamma_0 = n_{\text{gas}} v_\beta 4\pi R^2, \quad (10.3)$$

which gives the scattering rate of incoming particles having the most probable velocity v_β . To interpret Fig. 10.1 recall that the jump rate is given by the average collision rate of a particle with momentum U with the thermal background gas. Since the cross section is constant, the collision rate grows linearly for large momenta, while it saturates at a value close to Γ_0 for a vanishing U . The same behavior is found by the analytical result presented in [26].

10.1.2 Gaussian potential

To account for realistic scattering amplitudes, we chose as our second case an attractive Gaussian potential

$$V(r) = V_0 \exp\left(-\frac{r^2}{2d^2}\right). \quad (10.4)$$

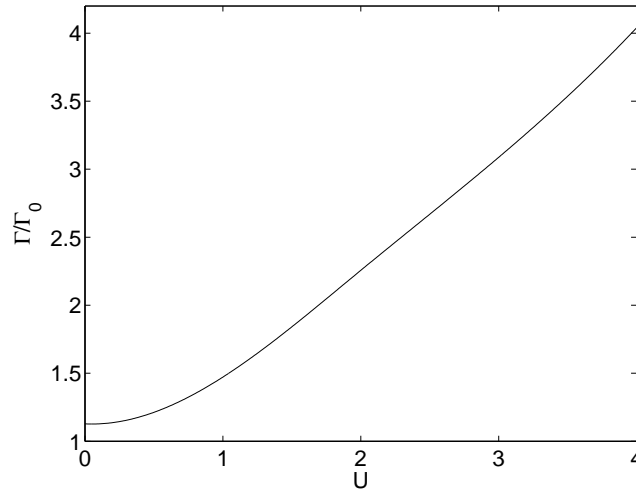


Figure 10.1: Jump rate Γ as a function of the momentum U assuming a constant scattering cross section. The result was obtained using a Monte Carlo integration with importance sampling. It agrees with the analytical result presented in [26].

Born approximation The scattering amplitude in the Born approximation can be obtained analytically using Eq. (9.11). The latter can be simplified for rotationally symmetric potentials $V(\mathbf{x}) = V(|x|) \equiv V(r)$, which yields

$$f_B(\mathbf{p}_f - \mathbf{p}_i) = -\frac{2m_*}{\hbar^2} \int_0^\infty dr r^2 \text{sinc}\left(\frac{qr}{\hbar}\right) V(r), \quad (10.5)$$

with $q = |\mathbf{p}_f - \mathbf{p}_i| = 2p \sin(\theta/2)$ denoting the momentum transfer and $\text{sinc}(x) \equiv \sin(x)/x$. Upon inserting the Gaussian potential (10.4), the scattering amplitude becomes

$$f_B(p, \cos \theta) = -\sqrt{\frac{\pi}{2}} \frac{2m_* V_0 d^3}{\hbar^2} \exp\left(-\frac{d^2 p^2}{\hbar^2} [1 - \cos \theta]\right). \quad (10.6)$$

Partial wave expansion The Born approximation is reliable only for weak interaction potentials, $V_0 \ll E_{\text{kin}}$; otherwise, one may apply the exact scattering amplitudes as obtained by means of the partial wave decomposition [52]

$$f(p, \cos \theta) = \sum_{l=1}^{\infty} (2l+1) f_l(p) P_l(\cos \theta), \quad (10.7)$$

with the Legendre-polynomials P_l and the partial scattering amplitudes f_l . The latter are related to the partial wave phase shifts δ_l by [52]

$$f_l(p) = \frac{\hbar}{p} e^{i\delta_l} \sin \delta_l. \quad (10.8)$$

Given the interaction potential, the phase shifts can be computed numerically by means of the *Johnson algorithm* [92].

A consistency test of the numerically calculated phase shifts is obtained for instance by analyzing the low and high energy limits, which should behave as

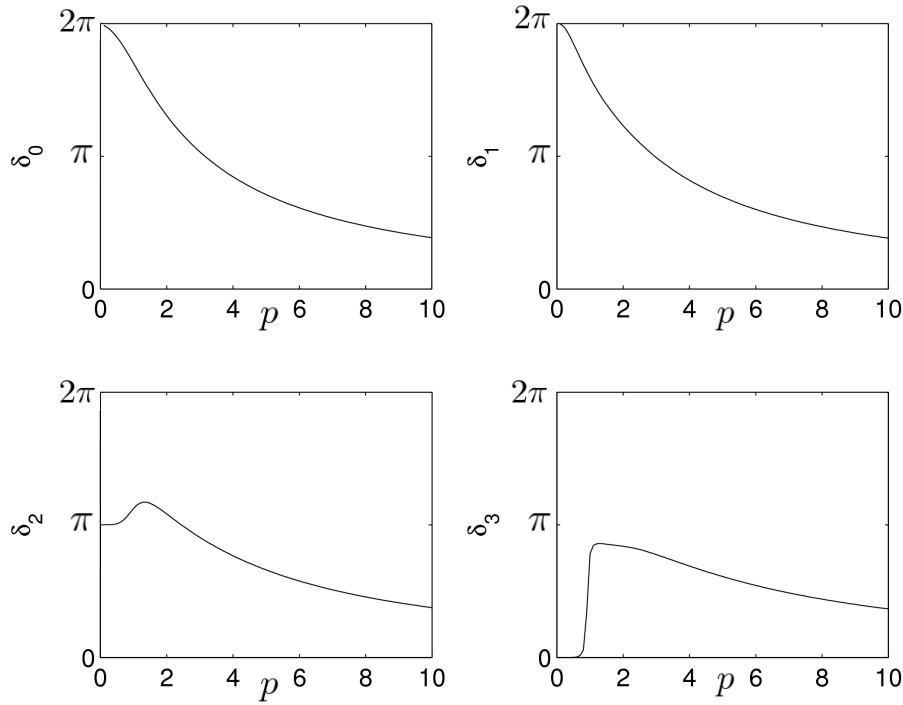


Figure 10.2: The first four phase shifts δ_l as a function of the relative momentum p for $m/M = 1$. The interaction potential is assumed to be a Gaussian (10.4) with $V_0 = -20$. The correctness of the simulation is confirmed by the low and high energy limits: the phase shifts vanish for high values of p , and they behave according to the Levinson theorem (10.9) for low energies. There are two bound states for $l = 0, 1$, one for $l = 2$, and zero for $l = 0$.

follows. For weak potentials or large energies, that is $V \ll p^2/2M$, the partial waves are hardly affected by the collision, so that the scattering amplitudes and phases vanish, $\delta_l(p \rightarrow \infty) = 0$. For small energies, on the other hand, they behave as [52]

$$\delta_l(p) \sim n_l \pi - a_l p^{2l+1}, \quad \text{for } p \rightarrow 0, \quad (10.9)$$

with the scattering lengths a_l . According to the *Levinson theorem* [52], the integer n_l equals the number of bound states with angular momentum l .

Numerical results We have calculated the phase shifts for the potential energies $V_0 = -1$ and $V_0 = -20$, and different mass ratios; Figure 10.2 shows the first four of them for $V_0 = -20$, $d = 1$, $\hbar = 1$ and $m = M$. Notably, the low energy limit, $p \rightarrow 0$, agrees with the Levinson-theorem (10.9), and also the high energy limit is correct, that is $\delta_l(p \rightarrow \infty) = 0$. Having the phase shifts at hand, the scattering amplitudes are obtained using Eqs. (10.8) and (10.7), where it is enough to take the first 30 partial waves, since the phase shifts become smaller with increasing angular momentum l . The numerically obtained f for $V_0 = -1$ is shown in Fig. 10.3 on the left-hand side. It differs substantially from the corresponding Born approximation shown on the right of Fig. 10.3.

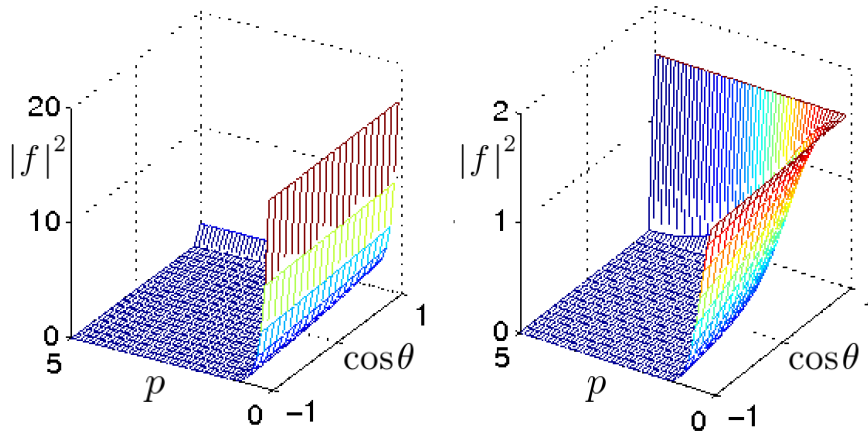


Figure 10.3: Square of the scattering amplitude f as a function of the relative momentum p and the scattering angle θ for $m/M = 1$. The interaction potential is assumed to be a Gaussian (10.4) with $V_0 = -1$. Left plot: numerical solution obtained by means of the partial wave decomposition. Right plot: Born approximation. The differences between the two amplitudes are significant (notice the different scalings of the z-axis).

As a further test of the correctness of this result, both sides of the optical theorem were calculated

$$\text{Im} [f(p, \theta = 0)] = \frac{p}{4\pi\hbar} \sigma(p), \quad (10.10)$$

with $\sigma(p) = 2\pi \int d(\cos\theta) |f(p, \cos\theta)|^2$ the total cross section. It yields a perfect agreement.

The numerically evaluated jump rate $\Gamma(U)$ corresponding to this scattering amplitude is shown in Fig. 10.4. It is obtained using a Monte Carlo integration of Eq. (9.45) with importance sampling, where the number of points is taken to be sufficiently large, in this case $n = 10^4$. The jump rate is given in units of the *effective collision rate*, as defined by the thermal average

$$\Gamma_{\text{eff}} \equiv n_{\text{gas}} \int_{\mathbb{R}^3} d\mathbf{p} \frac{p}{m} \mu(\mathbf{p}) \sigma(p). \quad (10.11)$$

The simulation shown by the solid line in Fig. 10.4 is based on the exact scattering amplitude (obtained by the partial wave decomposition and the Johnson algorithm), while the dashed corresponds to the Born approximation of f . One observes that the two results differ drastically, in particular for large interaction potentials V_0 , while they agree for large momenta p , where the two scattering amplitudes are close to each other.

The Gaussian interaction potential is applied in several examples below. In these cases, the system of units is defined by setting $\hbar = 1$, $m = 1$ and $d = 1$; moreover, we chose $k_B T = 1$ for the temperature of the gas environment and the gas density is set to unity, $n_{\text{gas}} = 1$.

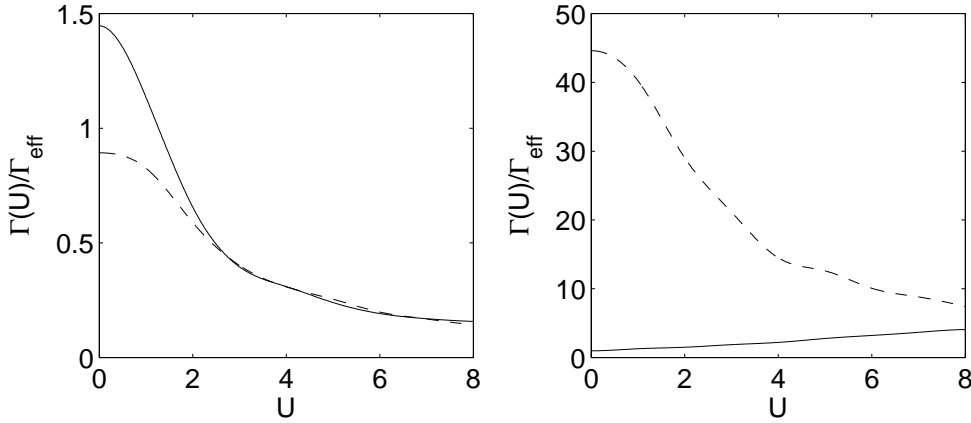


Figure 10.4: Jump rate Γ as a function of the momentum U for a mass ratio $M/m = 100$ and a Gaussian interaction potential with $V_0 = -1$ (left) and $V_0 = -20$ (right). The solid line corresponds to the exact scattering amplitude computed with the partial wave decomposition and the Johnson algorithm. The dashed line was obtained in Born approximation. For large interaction potentials, the results deviate strongly.

10.2 Decoherence in momentum

Let us now apply the Monte Carlo algorithm presented previously to the analysis of decoherence effects in momentum space. For this purpose, we chose as initial state a superposition of two momentum eigenstates,

$$|\psi(0)\rangle = \alpha(0)|\mathbf{U}(0)\rangle + \beta(0)|\mathbf{V}(0)\rangle, \quad (10.12)$$

which are taken to have the form

$$\mathbf{U}(0) = -\mathbf{V}(0) = (U_0, 0, 0). \quad (10.13)$$

Since the states $|\mathbf{U}(0)\rangle$ and $|\mathbf{V}(0)\rangle$ are genuine momentum eigenstates, any collision necessarily leads to an orthogonal state. It follows that the coherences decay exponentially

$$\frac{|\langle \mathbf{U}(0) | \rho(t) | \mathbf{V}(0) \rangle|}{|\langle \mathbf{U}(0) | \rho(0) | \mathbf{V}(0) \rangle|} = e^{-\Gamma(U_0)t}, \quad (10.14)$$

with the decay rate given by the total collision rate $\Gamma(U_0)$.

Alternatively, one may view the states $|\mathbf{U}(0)\rangle$, $|\mathbf{V}(0)\rangle$ as representing states which are well localized in momentum space, but with a finite width greater than the typical momentum transfer. Here a suitable measure for the degree of coherence is the ensemble average of the coherences exhibited by the individual quantum trajectories $|\psi(t)\rangle$ [26], that is

$$C(t) = \mathbb{E} \left[\frac{|\langle \mathbf{U}(t) | \psi(t) \rangle \langle \psi(t) | \mathbf{V}(t) \rangle|}{|\langle \mathbf{U}(0) | \rho(0) | \mathbf{V}(0) \rangle|} \right]. \quad (10.15)$$

To evaluate this term, recall that the quantum trajectories remain in a superposition of two momentum eigenstates during the time evolution, such that $|\psi(t)\rangle$ has the form

$$|\psi(t)\rangle = \alpha(t)|\mathbf{U}(t)\rangle + \beta(t)|\mathbf{V}(t)\rangle. \quad (10.16)$$

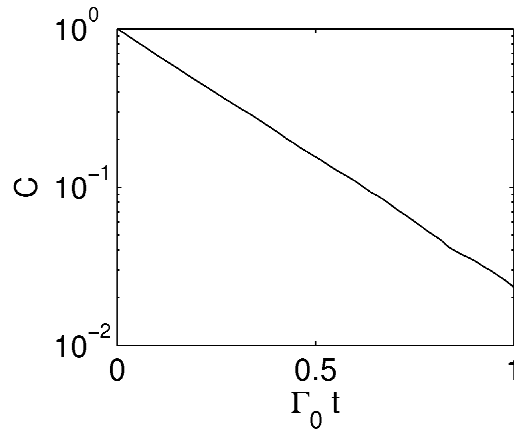


Figure 10.5: Semi-logarithmic plot of the “coherence” $C(t)$ defined in (10.17) for the state (10.12) with $U_0 = 4$. The interaction is described by s-wave hard-sphere scattering and the mass ratio is $m/M = 1$. The decoherence rate, which is obtained from an average over $5 \cdot 10^3$ trajectories, agrees with the result presented in [26].

By inserting this expression into equation (10.15), one finds [26]

$$C(t) = 2\text{E} [|\alpha(t)\beta(t)|] . \quad (10.17)$$

Simulation results Figure 10.5 shows a semi-logarithmic plot of the coherence $C(t)$ for a constant cross section, an initial momentum $U_0 = 4$, equal amplitudes $\alpha(0) = \beta(0) = 1/\sqrt{2}$ and the mass ratio $m/M = 1$. It reveals an exponential decay of the coherence; the corresponding decay rate agrees with the result presented in [26].

The simulation results for the Gaussian interaction potential are shown in Fig. 10.6, where we chose an initial momentum $U_0 = \sqrt{6}$ and, like above, a mass ratio $m/M = 1$ and equal amplitudes. The left-hand side of this plot represents a weak interaction potential, whereas a strong one is assumed on the right. In the latter case, the result obtained with the exact scattering amplitude (solid line) differs markedly from the corresponding Born approximation (dashed line).

These results show that the full QLBE (9.2) may lead to physical predictions which deviate significantly from the ones obtained with the QLBE in Born approximation (9.12), if the interaction potential is sufficiently strong. A similar conclusion is drawn below, when studying relaxation rates.

Experimental tests The design of experimental tests for decoherence effects in momentum space is a challenging task [12, 67, 93]. Such a setup would have to provide on the one hand a source of states having momentum coherences (which in turn requires the preparation of non-stationary beams), and on the other hand it would require an interferometric measurement apparatus able to detect momentum coherences. A further difficulty lies in the inevitable presence and dominance of position decoherence. During the free evolution, a superposition state of different momenta evolves into a superposition of spatially separated wave packets, which is affected by decoherence mechanisms in position space [12].

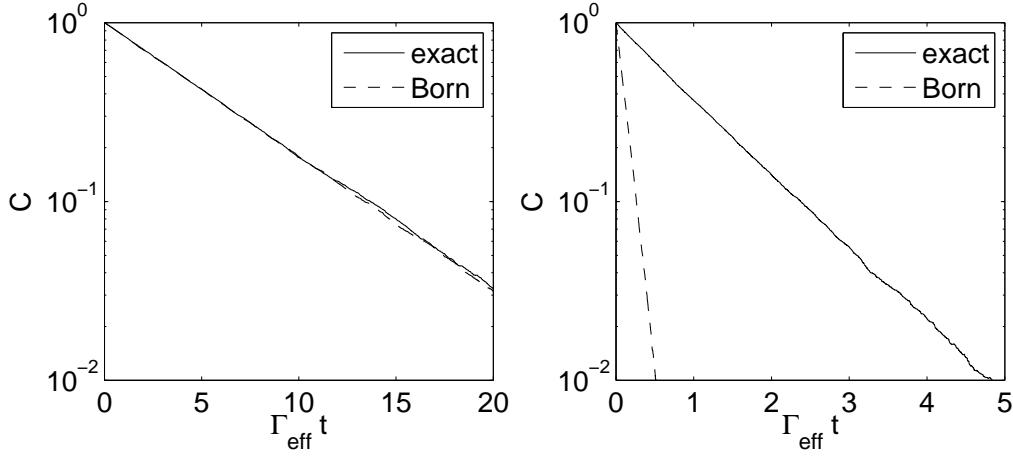


Figure 10.6: Similar to Fig. 10.5 but with an initial momentum $U_0 = \sqrt{6}$ and a Gaussian interaction potential (10.4) with $V_0 = -1$ (left) and $V_0 = -20$ (right). The solid line is obtained using the exact scattering amplitude, while the dashed line corresponds to the Born approximation. The predictions of the decoherence rates differ substantially in case of the large interaction potential with $V_0 = -20$.

Position decoherence, in contrast, has already been observed experimentally in Vienna [16] in fullerene interference experiments. The following section therefore focuses on the theoretical prediction of spatial decoherence effects based on the Monte Carlo unraveling of the QLBE.

10.3 Decoherence in position

10.3.1 Measuring spatial coherences

Let us now quantify the loss of spatial coherences $\rho(\mathbf{X}, \mathbf{X}') \equiv \langle \mathbf{X} | \rho | \mathbf{X}' \rangle$. To this end, we need to be able to measure $\rho(\mathbf{X}, \mathbf{X}')$ given the quantum trajectories in momentum representation, $|\psi(t)\rangle = \sum_{j=1}^N \alpha_j(t) |\mathbf{U}_j(t)\rangle$. For this purpose, it is convenient to express the position variable \mathbf{X} in units of the thermal wavelength Λ_{th} (3.27),

$$\mathbf{S} \equiv \frac{\mathbf{X}}{\Lambda_{\text{th}}}. \quad (10.18)$$

The spatial coherences are then obtained by taking the ensemble average of the coherences of the individual quantum trajectories, that is

$$\rho(\mathbf{S}, \mathbf{S}', t) = \mathbb{E} [\langle \mathbf{S} | \psi(t) \rangle \langle \psi(t) | \mathbf{S}' \rangle]. \quad (10.19)$$

By inserting the momentum representation of $|\psi(t)\rangle$ into this expression, we find

$$\begin{aligned} \rho(\mathbf{S}, \mathbf{S}', t) & \quad (10.20) \\ &= \sum_{j,k}^N \mathbb{E} [\alpha_j(t) \alpha_k^*(t) \langle \mathbf{S} | \mathbf{U}_j(t) \rangle \langle \mathbf{U}_k(t) | \mathbf{S}' \rangle] \\ &= \frac{1}{(2\pi)^3} \sum_{j,k}^N \mathbb{E} \left[\alpha_j(t) \alpha_k^*(t) \exp \left(\frac{i}{\hbar} M v_\beta \Lambda_{\text{th}} [\mathbf{S} \cdot \mathbf{U}_j(t) - \mathbf{S}' \cdot \mathbf{U}_k(t)] \right) \right]. \end{aligned}$$

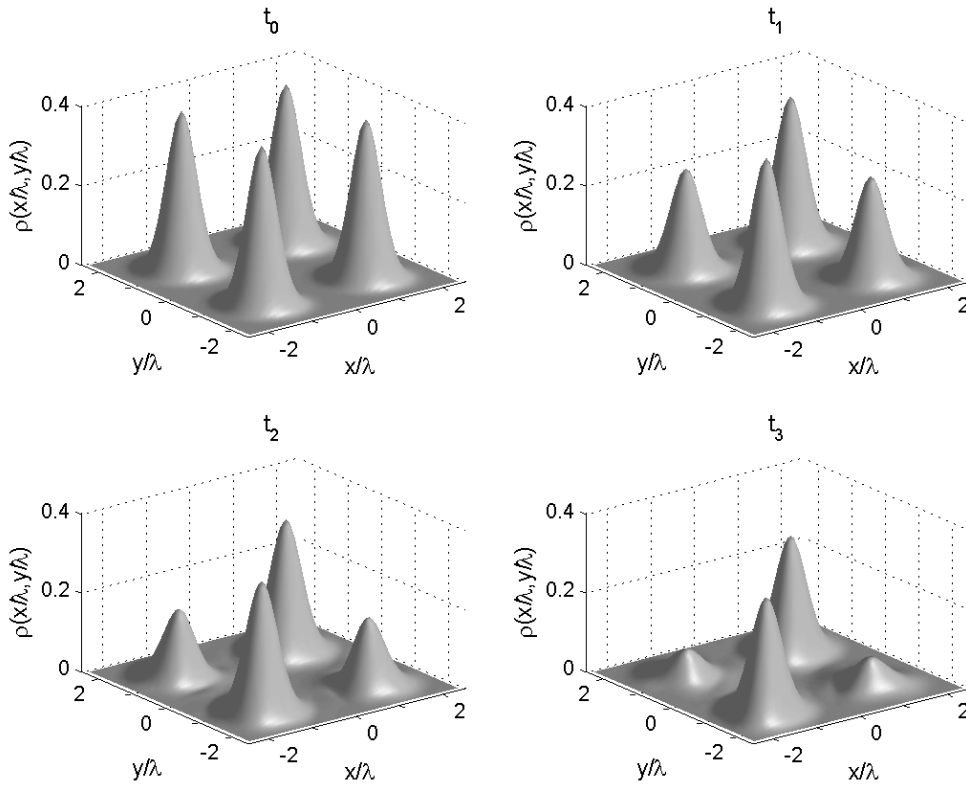


Figure 10.7: Evolution of the density matrix in position representation for an initial superposition of two Gaussian wave packets, obtained by solving the three-dimensional QLBE for s-wave hard-sphere scattering. The spatial coherences $\rho(x/\lambda, y/\lambda)$ are expressed in units of the thermal wavelength $\lambda \equiv \Lambda_{\text{th}}$.

This formula allows us to compute the coherences $\rho(\mathbf{S}, \mathbf{S}', t)$ by means of the amplitudes $\alpha_j(t)$ and the scaled momenta $\mathbf{U}_j(t)$.

Localization in one spatial direction A typical application of this formalism is the description of particles flying through an interferometer which contains slits or grids. After passing a grid, the particle is localized in one spatial direction, while it typically has a definite momentum (or an incoherent thermal distribution of momenta) in the other two directions. We therefore restrict the discussion from now on to initial states of the form

$$|\psi(0)\rangle = \sum_{j=1}^N \alpha_j(0) |U_j(0), V(0), W(0)\rangle, \quad (10.21)$$

where $|U_j(0), V(0), W(0)\rangle$ denote scaled eigenstates of the momentum operator $\mathbf{P} \equiv (P_x, P_y, P_z)$. By taking N to be sufficiently large, (10.21) may represent states which are localized in one spatial direction. Due to the conservation of momentum superpositions, the ensuing quantum trajectories have the structure

$$|\psi(t)\rangle = \sum_{j=1}^N \alpha_j(t) |U_j(t), V(t), W(t)\rangle. \quad (10.22)$$

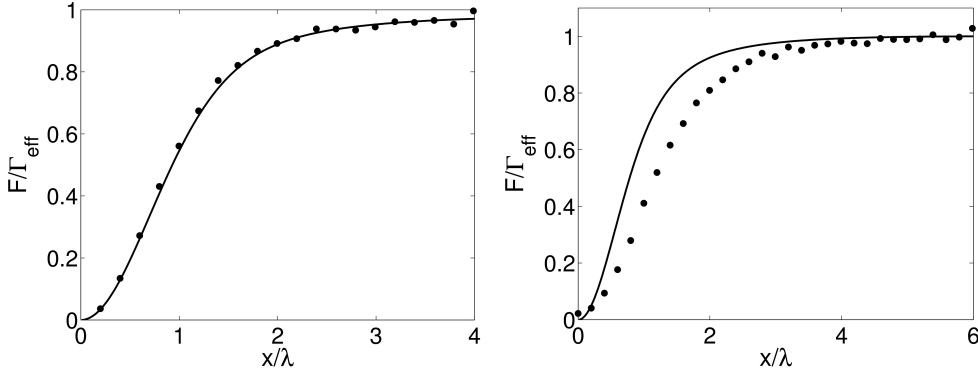


Figure 10.8: Decay rate of the spatial coherences as a function of the separation x/λ , $\lambda \equiv \Lambda_{\text{th}}$, for a Gaussian interaction potential and the mass ratios $M/m = 100$ (left) and $m = M$ (right). The solid line shows the prediction of pure collisional decoherence, Eq. (3.52), and the filled circles give the result of the stochastic simulation of the QLBE. For $M \gg m$, the predictions of the two models agree, while there are deviations visible for $m = M$. The localization rate saturates in all cases at the average collision rate Γ_{eff} . For $m = M$ and $x = 0$, the prediction of the QLBE does not vanish, since there is a loss of the populations due to diffusion.

The measurement of spatial coherences (10.20) can in this case be simplified, by focusing on the coherences in x -direction,

$$\begin{aligned} & \rho([S, 0, 0], [S', 0, 0], t) \\ &= \frac{1}{(2\pi)^3} \sum_{j,k}^N \mathbb{E} \left[\alpha_j(t) \alpha_k^*(t) \exp \left(\frac{i}{\hbar} M v_\beta \Lambda_{\text{th}} [S U_j(t) - S' U_k(t)] \right) \right]. \end{aligned} \quad (10.23)$$

Simulation result To visualize the evolution of the density matrix in position representation, consider an initial superposition of two resting Gaussian wave packets, with scaled mean positions $\langle \mathbf{S} \rangle_{1,2} = \pm 1.2$ and width $\sigma_{1,2} = 0.2$ (in units of Λ_{th}). This state may be written in the form (10.22), by using a finite dimensional representation of the corresponding Fourier transform. Figure 10.7 depicts the ensuing evolution of the matrix elements (10.23), obtained by solving the QLBE under the assumption of s-wave hard-sphere scattering and equal masses $m = M$. It shows four snapshots of the density matrix for the scaled times $t\Gamma_0 = (0, 1/3, 2/3, 4/3)$. The simulation is based on 10^3 realizations of the stochastic process and the state is represented using 55 momentum eigenstates.

10.3.2 Measuring the localization rate

As discussed in Sect. 9.2.2, the QLBE simplifies to pure collisional decoherence, if one assumes the tracer particle to be much heavier than the gas particles. In this model, the decay rate F of spatial coherences is a function of the distance $|\Delta \mathbf{X}|$ only; it does not depend on the particular matrix elements of the state, see Eq. (3.49). Hence, the decoherence process is completely characterized by the localization function $F(|\Delta \mathbf{X}|)$.

By evaluating the decoherence rates for various mass ratios and initial states, we found that this behavior holds as well in regimes where the QLBE differs from the model of collisional decoherence. This suggests that the decoherence dynamics of the QLBE is generally characterized by a one-dimensional function $F(|\Delta\mathbf{X}|)$.

Figure 10.8 shows the localization rate for a Gaussian interaction potential with $V_0 = -1$ and the mass ratios $M/m = 100$ (left) and $m/M = 1$ (right). The filled circles give the decay rate as evaluated from (10.23), obtained by 5×10^4 realizations of the Monte Carlo unraveling of the QLBE. The solid line represents the localization rate of collisional decoherence (3.52), calculated by numerical integration.

As expected, one finds a perfect agreement between the predictions of collisional decoherence and the solution of the QLBE if the test particle mass is much larger than the gas mass, $M/m = 100$. This is a further confirmation of the accuracy of the stochastic algorithm.

Moreover, it turns out that the results of the two models do not differ substantially even for equal masses $m = M$. This holds in particular for large distances, where the decay rates converge to the average collision rate Γ_{eff} (all cases). In this limit, one collision is enough to reveal the full ‘which path’ information, so that a saturation at Γ_{eff} is expected. For equal masses the prediction of the QLBE does not tend to zero in the limit of small distances, $F(0) > 0$. This is due to the contribution of quantum diffusion, which is naturally more pronounced when the test particle is lighter.

10.4 Interference and decoherence

As an application of the previous two sections, and as an illustration of the interplay between coherent and incoherent dynamics, let us study how the formation of interference patterns is affected by the interaction with the background gas. To this end, consider the scenario depicted in Fig. 10.9. Here the x -component of the three-dimensional initial state is prepared in a superposition of two counter-propagating coherent states $\psi_{1,2}$, while the other two components have a definite momentum. In the course of the evolution the wave packets start overlapping, which leads to interference, that is to oscillations of the spatial populations $\rho(x, x, t)$ in x -direction. The frequency of these oscillations is given by the de-Broglie wavelength λ_{dB} associated to the relative momentum of the coherent states. Besides this coherent effect, one observes a signature of decoherence, which manifests itself in the loss of fringe visibility. This becomes apparent in particular in the panel at the bottom of Fig. 10.9.

Details of the simulation Figure 10.9 is obtained by the Monte Carlo unraveling of the QLBE, assuming s-wave hard-sphere scattering and a mass ratio $M/m = 100$. It shows three snapshots of the populations of the density matrix for the scaled times $\Gamma_0(t_0, t_1, t_2) = (0, 9, 18)$. The simulation is based on 2.5×10^4 realizations of the stochastic process.

The parameters of the simulation are conveniently expressed in units of the de-Broglie wavelength λ_{dB} and the scattering rate Γ_0 (10.3), which define the dimensionless variables

$$S_{\text{dB}} \equiv \frac{X}{\lambda_{\text{dB}}}, \quad U_{\text{dB}} \equiv \frac{P}{M\lambda_{\text{dB}}\Gamma_0}. \quad (10.24)$$

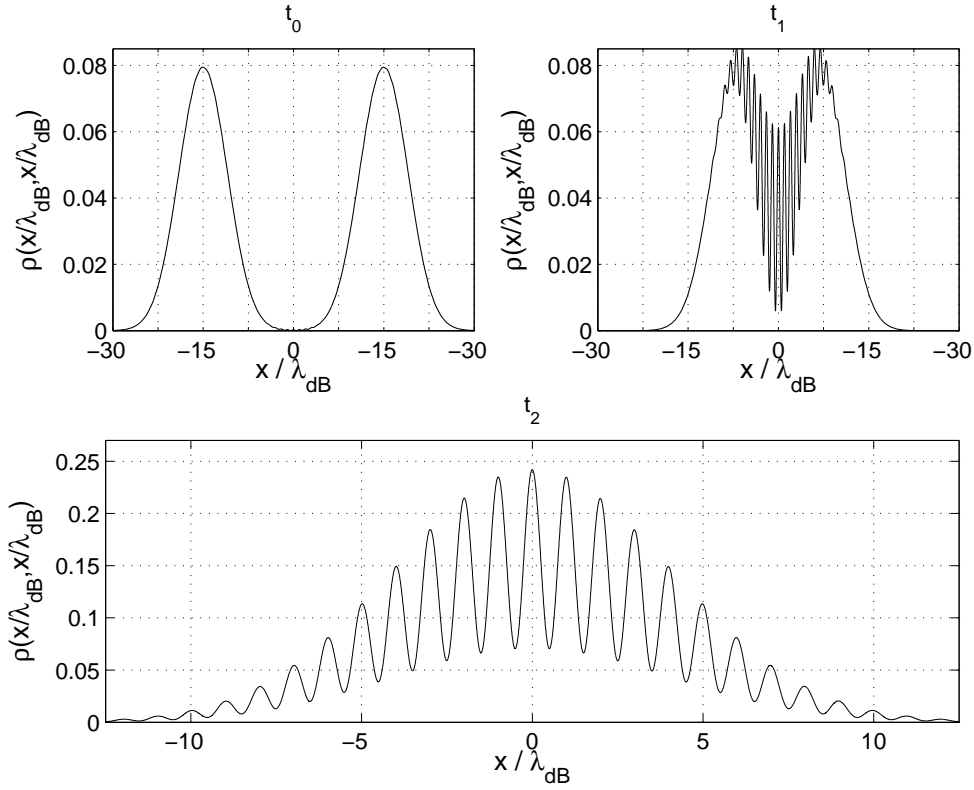


Figure 10.9: Evolution of the populations of the density matrix $\rho(x/\lambda_{\text{dB}}, x/\lambda_{\text{dB}})$ for an initial superposition of two counter-propagating coherent states. It is obtained by solving the QLBE for s-wave hard-sphere scattering. The figure shows three snapshots of the dynamics at times $\Gamma_0(t_0, t_1, t_2) = (0, 9, 18)$. Due to quantum coherence, one observes interference fringes with frequency λ_{dB} (the de-Broglie wavelength). Besides that, there is a signature of decoherence given by the loss of fringe visibility.

In this system of units the position and momentum expectations of the coherent states $\psi_{1,2}$ read as $\langle S_{\text{dB}} \rangle_{1,2} = \mp 15$ and $\langle U_{\text{dB}} \rangle_{1,2} = \pm 0.9$; their width is characterized by the standard deviation $\sigma_{1,2}/\lambda_{\text{dB}} = 4$. Furthermore, the de-Broglie wavelength is fixed by setting $\lambda_{\text{dB}}/\Lambda_{\text{th}} = 2.5 \times 10^{-2}$.

As mentioned above, an interesting quantity is the fringe visibility, which quantifies the loss of quantum coherence. It is here defined pragmatically as the difference between the first maximum and the first minimum, divided by their sum. For the visibility of the interference pattern in the last snapshot (Fig. 10.9, bottom), we find

$$\text{vis}(t_2) \simeq 55\%. \quad (10.25)$$

Estimation of the visibility using collisional decoherence To understand this result quantitatively, let us estimate the decay rate of the visibility by means of the integrated localization rate,

$$\text{vis}(\tau) = \exp\left(-\int_0^\tau d\tau' F[S(\tau')] \tau'\right) \text{vis}(0), \quad (10.26)$$

where $S(\tau) = |\langle X(\tau) \rangle_1 - \langle X(\tau) \rangle_2| / \Lambda_{\text{th}}$ denotes the distance of the coherent states in units of the thermal wavelength at time τ . By noting that the state moves in absence of an external potential, one finds

$$S(\tau) = \frac{\lambda_{\text{dB}}}{\Lambda_{\text{th}}} (|\langle S_{\text{dB}} \rangle_1 - \langle S_{\text{dB}} \rangle_2| - \tau |\langle U_{\text{dB}} \rangle_1 - \langle U_{\text{dB}} \rangle_2|). \quad (10.27)$$

Since the tracer particle is much heavier than the gas molecules, $M \gg m$, the dynamics described by the QLBE should be well approximated by the master equation of pure collisional decoherence, see Sect. 9.2.2. It follows that F is described by the formula (3.52), which can be evaluated analytically in the case of s-wave hard-sphere scattering. This yields

$$F(S) = 2\sqrt{\pi} n_{\text{gas}} R^2 v_{\beta} [4 - S^{-1} \exp(-4\pi S^2) \operatorname{erfi}(2\sqrt{\pi} S)], \quad (10.28)$$

where $\operatorname{erfi}(x)$ denotes the imaginary error function (5.71). The result follows from Eqs. (5.62), (5.63), (5.67) and (5.70) together with $v_{\beta} = 2\sqrt{\pi}\hbar / (m\Lambda_{\text{th}})$.

The visibility (10.26) may then be obtained by numerical integration, which yields

$$\operatorname{vis}(t_2) \simeq 56\%. \quad (10.29)$$

This result is in good agreement with the one obtained by the stochastic solution of the full QLBE, see Eq. (10.25).

10.5 Relaxation and thermalization

Thus far, we have been concerned with the short-time dynamics induced by the QLBE. In this section, let us study the long-time behavior of the energy and momentum expectation values. Before describing the numerical results, a short summary of the expected results is given. This discussion is based on the analytical treatment in [12].

Approach to thermal equilibrium Similar to the H -theorem of the non-linear Boltzmann equation [87], the QLBE satisfies an entropy inequality [12]. In contrast to the H -theorem, it is formulated in terms of the quantum relative entropy

$$S(\rho_A | \rho_B) \equiv k_B \operatorname{Tr}[\rho_A \ln \rho_A] - k_B \operatorname{Tr}[\rho_A \ln \rho_B]. \quad (10.30)$$

It states that the time derivative of the entropy of the solution of the QLBE $\rho_t = e^{\mathcal{L}t} \rho_0$ relative to the stationary solution ρ_{EQ} is non-positive [12],

$$\frac{d}{dt} S(\rho_t | \rho_{\text{eq}}) \leq 0. \quad (10.31)$$

Here the equality sign holds if and only if ρ_t equals the equilibrium state [12]. Since the quantum relative entropy is a measure for the distinguishability of two quantum states, it follows that the solution of the QLBE approaches asymptotically the stationary solution.

Moreover, using detailed balance and assuming the momenta of the gas particles to be Maxwell-Boltzmann distributed, one can show [12] that the stationary

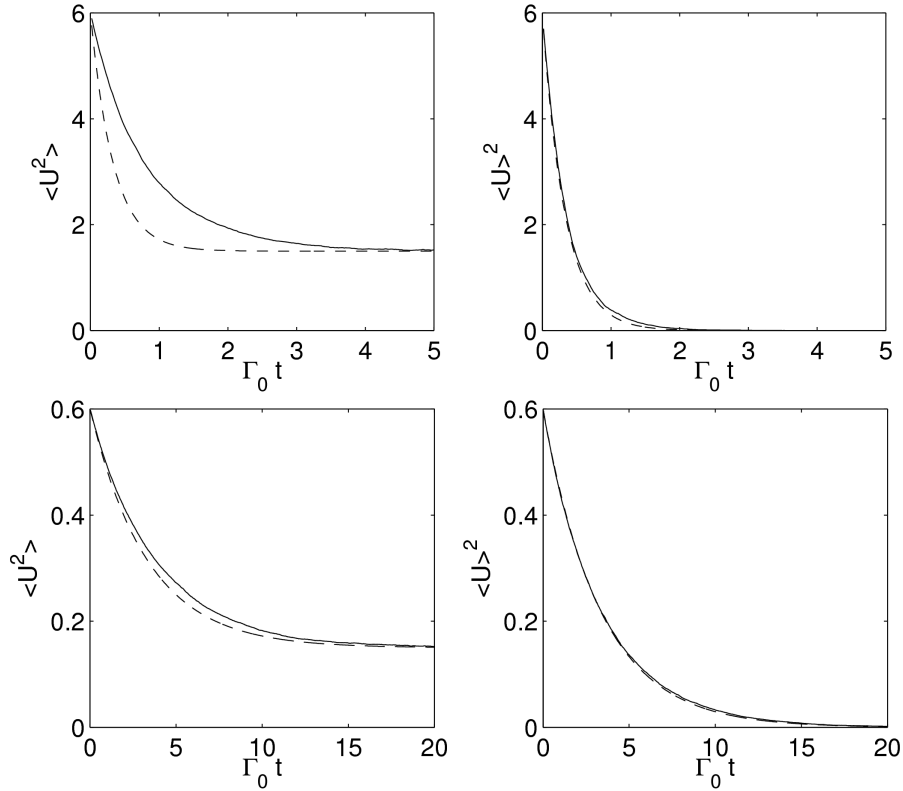


Figure 10.10: Energy and momentum relaxation assuming a constant cross section and mass ratios $M/m = 1$ (top) and $M/m = 10$ (bottom). The solid line shows the solution of the QLBE obtained by averaging over 10^4 trajectories. The dashed line corresponds to the analytic solution of the Caldeira-Leggett (CL) equation (10.35). The results are identical with the ones obtained in [26].

solution of the QLBE is given by the corresponding thermal state. The average kinetic energy of the solution of the QLBE must therefore asymptotically approach the thermal energy $3/(2\beta)$. Expressed in dimensionless units, this means that [12]

$$\langle U^2 \rangle_t \rightarrow \langle U^2 \rangle_{\text{eq}} = \frac{3}{2} \frac{m}{M}, \quad \text{for } t \gg \gamma^{-1}, \quad (10.32)$$

with γ the relaxation rate. In addition, it follows that the average momentum $\langle U \rangle_t$ tends to zero for $t \gg \gamma^{-1}$.

Quantum Brownian limit As the reader may recall from Sect. 9.2.4, the QLBE reduces to the Caldeira-Leggett (CL) equation in Lindblad form (3.33) if the state is close to thermal and the tracer particle is much heavier than the gas particles, $M \gg m$. The corresponding evolution of the energy and momentum expectation values is then well understood, see Refs. [12, 29] and Sect. 3.3.3. Formulated in dimensionless units, it reads as [12, 29]

$$\langle U^2 \rangle_t = \langle U^2 \rangle_{\text{eq}} + (\langle U^2 \rangle_{t_0} - \langle U^2 \rangle_{\text{eq}}) e^{-4\gamma t}, \quad (10.33)$$

$$\langle U \rangle_t^2 = \langle U \rangle_{t_0}^2 e^{-2\gamma t}, \quad (10.34)$$

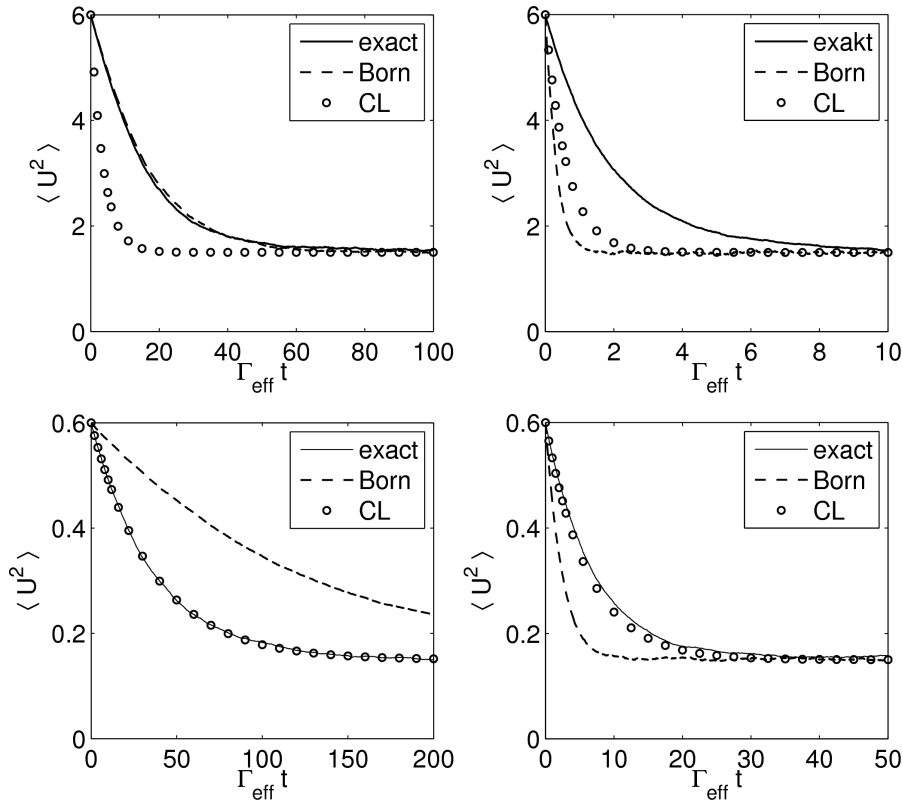


Figure 10.11: Energy relaxation using the exact scattering amplitude of the Gaussian interaction potential, the corresponding Born approximation, and the solution of the CL equation (9.14). We chose the potential energies $V_0 = -1$ (left) and $V_0 = -20$ (right) and the mass ratios $M/m = 1$ (top) and $M/m = 10$ (bottom). One obtains the correct equilibrium values (10.32), $3/2$ (top) and $3/20$ (bottom). The exact result agrees with the solution of the CL equation for heavy tracer particles (bottom). The Born approximation gives reliable results when the kinetic energy is much larger than the potential one (top left).

with $\langle U^2 \rangle_{\text{eq}} = 3m/(2M)$. According to [12], the relaxation rate γ can be expressed in terms of the gas density, the temperature, the mass ratio, and the scattering amplitude, see Eq. (9.14). For the constant cross section, this formula can be evaluated analytically, which yields [12]

$$\gamma = \frac{4}{3\sqrt{\pi}} \frac{m}{M} \Gamma_0. \quad (10.35)$$

Simulation results Figure 10.10 shows the energy and momentum relaxation process exhibited by the stochastic solution of the QLBE with constant scattering cross section (solid line). The initial state is here a momentum eigenstate with eigenvalue $U_0 = \sqrt{6}$. Such a state is sufficiently close to the thermal one, so that the quantum-Brownian limit holds for $M \gg m$. In this limit (bottom), one obtains a good agreement with the analytic solution, Eqs. (10.33) to (10.35), of the CL equation (dashed line). For equal masses, $m = M$, the results deviate noticeably (top). As expected, all of the solutions converge to the correct equilib-

rium values, that is the scaled energies converge to $3/2$ (top) and $3/20$ (bottom), while the scaled momenta tend to zero (right). Similar results are obtained by the QLBE in Born approximation [26].

The energy relaxation for the Gaussian interaction potential with $V_0 = -1$ (left) and $V_0 = -20$ (right) is shown in Fig. 10.11. Here the mass ratios are the same as above: $M/m = 1$ (top) and $M/m = 10$ (bottom). The solid line shows the solution of the QLBE based on the exact scattering amplitude, while the corresponding Born approximation is represented by the dashed line; both simulations are based on 5×10^3 trajectories. Furthermore, the prediction (10.33) of the CL equation is presented (dots). Here the relaxation rate was obtained by numerical integration of the right-hand side of Eq. (9.14). As in the previous example, the correct equilibrium values are approached asymptotically: $3/2$ (top) and $3/20$ (bottom). Moreover, it turns out that the predictions of the CL equation fit well in the quantum Brownian limit, that is for $M \gg m$. The Born approximation yields reliable results when the kinetic energy is much larger than the potential one (top left).

As in Sect. 10.2, we conclude that the full QLBE (9.2) may lead to physical predictions which deviate significantly from the ones obtained with the QLBE in Born approximation (9.12). This holds in particular for strong interaction potentials, where the corresponding scattering amplitudes are different. Furthermore, this section verifies that the expression (9.14) obtained in [11, 12] yields the correct relaxation rate in the quantum Brownian limit.

10.6 Diffusion

As a final discussion, let us study the simulation of quantum diffusion processes described by the QLBE. To this end, a localized initial state is prepared and the growth of the variance of the spatial populations is measured. Before discussing the numerical result, a short summary of analytical predictions is presented, based on the treatment in [12].

Quantum dispersion On short time scales, where the number of collisions is small, one expects the variance growth to be dominated by quantum dispersion. This implies that the variance growth is described by the parabolic behavior

$$\text{Var}(X, t) = \text{Var}(X, 0) + \frac{\hbar^2}{4M^2 \text{Var}(X, 0)} t^2, \quad (10.36)$$

where an initial state of minimum uncertainty is assumed.

Classical diffusion After time scales after which many collisions have occurred, the variance growth is expected to be dominated by classical diffusion, where the corresponding diffusion constant can be estimated by the following consideration.

As discussed in Sect. 9.2.1, the QLBE approaches asymptotically the classical linear Boltzmann equation (CLBE). The latter can be simplified, by considering the *Brownian limit*, that is the limit of heavy tracer particles, $M \gg m$, with a momentum P close to the typical thermal value $P_\beta = \sqrt{2M/\beta}$ [12, 94, 95]. Under these conditions, the CLBE (9.7) reduces to the classical Kramers equation, which

reads as [12]

$$\partial_t w(\mathbf{P}) = \eta \sum_{i=1}^3 \left(\frac{\partial}{\partial P_i} [P_i w(\mathbf{P})] + \frac{M}{\beta} \frac{\partial^2}{\partial P_i^2} w(\mathbf{P}) \right), \quad (10.37)$$

with momentum distribution $w(\mathbf{P})$ and friction coefficient η . The latter can be expressed in terms of the microscopic details of the gas [12,96], giving $\eta = 2\gamma$, with γ the relaxation rate appearing in the Caldeira-Leggett equation, see Sect. 9.2.4, Eq. (9.14).

The important point to note is that the Kramers' Fokker-Planck equation leads to diffusion, that is to a linear growth of the variance [97]

$$\text{Var}(X, t) = \text{Var}(X, 0) + 2Dt, \quad (10.38)$$

with diffusion constant $D = \eta M / \beta$ [97]. This implies that

$$\text{Var}(X, t) = \text{Var}(X, 0) + \frac{1}{\beta M \gamma} t. \quad (10.39)$$

In case of a constant cross section, γ can be evaluated analytically [12], which yields Eq. (10.35). In conclusion, Eqs. (10.39) and (10.35) provide an analytical prediction for the diffusion constant, assuming the limit $M \gg m$.

Simulation results The solid line in Fig. 10.12 shows the variance growth of the spatial populations, obtained by solving the QLBE for s-wave hard-sphere scattering and mass ratios $M/m = 100$ (left) and $M/m = 1$ (right). This stochastic simulation is based on 4×10^3 trajectories. For the initial state, we chose a Gaussian with width $\text{Var}(X, 0) / \Lambda_{\text{th}}^2 = 1.6 \times 10^{-3}$ (left) and $\text{Var}(X, 0) / \Lambda_{\text{th}}^2 = 1.6 \times 10^{-1}$ (right).

To interpret the results, let us first discuss the panel on the left-hand side. Here the solution of the QLBE starts for small times with a quadratic dependence, as expected by the quantum dispersion Eq. (10.36) (dashed line). However, the slope of the parabola is steeper than expected, which is presumably due to the fact that the time scale shown in Fig. 10.12 is of the order of 10 to 10^2 collisions. The dynamics is therefore affected by incoherent effects.

For large times the curve goes over to a straight line, as expected for classical diffusion. A linear fit to this linear part is shown by the filled dots; its slope is approximately 7.5×10^{-6} . From the analytical considerations presented above, one expects a straight line of the form

$$\begin{aligned} \frac{\text{Var}(X, t)}{\Lambda_{\text{th}}^2} &= \frac{\text{Var}(X, 0)}{\Lambda_{\text{th}}^2} + (\beta M \gamma \Lambda_{\text{th}}^2 \Gamma_0)^{-1} t \Gamma_0 \\ &= 1.6 \times 10^{-3} + 6.7 \times 10^{-6} t \Gamma_0. \end{aligned} \quad (10.40)$$

The relative error between the analytical prediction and the simulation result for the slope is around 12%.

For equal masses (right panel) one obtains a straight line even for small times, which shows that classical diffusion is dominant over quantum dispersion. The slope of the curve is about 3.2×10^{-2} , implying that the diffusion constant is much stronger for light test particles. These results cannot be predicted by the Kramers' Fokker-Planck equation, since the latter holds in the Brownian limit only.

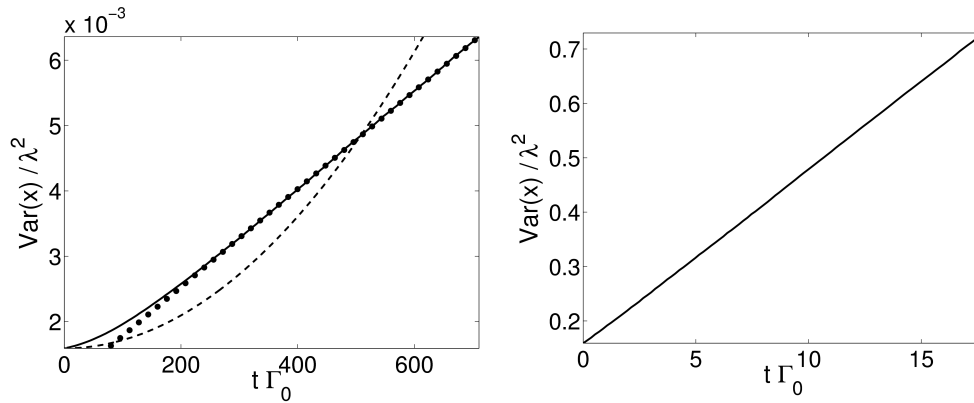


Figure 10.12: The solid line shows the variance of the spatial populations, obtained by solving the QLBE for s-wave hard-sphere scattering and mass ratios $M/m = 100$ (left) and $M/m = 1$ (right). Left plot: the curve goes over from a quadratic behavior (quantum dispersion) to a straight line (classical diffusion). The dashed parabola shows the theoretical prediction of quantum dispersion. The dotted straight line gives a linear fit to the solid line. Its slope is close to the diffusion constant predicted by the Kramers' Fokker-Planck equation (relative error: 12%). Right plot: the variance growth is dominated by classical diffusion, since the test particle is relatively light, $M = m$.

10.7 Summary

In this chapter we applied the Monte Carlo algorithm introduced in the previous chapter to specific examples where a test particle interacts with an ideal gas environment either by s-wave hard-sphere scattering or by a Gaussian interaction potential. It is demonstrated how important physical observables can be extracted from the simulated quantum trajectories, allowing us to monitor a variety of physical processes. These phenomena include pure quantum effects, such as the appearance of interference patterns, as well as incoherent features, for example relaxation and diffusion. The results were used to test the range of validity of the various limiting forms of the QLBE. For instance, we found an agreement with the predictions of the Caldeira-Leggett equation in the quantum Brownian limit, while the simulations agree with the solutions of pure collisional decoherence for short-time scales and heavy test particles. Moreover, it turns out that the full QLBE agrees with the simplified QLBE in Born approximation for weak interaction potentials.

Chapter 11

Conclusions

11.1 Pointer states and the orthogonal unraveling

In this thesis, we related the nonlinear double bracket equation discussed in [6–8] to a specific orthogonal unraveling of Markovian quantum master equations. This yields two sufficient criteria, which guarantee the existence of pointer states: (1) the double bracket equation must exhibit stable fixed points or solitons, (2) which are characterized by a vanishing entropy production rate. By applying these criteria to a particle in an ideal gas environment, it is shown that the corresponding pointer states are exponentially localized solitonic wave packets, which form an overcomplete basis. For sufficiently strong collisions with the background gas, these solitonic wave packets move according to the classical equations of motion. Since the dynamics of the system is asymptotically represented by an ensemble of these localized trajectories, it thus helps to explain the emergence of classical trajectories within the quantum framework.

In order to study the formation of pointer states, we applied the orthogonal unraveling to specific initial states which are superpositions of a finite number of localized wave packets. This way, the orthogonal unraveling was reduced from an infinite-dimensional unraveling to a stochastic process in \mathbb{C}^N , which can easily be implemented. As a result, it is found that after the decoherence process the statistical weights of the pointer states are given by the Born rule, that is by the overlap of the initial state with the initial pointer states.

Finally, a simple model is presented which admits the estimation of the pointer state width based on the microscopically defined localization rate of the master equation. By applying this model to three-dimensional settings and realistic interaction potentials, one obtains an expression that relates the width of the pointer states to the mean free path and the thermal wave length of the gaseous environment. This result allows us in particular to estimate the coherence length in an interacting thermal gas.

Future studies might consider the emergence and dynamics of pointer states in dissipative quantum systems. We note that this part of the thesis relies on the model of pure collisional decoherence which does not describe long-time effects such as dissipation or thermalization. As a next step, one might determine the pointer states of a more involved model such as the quantum linear Boltzmann equation. For large mass ratios, one expects that the pointer states then evolve according to a Langevin equation, thus explaining the emergence of classical Brownian motion within the quantum framework.

Apart from the investigation of specific open quantum systems, it might be interesting to analyze the double bracket equation for general Lindblad master equations. It would certainly be worth to investigate under which conditions the double bracket equations exhibits (localized) stationary or solitonic solutions.

Besides these mathematical issues, it remains an open problem to find experimental signatures of pointer states. This could potentially be done by measuring longitudinal coherences in atomic beams, as in the experiments described in [67,93]. An alternative idea is to observe pointer states indirectly by exploiting our predictions for the coherence length of interacting thermal gas. This relation could possibly be used for the prediction of the critical temperature of phase transitions, such as the Bose-Einstein condensation of interacting Bose systems. A textbook argument states that the condensation occurs whenever the coherence length is close to the mean particle distance. While this argument is typically used in the context of ideal Bose gases, it has also been applied in some articles [68,69] to determine the critical temperature of interacting systems. Since our theory yields the temperature dependence of the coherence length of interacting gases, it might be applicable to such scenarios.

11.2 Stochastic simulation of the quantum linear Boltzmann equation

The second part of the thesis presents a stochastic algorithm, which admits the solution of the full quantum linear Boltzmann equation (QLBE) for a given interaction potential. It is based on the translational invariance of the QLBE, and admits the efficient propagation of superpositions of momentum eigenstates. Since the computation time scales almost linearly with the number of basis states, it can however be used in practice to simulate arbitrary states, such as spatially localized ones. This enables us to simulate many important physical processes, ranging from short-time effects, such as the loss of fringe visibility in interference experiments, to long-time phenomena, for example relaxation and thermalization.

These results were used to determine the range of validity of the different limiting forms of the QLBE, including the collisional decoherence model, the quantum Brownian limit and the classical linear Boltzmann equation. Moreover, we compared these simulations to the corresponding predictions of the simplified QLBE in Born approximation. Here it is found that the full QLBE may lead to physical predictions which deviate significantly from the ones obtained with the QLBE in Born approximation, if the interaction potential is sufficiently strong.

As an application of these results, one might consider interference experiments with test particles, such as electrons or small molecules, which are light compared to the gas particles. Their loss of quantum coherence due to the interactions with a background gas is inaccessible with previous methods, since all of them rely on the limit of heavy tracer particles.

On the theoretical side, it remains an open problem to design algorithms which admit the solution of the QLBE in presence of an external potential. Recall that the Monte Carlo algorithm presented in this thesis relies on the translational invariance of the QLBE. However, this symmetry is broken if an external potential is applied, such that the algorithm is no longer applicable. Presumably it is then necessary to perform the simulations on a three-dimensional grid.

Bibliography

- [1] W. H. Zurek, *Pointer Basis of Quantum Apparatus: Into What Mixture Does the Wave Packet Collapse?*, Phys. Rev. D **24**, 1516–1525 (1981).
- [2] E. Joos and H. D. Zeh, *The Emergence of Classical Properties Through Interaction with the Environment*, Z. Phys. B: Condens. Matter **59**, 223–243 (1985).
- [3] D. Giulini, E. Joos, C. Kiefer, J. Kupsch, O. Stamatescu, and H. D. Zeh, *Decoherence and the Appearance of the Classical World in Quantum Theory*, Springer, Berlin, 1996.
- [4] W. H. Zurek, *Decoherence, Einselection, and the Quantum Origins of the Classical*, Rev. Mod. Phys. **75**, 715–775 (2003).
- [5] W. H. Zurek, S. Habib, and J. P. Paz, *Coherent states via decoherence*, Phys. Rev. Lett. **70**, 1187–1190 (1993).
- [6] L. Diósi and C. Kiefer, *Robustness and Diffusion of Pointer States*, Phys. Rev. Lett. **85**, 3552–3555 (2000).
- [7] N. Gisin and M. Rigo, *Relevant and irrelevant nonlinear Schrödinger equations*, J. Phys. A: Math. Gen. **28**, 7375–7390 (1995).
- [8] W. T. Strunz, *Decoherence in Quantum Physics*, Lect. Notes Phys. **611**, 199–233 (2002).
- [9] J. Eisert, *Exact Decoherence to Pointer States in Free Open Quantum Systems is Universal*, Phys. Rev. Lett. **92**, 210401 (2004).
- [10] K. Hornberger, *Master equation for a quantum particle in a gas*, Phys. Rev. Lett. **97**, 060601 (2006).
- [11] K. Hornberger and B. Vacchini, *Monitoring derivation of the quantum linear Boltzmann equation*, Phys. Rev. A **77**, 022112 (2008).
- [12] B. Vaccini and K. Hornberger, *Quantum linear Boltzmann equation*, Phys. Rep. **478**, 71–120 (2009).
- [13] K. Hornberger, *Monitoring approach to open quantum dynamics using scattering theory*, Europhys. Lett. **77**, 50007 (2007).
- [14] M. R. Gallis and G. N. Fleming, *Environmental and Spontaneous Localization*, Phys. Rev. A **42**, 38–48 (1990).

- [15] K. Hornberger and J. E. Sipe, *Collisional Decoherence Reexamined*, Phys. Rev. A **68**, 012105 (2003).
- [16] K. Hornberger, S. Uttenthaler, B. Brezger, L. Hackermueller, M. Arndt, and A. Zeilinger, *Collisional Decoherence Observed in Matter Wave Interferometry*, Phys. Rev. Lett. **90**, 160401 (2003).
- [17] L. Hackermüller, K. Hornberger, B. Brezger, A. Zeilinger, and M. Arndt, *Decoherence in a Talbot Lau Interferometer: The Influence of Molecular Scattering*, Appl. Phys. B **77**, 781–787 (2003).
- [18] K. Hornberger, J. E. Sipe, and M. Arndt, *Theory of Decoherence in a Matter Wave Talbot-Lau Interferometer*, Phys. Rev. A **70**, 053608 (2004).
- [19] B. Vacchini, *Quantum and Classical Features in the Explanation of Collisional Decoherence*, J. Mod. Opt. **51**, 1025–1029 (2004).
- [20] B. Vacchini, *Theory of Decoherence due to Scattering Events and Lévy Processes*, Phys. Rev. Lett. **95**, 230402 (2005).
- [21] L. Diósi, *Stochastic pure state representation for open quantum systems*, Phys. Lett. **114A**, 451–454 (1986).
- [22] M. Rigo and N. Gisin, *Unravellings of the master equation and the emergence of a classical world*, Quantum Semiclass. Opt. **8**, 255–268 (1996).
- [23] G. C. Ghirardi, A. Rimini, and T. Weber, *Unified Dynamics for Microscopic and Macroscopic Systems*, Phys. Rev. D **34**, 470–491 (1986).
- [24] A. Bassi and G. Ghirardi, *Dynamical Reduction Models*, Phys. Rep. **379**, 257–426 (2003).
- [25] B. Vacchini, *On the precise connection between the GRW master equation and master equations for the description of decoherence*, J. Phys. A: Math. Gen. **40**, 2463–2473 (2007).
- [26] H. Breuer and B. Vacchini, *Three-dimensional Monte Carlo simulations of the quantum linear Boltzmann equation*, Phys. Rev. E **76**, 36706 (2007).
- [27] K. Mølmer, Y. Castin, and J. Dalibard, *Monte Carlo wave-function method in quantum optics*, J. Opt. Soc. Am. B **10**, 524–538 (1993).
- [28] K. Mølmer and Y. Castin, *Monte Carlo wavefunctions in quantum optics*, Quantum Semiclass. Opt. **8**, 49 (1996).
- [29] H.-P. Breuer and F. Petruccione, *The Theory of Open Quantum Systems*, Oxford University Press, Oxford, 2002.
- [30] E. B. Davies, *Quantum Theory of Open Systems*, Academic Press, London, 1976.
- [31] M. A. Nielsen and I. L. Chuang, *Quantum Computation and Quantum Information*, Cambridge University Press, Cambridge, 2000.

- [32] L. P. Hughston, R. Jozsa, and W. K. Wootters, *A complete classification of quantum ensembles having a given density matrix*, Phys. Lett. A **183**, 14–18 (1993).
- [33] P. Kok and S. L. Braunstein, *Postselected versus nonpostselected quantum teleportation using parametric down-conversion*, Phys. Rev. A **61**, 042304 (2000).
- [34] P. A. Horn and C. R. Johnson, *Matrix Analysis*, Cambridge University Press, New York, 1985.
- [35] W. F. Stinespring, *Positive Functions on C^* -algebras*, Proc. Amer. Math. Soc. **6**, 211 (1955).
- [36] R. Alicki and K. Lendi, *Quantum Dynamical Semigroups and Applications*, Springer, Berlin, 1987.
- [37] G. Lindblad, *On the generators of quantum dynamical semigroups*, Commun. Math. Phys. **48**, 119–130 (1976).
- [38] C. W. Gardiner, *Handbook of Stochastic Methods*, Springer, New York, 1985.
- [39] K. Hornberger, *Introduction to Decoherence Theory*, in *Entanglement and Decoherence. Foundations and Modern Trends*, edited by A. Buchleitner, C. Viviescas, and M. Tiersch, volume 768 of *Lect. Notes Phys.*, pages 221–276, Springer, Berlin, 2009.
- [40] V. Gorini and A. Kossakowski, *Completely positive dynamical semigroups of N -level systems*, J. Math. Phys. **17**, 821–825 (1976).
- [41] A. S. Holevo, *A note on covariant dynamical semigroups*, Rep. Math. Phys. **32**, 211–216 (1993).
- [42] A. S. Holevo, *On conservation of covariant dynamical semigroups*, Rep. Math. Phys. **33**, 95–110 (1993).
- [43] A. S. Holevo, *On translation-covariant quantum Markov equations*, Izv. Math. **59**, 427–443 (1995).
- [44] A. S. Holevo, *Covariant quantum Markovian evolutions*, J. Math. Phys. **37**, 1812–1832 (1996).
- [45] F. Petruccione and B. Vacchini, *Quantum description of Einstein’s Brownian motion*, Phys. Rev. E **71**, 046134 (2005).
- [46] H. J. Carmichael, *Statistical Methods in Quantum Optics 1*, Springer, Berlin, 1999.
- [47] A. O. Caldeira and A. J. Leggett, *Path Integral Approach to Quantum Brownian Motion*, Physica A **121**, 587–616 (1983).
- [48] R. P. Feynman and F. L. Vernon, *The Theory of a General Quantum System Interacting with a Linear Dissipative System*, Ann. Phys. (N.Y.) **24**, 118 – 173 (1963).

- [49] L. Diósi, *On high temperature Markovian equation for quantum Brownian motion*, Europhys. Lett. **22**, 1–3 (1993).
- [50] F. M. Ramazanoglu, *The approach to thermal equilibrium in the Caldeira-Leggett model*, J. Phys. A: Math. Gen. **42**, 265303 (2009).
- [51] W. H. Zurek, *Decoherence and the transition from quantum to classical*, Phys. Today **44**(10), 36 (1991).
- [52] J. R. Taylor, *Scattering Theory*, John Wiley & Sons, New York, 1972.
- [53] L. Mandel and E. Wolf, *Optical Coherence and Quantum Optics*, Cambridge University Press, Cambridge, 1995.
- [54] J. M. Raimond, M. Brune, and S. Haroche, *Colloquium: Manipulating Quantum Entanglement with Atoms and Photons in a Cavity*, Rev. Mod. Phys. **73**, 565–582 (2001).
- [55] S. Haroche, *Mesoscopic superpositions and decoherence in quantum optics*, in *Quantum entanglement and information processing*, edited by D. Estève, J.-M. Raimond, and J. Dalibard, Les Houches 2003, Elsevier, Amsterdam, 2004.
- [56] Zurek, *Preferred States, Predictability, Classicality and the Environment-Induced Decoherence*, Progr. Theor. Phys. **89**, 281–312 (1993).
- [57] W. T. Strunz, *Decoherence in Quantum Physics*, in *Coherent Evolution in Noisy Environments*, edited by A. Buchleitner and K. Hornberger, Lecture Notes in Physics 611, Berlin, 2002, Springer.
- [58] B. L. Hu, J. P. Paz, and Y. Zhang, *Quantum Brownian motion in a general environment: Exact master equation with nonlocal dissipation and colored noise*, Phys. Rev. D **45**, 2843–2861 (1992).
- [59] J. A. Fleck, J. R. Morris, and M. D. Feit, *Time-dependent propagation of high energy laser beams through the atmosphere*, Appl. Phys. A **10**, 129–160 (1976).
- [60] M. D. Feit, J. A. Fleck, and A. Steiger, *Solution of the Schrödinger equation by a spectral method*, J. Comput. Phys. **47**, 412–433 (1982).
- [61] J. Klauder and B. Skagerstam, *Generalized phase-space representation of operators*, J. Phys. A: Math. Gen. **40**, 2093 (2007).
- [62] D. J. Griffiths, *Introduction to quantum mechanics*, Prentice Hall, New Jersey, 1995.
- [63] I. M. Ryshik and I. S. Gradstein, *Tables of series, products and integrals*, Veb Deutscher Verlag der Wissenschaften, Berlin, 2nd edition, 1963.
- [64] F. Schwabl, *Statistische Mechanik*, Springer, Berlin, 2nd edition, 2004.
- [65] F. Ehlotzky, *Quantenmechanik und ihre Anwendungen*, Springer, Berlin, 2005.

- [66] D. E. Miller, J. R. Anglin, J. R. Abo-Shaeer, K. Xu, J. K. Chin, and W. Ketterle, *High-contrast interference in a thermal cloud of atoms*, Phys. Rev. A **71**, 043615 (2005).
- [67] R. Rubenstein, D. A. Kokorowski, A. Dhirani, T. Roberts, S. Gupta, J. Lehner, W. Smith, E. Smith, H. Bernstein, and D. E. Pritchard, *Measurement of the density matrix of a longitudinally modulated atomic beam*, Phys. Rev. Lett. **83**, 2285–2288 (1999).
- [68] S. M. Apenko, *Critical temperature of the superfluid transition in Bose liquids*, Phys. Rev. B **60**, 3052–3055 (1999).
- [69] S. M. Apenko, *Superfluid transition temperature from the Lindemann-like criterion*, Phys. Rev. B **62**, 9041–9049 (2000).
- [70] S. E. Shreve, *Stochastic Calculus for Finance II: Continuous-Time Models*, Springer, New York, 2nd edition, 2008.
- [71] B. Øksendal, *Stochastic Differential Equations: An Introduction with Applications*, Springer, Berlin, 2003.
- [72] W. H. Press, S. A. Teukolsky, W. T. Vetterling, and B. P. Flannery, *Numerical recipes: the art of scientific computing*, Cambridge University Press, Cambridge, 2007.
- [73] R. L. Stratonovich, *Introduction to the Theory of Random Noise*, Gordon and Breach, New York, 1963.
- [74] J. Hull, *Options, Futures and other Derivatives*, Prentice-Hall, Englewood Cliffs, 7th edition, 2008.
- [75] D. Williams, *Probability with Martingales*, Cambridge University Press, Cambridge, 1991.
- [76] E. Wong and M. Zakai, *On the convergence of ordinary integrals to stochastic integrals*, Annals Mathem. Statistics **36**, 1560 (1965).
- [77] H. Carmichael, *An Open Systems Approach to Quantum Optics*, Springer, Berlin, 1993.
- [78] N. Gisin and I. Percival, *The quantum-state diffusion model applied to open systems*, J. Phys. A: Math. Gen. **25**, 5677–5677 (1992).
- [79] I. Percival, *Quantum state diffusion*, Cambridge University Press, Cambridge, 1998.
- [80] C. W. Gardiner and P. Zoller, *Quantum Noise*, Springer, New York, 2000.
- [81] T. A. Brunn, *A simple model of quantum trajectories*, Am. J. Phys. **50**, 719–737 (2002).
- [82] P. E. Kloeden and E. Platen, *Numerical Solution of Stochastic Differential Equations*, Springer, Berlin, 3rd edition, 1999.

- [83] H. M. Wiseman and L. Diósi, *Complete parametrization, and invariance, of diffusive quantum trajectories for Markovian open systems*, Chem. Phys. **268**, 91–104 (2001).
- [84] L. Diósi, *Orthogonal jumps of the wavefunction in white-noise potentials*, Phys. Lett. A **112**(6-7), 288–292 (1985).
- [85] L. Diósi, *Quantum stochastic processes as models for state vector reduction*, J. Phys. A: Math. Gen. **21**, 2885–2898 (1988).
- [86] N. A. Smith and R. W. Tromble, *Sampling uniformly from the unit simplex*, Tech. Rep, Johns Hopkins University (2004).
- [87] C. Cercignani, *Theory and application of the Boltzmann equation*, Scottish Academic Press, Edinburgh, 1975.
- [88] B. Vacchini, *Translation-Covariant Markovian Master Equation for a Test Particle in a Quantum Fluid*, J. Math. Phys. **42**, 4291–4312 (2001).
- [89] B. Vacchini, *Non-Abelian linear Boltzmann equation and quantum correction to Kramers and Smoluchowski equation*, Phys. Rev. E **66**, 027107 (2002).
- [90] B. Vacchini and K. Hornberger, *Relaxation dynamics of a quantum Brownian particle in an ideal gas*, Eur. Phys. J. Special Topics **151**, 59–72 (2007).
- [91] C. W. Gardiner, A. S. Parkins, and P. Zoller, *Wave-function quantum stochastic differential equations and quantum-jump simulation methods*, Phys. Rev. A **46**, 4363–4381 (1992).
- [92] B. Johnson, *The multi-channel log-derivative method for scattering calculations*, Journal of Comp. Phys. **13**, 445–449 (1973).
- [93] R. Rubenstein, A. Dhirani, D. Kokorowski, T. Roberts, E. Smith, W. W. Smith, H. Bernstein, J. Lehner, S. Gupta, and D. Pritchard, *Search for Off-Diagonal Density Matrix Elements for Atoms in a Supersonic Beam*, Phys. Rev. Lett. **82**, 2018–2021 (1999).
- [94] J. W. S. Rayleigh, *Dynamical problems in illustration of the theory of gases*, Phil. Mag. **32**, 424–445 (1891).
- [95] M. S. Green, *Brownian motion in a gas of noninteracting molecules*, J. Chem. Phys. **19**, 1036–1046 (1951).
- [96] L. Ferrari, *An improved differential form of the Boltzmann collision operator for a Rayleigh gas (or Brownian particles)*, Physica A **142**, 441–466 (1987).
- [97] N. G. Van Kampen, *Stochastic processes in physics and chemistry*, Elsevier, Amsterdam, 2nd edition, 2006.

Name Marc Busse
Geburtsdatum 05. April 1980
Geburtsort Starnberg
Familienstand ledig

Schulbildung

1986 – 1990 Volksschule Fürstenfeldbruck
1990 – 1999 Gymnasium Starnberg
25. Juni 1999 **Abitur**
Leistungskurse Physik und Chemie

1999 – 2000 Zivildienst

Studium der Physik

2000 – 2006 Ludwig-Maximilians-Universität München
10. Mai 2002 **Physik Vordiplom**
Feb. – Nov. 2003 University of Auckland, Neuseeland
15. Mai 2006 **Physik Diplom**
Betreuer Prof. Dr. A. Buchleitner
“Verschränkung in offenen Quantensystemen”
angefertigt am Max-Planck-Institut für Physik
komplexer Systeme, Dresden

Juli – Okt. 2006 Praktikum bei Converium Holding AG, Zürich

Promotion in Physik

Seit Dez. 2006 Arnold-Sommerfeld-Zentrum für Theoretische Physik,
LMU, München
Betreuer Priv. Doz. Dr. K. Hornberger

Stipendien

Feb. – Nov. 2003 Jahresstipendium,
Deutschen Akademischen Austauschdienst (DAAD)